Cellular Mechanisms of Organ-Specific Metastasis of Ewing's Sarcoma

Henrike Knizia

Student number: 089160064

A thesis submitted in part requirement for the degree of Doctor of Philosophy from the

Faculty of Medical Sciences at Newcastle University,

Newcastle upon Tyne, UK

March 2011

Leukaemia Stem Cell Research Group, Northern Institute for Cancer Research, Paul O'Gorman Building, Medical School, Framlington Place, University of Newcastle, Newcastle-upon-Tyne, NE2 4HH, UK.

“When a plant goes to seed, its seeds are carried in all directions;

but they can only grow if they fall on congenial soil.”

Sir Stephen Paget

Author's declaration

I hereby declare that no parts of the work referred to in this thesis have previously been submitted in support of an application for another degree or qualification of this or any other University.

Cloning work was performed in cooperation with Dr. Frida Ponthan and Dr. Olaf Heidenreich, histology was supported by Dr. Christopher Bacon and imaging was supported by the imaging groups in Münster and Newcastle upon Tyne.

Parts of the work of this thesis in hand were performed at the Westfälische Wilhelms-University and University Hospital Münster, Germany.

Henrike Knizia

March 2011

Abstract

Ewing's sarcoma is the second most common bone tumour in children and adolescents. The prognosis is mainly influenced by the occurrence of primary metastasis. Although great improvement in treatment has been achieved, still only 2/3 of patients with localized disease can be cured. Furthermore, the 3-year event free survival in patients with lung metastases is only ~50%, and is less than 20% in patients with bony metastases. Metastatic models of Ewing's sarcoma developed in this study using cell lines in immunocompromised mice show a pattern of disease spread similar to that found in patients, providing a suitable system for studying the metastatic process likely occurring in the course of Ewing's sarcoma. The comparison of microarray gene expression patterns revealed interesting candidate genes for diagnosis and identified putative metastasis-specific targets that might be exploited in the development of new treatment approaches. However, it will be necessary to additionally analyse these patterns in primary material.

One gene that formerly has been shown to play a role in the metastasis to bones in a variety of cancer types is CXCR4, which encodes for the cytokine receptor of CXCL12 (SDF-1), and which plays a role in the metastasis to bones in a variety of other cancer types. As Ewing's sarcoma cells express CXCR4, a shRNA vector was constructed, transduced and stably expressed to investigate the role of the CXCR4/CXCL12 axis in Ewing's sarcoma cells via RNA interference. This stability provides the possibility of an *in vitro* and furthermore an *in vivo* use for investigations.

In order to investigate the biology of bone malignancy and especially the interaction of tumour cells with cells of the microenvironment of the bone

directly, an orthotopic model for Ewing's sarcoma was developed. Additionally, osteosarcoma as a further primary bone sarcoma and prostate carcinoma as a cancer type with frequent bone metastases were tested in this model. The previously described technique of intrafemoral transplantation was used in this model. Using small animal imaging techniques such as nano computed tomography and magnetic resonance imaging in combination with histology it could be shown that the transplanted cells led to the development of orthotopic tumours presenting a comparable picture to the clinical situation. This model will be further used for research projects performed in the Northern Institute for Cancer Research on the effectiveness of drugs targeting Ewing's sarcoma cells.

Acknowledgments

My special thanks go to my supervisor Prof. Dr. Josef Vormoor for giving me the opportunity to study for a PhD and develop as a researcher. Many thanks also to Dr. Marc Hotfilder and Dr. Georg Hempel in Münster for their support during the first phase of my PhD.

My dear colleagues: thank you very much for all the fun and for bearing me during the stressful times. Thanks, Patricia for sharing all your expertise, thanks Mike for all the hard work, help and expertise on mice and spending all this time down there in the CBC. Thanks to Klaus and Kerrie for company in the CBC. Thanks to Hesta and Annegret for their sorting support and to Andrea, Christoph, Rebekka and the girls from the KMT ward for the scientific exchange and discussions. I made a lot of good friends that contributed to the success of my thesis: Miriam, Mirjam, Andreas, Stephan and more in Münster, Patricia, Christine, Lisa, Klaus & Co. and more in Newcastle. Thanks for a great time!

Furthermore, my thanks go to all the collaborators for their help and support, especially to Gilberto Almeida, Ian Wilson, Dr. Ross Maxwell, Dr. Chris Bacon and Kieran O'Toole.

I would like to thank the Deutsche Krebshilfe, the Bone Cancer Research Trust, the North of England's Children's Cancer Research Fund and the Newcastle Healthcare Charity for funding parts of my studies.

My very special thanks go to my dear parents, my dear little brother Jan and the rest of my siblings and family for always being such a great support, lending an ear and taking so much care!

Table of Contents

List of Figures

List of Tables

List of Abbreviations

APC – Allophycocyanin

BM – Bone marrow

BMPs – Bone Morphogenic Proteins

BSA – Bovine serum albumin

CaP – Carcinoma of the prostate

CD – Cluster of differentiation

CSC – Cancer stem cell

CT – Computed tomography

d – day

ddH_2O – Distilled, deionised water

DMSO – Dimethylsulfoxide

dNTP – Deoxyribonucleotide triphosphate

ddNTP – Dideoxynucleoside triphosphate

E. coli – Escherichia coli

EDTA – Ethylediaminetetraacetic acid

eGFP – Enhanced green fluorescence protein

(EI)CESS – European Intergroup Cooperative Ewing's Sarcoma Study

EMT – Epithelial-to-mesenchymal transition

ES – Ewing's sarcoma

ES/PNET – Ewing's sarcoma/Primitive neuroectodermal tumours

et al. – et alia (*lat.* and others)

EURO-E.W.I.N.G. – EUROpean Ewing tumour Working Initiative and National Groups

FACS – Fluorescence activated cell sorting

FDG – ^{18}F-2-Fluor-2-deoxy-D-glucose

FCS – Foetal calf serum

FITC – Fluorescein isothiocyanate

FOV – Field of view

FSC – Forward scatter parameter

G – Gauge, used to specify diameter of a needle

h – hour

IDDM – insulin-dependent diabetes mellitus

i. f. – Intrafemoral

i. p. – Intraperitoneal

IPA – Ingenuity pathway analysis

i. t. – Intratibial

i. v. – Intravenous

kVp – Peak kilovoltage

LB – Lysogeny broth

MMP1 - Matrix metalloproteinase 1

MMPs – Matrix metalloproteinases

MRI – Magnetic resonance imaging

MSC – Mesenchymal stem cell

MTT – 3-([4,5-Dimethylthiazol-2-yl]-2,5-dimethyltetrazoliumbromide

NOD – Non-obese diabetic

NSG – NOD.Cg-*Prkdcscid Il2rgtm1Wjl*/SzJ

OD – Optical density

OS – Osteosarcoma

PAA – Polyacrylamide

PAGE – Polyacrylamide gel electrophoresis

PBS – Phosphate buffered saline

PCR – Polymerase chain reaction

PE – Phycoerthrin

PET – Positron emission tomography

PNET – Primitive neuroectodermal tumours

qRT-PCR – quantitative reverse transcriptase polymerase chain reaction

RPMI – Roswell Park Memorial Institute medium

s. c. – Subcutaneous

scid – Severe combined immunodeficiency

SSC – Side scatter parameter

TBE – Tris/boric acid/EDTA buffer

T_E – Echo time

T_R – Repetition time

Only terms used more than three times were abbreviated. Gene names, general biologic terms and SI units were not included.

1. Chapter – Background and Introduction

Ewing's sarcoma/Primitive neuroectodermal tumour (ES/PNET) is a rare disease and its diagnosis can still be fatal for patients. However, over the past decades outcome of patients has significantly improved. While 30 years ago more than 90% of patients would die nowadays the long-term survival rates have improved to 60-70% for patients with localised disease. Regardless, relapse rates of over 30% are still unacceptably high and these patients usually have a very poor prognosis (Leavey et al., 2008). Patients with systemic disease still have a poor prognosis (Paulussen et al., 2008).

Improved treatment of this malignant tumour has been achieved through application of multimodal treatments including local management as well as the introduction of chemotherapeutic approaches. The lack of alternatives to chemotherapeutic treatment approaches shows the necessity of basic and translational research to discover more specific, accurate, and effective targets for molecular therapies and diagnosis of ES/PNET.

1.1 Ewing's sarcoma

ES/PNET was first described by Lücke and Hildebrand but in 1921 the US-American pathologist James Ewing was the first to publish an elaborate characterisation of the disease which he described as a "diffuse endothelioma" and an "endothelial myeloma". This approach characterised the disease as being distinct from lymphoma and other types of cancer (Lücke, 1866; Hildebrand, 1890; Ewing, 1921, 1924).

1.1.1 Epidemiology

ES/PNET is the second most common primary malignant tumour of the bone in Caucasian children and adolescents with a median age at diagnosis of 15 years. In the UK it accounts for 39% of primary malignant tumours of the bone with a yearly incidence of approximately three new diagnoses per one million children under the age of 15 years and approximately 2.4 new diagnoses per one million adolescents between 15 and 25 years according to the (EI)CESS studies (European Intergroup Cooperative Ewing's Sarcoma Study). However, since new molecular tools for diagnoses have been introduced, more and more cases of unclassified sarcomas are identified as ES/PNET. This results in a growing number of diagnoses of ES/PNET in patients older than 20 years and a decreasing number of cases in patients aged 30 and older (Pieper et al., 2008).

More than 50% of new diagnoses are made for children and adolescents in their second decade of life and men are affected with an overall ratio of 1.5:1, which even increases with age (see Figure 1.1) However, data for the ratio between male and female patients vary between different studies.

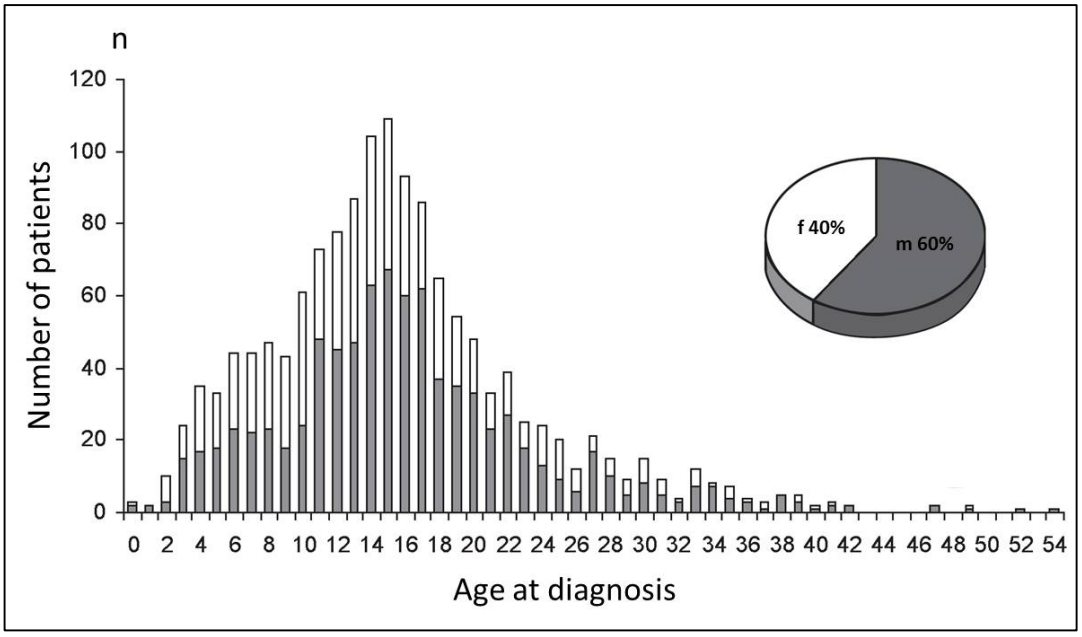

Figure 1.1: Age and sex distribution of patients with ES/PNET at the date of the initial diagnosis. Data based on 1426 patients of the (EI)CESS studies; f; female; m, male; n, number (Jürgens et al., 2006).

The incidence of ES/PNET in the African or Asian populations in very low, suggesting a genetic predisposition, although the formal evidence for this is limited (Fraumeni and Glass, 1970; Li et al., 1980; Hense et al., 1999).

1.1.2 Clinical presentation and diagnosis

Typically, patients present with diffuse pain which very often at first is thought to be caused by a trauma or "growth pain". However, there is no correlation between ES/PNET and traumas. Usually, the pain increases with physical activity but persists also in periods of recovery and during the night. This pain advances and results from the expansion of the periosteum caused by the

formation of new bone which ultimately leads to a swelling of the effected region. This swelling is very often misinterpreted as an inflammation.

The primary tumour is most frequently localised in the *os ilium* of the pelvis or the long bones of the extremities with the femur being affected in 20% of the cases (see Figure 1.2). Usually, the localisation in the long bones is diaphysial opposed to the metaphysical localisation of osteosarcoma (Hauben and Hogendoorn, 2010).

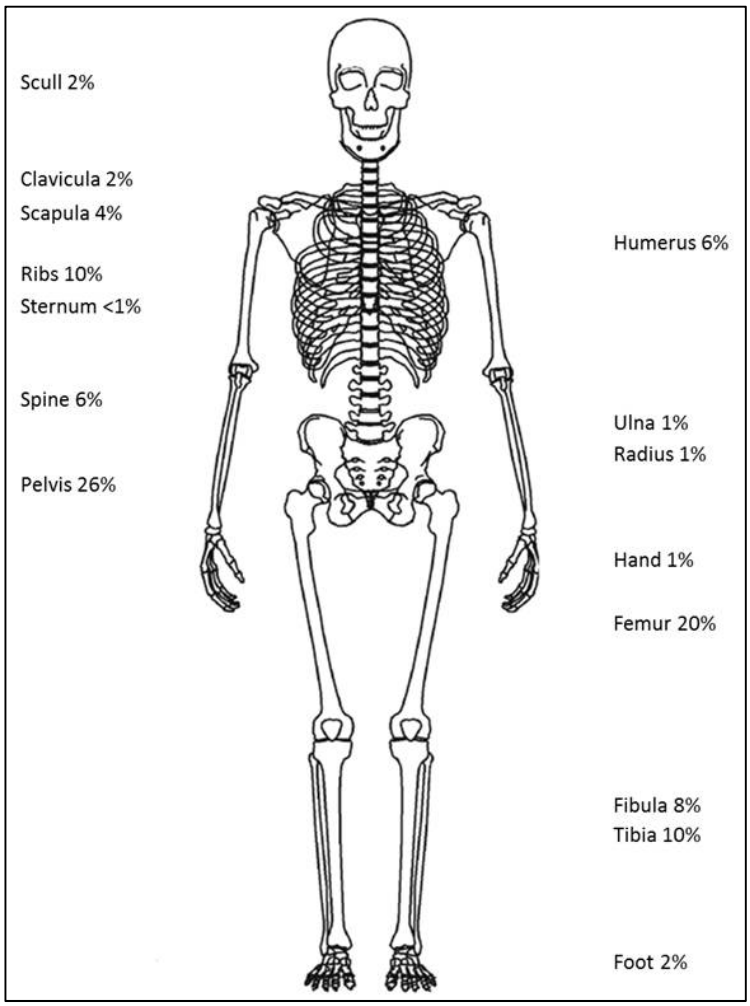

Figure 1.2: Skeletal dissemination of primary ES/PNET. Data based on 1426 patients of (EI)CESS studies (modified from Bernstein et al., 2006).

Further symptoms include increased body temperature or, depending on localisation and size of the tumour, neurological deficits. These symptoms are more common in advanced and metastatic stages of the disease and can be of indirect prognostic value (Widhe and Widhe, 2000; Bernstein et al., 2006).

The first tool for diagnosis of a suspected osseous lesion is imaging. Usually a radiograph in two planes is performed and images are investigated for tumour related osteolysis, Codman triangles (detachment of the periosteum from the bone) and formation of new bone (spiculae of calcification in the soft tissue mass of the tumour). To be able to more precisely evaluate the extent of the lesion and the location of the tumour in relation to blood vessels and nerves, magnetic resonance imaging (MRI) is performed (Bernstein et al., 2006).

1.1.3 Adverse factors and prognosis

Numerous factors are associated with poor prognosis in ES/PNET patients. The most unfavourable marker, which is important to clarify during initial staging, is the presence of metastases. Approximately, a quarter of patients present with metastatic disease at the time point of diagnosis (see Figure 1.3; further discussed in chapter 4). An additional important prognostic factor is age of the patient at the time of diagnosis. Patients younger than 10 years have a better outcome than older patients (Grier et al., 2003; Paulussen et al., 2007). A further unfavourable factor is a tumour volume larger than 200ml. Very often this is the case for tumours located in the pelvis as these are recognised and diagnosed relatively late. The response of the tumour to chemotherapy can be evaluated after surgical resection and gives evidence for prognosis as well (Paulussen et al., 2001).

The site of the primary tumour can also impact on prognosis. Patients with tumours located in the axial skeleton have a worse prognosis than patients with primary tumours in other sites as these are usually more difficult to treat and may not come into consideration for surgery (Cotterill et al., 2000a).

Taking the evidence based importance of these adverse prognostic factors into account several current therapeutic approaches and regimens are stratified accordingly.

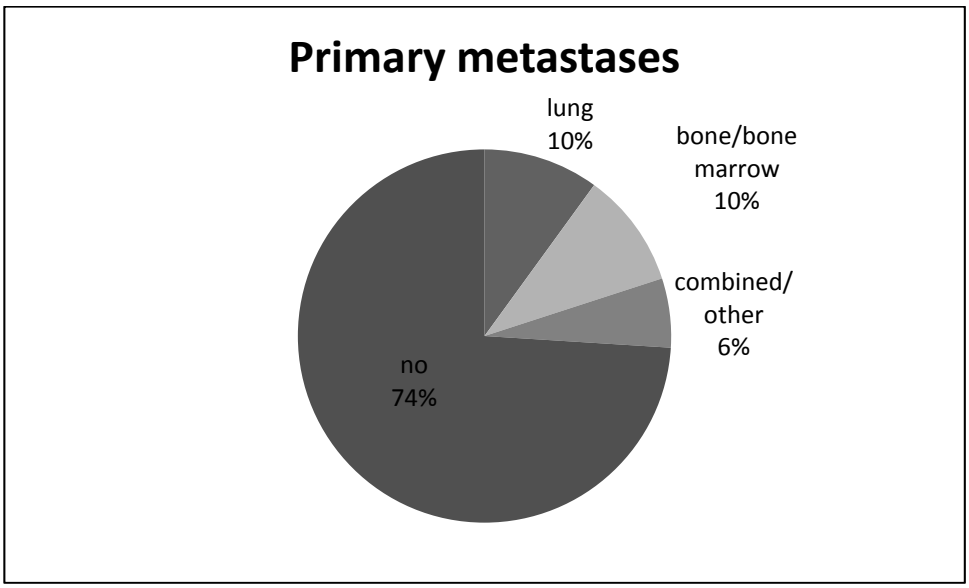

Figure 1.3: Percentage dissemination of primary metastases to organs. Data based on 1426 patients of (EI)CESS studies (modified from Bernstein et al., 2006).

1.1.4 Pathology

Macroscopically, ES cells of the bone, primitive neuroectodermal tumours (PNET) and Askin's tumours of the thoracic wall are histochemically characterised through a monomorphic appearance of small blue round cells

(routine hematoxylin and eosin staining). This predominance of blue staining is due to the fact that the tumour cells consist predominantly of a nucleus and scant cytoplasm. The existing glycogen inclusions can be visualised through periodic acid-Schiff staining (Roessner and Jürgens, 1993).

When characterising cells of these types of tumours immunhistochemically, 95% show positivity for the MIC2-antigen (CD99). However, CD99 is also expressed by other cell types and has a high incidence of expression in myeloid haematopoietic neoplasms. This limits the use of CD99 for differential diagnosis (Zhang et al., 2000).

To be able to further distinguish between the different tumour types, the presence of neuronal markers is also tested. Tumours that lack neuronal markers are termed as classical ES. However, tumours with two or more neuronal markers such as S-100 protein, neuron-specific enolase or synaptophysin are named PNET (Schmidt et al., 1991).

Today, the World Health Organisation classification no longer distinguishes between the three types of tumours as their biology is very similar and there is no evidence that the prognosis for patients with PNET and Askin's tumours differs from prognosis for patients with classical ES. Therefore, the currently used term is Ewing's sarcoma/primitive neuroectodermal tumours (ES/PNET; Dirksen and Jürgens, 2010).

1.1.5 Genetic background

Regardless of neuronal markers, ES/PNETs are classified as a biologic entity through the common chromosomal translocation they harbour. They represent

the first group of sarcomas for which a chromosomal translocation was characterized (Delattre et al., 1992, 1994). This molecular similarity is widely believed to play a major role in tumour pathology and biology.

1.1.5.1 Chromosomal translocations in Ewing's sarcoma

CD99-positive tumours are classified as ES/PNET+ve when a translocation exists between the *EWS* gene (Ewing's sarcoma breakpoint region 1, also known as *EWSR1*) at 22q12 and a member of the *ETS* (E26 transformation specific gene) family of transcription factors. In 85% of ES/PNET cases a translocation t(11;22)(q24;q12) is detected which fuses *EWS* to the gene *FLI1* (Friend leukaemia virus integration 1). This results in the fully functional but aberrant fusion transcript EWS-FLI1 (Delattre et al., 1992; Zucman et al., 1993; Delattre et al., 1994). In half of such cases, this translocation results in a fusion protein consisting of the first 264 N-terminal amino acids of the EWS protein (breakpoint in intron 7) and the 233 C-terminal amino acids of FLI1 (breakpoint in intron 5), which is termed "type 1" fusion protein (see Figure 1.4). There are further EWS-FLI1 fusion proteins involving slightly different breakpoints of the two genes (Delattre et al., 1992; Plougastel et al., 1993; Zucman et al., 1993).

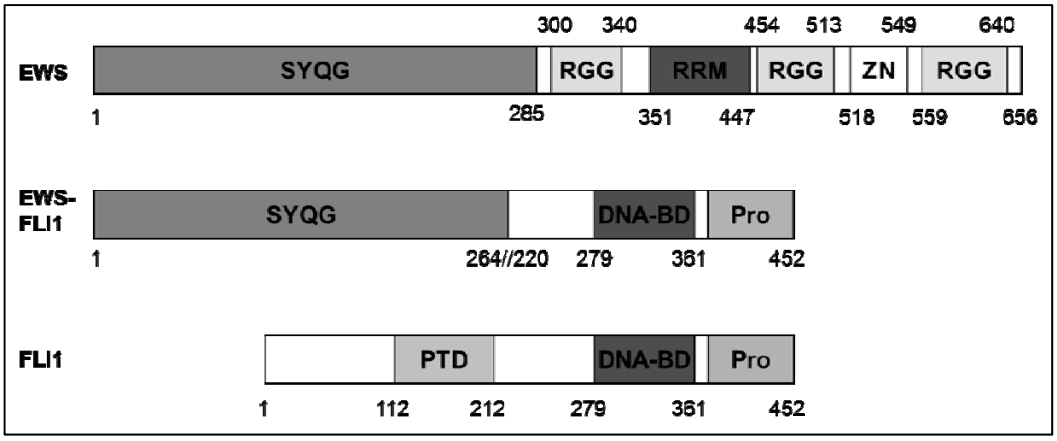

Figure 1.4: Scheme of the proteins EWS and FLI1 as well as the EWS-FLI1 fusion protein type 1. DNA-BD, DNA-binding domain; Pro, proline-rich activation domain; PTD, pointed domain; RGG, arginine-glycine-glycine-rich region; RRM, RNA-recognition motif; SYQC, serine-tyrosine-glutamine-glycine-rich region; ZN, zinc finger (modified from (Janknecht, 2005).

All possible *EWS-FLI1* translocations create fusion proteins consisting of the potent transactivation domain of the EWS protein and the DNA binding and proline-rich transcription-advancing domains of FLI1. Thus, the aberrant fusion proteins are potent transcription factors that are capable of binding to DNA (Bailly et al., 1994; Mao et al., 1994; Lessnick et al., 1995).

Approximately 10% of ES/PNETs harbour a t(21;22)(q22;q12) translocation between *EWS* and the *ETS* gene *ERG* (*ETS*-related gene). Further translocation partner genes of *EWS* include *ETV1* (*ETS* variant gene 1), *FEV* (fifth Ewing's sarcoma variant) and *E1AF* (E1A enhancer binding protein) (Jeon et al., 1995; Kaneko et al., 1996; Peter et al., 1997; Sorensen et al., 1994; Urano et al., 1996; Zucman et al., 1993). All different forms of translocations produce chimeric proteins that function as potent aberrant transcription factors because the transactivation domain of *EWS* is fused to a DNA-binding domain of a member of the *ETS*-family of transcription factors (Uren et al., 2004a; Janknecht, 2005).

Recently, it has been shown that neither the fusion partner nor the different breakpoints (different types of EWS/FLI) are of prognostic relevance (Le Deley et al., 2010; van Doorninck et al., 2010).

1.1.5.2 Further aberrations

In 80% of the cases there are molecular abnormalities discovered in addition to the characteristic translocations between *EWS* and members of the *ETS* family of transcription factors (Roberts et al., 2008). However, numbers vary in different studies. In the majority of cases these non-random chromosomal aberrations are chromosomal gains with number changes. Most often a trisomy of chromosome 8, as well as chromosomes 2, 12 and 20 can be detected. Additional structural aberrations are less common and appear as unbalanced rearrangements involving chromosomes 1 and 16 with a net gain of 1q and loss of 16q (Hattinger et al., 2002). Different studies suggest that these chromosomal gains may be of prognostic value or may even lead to a worse prognosis for patients (Armengol et al., 1997; Hattinger et al., 2002; Roberts et al., 2008).

1.1.6 Mechanisms of fusion transcripts in tumorigenesis

In vitro studies have proven that the EWS-ETS fusion proteins contribute to tumorigenesis and behave as oncoproteins. This was established using NIH3T3 cells transformed following transfection and ectopic expression of *EWS-FLI1* (May et al., 1993a, 1993b; Lessnick et al., 1995; Thompson et al., 1999).

Furthermore, antisense experiments in ES/PNET cells led to growth impairment, increased apoptosis rates and prevention of tumour formation *in vivo* proving that the fusion protein is also critically important for maintaining the ES/PNET phenotype (Lambert et al., 2000; Prieur et al., 2004; Siligan et al., 2005).

Recently, development of new techniques has allowed detailed investigations of direct and indirect downstream target genes of chimeric fusion proteins, including investigations elucidating the function of EWS-FLI1 as an aberrant transcription activator and repressor. Amongst other functions, genes that are transactivated are involved in cell survival and proliferation, such as *IGF1* (Cironi et al., 2008) and *Myc* (Sollazzo et al., 1999), or differentiation (*SOX2*; (Riggi et al., 2010). Repressed genes include, amongst others, *TGFB2* (Hahm, 1999) and *IGFBP3* (Prieur et al., 2004).

Important cellular signalling pathways activated in ES/PNET include amongst others the Wnt signalling pathway and the insulin growth factor 1 (IGF1) mediated tyrosine kinase pathway. In ES/PNET cell lines Wnt/Frizzled-signalling has been shown to be functional with the canonical Wnt/β-catenin signalling enhancing motility of cells and thus probably contributing to metastasis of ES/PNET (Uren et al., 2004b; Endo et al., 2008; Navarro et al., 2010). The interplay of IGF1 and its receptor IGF1R and subsequently downstream targets of this pathway have been shown to be effected by *EWS-FLI1* knockdown (Herrero-Martín et al., 2009). This in turn influences growth and maintenance of the tumour.

Other functions of fusion transcripts and proteins are currently further investigated, including RNA binding, aberrant RNA splicing and protein-protein interactions (Watson et al., 1997; Yang et al., 2000; Toretsky et al., 2006).

Although progress has been made in identifying downstream targets, it has become clear that the identification of the cell of origin in ES/PNET is immensely important. It is possible to transform the immortalised cell line NIH3T3 but so far transformation experiments with native murine and human fibroblasts has not been successful, primarily because expression of *EWS-FLI1* leads to cell cycle arrest (Lessnick et al., 2002).

All this underlines the importance of further investigations for the cell of origin as the fusion transcript seems to have different effects on varying cell types. Furthermore, in this context the role of additional aberrations has to be kept in mind as well.

1.1.7 Potential cell of origin of Ewing's sarcoma

As mentioned before, all ES/PNET harbour an in-frame *EWS-ETS* translocation. This translocation and the resulting fusion transcripts act on the affected cells with complex mechanisms of which the function as an aberrant transcription factor is best known. The specificity of the *EWS-FLI1* and other *EWS-ETS* fusions for ES/PNET tumours suggests that the cell of origin is critical for EWS-FLI1-induced oncogenesis. However, despite elaborate and extensive investigations the cell of origin is currently still unknown (Prieur et al., 2004).

On the one hand, historically and histologically, for a long time ES/PNET has been thought to be of neuroectodermal origin as early neural markers and other features can be detected that are typically found in primitive neuroectodermal cells (Cavazzana et al., 1987). Although these findings strongly suggested the origin to be neuroectodermal the fact that these neural markers are just found in a

minority of cases and the fact that *EWS-FLI1* induces neuroectodermal differentiation and upregulation of a number of genes associated with early neural differentiation raise the assumption that the cell of origin might not necessarily be of neuroectodermal origin (Teitell et al., 1999; Hu-Lieskovan et al., 2005b). This is why, the finding suggest that occasional neuroectodermal features of ES/PNET cells are a direct result of the fusion transcrips rather than the cell of origin.

On the other hand, there is evidence that ES/PNET might originate from a mesenchymal stem cell (MSC). As all bones of the skeleton except the cranial bones and the cells of the bone marrow originate from the mesenchyme and ES/PNET most often arise in the long bones or the pelvis it seems to be plausible that the cell of origin of ES/PNET is a resident of the bone. Besides, MSC from the bone marrow show some characteristics of neuroectodermal cells (Olsen et al., 2000; Takashima et al., 2007) which could explain neuroectodermal features of ES/PNET cells. Admittedly, the term of MSCs is not exact enough. One of the problems is that extraction of MSCs from bone marrow leads to a mixture of cells enriched from all adherent cells through selection of specific surface markers (Bianco et al., 2008; Lin et al., 2011). This implies that more defined extraction terms will have to be identified as there is evidence of more than one type of pluripotent non-haematopoietic cell within the bone marrow (Colter et al., 2001; Jiang et al., 2002). The current definition of MSC is that of multipotent stem cells that are able to differentiate into mature cell types, including osteoblasts, chondrocytes (cartilage cells) and adipocytes (fat cells) (Beyer Nardi and da Silva Meirelles, 2008).

However, approaching from the opposite side, a subpopulation of $CD133^+$ tumour cells from ES/PNET has been identified and characterised. These are characterised through a high degree of plasticity similar to MSCs and are able to initiate and promote the growth of tumours in *in vivo* experiments with immunodeficient mice (Suvà et al., 2009).

Furthermore, there is more direct evidence supporting the hypothesis of a MSC-like cell as origin of ES/PNET. *EWS-FLI1* knockdown experiments in ES/PNET cell lines leave the cells with the ability to differentiate into a range of comparable cell types as MSCs are able to differentiate into (Tirode et al., 2007). The identified "core" EWS-FLI1 transcriptional pattern achived through knockdown of the fusion transcript could be shown to resemble the one of human MSCs (Hancock and Lessnick, 2008; Kauer et al., 2009).

Additionally, knock-in experiments with murine MSCs produce transformed cells that form sarcomas *in vivo* (Castillero-Trejo et al., 2005; Riggi et al., 2005). Transfection of human MSCs did not lead to tumour formation after transplantation into immunocompromised mice but the cells took on an ES/PNET -like morphology and CD99 expression was upregulated (Miyagawa et al., 2008; Riggi et al., 2008).

It seems that due to the additional genetic changes in ES/PNET cells these cannot be reverted to normal MSCs by a simple knockdown of *EWS-FLI1*. Although a lot of data is suggestive that MSCs are the cell of origin for ES/PNET additional studies are necessary and the phenotype for extraction of MSCs needs to be further defined. This leads to the assumption that they cannot yet be definitely understood as the cell of origin (Lin et al., 2011).

1.1.8 Current treatment and studies

Shortly after the first description of ES/PNET it was clear that the tumours are sensitive to radiotherapy (Ewing, 1939). However, only since the 1970s it was possible to achieve a cure of the disease and increase survival rates because multimodal multidisciplinary treatment was developed applying neoadjuvant systemic chemotherapy and local therapy consisting of surgery and/or radiotherapy (Stiller et al., 2001). Today, current regimens reach a 5-year survival of up to 75% of patients with localised disease (Paulussen et al., 2001).

Currently, surgical therapy following initial chemotherapy is performed when the primary tumour is located in the extremities, the thoracic wall or the pelvis as long as the sacrum is not involved. Through the development of novel surgical techniques, including amongst others extendable endoprostheses for children and adolescents, nowadays, limb salvage can often be achieved (Kotz et al., 2002). Postoperative radiotherapy care has to be considered and the dosage depends on histologic response of the tumour to chemotherapy and the success of surgery. The combination of surgery and radiotherapy opposed to radiotherapy alone increases survival rates by 15-20% (Schuck et al., 2003).

First studies in the early 1960s proved the sensitivity of ES/PNET to cytostatics (Sutow and Sullivan, 1962). About a decade later, first combinations of cytostatics were tested in clinical trials and a combination of VACD (vincristine, actinomycin D, cyclophosphamide, doxorubicin) soon became standard in many trials for non-metastatic disease. Local control and event free survival could be improved but at the same time increased doses of doxorubicin lead to greater cardiac morbidity (Nesbit et al., 1990; Burgert et al., 1990).

Subsequently, inclusion of ifosfamide (I) and etoposide (E) showed improvement of ES/PNET of patients with localised disease as well as better prognoses for relapsed patients (Craft et al., 1998; Grier et al., 2003).

During the course of the EICESS-92 trial patients were divided into standard risk and high risk groups (tumour volume </≥ 200ml). Standard risk patients did not benefit from the VAID regime opposed to VACD and there was no significant benefit for high risk patients when treated with an EVAID regime compared to patients treated with VAID. Despite the insufficient power of the study, however, etoposide might be beneficial to those patients (Paulussen et al., 2008).

To be able to recruit more patients the EURO-E.W.I.N.G.99 (EUROpean Ewing tumour Working Initiative of National Groups - Ewing tumour studies 1999) trial was initiated bringing together major European study groups. The aims of the study are to address whether further increases in treatment intensity will lead to further benefits for patients as well as to further improve survival of patients with poorer prognosis and to decrease long-term effects of toxicity. Furthermore, the effect of a myeloablative therapy with haematopoietic stem cell rescue in high risk patients will be investigated (Rodriguez-Galindo et al., 2003).

Up to today it is not possible to make a reliable statement about the outcome of the study although first results are published (Ladenstein et al., 2010) and final results are awaited to be published.

1.2 Bone Biology

One of the major specialised tissues of the human body is bone, a composite tissue of inorganic materials, organic matrix and cells. Bone does not only have a

mechanical function of giving the body structural support, allowing movement by supporting musculature and protecting vital organs but also has biological and metabolic functions. These functions include maintenance of mineral homeostasis and acid-base balance as well as keeping a reservoir of growth factors and cytokines. Furthermore, bone provides within the bone marrow cavity an environment for haematopoiesis (Clarke, 2008).

1.2.1 Bone structure

There are two different types of bone structure. Trabecular bone (also referred to as cancellous or spongy bone) is made of characteristic irregular branches giving it a honey comb appearance. The emerging cavity contains the bone marrow. Due to its fine branches and the close proximity to the bone marrow, trabecular bone is more metabolically active than cortical bone.

Trabecular bone is surrounded by cortical bone giving bones the typical smooth, white appearance. It makes up 80% of the dry weight of the total bone mass and accounts for the mechanic stability of bones due to its compactness (Safadi et al., 2009).

1.2.1.1 Molecular structure

The inorganic compound makes up 60% of the try weight of bone tissue and consists mainly of crystalline calcium phosphate salts (hydroxyapatite, $Ca_{10}(PO_4)_6(OH)_2$), carbonate, fluoride, magnesium, acid phosphate and citrate.

To resist applied forces, calcium hydroxyapatite crystals are arranged in parallel to collagen fibres. This orientation maximises resistance to stretch (type I collagen) and compression (calcium hydroxyapatite salt) forces (Sela et al., 1987; Safadi et al., 2009).

The organic matrix produces mainly type I collagen which is synthesised intracellularely as tropocollagen. When cells export tropocollagen, fibrils are formed. Proteoglycans, glycoproteins, phospholipids, phosphoproteins and various growth factors are part of the organic matrix as well. This means besides mechanical functions bone tissue also fulfils the function as a reservoir for inorganic ions and is involved in metabolic processes through the active participation in the calcium/phosphate balance and release of growth factors and other components resting within the bone tissue (Safadi et al., 2009).

According to the pattern in which collagen and other proteins form the osteoid, there are two types of bone tissue – woven and lamellar bone. Woven bone is characterised by a rather high number of osteocytes and a disorganised appearance due to randomly orientated collagen fibres. This disorganisation accounts for a weaker structure. It is mainly found in sites of rapid growth such as the embryonic skeleton and later at sites of fractures (Price et al., 1994).

Lamellar bone is the mature form of bone which grows slowly and in parallel lines of deposited bone, the collagen fibres are highly organised and run in opposite directions to maximise mechanical stability. Usually it is deposited on pre-existing bone (Khurana and Safadi, 2009).

The secondary structure of lamellar bone accounts for the high level of organisation of compact bone (see Figure 1.5).

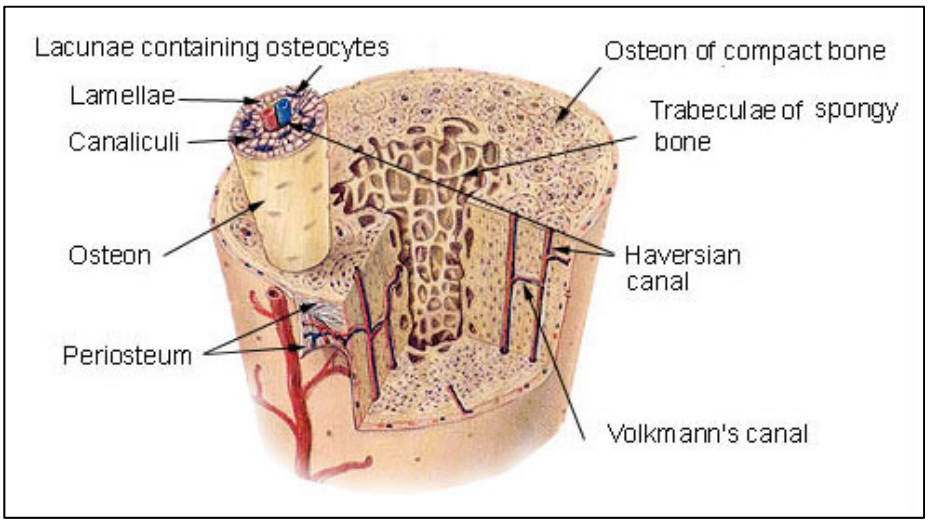

Figure 1.5: Scheme of the cross section of a typical human long bone (Standring and Gray, 2008).

The part of the bone formed by compact bone (surrounding the trabecular bone part in the centre of the bone) consists of closely packed osteons (also called Haversian systems). Each osteon consists of a Haversian canal in the centre through which blood and lymphatic vessels as well as nerves run. The canal is surrounded by 5-15 concentric layers, or lamellae, of compact bone tissue arranged in parallel to the long axis of the bone. Volkmann's canals connect Haversian canals to each other as well as to the blood system of the body (Safadi et al., 2009).

Between layers osteocytes are located in spaces termed lacunae. These are interconnected through canaliculi and connected to the Haversian channel to provide all cells equally with nutrition. The entity of tubular osteons is surrounded by outer circumferential lamellae that lie underneath the periosteum and in parallel to it. The periosteum is a fibrous layer coating the entire bone

except at joints where articular cartilage covers the bone surface. It consists of an outer connective tissue layer containing fibroblasts, nerves and blood vessels supplying the bone tissue and an inner cambium layer containing osteoprogenitor cells.

The inner circumferential lamellae are located next to the endosteum, which is a membranous layer. The endosteum covers the inner surface of cortical bone, trabecular bone and the Haversian and Volkmann's canals and contains blood vessels, osteoblasts and osteoclasts (Clarke, 2008; Safadi et al., 2009).

The rods and plates forming the structure of trabecular bone consist of so-called packets (trabecular osteons). These have a semilunar shape and consist of concentric lamellae.

1.2.1.2 Cellular structure

The existence of bone and its continuous remodelling relies on the precise equilibrium between the different types of cells present in this tissue.

Within the bone marrow there is a small population of MSCs which are distinct from the haematopoietic stem cells. These MSCs are capable of giving rise to various cell types one of them being osteoprogenitor cells. Osteoprogenitor cells differentiate to different cell types (Pittenger et al., 1999). One of those cell types is the osteoblast which is a bone-forming, large and mononuclear cell that deposits osteoid (organic bone matrix). This is why one of the characteristics of osteoblasts are large Golgi structures and an extensive endoplasmic reticulum. Subsequently, the osteoid becomes mineralised through the secretion of alkaline phosphatase and non-collageneous, calcium- and phosphate-binding proteins.

However, osteoblasts are heterogeneous in their expression of gene patterns which may explain different microarchitecture of skeletal sites, site-specific disease manifestation and regional differences in response to drug treatments (Harada and Rodan, 2003; Clarke, 2008).

Another type of cell is the osteocyte which resides within the bone tissue and maintains the structure of it. It originates from formerly active osteoblasts and changes shape throughout the production of mineralised bone. When trapped in the lacunae between the lamellae of bone osteocytes keep in contact with each other via canaliculi (Safadi et al., 2009).

Furthermore, there are protective lining cells that cover the surface and are thought to be quiescent osteoblasts. They form the endosteum and underlie the periosteum on mineralised bone. Usually, lining cells are found in close proximity to osteoblasts and interact with those (Clarke, 2008).

Osteoclasts are antagonising osteoblasts. They are multinucleated and originate from mononuclear precursor cells of the monocyte-macrophage lineage (Boyle et al., 2003). Osteoclasts are able to bind to the bone surface because they express integrin receptors that bind collagen, fibronectin and laminin of the bone matrix (Ross and Teitelbaum, 2005). Upon binding to the bone matrix, the osteoclast becomes polarised and apical a ruffled border is formed. The cytoskeleton of the osteoclast forms a ring to seal in the periphery of the osteoclast's attachment to the bone surface (Howship's lacuna or resorption pit). Subsequently, acidified vesicles export proteins via the ruffled border into the Howship's lacuna. Amongst others matrix metalloproteinases (such as MMP-1) and cathepsins (such as pro-cathepsin K) are secreted, the latter of which are activated through exocytosis within the acidic milieu of the Howship's lacunae. The acidified

condition is achieved through secretion of H^+ ions via H^+-ATPase and chloride channels (Väänänen et al., 2000). While enzymes cause resorption of the organic part of the bone matrix, the acidic milieu leads to solubilisation of the crystalline calcium hydroxyapatite.

1.2.1.3 Macroscopic structure

The formerly mentioned macroscopic structures of cortical and trabecular bone are not found in all bones. In the adult human body trabecular bone can only be found in the metaphysis and epiphyses of long bones, the vertebral bodies and flat bones. This has the advantages of skeletal weight reduction without compromising strength (Price et al., 1994; Clarke, 2008). Consequently, ratios of cortical and trabecular bone structures vary between different bones; for example the ratio is 25:75 in vertebrae whereas it is 95:5 in the radial diaphysis. Due to these findings, bones are classified into four main groups: long bones (e.g. femurs, tibiae, humeri), short bones (e.g. carpal and tarsal bones), flat bones (e.g. skull, ribs) and irregular bones (e.g. vertebrae).

Long bones consist of a diaphysis (hollow shaft), a cone-shaped metaphysis below growth plates and a rounded epiphysis above growth plates. While the metaphysis and the epiphysis are mainly made up of trabecular meshwork surrounded by a thin layer of cortical bone, the diaphysis is primarily composed of dense cortical bone (Clarke, 2008).

1.2.2 Bone remodelling

Throughout life, bone tissue is constantly remodelled giving it an adaptive and regenerative capacity. Remodelling of bone takes place alongside the processes of growth and skeletal modelling taking place in childhood. This means, remodelling already starts before birth and continues until death. It is achieved through the simultaneously, and normally counterbalanced, processes of bone formation and resorption (Clarke, 2008; Safadi et al., 2009).

There are different aspects of the randomness of remodelling sites in the human skeleton. On the one hand, to achieve one of the goals of remodelling, i.e. maintaining the balance of essential minerals, remodelling does not have to target a specific site and thus mostly occurs randomly. On the other hand, to achieve the goals of maintenance of stability, adaption to mechanical stress and repair of damage, remodelling has to be targeted (Burr, 2002).

Studies with genetically modified mice have shown that net bone formation occurs when mice are deficient for normal osteoclasts. Net resorption takes place when mice cannot develop fully functional osteoblast. This suggests that the two types of cells do not require each other to function or be activated but that balance in bone metabolism can only be achieved with both cell types controlling each other (Corral et al., 1998; Kong et al., 1999). In humans defects in the fine equilibrium of bone remodelling leads to a variety of different bone diseases including osteoporosis, osteopetrosis and Paget's disease.

The process of remodelling not only involves osteoclasts and osteoblasts but as well osteocytes and lining cells. The tightly coupled cells function together as the basic multicellular unit and perform the four sequential phases of remodelling: initiation, resorption, reversal and formation.

However, due to the complexity of remodelling this subchapter can only selectively highlight some of the more important processes of remodelling (Sims and Gooi, 2008).

1.2.2.1 Initiation and activation of osteoclasts

Haematopoietic myelomonocytic osteoclast precursor cells are attracted to the site of remodelling, where they fuse and subsequently bind to the bone surface as multinucleated cells (see Figure 1.6). Cells of the osteoblasts lineage (pre-osteoblasts, mature osteoblasts, lining cells and osteocytes) play a critical role in each of those steps (Sims and Gooi, 2008).F

One the one hand, chemoattractants released by the osteoblast-lineage are responsible for the control of the movement of osteoclast-precursors towards each other and the bone surface. These factors might be directly released by osteoblasts and/or lining cells, bone matrix-derived (osteocalcin, α_2 HS-glycoprotein, collagen I fragments, aging of bone resulting in isomerisation of collagen I) or set free through apoptosis of osteocytes (see further below). In more detail, factors released by osteoblast-lineage cells include CXCL12 (chemokine (C-X-C motif) ligand 12; also referred to as SDF-1, stromal-derived factor 1), CCL3, CCL5 and CCL7 (chemokine (C-C motif) ligands 3, 5 and 7). In addition to promotion of osteoclast formation these factors increase chemotaxis of osteoclast-precursors *in vitro* (Yu et al., 2003, 2004). It could also be shown that some of these factors play a role in osteoclast-precursor attraction in pathological conditions such as multiple myeloma or bone metastases caused by breast and prostate cancer, but their role in

non-pathological remodelling remains to the greatest extend unclear (Aggarwal et al., 2006; Guise et al., 2006).

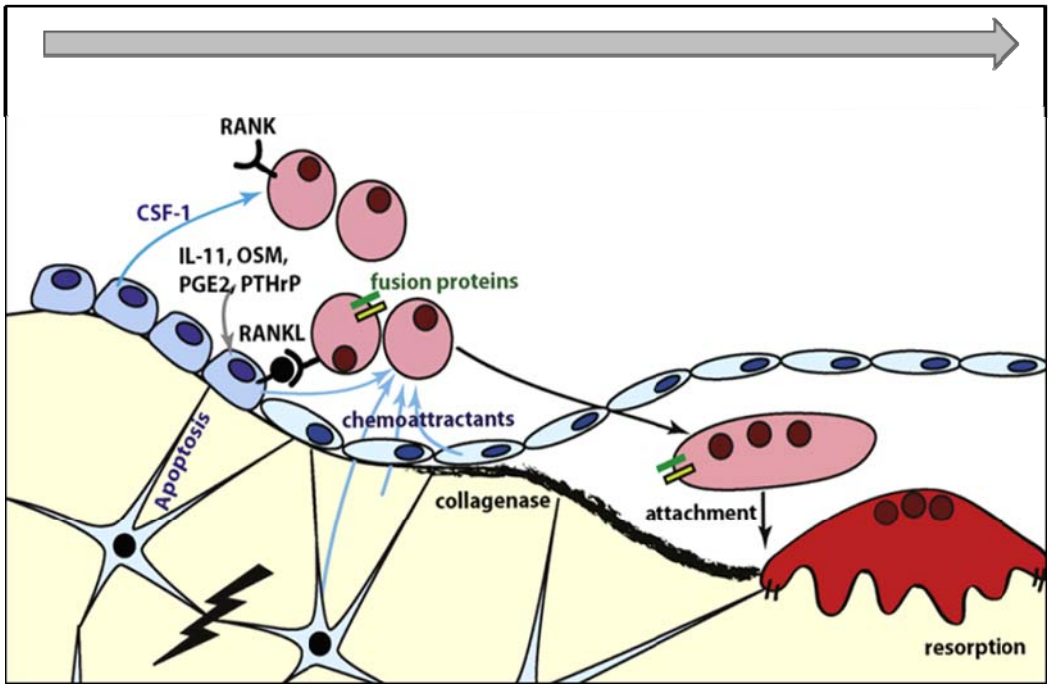

Figure 1.6: Initiation of osteoclast formation (osteoclast-lineage cells shown in red shades, osteoblast-lineage cells shown in blue shades). Proliferation of osteoclast precursors (light red cells) and expression of RANK is stimulated through CSF-1 produced by osteoblasts. Locally acting factors such as IL-11, OSM, PGE2 and PTHrP (grey arrow) and microdamage-induced osteocyte apoptosis (lightning) induce RANKL (receptor activator of NF-κB ligand) expression on osteoblasts. chemoattractants (blue arrows) released from osteoblast-lineage cells and bone matrix attract osteoclast precursors. Resulting interaction between RANKL and RANK leads to expression of fusion proteins (green blocks). Lining cells (light blue) prepare the bone surface (collagenases) and lift off to form the bone remodelling compartment, in which osteoclast precursors enter. They attach to the bone surface as resorbing osteoclasts (red cell) (Sims and Gooi, 2008).

A lot of cytokine receptors that stimulate bone resorption through initiation of osteoclast formation are expressed in cells of the osteoblast-lineage. This proves

that at least to parts osteoblast-lineage cells are required for the formation and activation of osteoclasts (Suda et al., 1999). Subsequent to osteoblasts binding, indirectly acting osteoclast-activating factors like IL-11 (interleukin 11), PGE2 (prostaglandin E2), OSM (oncostatin M) and PTHrP (parathyroid hormone-related protein), intracellular signalling is activated. In most cases intracellular signalling results in osteoclast-activation mediated through RANKL (receptor activator of NF-κB ligand) which is presented on the osteoblast cell surface. A further important factor produced by osteoblasts is the soluble TNF receptor superfamily member OPG (osteoprotegerin), which inhibits osteoclast formation (Yasuda et al., 1998; Horwood et al., 1998; Liu et al., 1998; Palmqvist et al., 2002). The very complex interactions leading to the activation of osteoclasts are only described to parts in Figure 1.6.

Further to released factors, the interruption of a physiological link between osteocytes and existing osteoclasts, as well as the release of certain factors such as cytokines and prostaglandins through apoptosis of osteocytes, might trigger the osteoclast formation (Sims and Gooi, 2008).

1.2.2.2 Attachment of osteoclasts to and resorption of bone material

Attachment of osteoclasts to the bone surface depends on the activity of terminally differentiated lining cells deriving from the osteoblast-lineage. These lining cells are thought to prepare the bone surface for resorption by releasing collagenase to destroy the fine layer of non-mineralised matrix on which they are located (Chambers and Fuller, 1985). This causes the lift off of lining cells from the bone surface and formation of a cover underneath which a space is created.

This space serves as a temporary bone remodelling compartment where the bone surface is exposed to osteoclasts for resorption as well as to osteoblasts for subsequent bone formation, but it still remains unclear, how both cell types enter the bone remodelling compartment. It has to be mentioned that the bone remodelling compartment is highly supplied with blood vessels indicating that stromal derived osteoblasts might be able to arrive via the blood stream (Parfitt, 2001; Sims and Gooi, 2008).

The attachment itself occurs when osteoclast-expressed integrins bind to an arginine-glycine-aspartic acid sequence of bone matrix proteins such as osteopontin and bone sialoprotein which have been laid down within the matrix by osteoclasts in previous cycles of remodelling (Ross and Teitelbaum, 2005). Polarisation of the osteoclast attached to the bone surface and sealing of the resorptive pit allows directed and selective resorption (see chapter 1.2.1.2).

When resorption and recycling of matrix components is completed, osteoclasts die through apoptosis and detach from the bone surface. Currently, it is unknown whether the apoptotic process is initiated by the osteoclast itself or whether the osteoblast-lineage cells are involved.

1.2.2.3 Reversal

The process of reversal is still not known entirely. After apoptosis of osteoclasts mononuclear cells of unknown origin enter the resorptive pit. These are thought to be haematopoietic phagocytes as well as osteoblast-lineage cells that might complete the process of resorption through release of MMPs and serine proteases

as well as prepare the bone surface by formation of a "reversal line" (Tran Van et al., 1982; Everts et al., 2002).

Amongst several influences that activate osteoblasts, osteoclast-secreted factors play a role in this activation (Matsuo and Irie, 2008) as well as factors released from the bone matrix during resorption (see Figure 1.7). These factors include IGF-1 and -2 (insulin-like growth factor 1 and 2), BMPs (bone morphogenic proteins) (Schmid et al., 1992; Harris et al., 1994).

The process of reversal requires more detailed research to be entirely understood.

1.2.2.4 Formation of new bone material

To achieve bone formation osteoblasts have to mature from progenitors. Osteoblastogenesis has been shown to be influenced by a number of different pathways. One of the more prominent ones is the Wnt/β-catenin pathway (also referred to as canonical wnt (wingless) signalling) which mediates cell fate determination, proliferation and survival through increase of β-catenin levels. Furthermore, alteration of the expression pattern of genes occurs due to the transcription factor Lef/Tcf (Lymphoid enhancer factor/T cell factor) binding β-catenin (Westendorf et al., 2004). As a consequence of downstream signalling, β-catenin accumulates in the cytoplasm, translocates to the nucleus, and alters gene expression (Krishnan et al., 2006).

Further promoters of osteoblastogenesis are BMPs which belong to the large superfamily of TGFβ. *In vitro* BMPs are capable of causing differentiation of myoblastic cell lines into osteoblast-lineage cells. Besides, induction of osteoblast specific proteins such as alkaline phosphatase, osteocalcin and

transcription factor Runx2/Cfba1 (member of the Runt-related family of transcription factors) could be achieved through a SMAD-dependent downstream signalling (Katagiri et al., 1994). Intracellular SMAD proteins are transduce extracellular signals mediated through transforming growth factor beta ligands to the nucleus where they activate downstream TGF-β gene transcription.

Following osteoblast differentiation formation of new bone is achieved by the secretion of collagen I and other proteins and factors through osteoblasts. This organic part of the bone material gets mineralised most probably through alkaline phosphatase (Wennberg et al., 2000).

Further factors from different other cell types seem to be required to initiate bone formation (see Figure 1.7). A direct contact-dependent mechanism between osteoclasts and osteoblasts seems to play a role although direct contact of osteoclasts and osteoblasts can usually not be observed in histology (Zhao et al., 2006).

Furthermore, osteoblasts use contact-dependent mechanisms (e.g. gap-junctions) as well as expression of membrane-bound and secreted factors to "communicate" with each other. Factors like ephrines, PTHrP and sclerostine for example are expressed at all stages of differentiation (Sims and Gooi, 2008).

At the end of the remodelling cycle, osteoblasts become quiescent and cover the bone surface as lining cells or become osteocytes when they remain within the bone tissue.

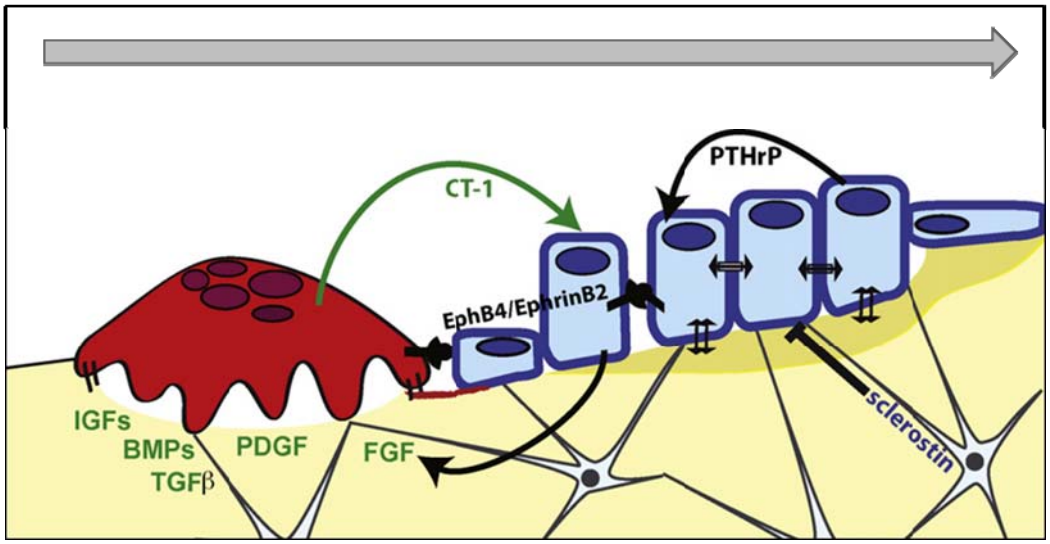

Figure 1.7: Control of bone formation in remodelling (osteoclast shown in red, osteoblast shown in blue). Osteoclastic bone resorption releases factors previously embedded by osteoblasts in the bone (green), including IGFs, BMPs, TGFβ, PDGF and FGF. These and factors produced and released by osteoclasts including cardiotrophin-1 (CT-1), stimulate osteoblast differentiation and bone formation. Lining cells prepare the bone surface for osteoid deposition (blue cell releasing red substance). EphB4, expressed by both osteoclasts and osteoblasts, interacts with ephrinB2, expressed by the osteoblast lineage to stimulate bone formation. This is further enhanced by PTHrP. Osteoblasts also sense the resorption pit (double arrows) and communicate with each other (boxed double arrows) to determine the quantity of new bone required. Negative feedback from osteocytes within the bone matrix through sclerostin production inhibits the process of bone formation. At the completion of matrix deposition, osteoblasts differentiate into osteocytes or lining cells (Sims and Gooi, 2008).

1.2.3 Cancer metastasis to the bone

The concept of organ-specific metastasis dates back to the pioneering work of Dr. Steven Paget. More than 120 years ago he described his "seed and soil" hypothesis for metastasis which claims that a metastasising cancer cell (seed) needs a congenial local microenvironment (soil) to grow a metastasis (Paget, 1889). More than 80 years later this hypothesis was proven with advanced methods showing that although cancer cells reached the blood stream

development of metastasis could only be observed in specific organs (Fidler and Kripke, 1977; Hart and Fidler, 1980).

1.2.3.1 Clinical picture of bone metastases

After lung and liver, bone tissue is the third most common site for metastatic tumours and metastatic carcinoma is the most frequent malignancy occurring in the skeleton of humans. Preferred sites of metastasis are spine, pelvis, femur and ribs (Berrettoni and Carter, 1986; Hauben and Hogendoorn, 2010). Bone metastases may lead to complications in many malignancies. Bone tissue involvement can worsen the clinical picture and impair the quality of life immensely and increases morbidity significantly. Amongst the most common skeletal complications are pain, hypercalcemia, spinal cord compression and pathological fractures (Coleman, 2006).

1.2.3.2 General mechanisms of metastasis

It has been suggested that the complex mechanism of metastasis can be separated into two phases. The first phase, the physical translocation of a cancer cell, involves intravasation and extravasiation. Intravasation includes the invasion of the surrounding tissue of the primary tumour and entry to the lymph and blood system. Extravasation takes place, when the cell survives and translocates via the blood stream to microvessels of distant tissues and enters this tissue from the blood stream.

The second phase describes the colonisation, involving survival in the new microenvironment, adaption and finally proliferation to form a secondary tumour. The complexity and many different aspects of the second phase of metastasis still remain to be investigated to a greater extent (Chaffer and Weinberg, 2011).

One aspect of the first phase that has been investigated during the last decades is the epithelial-to-mesenchymal transition (EMT) that mainly plays an important role as cell-biological program in early embryonic morphogenesis (Thiery et al., 2009). EMT involves dedifferentiation of cells and improvement of their motility by reduction of cell-cell-contacts and thus adhesion. However, recently it could be shown for breast cancer that non-CSCs can transform into CS-like cells due to EMT. This might be a key mechanism by which dissemination of cancer takes place (Mani et al., 2008; Morel et al., 2008; Thiery et al., 2009).

In carcinoma, the activation of this EMT-program in tumourigenesis calls for signalling between cancer cells and their neighboring stromal cells so that a variety of different cell types are attracted to the surrounding stroma. These cells lead to the formation of a "reactive" stroma leading to an inflammation and finally in the release of EMT-inducing molecules. This triggers the expression of certain EMT transcription factors by the carcinoma cells resulting in the EMT programm (Yang and Weinberg, 2008; Chaffer and Weinberg, 2011).

However, the concept of EMT as a mediator of dissemination and subsequently metastasis as well as the mechanisms of colonisation as the second phase of metastasis still have to be investigated in other types of cancers and sarcomas as such.

1.2.3.3 Mechanisms of metastasis to the bone

Regarding the site of bone metastases of different types of cancers, it is obvious that these are mainly affecting bone regions which contain red bone marrow, which consists mainly of haematopoietic tissue. This might play a role in the process of metastasis to the bone (marrow) because properties of circulation, cells and extracellular matrix in the bone might support homing and growth of metastasised cancer cells. Furthermore, post-mortem studies in animals and humans have shown that venous blood from breast and pelvis does not only flow into the *vena cava* but also into a vertebral-venous plexus. This might, to a certain extent, explain the tendency of breast, prostate and other cancer types to metastasise to bones at certain anatomical sites (Batson, 1940; Coleman, 2006).

Disseminating tumour cells become attracted to certain regions and are physically trapped in the capillary beds of a variety of tissues. However, the tumour cells have to interact with the local tissue and this is only possible in tissues that offer the appropriate microenvironment for survival and growth to which the disseminating cell has to adapt. This process of communication plays a critical role in homing and establishment of metastatic disease. In more detail this involves degradation of extracellular matrix, secretion of appropriate growth factors, chemokines and cytokines, and expression of receptors on tumour cells (Nannuru and Singh, 2010).

Furthermore, it is thought that bone metastasis can be described as a vicious circle in which tumour cells get attracted by growth factors released from bone tissue through normal osteoclastic resorption during bone remodelling. This leads to enrichment of the microenvironment and leads to increased tumour cell growth and alteration of tumour cell phenotypes. This, in turn, influences the

cells of the bone microenvironment and disturbs the fine equilibrium between osteoblasts and osteoclasts (Bussard et al., 2008).

1.2.3.4 Metastasis in Ewing's sarcoma

Metastatic disease is one of the most important factors influencing prognosis, disease and the choice of treatment in ES/PNET (for more details see chapter 4). ES/PNET is known to be a systemic disease with patients most commonly dying from lung metastases (Cotterill et al., 2000; Grier et al., 2003; Paulussen et al., 2008).

Until today, the process of detatchment form the primary tumour has been investigated in ES/PNET. It is known that activation of certain downstream signalling pathways is important for anchorage-independent survival and growth, such as PI3K/Akt. Furthermore, the activation of tyrosin-kinase receptors involving IGF-1R (insulin-like growth factor 1 receptor) may not only be important in the survival of detached ES/PNET cells but as well in maintenance of a malignant phenotype (Strauss et al., 2010).

As a further mechanism promoting tumour development, growth and a metastatic phenotype chromatin modifications are increasingly recognized in different cancer types and as well ES/PNET. EZH2 (histone methyltransferase Enhancer of Zeste, Drosophila, Homolog 2), the enzymatic subunit of the polycomb PRC2 complex has been shown to methylate histone H3K27. This ultimately leads to gene silencing.

EWS-FLI1 was found to be bound to the promoter of EZH2 *in vivo* and its downregulation suppressed tumour development and metastasis *in vivo* (Burdach et al., 2009).

The exact mechanisms of metastasis in ES/PNET as such still remain unclear. With micrometastases in many cases being resistant to chemotherapy and responsible for a high risk of relapse and a worse outcome for patients (Schleiermacher et al., 2003; Strauss et al., 2010) it is crucial to investigate the development of metastasis in order to improve treatment strategies and patient outcome.

1.2.3.5 Degradation of extracellular matrix

Proteases are released by tumour cells metastasising to the bone as well as by bone cells themselves to degrade extracellular matrix. Tumour cells require these to invade into bone tissue.

MMPs are zinc-dependent endoproteases employed for this purpose. Breast cancer cells and other cells of further malignancies can express different MMPs at high levels and this correlates with a poor prognosis (Leppä et al., 2004). Additionally, TIMPs (tissue inhibitor of metalloproteinases) are often inhibited in malignant and non-malignant cells during the metastatic process. *In vitro* inhibition of MMPs and addition of TIMP1 and TIMP2 to cultures of breast cancer cell lines lead to reduced adherence and migration (Zhao et al., 1999; Saad et al., 2000).

More recently, the role of MMP-7 and MMP-9 has been investigated. Both proteases seem to contribute to osteolytic metastatic lesions. While MMP-7

solubilises RANKL (presented on the osteoblast cell surface, usually leads to osteoclast-activation; see chapter 1.2.2.2) in prostate cancer models of bone metastases, MMP-9 is thought to be involved in osteoclast recruitment (Dong et al., 2005; Lynch et al., 2005).

Cathepsins have been shown to be vital for differentiation and activation of osteoclasts. Cathepsin G has been shown to mediate activation of MMP-9 and thus promote bone destruction. Targeting cathepsin G inhibits tumour vascularisation through reduced levels of VEGF (vascular endothelial growth factor) and chemoattractant protein-1 (Ishikawa et al., 2001; Wilson et al., 2009, 2010).

1.2.3.6 Growth factors and cytokines

The bidirectional interaction between tumour cells and stromal cells of the bone microenvironment has been investigated extensively. On both sides this interplay induces production of growth factors and cytokines leading to complex signalling cascades. These factors can be categorised into bone-resorbing and bone-forming factors (Mundy, 2002).

Amongst many factors that promote resorption the role of different cytokines and growth-factors in metastasis of cancer to the bone has been investigated and they often act in a RANKL-dependent way. Thus, differentiation of newly recruited osteoclast precursors to active osteoclasts is triggered (Thomas et al., 1999; Bendre et al., 2005). The limiting step in this interaction is the direct cell-to-cell contact between RANKL-expressing osteoblasts and RANK-expressing osteoclasts.

However, promotion of RANK-RANKL interaction can be achieved through cleavage of the membrane bound form of RANKL into a fully functional soluble RANKL. MMP-7 and cathepsin G are able to cleave the membrane bound form of RANKL. Their expression and thus promotion of osteoclast activation could be shown in different types of cancers metastasising to the bone (Lynch et al., 2005; Thiolloy et al., 2009).

A form of promotion of osteoblastic metastases of the bone could be achieved through endothelins. Osteoblasts produce ET_A and ET_B receptors (endothilin A and B receptors) and thus bind ET-1 (endothelin 1) which triggers mitogenesis and consequently proliferation of osteoblasts via the Wnt/β-catenin signalling pathway (Clines et al., 2007).

Thus, tumour cell derived ET-1 might stimulate osteoblasts as well as promote tumour cells themselves in an autocrine fashion (Takuwa et al., 1990; Chiao et al., 2000; Guise and Chirgwin, 2003).

As mentioned before, the bone matrix is rich in a range of growth factors such as IGF-1 and -2, TGF-β, BMPs, FGF (fibroblast growth factor) and PDGF released during osteolysis. These additionally promote proliferation and survival of tumour cells in the bone microenvironment which closes the "vicious cycle" of metastasis to the bone.

1.2.3.7 Chemokines and their receptors

Chemokines and their G-protein-coupled receptors play an important role in the interaction of tumour cells and the bone microenvironment. Chemokines, secreted by tumour cells or through degradation of the extracellular matrix,

provide a chemotactic signal to cells expressing the appropriate receptors. This attraction is likely to be responsible, at least in part, for distant organ-specific metastasis (Nannuru and Singh, 2010).

The first two chemokine receptors, which initiated the idea of chemokine driven metastasis to bone, were CCR7 and CXCR4. These are highly expressed in breast cancer cells while the associated ligands CCL21 and CXCL12 are expressed in bone as well as lung and lymph nodes (Müller et al., 2001). Furthermore, evidence for expression of CXCR4 could also be found in prostate cancer cells where interaction of CXCR4 with CXCL12 has amongst others the effect of increasing MMP-9 expression which subsequently promotes invasiveness of tumour cells (Chinni et al., 2006). There are many more effects of the CXCR4/CXCL12-axis but it can be reasoned in general that this leads to the establishment of the cancer stem-like cell niche where high levels of CXCL12 recruit a population of highly tumorigenic cells promoting cell survival, proliferation, angiogenesis, and further metastasis (Wennberg et al., 2000; Chinni et al., 2008).

The CCL22/CCR4-axis attracts lung cancer cells to the bone marrow (Nakamura et al., 2006). Conversely, CCL2 expression seems to inhibit the metastasis of breast cancer cells to bone and lung (Takahashi et al., 2009).

1.3 The CXCL12/CXCR4-axis

Chemokines are a subgroup of cytokines with the ability to chemically attract cells expressing the appropriate chemokine receptor. Thus, chemokines are major regulators of cell trafficking and adhesion.

Chemokine receptors are seven-span transmembrane proteins which are coupled to G proteins. All chemokines present the N-terminus at the cell surface and the C-terminus to the cytoplasm with three extra- and three intracellular loops. One of the latter interacts with heterotrimeric G proteins. As mentioned before, this initiates a signalling cascade (Sun et al., 2010).

1.3.1 Role of the CXCL12/CXCR4 axis

For years, the interaction between CXCL12 and CXCR4 was thought to be exclusive. Just recently the picture of CXCL12 changed when it became clear that CXCR4 is not its only receptor. A new receptor was identified on murine fetal liver cells which was still able to bind CXCL12 after CXCR4 knockout (Burns et al., 2006). However, the work at hand will focus on the interaction of CXCL12 with the receptor CXCR4.

So far, there is a variety of tasks known which the axis of CXCL12/CXCR4 fulfils: it is primarily thought to regulate the migration of haematopoietic stem cells into and out of the bone marrow, and facilitates the cells transmigration through endothelial cell barriers (Möhle et al., 1997; McGrath et al., 1999). Furthermore, it is a key regulator of B cell lymphopoiesis and leukocyte migration (Nagasawa et al., 1996).

Additionally to those functions in the adult body, in mice genetically deleted of CXCL12, early stage embryos exhibit profound defects in the formation of large vessels, septal malformation during cardiac development and abnormal brain development (Nagasawa et al., 1996). Eventually, between days 15 and 18 of gestation embryonic lethality is observed. Other investigations demonstrated that

CXCL12 can induce angiogenesis *ex vivo* and *in vivo* (Tachibana et al., 1998; Salcedo et al., 1999).

CXCL12 has two major isoforms due to alternative splicing. The predominant α-isoform is involved in many local tissue-specific physiological processes and is expressed in nearly all organs. In blood it rapidly undergoes proteolysis. CXCL12β is more resistant to proteolysis and is mainly found in highly vascularised organs such as liver, spleen and kidneys (Janowski, 2009). There are four more isoforms of CXCL12 which, however, have to be further investigated (Yu et al., 2006).

In the bone marrow, CXCL12 is mainly produced by osteoblast-derived lining cells and regulates the migration of $CD34^+$ cells. The homology of the human and the murine variants of CXCL12 contribute amongst other factors to human $CD34^+$ cells being able to repopulate the bone marrow of NOD/Scid mice (Ponomaryov et al., 2000; Jung et al., 2006; Janowski, 2009).

CXCR4 is highly conserved and binds CXCL12 as a ligand. It is mainly expressed during development but later on it mediates migration of resting leukocytes and haematopoietic progenitors and plays a role in the immune system (Zou et al., 1998; Aiuti et al., 1999).

The interaction of ligand and receptor leads to intracellular binding of a G protein complex to CXCR4. This causes the dissociation of the subunits of the G protein complex resulting in the activation of multiple downstream effectors of ERK1/2 (extracellular-signal-regulated kinase 1 and 2), different MAPKs (mitogen-activated protein kinases), and AKTs (v-akt murine thymoma viral oncogene homologs) (Lee et al., 2007; Lu et al., 2009).

The role of the CXCL12 and CXCR4 as mediators of migration and initiator of angiogenesis offers a high possibility for this axis to play a role in cancer as well.

1.3.2 The CXCL12/CXCR4 axis in cancer metastasis

Lapidot and co-workers suggested the concept of cancer stem cells by studying on leukaemia (Bode et al., 1992; Lapidot et al., 1994). Further investigations on different cancer types suggest indeed, that there is evidence for specific cancers arising from quiescent tissue-committed stem cells (cell of origin) acquiring several mutations over time. Furthermore, during the development of the specific tumours some cells remain in a quiescent, stem cell-like state allowing metastasis and relapse (cancer maintaining stem cell). This is due to their relative resistance to chemotherapeutics which target rapidly dividing cells. Recently, research has shown that these cancer stem cells play a pivotal role in many cancer types such as breast, prostate and brain cancers (Dontu et al., 2003; Singh et al., 2004; Collins and Maitland, 2006) and seem to share molecular mechanisms with normal stem cell trafficking as displayed in Figure 1.8 (Kucia et al., 2005).

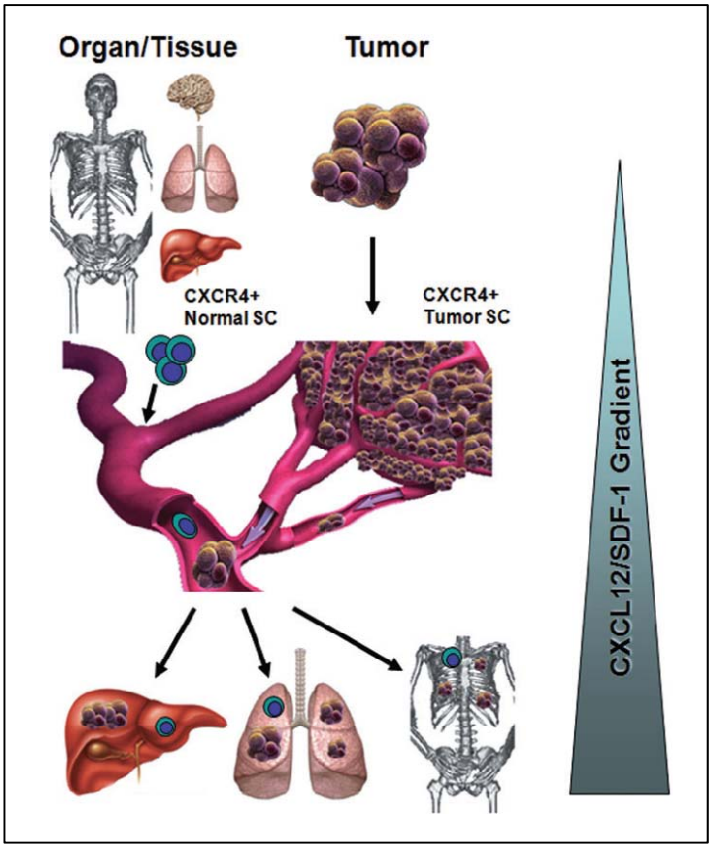

Figure 1.8: Hypothetical role of the CXCL12/CXCR4 axis in migration of normal stem cells (SC) and metastasis of malignant stem cells (cancer SC). Cells (**I**) leave their stem cell niches (SC) or primary tumour (cancer SC) and enter circulation, (**II**) arrive at the site of homing (SC) or metastasis (cancer SC) via the peripheral blood or lymph, (**III**) adhere to the endothelium, (IV) invade tissues, and (V) proliferate and expand at a location that provides a supportive environment (Furusato et al., 2010).

As CXCR4 is expressed on stem cells of various organs as well as on many tumour cells themselves, researchers suggest that these tumour types arise from $CXCR4^+$ stem cells (Furusato et al., 2010). So far, some cancers that are positive for CXCR4 have been shown to metastasise and home to bone via the blood stream in a CXCL12-dependent way (Geminder et al., 2001; Müller et al., 2001; Sun et al., 2003). Therefore, metastases of breast and prostate tumours can be found in tissues excreting high levels of CXCL12 such as lymph nodes, lung,

liver and bone marrow (Allinen et al., 2004; Gladson and Welch, 2008). The hypothesis of the CXCL12/CXCR4-dependent homing is supported by findings of *in vivo* studies where neutralising antibodies against CXCR4 inhibited metastasis (Du et al., 2008).

CXCR4 is overexpressed in a variety of different cancer types, and cancer cell lines such as for example breast cancer, prostate cancer, and melanoma. However, it is conspicuous that in all cases the originating tissue does not express CXCR4 (Müller et al., 2001; Scotton et al., 2001; Sun et al., 2003). Therefore, CXCR4 expression of cancer cells might not be due to transformation of a CXCR4-positive mesenchymal stem cell but a consequence of the malignant programme that drives the metastatic phenotype.

The up-regulation might be caused by different mechanisms. One of those might be the induction of CXCR4 expression through VGEF, which in turn can be up-regulated itself through the transcription factor HIF-1 (hypoxia-inducible factor 1) under hypoxic conditions. This has been shown to be the case for glioblastoma (Zagzag et al., 2006).

The interesting and important role CXCL12/CXCR4 seems to play in different types of cancers suggests a potential role of this axis in ES/PNET as well. This, however, still needs to be investigated.

1.3.3 Potential role of CXCL12/CXCR4 axis in Ewing's sarcoma

Until today, no research results have been published that had the direct aim to investigate on the role of CXCL12/CXCR4 in ES/PNET. However, different projects revealed interesting results that involved CXCL12/CXCR4.

Recently, data was published describing a novel method of gene expression analysis called intercohort gene expression co-analysis. This study shows that higher CXCR4 expression correlates with metastatic behaviour of ES/PNET. Furthermore, the patient group with ES/PNET cells highly expressing CXCR4 and CXCR7 had the worst survival rates (Bennani-Baiti et al., 2010).

Knockdown experiments targeting the fusion transcript EWS/FLI1 revealed that CXCR4 expression seems to be directly or indirectly regulated through the aberrant transcription factor EWS/FLI1 (Chansky et al., 2004; Bennani-Baiti et al., 2010).

Additionally to this, HIF-1 might be responsible for the expression of CXCR4 in ES/PNET. As mentioned previously, HIF-1 can up-regulate VEGF expression, which in turn can up-regulate CXCR4 expression. In ES/PNET HIF-1α influences the expression of EWS/FLI1 and may also be responsible for up-regulation of CXCR4 via VEGF. This, however, needs to be investigated further (Aryee et al., 2010).

To date, there is still a need for a direct experimental proof of a role of the CXCL12/CXCR4-axis in the metastasis of ES/PNET. But taking its high expression in nearly all ES cell lines and many primary tumours as well as the role of this axis in other cancers into account there is strong indication for CXCR4 involvement in the organ-specific metastasis of ES/PNET.

2. Chapter – Hypothesis and aims

The main aim of this thesis was to investigate different aspects of the cellular mechanisms of organ-specific metastasis in ES/PNET. In different studies on ES/PNET it has been observed that the occurrence and location of primary metastases in ES/PNET plays an important role for the outcome of patients. These studies revealed as well that metastasis to distinct organs leads to different survival rates in patients. Thus, the overall hypothesis of this thesis was that cells metastasising to different organs would be distinct from each other. Especially, it was thought that this would be manifested in the expression of genes, *in vitro* and *in vivo* behaviour.

As CXCR4 has been shown to play a role in the metastasis of other cancer types and has been shown to be expressed in ES/PNET it was hypothesised to have a potential role in the metastatic behaviour of this sarcoma type as well.

More specifically the aims were as follows:

- to isolate organ-specific ES/PNET subclones employing the established i. v. metastasis model for ES/PNET.

- on-going from this to identify organ-specific gene expression signatures using microarray analyses.

- to create a stable knockdown vector against CXCR4 for further investigations on its role in the metastasis of ES/PNET.

- to develop and characterise an orthotopic model for ES/PNET to investigate the interaction of ES/PNET cells in the appropriate microenvironment.

The development of an orthotopic model for ES/PNET is justified by the need of investigation of the interaction of the tumour cells in the microenvironment of the bone. Employment of such an orthotopic preclinical model would facilitate fundamental research on the biology of ES/PNET. Furthermore, it would provide an improved tool for drug development as compared with current subcutaneous (s. c.) models.

3. Chapter – Materials and Methods

3.1 General devices and materials

If not stated otherwise or directly in the correlating chapter the following equipment and materials were used:

3.1.1 Equipment

ABI 7000 Real Time detection system, Applied Biosystems, Warrington, UK

ABI 7500 Fast Real-Time PCR system, Applied Biosystems

ABI 7000 SDS program, Applied Biosystems

ABI 7900HT Sequence detection system, Applied Biosystems

ABI SDS 2.2, Applied Biosystems

Agarose gel electrophoresis unit, BIO-Rad, Hemel-Hempsted, UK

FACSCalibur, Becton Dickinson, Oxford, UK

FACSCanto, Becton Dickinson

MINI-PROTEAN II electrophoresis cell, BIO-Rad

ND-1000 spectrophotometer, Nanodrop Technologies Ltd., Wilmington, USA

Spectramax 250 multiwell plate reader, Molecular devices, Crawley, UK

Centrifuge 5415C, Eppendorf AG, Germany

Centrifuge 5415R, Eppendorf AG

L870M Ultracentrifuge, Beckman Coulter, UK

Allegra® X-12 benchtop centrifuge, Beckman Coulter, High Wycombe, UK

Bio Mat^2 Class II Microbiological Safety Cabinet, Medical Air Technology Ltd., Oldham, UK

CO_2 Incubator, Sanyo E&E Europe, Loughborough, UK

Sub-Cell® GT gel-electrophoresis chamber, BIO-Rad

ChemiDoc XRS+ system, BIO-Rad

GeneAmp® PCR System 2700, Applied Biosystems

Thermomixer comfort, Eppendorf AG

3.1.2 Material

Costar® Cell culture flask, different sizes, Corning Incorporated, USA

CryoTubes, Nunc A/S, Denmark

Costar® cell culture plates, different sizes, Corning Incorporated, USA

FACS tubes, BD Bioscience, Oxford, UK

3.1.3 Kits

Maxiprep Endofree Plasmid Isolation Kit, Qiagen, Crawley, UK

QIAprep Spin MiniPrep Kit, Qiagen

RNeasy kit, Qiagen

QIAShredder spin colums, Qiagen

3.1.4 Chemicals

If not stated otherwise, chemicals were purchased from Sigma-Aldrich (Poole, UK) or Fisher Scientific (Loughborough, UK).

3.2 Microbiological work

3.2.1 Bacteria

Escherichia coli K12 JM109

A suspension of *Escherichia coli (E. coli)* K12 JM109 grown in minimal media and cryopreserved in 50 % glycerol was purchased from Promega (Southhampton, UK). Competent bacteria were produced from this stock.

Genotype: F´ *traD36 proA*$^{+}$*B*$^{+}$ *lacI*^{q} *Δ(lacZ)M15/ Δ(lac-proAB) glnV44 e14*$^{-}$ *gyrA96 recA1 relA1 endA1 thi hsdR17*

Escherichia coli K12 ER2925

A suspension of *E. coli* ER2925 grown in Lysogeny broth (LB) and cryopreserved in 50 % glycerol was purchased from New England BioLabs (Hitchin, UK). This strain is *dam*$^{-}$ and *dcm*$^{-}$ and was used for the production of plasmids in which the restriction site XbaI was used.

Genotype: *ara-14 leuB6 fhuA31 lacY1 tsx78 glnV44 galK2 galT22 mcrA dcm-6 hisG4 rfbD1 R(zgb210::Tn10)TetS endA1 rpsL136 dam13::Tn9 xylA-5 mtl-1 thi-1 mcrB1 hsdR2*

3.2.2 Plasmids

Table 3.1 lists all plasmids purchased, used and constructed for the projects of this work.

Table 3.1: List of purchased and constructed vectors.

Plasmid	**Antibiotic resistance**	**Manufacturer/Co-operator**
pSUPER	Ampicillin	Oligoengine, Seattle, USA
pSUPERshMA6Mut1	Ampicillin	Dr. Frida Ponthan
pSUPERshCXCR4	Ampicillin	Henrike Knizia
pEPI-EGFP	Kanamycin	Prof. Lipps, University of Witten/Herdecke, Germany
pEPI shCXCR4	Kanamycin	Henrike Knizia
pEPI shMA6Mut1	Kanamycin	Henrike Knizia

For the selection of bacteria carrying the designated plasmid the adequate antibiotic was added to the culture medium.

3.2.3 Media, additives and growth conditions

Table 3.2 and 3.3 describe the medium and additives used to cultivate and select bacteria. Medium was sterilised before use for 20 minutes at 121°C and 2×10^5 Pa. To create selection pressure antibiotics were added after cooling down the media. Cultures were incubated at 37°C in a shaking incubator either overnight or until the designated density was obtained. To produce agar plates 1.8% (w/v) agar was added to the medium prior to autoclaving.

Table 3.2: Recipe for Lysogeny broth (LB).

LB medium	
Bacto-tryptone	1% w/v
Yeast extract	0,5%w/v
NaCl	1%w/v
ddH_2O	*ad* 1000ml
	pH 7.5

Table 3.3: Antibiotics and used concentrations.

Antibiotic	**Stock solution**	**End concentration**
Ampicillin	50mg/ml	50µg/ml
Kanamycin	50mg/ml	50µg/ml

3.2.4 Strain conservation

For short term conservation strains were maintained on LB agar plates with the appropriate antibiotics. These plates were sealed with Parafilm® M (American National Can Company, Chicago, USA) and stored inverted at 4°C in a designated refrigerator.

For long term conservation *E. coli* strains were stored as glycerine-suspensions. Therefore, bacteria were cultivated overnight in liquid LB medium with the appropriate antibiotics. Aliquots of the bacteria solution were brought to an end concentration of 20% (v/v) with sterile glycerine and stored in a screw cap glass tube at -80°C.

To reactivate the frozen bacteria a sterilised inoculation loop was used to pick up the frozen stock and inoculate a LB culture with the adequate antibiotics.

3.2.5 Preparation of competent *Escherichia coli*

A 5ml culture of bacteria was incubated overnight at 37°C in LB medium. The culture was transferred into a sterilised 200ml conical flask and 25-50ml of fresh LB medium was added (the dilution should at least be 1/100). The diluted culture was grown to an optical density at 600nm (OD_{600}) of 0.2-0.5, which was examined every 30 minutes. After the required OD_{600} was reached the culture was split and transferred into 50ml tubes and incubated on ice for 10 minutes. The bacteria were centrifuged for 10 minutes at 1000g at 4°C and the supernatant discarded. The required number of 1.5ml reaction tubes were pre-chilled on ice and the pellet was resuspended in ice-cold TSS buffer (see Table 3.4; 10% of the former culture volume). The solution was mixed gently, to dissolve all aggregates. From this solution 100µl aliquots were added to the chilled 1.5ml reaction tubes and these were immediately transferred from ice to a -80°C freezer.

For each batch of competent bacteria a positive control was performed and the transformation efficiency calculated.

Table 3.4: Recipe for TSS buffer.

TSS buffer	**End concentration**
Polyethylene glucol 8000 (PEG)	10% (v/v)
DMSO (Dimethyl sulfoxid)	5% (v/v)
$MgCl_2$	30mM
LB medium	*ad* 50ml

The solution was filter sterilised (0.22µm filter) and stored at 4 or -20°C.

3.2.6 Transformation of plasmids into competent *Escherichia coli*

The method is based on a heat shock treatment of competent *E. coli* with the purpose to transfer plasmid-DNA. Subsequent, the plasmid amplified occurs following the incubation and growth of the bacteria.

The competent bacteria (in 100µl aliquots), were thawed on ice prior to the addition of 0.1-50ng of purified plasmid and 2µl of a ligation mix. The mix was incubated on ice for 30 minutes to allow the plasmids to bind to the surface of the bacteria. The heat shock was performed at 42°C in a water bath for 45 seconds, followed by incubation on ice for 2 minutes. Next, 450µl of ice cold SOC-Medium was added (see Table 3.5), and the transformed *E. coli* were incubated for 1 h at 37°C to facilitate recovery.

The transformed bacteria were centrifuged in a 1.5ml reaction tube at full speed using a benchtop microcentrifuge at 1200g, the supernatant was discarded and the bacteria were resuspended in the remaining liquid on the pellet and placed on a pre-warmed LB agar plate (containing the appropriate antibiotic as a selection

marker if required). The bacteria were spread on the agar plate with a Drigalski-applicator and incubated overnight at 37°C in an inverted position.

Table 3.5: SOC-Medium.

SOC-Medium	
Tryptone (pancreatic digest of casein)	2% (w/v)
Yeast extract	0.5% (w/v)
NaCl	10mM
KCl	2.5mM
$MgSO_4$	20mM
Glucose	200mM

The glucose solution had to be sterilised before adding it to the recipe. Adjust to pH 7.0.

3.3 Nucleic acid methods

3.3.1 Isolation of plasmid DNA from bacteria

A QIAprep Spin MiniPrep Kit (Qiagen) was used to extract plasmid DNA from cultured bacteria according to the manufacturer's instructions, as follows:
Bacteria carrying the plasmid were cultivated overnight at 37°C with shaking and 2ml of this culture was centrifuged for 5 minutes at 8000g in a microcentrifuge.

The bacterial pellet was re-suspended in 250µl of buffer P1 (Qiagen) and bacteria were lysed by adding 250µl of buffer P2 (Qiagen) and incubated for 5 minutes at room temperature. Lysis was terminated by adding 350µl of neutralising buffer N3 (Qiagen) and inverting the reaction tubes cautiously. To sediment the resulting precipitates the solution was centrifuged for 10 minutes at full speed in a benchtop microcentrifuge. The supernatant was transferred to a QIAprep spin column, centrifuged at full speed for 1 minute and the flow-through was discarded. Column-bound DNA was washed with 500µl PB buffer (Qiagen), and then washed with 750µl of PE buffer (Qiagen). The flow-through was discarded following each wash step. To ensure complete removal of residual ethanol, the spin column was transferred into a new 2ml reaction tube and centrifuged again for 1 minute at full speed to dry the column. To elute the column-bound DNA 50µl of EB buffer (Qiagen) were added to the column, the column incubated for 5 minutes and the resuspended DNA centrifuged for 5 minutes at full speed.

Plasmids were stored at -20°C until further use.

3.3.2 Isolation of plasmid DNA from bacteria under endotoxin-free conditions

Plasmids used for work carried out on mammalian cells samples must be endotoxin-free. Endotoxins produced by bacteria are harmful for mammalian cells and therefore have to be removed. This was achieved using the Maxiprep Endofree Plasmid Isolation Kit (Qiagen).

To isolate a plasmid in larger quantities, 2ml of a pre-culture were used to inoculate a 100-150 ml overnight-culture in LB-medium with the require

antibiotic that was incubated at 37°C on a shaking platform. The next day, the bacteria were harvested by centrifugation at 6000g for 15 minutes at 4°C. The pellet was re-suspended in 10ml buffer P1 (Qiagen) and lysed by the addition of 10ml buffer P2 (Qiagen). To ensure a complete lysis, the sealed tube was inverted and subsequently the mixture was incubated for 5 minutes at room temperature. During the incubation the QIAfilter cartridge was prepared.

The lysis was neutralised by the addition of 10ml pre-chilled buffer P3 (Qiagen), vigorous inversion and incubation on ice for 20 minutes. The mixture was applied to the barrel of the filter cartridge, incubated for an additional 10 minutes and filtered into a new 50ml tube. Where required an endotoxin removal step was performed by adding 2.5ml of buffer ER (Qiagen) to the filtered lysate and incubation for 30 minutes on ice. During the incubation, the QIAGEN-tip 500 columns were equilibrated by applying buffer QBT (Qiagen). Subsequently, the mixture was centrifuged for 30 minutes with 20,000g at 4°C. The supernatant was applied to the equilibrated QIAGEN-tip 500, allowed to enter the resin by gravity flow and washed twice with 30ml of buffer QC (Qiagen). Plasmid DNA was eluted with buffer QF (Qiagen).

3.3.3 Isolation of genomic DNA from mammalian cells

To be able to investigate genetic features such as fusion genes it was necessary to isolate the genomic DNA of cells. To acquire genomic DNA the QIAamp DNA Mini Kit (Qiagen) was used.

Five million cells were centrifuged at 300g for 5 minutes. Cells were re-suspended in 200µl of phosphate-buffered saline (PBS; GIBCO, Invitrogen)

and 4µl of DNase-free RNase (100mg/ml) were added. The suspension was incubated for 2 minutes at room temperature. Cells were lysed by adding 200µl buffer AL (room temperature, Qiagen) and 20µl Proteinase K. The samples were mixed by vortexing, briefly microcentrifuged and incubated for 10 minutes at 70°C. Then 200µl of absolute ethanol was added and the solution was transferred to a QIAamp DNA spin column placed in a 2ml collection tube. By centrifugation at 6000g for 1 minute the DNA bound to the column matrix. The flow-through was discarded and the column was washed once with 500µl buffer AW1 (Qiagen) and subsequently with 500µl buffer AW2 (Qiagen) by centrifugation at 6000g. Again, the flow-through was discarded. To avoid a possible negative effect of remaining ethanol on subsequent reactions, the column was centrifuged once again at full speed for 3 minutes. To elute bound DNA from the column it was transferred into a 1.5ml reaction tube, incubated with 100µl of buffer AE (Qiagen) for 1 minute and centrifuged for 1 minute at full speed.

DNA was stored at -20°C if not used immediately.

3.3.4 Isolation of RNA from mammalian cells

RNA from mammalian cells was isolated using the RNeasy kit and QIAShredder spin columns (both Qiagen). Therefore, cells were harvested and counted as usual. One $x10^6$ cells were pelleted at 300g. The cell pellet was resuspended in 350µl of RLT buffer (Qiagen). Additionally, the cells were disrupted mechanically using QIAShredder columns.

One volume of 70% ethanol was added to the homogenized lysate. Up to 700µl of the sample were transferred to an RNeasy spin column placed in a 2ml collection tube and centrifuged for 15 seconds at 8000g. The flow-through was discarded.

To wash the spin column, 700µl of buffer RW1 (Qiagen) and twice 500µl buffer RPE (Qiagen) were added to the spin column. With both buffers the column was centrifuge for 15 seconds (for 2 minutes during the last wash step) at 8000g and the flow-through discarded. The spin column was placed in a new 1.5ml collection tube and 30-50µl RNase-free water was applied directly to the spin column membrane. To elute the RNA, the sample was centrifuged for 1 minute at 8000g.

RNA was quantified and stored at -20°C until further use.

3.3.5 Determination of the concentration of DNA and RNA samples

A NanoDrop® ND-1000 spectrophotometer was used to determine the concentration of DNA and RNA samples after isolation.

Briefly, 1.2µl was applied onto the pedestal of the spectrophotometer and measured at 260nm and given in ng/µl. Additionally, by calculation of the ratio of the absorbance at 260 and 280nm the purity of the DNA sample was checked. DNA absorbs maximally at 260nm while proteins absorb maximally at 280nm. An $OD_{260/280}$ ratio of 1.8 would indicate highest purity. However, values above 1.4 are considered as sufficient.

3.3.6 Polymerase chain reaction

To amplify specific genes the technique of polymerase chain reaction (PCR) was used. If required for genomic DNA, a prolonged denaturation step prior to addition of the polymerase and start of the PCR has been applied to avoid problems.

After pipetting the PCR reaction-mix (see Tables 3.6, 3.8 and 3.9) into a 200µl PCR tube, 5-25 µl of DNA-sample (200ng-1µg DNA) was added and the mixture was overlaid with 20µl of mineral oil (PCR-grade). A negative control containing water instead of sample was included.

If a hot-start PCR was performed, the samples were put into the thermal cycler and denatured for 10 minutes at 95°C, before adding the Taq (*Thermus aquaticus*) polymerase and starting the actual PCR programme described in Table 3.7.

Table 3.6: Recipe for PCR master mix.

PCR master mix	**50 µl**
10x Brady buffer	1x
3' primer	0,2µM
5' primer	0,2µM
dNTPs	0,2mM
Taq-Polymerase (GibcoBRL Taq-Polymerase)	0,2U
ddH_2O	*ad* 50µl

Table 3.7: PCR cycling conditions.

Temperature	Time	cycles
95°C	10 minutes	1
95°C	1 minute	
56-68°C	50 seconds	35
72°C	1 minute	
10°C	hold	1

dNTPs

The different 100mM dNTP stocks (25µmol in 250µl; Boehringer, Mannheim, Germany) were combined and diluted to 1:50 in distilled, deionised water (ddH_2O).

Table 3.8: Recipe for 10x Brady buffer.

10x Brady buffer	50 µl
Tris/HCl pH8,3	100mM
KCl	500mM
$MgCl_2$	15-50mM
BSA	1mg/ml
Triton X-100	0,5% (v/v)
ddH_2O	*ad* 1000µl

Table 3.9: PCR primers for ES fusion transcript EWS-FLI1 (embedded PCR).

Gene	5' sense	3' antisense
	EWS	FLI-1
1. PCR	CCACTAGTTACCCACCCCAAAC	AACTCCCCGTTGGTSCCYTCC
	EWS	FLI1
2. PCR	TCCTACAGCCAAGCTCCAAGTC	GAATTGCCACAGCTGGATCTG

3.3.7 Digestion of DNA using restriction endonucleases

The sequence-specific hydrolysis of the DNA backbone was achieved by using restriction endonucleases of the type II (Fermentas, York, UK). These are able to recognise sequences that are palindromic and produce single strand cohesive ends or blunt ends.

For a typical restriction digest a reaction volume of 20µl was used and the mix was prepared with ddH_2O (see Table 3.10):

Table 3.10: Recipe for restriction reactions.

Restriction reaction	
dsDNA	0.7pmol
Buffer (10x)	1x
Restriction enzyme	5U

The volume of the restriction enzyme should not exceed 10% of the total volume as the glycerol supplied with the enzyme will inhibit the reaction. Thus, only

0.5µl of enzyme, typically 10Units/µl (U/µl) were used when carrying out double digests.

The reaction mixture was incubated in a water bath or heating block at 37°C for 1 hour and heat inactivated at 65°C or 80°C according to manufacturer's information.

3.3.8 Hybridisation of DNA-oligo single strands

Lyophilised sense and antisense oligonucleotides were re-suspended in hybridisation buffer (see Table 3.11 and 3.12), adjusting the stock to a concentration of 100µM each. Both stocks were combined to a final concentration of 10µM in 10x buffer O+ (Fermentas) and ddH_2O. To denature possible secondary structures the mix was heated for 30 seconds at 95°C. Subsequently, the thermomixer (Eppendorf) was switched off and the hybridisation mix was allowed to slowly cool down to room temperature within the heat block. During the cooling down process hybridisation could occur during which the complimentary strands annealed. The generated duplexes were stored at -20°C until further use.

Table 3.11: Hybridisation buffer used for DNA oligos.

Hybridisation buffer	
NaCl	100mM
Tris	25mM
	pH 7.5

Table 3.12: Oligonucleotides for cloning of shRNA-plasmids, 5' - 3' (Purimex, Grebenstein, Germany).

Gene	**Orientation**	**Sequence**
CXCR4	Sense	GATCCCCCACCCTGTTTCCGTGAAGAATTCAAGAGAT
		TCTTCACGGAAACAGGGTTTTTCTAGAAAG
	Antisense	TCGACTTTATAGAAAAACCCTGTTTCCGTGAAGAATC
		TCTTGAATTCTTCACGGAAACAGGGTGGGG
MLL/AF4	Sense	GATCCCCGAGAAAAGCAGACCTACTCCATTCAAGAG
		ATGGAGTAGGTCTGCTTTTCTCTTTTTG
	Antisense	TCGACAAAAAGAGAAAAGCAGACCTACTCCATCTCT
		TGAATGGAGTAGGTCTGCTTTTCTCGGG

3.3.9 Isolation of DNA-fragments from agarose gels

Following restriction digestion of plasmid DNA and agarose gel electrophoresis, linearised DNA fragments of interest were isolated from the agarose gel. DNA band is illuminated using a UV light source and the specific band is excised using a sterile scalpel blade. The DNA was extracted from the gel using the QIAquick Gelextraction Kit (Qiagen).

The excised agarose gel piece containing the DNA was put into a 2ml reaction tube and weighed on a balance. Three volumes of QG buffer (Qiagen; 100µl buffer equivalent to 100mg agarose gel) were added to and the mixture was incubated for 10-15 minutes at 50°C until complete dissolution of the gel piece. One volume of isopropanol was added to the reaction mixture, up to 700µl were applied onto a QIAquick spin column and the DNA bound to the matrix by centrifugation for 1 minute at full speed in an microcentrifuge. Subsequently, the flow-through was discarded and the column was washed with 500µl of QG buffer and again centrifuged for 1 minute at full speed to remove any residual agarose or QG buffer. Flow-through was thrown away and the column was washed with 750µl of PE buffer (Qiagen). The column was transferred to a new 2ml collection tube and dried by centrifugation at full speed for 1 minute. DNA was eluted from the column by incubation with 30µl of pre-warmed EB buffer (Qiagen) and centrifugation for 5 minutes at full speed.

3.3.10 Ligation of DNA-fragments

DNA-fragments that were obtained from gel extraction, restriction digests or hybridisation were ligated to obtain the required complete circular plasmid with insert suitable for subsequent transformation.

Therefore, a ligation reaction consisting of the plasmid DNA and insert DNA was carried out using T4 DNA ligase (Fermentas). This enzyme catalyses the ligation between the phosphate group of one strand of DNA with the hydroxyl group of the other. The amount of plasmid to insert used in this work was 1:3 and 1:6 ratio of vector to insert respectively. Typically, 1U of T4 DNA ligase per µg

DNA, 1µl T4 ligase buffer (Fermentas), vector and insert mixture was made up to 10-15µl with ddH_2O and incubated overnight at 14°C.

Transformation of competent *E. coli* was subsequently carried out using 1-2µl of the ligation mixture and the rest was stored for short term storage at -20°C.

3.3.11 Agarose gel electrophoresis for separation of DNA-fragments

Agarose gel electrophoresis allows the separation of DNA fragments according to their size and possible secondary structures (for example intact plasmids). To achieve separation DNA samples were loaded onto a 0.8-2% agarose gel according to their expected size, in which a higher concentration of agarose is used to separate smaller fragments. Due to the negative charge of the sugar-phosphate backbone of the DNA, it migrates towards the positive electrode once an electrical current is applied.

Loading dye buffers and DNA ladders were applied to be able to monitor the degree of migration in the agarose gel and to size fragments. Loading buffer consisted of bromophenol blue, glycerol and Tris (Fermentas). Four µl of this loading buffer was mixed with 16µl of DNA sample for loading onto the gel.

The appropriate amount of agarose powder (Invitrogen) was completely resuspended in 1x Tris/boric acid/EDTA (ethylediaminetetraacetic acid) (TBE; see Table 3.13) buffer by heating in a microwave and poured into a casting stand (Agarose gel electrophoresis unit, BIO-Rad). A comb was placed into the stand and the gel was allowed to set for 30 minutes. The gel was transferred to an electrophoresis tank filled with TBE, and DNA samples mixed with loading dye were loaded into the pockets formed by the comb. To allow band size

approximation 5µl of DNA ladder (Fermentas) was loaded alongside the DNA samples. The type of ladder was chosen before to match the sizes of the DNA samples. A voltage of 80V was impressed for approximately 45 minutes.

The gel was transferred into a tank containing water and ethidium bromide and allowed to stain for 10-15 minutes. Ethidium bromide intercalates the DNA, which then can be visualised by using the fluorescence of ethidium bromide when visualised by ultraviolet light. The DNA was visualised and recorded using a BIO-Rad system.

Table 3.13: Recipe for TBE buffer.

TBE buffer	**1x**
Tris base	89mM
Boric acid	89mM
EDTA-Na_2	2mM
ddH_2O	*ad* 1000ml
	pH 8.0

3.3.12 Reverse transcription polymerase chain reaction

Total RNA isolated from cells was used to synthesis cDNA with the Revert Aid H Minus First Strand cDNA Synthesis kit (Fermentas) in a reverse transcription polymerase chain reaction (RT-PCR) using the recipe described in Table 3.14.

Table 3.14: Recipe for the reaction mix for RT-PCR.

Reaction mix	**12µl**
RNA	500ng - 1µg
Random hexamers (100 µM)	8,3µM
ddH_2O	*ad* 12µl

The PCR programme starts with 5 minutes at 70°C. Afterwards it is paused at 4°C. During the pause 8µl master mix (see Table 3.15) are added to the samples on ice.

Table 3.15: Recipe for RT-PCR reaction master mix.

Reaction master mix	**8µl**
buffer (5x)	1x
dNTP mix (10 mM)	2,5mM
RiboLock inhibitor	20Ul
MuMLV RT Pol	200U

The samples were put back into the PCR machine and the program was continued with 10 minutes at 25°C, 60 minutes at 42°C and 10 minutes at 70°C. On ice 30µl ddH_2O were added and the samples were store at -20°C until further use.

3.3.13 Quantitative real time polymerase chain reaction

To detect and simultaneously quantify the expression of specific targeted genes, cDNA (can range from 200ng transcribed RNA to up to 5µg RNA, standard condition is 1µg transcribed RNA) derived from total RNA was used in a quantitative real time polymerase chain reaction (qRT-PCR) using the reaction mix described in Table 3.16. For detection of the amplicon SYBR® Green QCR Supermix w/ROX (Invitrogen, Paisley, UK) was used, which intercalates with dsDNA and on doing so emits a fluorescent signal of specific wave-length. ROX was used as a reference dye. The ABI 7500 Fast Real-Time PCR system (Applied Biosystems) was used.

Table 3.16: Recipe for the qRT-PCR reaction mix.

Reaction mix	**10µl**
Primer (10µM fw+rev mix)	300nM
SyBr-Green master mix (2x)	1x
cDNA	200ng - 5µg
ddH_20	*ad* 10µl

The master reaction mix was prepared without the sample cDNA and 8µl were added per well required of 384-well plate. The template cDNA was added to the appropriate wells to reach 10µl total reaction volume. The plate was sealed and briefly centrifuged.

The qRT-PCR was performed with the following temperature profile (Table 3.17). The signal was recorded at the 60°C-amplification step.

Table 3.17: qRT-PCR cycling conditions.

	cycles	**temperature**	**time**
Dissociation	(1x)	50°C	2 minutes
		95°C	10 minutes
Amplification	(40x)	95°C	15 seconds
		60°C	1 minute
Amplicon-dissociation	(1x)	95°C	15 seconds
		60°C	1 minute

All samples were performed in triplicate and water was used as a negative control to look for eventual primer dimers. Glycerinaldehyd-3-phosphat-dehydrogenase was used for normalisation and all primers were checked for quality by loading the qRT-PCR sample onto a DNA-polyacrylamide (PAA) gel and performing a polyacrylamide gel electrophoresis (PAGE) to check amplicon length and possible side products.

Analysis of the data was performed using ABI SDS 2.2 System software and by using the ΔΔCt method. Here, SYBR-Green was used as a reporter dye for accumulating amplification products. The intensity of the emitted SYBR Green signal can be assumed as being proportional to the amount of amplified DNA.

3.3.14 DNA polyacrylamide gel electrophoresis

The method of PAGE is especially performed for small amplicons typically generated by qRT-PCR primers as a vertical PAA gel in a TBE buffer system is used (see Table 3.13). This produces smaller mesh pore sizes and so leads to a higher resolution of the small amplicons. Typically, for an expected product size smaller than 50bp a 10%-TBE-PAA gel, for a product size of 50bp-300bp an 8%-TBE-PAA gel and for product sizes of 300bp-500bp a 6%-TBE-PAA gel would be performed.

To produce two TBE-PAA-gels the recipe described in Table 3.18 was used.

Table 3.18: Example for the recipe for an 8% TBE-PAGE gel.

8%-TBE-PAGE (example)	
40% Acrylamide/Bisacrylamide solution (37.5:1)	8% (v/v)
5x TBE buffer	1x
ddH_2O	*ad* 10ml
Ammonium persulfate, APS (10%)	0,1% (v/v)
Tetramethylethylenediamine, TEMED	0,17% (v/v)

If samples of a qRT-PCR had to be analysed the seal of the 348-well plate was punctured, 2µl 6x DNA loading buffer were added to the sample and 5µl of this/well were loaded on a gel.

3.3.15 DNA sequencing

Constructed plasmids were sequenced by Eurofins MWG Operon's sequencing service (Ebersberg, Germany). Primers were provided (see Table 3.19) as required and purchased before sequencing through Sigma.

Eurofins MWG Operon uses the Cycle Sequencing Technology (dideoxy chain termination/cycle sequencing), which is modified from the traditional Sanger sequencing method. The components are DNS, primer, heat-resistant DNA-polymerase, four dNTP's, four ddNTP's (dideoxy terminator nucleotides), which are labelled with four different fluorescent markers as well as buffer containing Mg^{2+} and K^{+} ions. The single primer binds to the DNA and is elongated in a linear manner until a ddNTP is bound. The polymerase is not able to elongate the fragment due to the dideoxy-characteristic of the nucleotide and the process is aborted.

An ABI 3730XL Sequencer (Applied Biosystems) was used.

Table 3.19: Sequencing primers.

Plasmid	Primer	sequence
pSUPER	T7 primer	AATACGACTCACTATAG
pEPI	Fwd pEPI	CTGAAAGAGATTGTAGAA

3.4 Mammalian cell culture

3.4.1 Cell lines

For *in vitro* and *in vivo* studies ES/PNET cell lines CADO-ES1, RD-ES, RM-82, TC-71, VH-64 and WE-68 were used. These 6 cell lines represent Ewing's sarcoma cells with different fusion transcrips and thus were chosen for the experiments (see Table 3.20).

The prostate carcinoma cell lines PC3M and LNCaP (both cell lines behave *in vivo* in a metastatic manner) and the OS cell line SaOS-2 (chosen as cells were isolated from primary site and have been shown to grow *in vivo*, see chapter 6.1.2.1) were used as an addition for the mouse model on bone malignancies (see Table 3.20).

Table 3.20: Type and origin of cell lines.

Cell line	Type	ES translocations	Origin	Co-operator
CADO-ES1	ES	t(21;22)(q22;q12)	pleural effusion	Dr. van Valen
RD-ES	ES	t(11;22)(q24;q12)	humerus	Dr. van Valen
RM-82	ES	t(21;22)(q22;q12	femur	Dr. van Valen
TC-71	ES	t(11;22)(q24;q12)	humerus (relapse)	T. J. Triche
VH-64	ES	t(11;22)(q24;q12)	pleural effusion	Dr. van Valen
WE-68	ES	t(21;22)(q22;q12	Fibula	Dr. van Valen
SaOS-2	OS		Primary site	Prof. Lunec
LNCaP	CaP		Lymph node metastasis	Prof. Robson
PC3M	CaP		Transplant from mouse (PC3)	Prof. Robson

3.4.2 Culture media and supplements

To produce growth medium, Roswell Park Memorial Institute (RPMI) 1640 medium, a modification of McCoy′s 5A Medium, containing 1000mg glucose/L pyridoxine HCL and $NaHCO_3$ was routinely supplemented with 10% (v/v) foetal calf serum (FCS) and 2mM L-glutamine. If necessary, 100IU/ml Penicillin and 100µg/ml Streptomycin were added to the medium.

To obtain cryopreservation medium, growth medium was additionally supplemented with 10% (v/v) DMSO and further 10% (v/v) of FCS to obtain a final concentration of 20% (v/v) FCS. DMSO prevents ice crystal formation within the cells during storage.

All media was stored at 4°C and pre-warmed to 37°C in a water bath before use.

3.4.3 Collagen coating of tissue culture plastic

To provide suitable conditions for ES/PNET derived cell lines all tissue culture plasticware had to be coated with collagen I. Rat collagen I (BD Bioscience) was diluted in a 0.1N HAc solution to a final concentration of 0.2mg/ml.

Cell culture flasks ($25cm^2$ and $75cm^2$) with filter-lid (Corning Incorporated) were coated with 1.5ml/flask or 4.5ml/flask, respectively. The collagen I-solution was left in the flasks for 2 days with the lid closed. After discarding the solution from the flasks these were left to dry with open lids in an activated safety cabinet overnight.

Tissue culture well plates (Corning Incorporated) were coated with the same collagen I-solution. 96-well plates were coated with 50µl/well of the solution and from this the amount of solution required was scaled up according to the size of the well plate (6-, 24-, 48-well).

3.4.4 General cell culture and cell harvesting

All mammalian cells were grown in 5% CO_2 humidified atmosphere in a 37°C incubator. The cells were passaged on a regular basis in a safety cabinet every 2-3 days at a ratio of 1:5 to 1:6 once a confluence of 80-90% was achieved.

Cells were detached from the coated cell culture plastic ware by washing off residual medium with PBS (see Table 3.21) before incubation at 37°C with pre-warmed 1:10 Trypsin/EDTA 10x (see Table 3.22) in PBS solution for approximately 1-2 minutes inside an incubator. The digestion of surface proteins was stopped by adding FCS-supplemented medium. The cells were centrifuged for 5 minutes at 300g to pellet them and the supernatant was discarded. The

remaining cell pellet was re-suspended in an appropriate volume of pre-warmed media to be used for further culturing or experiments.

Table 3.21: Recipe for PBS buffer.

PBS	
NaCl	137mM
KCl	2.7mM
Na_2HPO_4	4.3mM
	pH 7.4

PBS was prepared using PBS tablets resuspended in deionised water. The solution was autoclaved in house at >120°C for sterility.

Table 3.22: Recipe for Trypsin/EDTA solution.

Trypsin/EDTA solution	**10x**
Trypsin	0.5% (v/v)
EDTA	0.2% (w/v)
NaCl	0.9% (w/v)
	pH 7.4

If experiments were performed involving attachment abilities of the cells, a less drastic detachment method using cell dissociation buffer was performed (see Table 3.23):

Table 3.23: Recipe for cell dissociation buffer.

Cell dissociation buffer	
TrisHCl	0.04mM
EDTA	1mM
NaCl	0.15M
	pH 7.4

The buffer was sterilised by using a steam autoclave or sterile filters.

An appropriate amount of cell dissociation buffer was added to the previously washed cells and the cells were incubated for 10 minutes at 37^{o}C. Dissociated cells were collected in a tube, centrifuged at 300g and washed with pre-warmed PBS. Subsequently, cells could be used for experiments as required.

3.4.5 Cell counting

After harvesting, cells were routinely counted using an Improved Neubauer counting chamber (Hawksley, Lancing, UK). The particles of a trypan blue solution given to the cells get into the cells. Only viable cells are able to export these again and thus viable cells can be distinguished from dead cells and counted.

Briefly, cells were harvested as described before and 45µl of the cell solution were mixed with 5µl of a 0.4% Trypan blue solution. This mix was allowed to diffuse beneath the cover slip of the haemocytometer. Cells in 4x4 squares of the grid were counted under a light microscope using x20 magnification. The

average was divided by 4 (squares) and 10 (dilution) to obtain the number of cells in million per millilitre of the cell solution. Viable cells were distinguished by their ability to exclude the Trypan blue. Therefore, dead cells appeared blue while viable ones appeared bright and lighter.

3.4.6 Cell cryopreservation

All cells were routinely cryopreserved for long term storage at, ideally, an early passage number. After harvesting and counting of cells these were centrifuged and the pellet was re-suspended in an appropriate volume of cryopreservation medium to obtain an approximate density of $1x10^6$ cells/ml (see Table 3.24). One ml of the solution of cells was transferred into a cryo-tube (Nunc) and placed in an isopropanol filled container. Transferring the cells from room temperature to -80°C in an isopropanol filled container allows a gradual cooling of cells at a rate of 1°C per minute. For long-term storage cells were transferred to liquid nitrogen (-196°C).

Table 3.24: Recipe for cryopreservation medium.

Cryopreservation medium	
FCS	20% (v/v)
DMSO	10% (v/v)
RPMI	*ad* 50ml

3.5 *In vitro* assays on mammalian cells

3.5.1 Cytospin

Cells were harvested and counted as described before and $2x10^5$ cells in 200µl were pipetted into the cytofunnel placed on a glass slide. Cytospins were performed for 6 minutes at 115g using a Shandon CytoSpin III Cytocentrifuge (Thermo Fisher Scientific, Schwerte, Germany). Afterwards, the glass slides were dried for 10 minutes at the air and stained for 30 seconds in May-Grünwald and 4.5 minutes in Giemsa.

3.5.2 Cell viability assay using MTT

This assay is used to measure the proliferation of cells. To quantify living cells mitochondria are stained (indirect quantification) with 3-([4,5-Dimethylthiazol-2-yl]-2,5-dimethyltetrazoliumbromide (MTT). MTT is a yellow tetrazolium-salt that is soluble in water and taken up by mitochondria. Within the mitochondria this salt is reduced to a non-soluble blue formazan by mitochondrial dehydrogenases.

Usually this test was used to either determine the growth rate of cells or to quantify cells and their growth subsequent to a test (e.g. adhesion test).

Cells were either simply cultivated in 96-well plates or according to specific test conditions (see growth and adhesion assays).

Ten µl MTT (5mg/ml in PBS) was given into each well onto the cells using a Multipette plus (Eppendorf AG) and plates were incubated for 3 to 4 hours in an incubator at 37°C.

Afterwards the MTT-containing supernatant was aspirated and 100µl of lysis-buffer were pipetted onto the cells and plates were moved carefully back and forth to insure that the resulting solution is equally mixed (see Table 3.25).

The optical density of the solution was measured using an ELISA-reader (FLx800, BioTek, Winooski, USA) at 550nm, using a reference measurement at 630nm. Values measured at 630nm were subtracted from values measured at 550nm.

Table 3.25: Recipe for lysis buffer for mammalian cells.

Lysis buffer	
Dimethylformamid	50% (v/v)
ddH_2O	50% (v/v)
Sodium dodecyl sulfate	69.3mM

To remove all remaining solids the buffer was filtered after complete solution.

3.5.3 Adhesion assay

To test whether specific agents influence the adhesion of cells to collagen-coated cell culture flasks an adhesion assay was performed. It was essential to use a PBS^{2+} solution for collagen-coating of 96-well plates that was supplemented with

calcium and magnesium because a lot of adhesion molecules and their ligands require bivalent cations to function (see Table 3.26).

Cells were cultivated so they were 90% confluent at the time point of the experiment. The T25-culture was washed with PBS twice and cells were detached with 2ml cell dissociation buffer (see Table 3.23). The detaching of cells was stopped after 10 minutes by tapping the flask and adding 3ml of adhesion medium (see Table 3.27). Cells were centrifuged at 300g for 5 minutes and the supernatant was discarded. The pellet was resuspended in 2ml adhesion buffer and cells were counted using a haemocytometer.

Therefore, solutions were prepared containing $4x10^5$ cells/ml and different concentrations of the factor that was to be investigated. These solutions were incubated for 30 minutes at 37°C. Subsequently, 100µl/well were pipetted in triplicate into collagen-coated 96-well plates. Plates were incubated a 37°C for 30 minutes to allow cells to adhere to the collagen.

Afterwards, the plates were tilted cautiously to loosen non-adhered cells and the solution was aspirated. The cells were covered with 100µl adhesion medium and allowed to consolidate for 1 hour at 37°C.

To analyse the cell amounts a MTT assay was performed.

Table 3.26: Recipe for PBS^{2+} solution.

PBS^{2+} solution	
$CaCl_2$	1mM
$MgCl_2$	0.5mM
PBS	*ad* 500ml

The solution was sterile filtered.

Table 3.27: Recipe for adhesion medium.

Adhesion medium	
Bovine serum albumin	0.2%
Glutamine	1%
Penecillin/streptomycin	1%
RPMI	*ad* 500ml

Adhesion medium was filter sterilised.

3.5.4 Cell cycle analysis

This method measures the relative DNA-content of cells using a propidium iodide staining. Afterwards, cells are analysed by flow cytometry.

Cells were detached using Trypsin/EDTA, and counted. Two $x10^5$ up to $1x10^6$ cells were given into a FACS tube (BD Biosciences). After 5 minutes of centrifugation at 300g and room temperature cells were washed with PBS containing 2% FCS once and centrifuged again. The supernatant was discarded.

To fix cells and make them permeable, the cell pellet was drop-wise carefully resuspended in cold 70% ethanol (4-8°C) and incubated for 30 minutes at 4-8°C. Occasionally the cell solution was mixed by flicking the tube. After the incubation cells were pelleted by centrifugation for 5 minutes at 300g at room temperature and the supernatant was discarded.

Subsequently the pellet was resuspended in 500µl PBS containing 2% FCS, 20µl RNAse A stock solution (see Table 3.28; end concentration of 400µg/ml) and 100µl propidium iodide stock solution (end concentration of 10µg/ml; Carl Roth GmbH & Co. KG, Karlsruhe, Germany) and incubated for 1 hour in the dark.

After the incubation the solution was topped up with 2ml of PBS, centrifuged at 300g for 5 minutes at room temperature. The supernatant was discarded and the pellet resuspended in 100µl PBS.

Cells were analysed using a FACS Canto or flow cytometer (BD Biosciences).

Table 3.28: Recipe for RNAse A-solution.

RNAse A-solution	
RNAse A	10mg/ml
TrisHCl	10mM
NaCl	15mM
	pH7.5

3.5.5 Colony-forming assay

To investigate the potential to grow in colonies under non-adherent conditions colony-forming assays were performed. These give information about the ability of cells or cell lines to grow under substrate independent conditions.

Stocks of methylcellulose, 2% (v/v) BSA in RPMI medium and FCS were sterile filtered and used for the experiment. Each colony assay was performed in duplicate in 30mm petri dishes (Nunc).

Cells were detached using cell-dissociation buffer, counted and then diluted to achieve the required cell suspensions. The cell suspension was mixed with the serum-containing colony-forming assay medium using a 1.2 Gauge (G) needle and a 5ml-syringe (see Table 3.29).

Table 3.29: Recipe for serum-containing colony-forming assay medium.

Colony-forming assay medium	**5ml**
Methylcellulose	45% (v/v)
FCS	15% (v/v)
RPMI	16% (v/v)
Cell suspension in RPMI	24% (v/v)

The cells were plated carefully into the dishes avoiding the development of air bubbles. Per cell line two dishes with 500 cells/ml and two dishes with 1000 cells/ml were prepared. Colonies were counted after 14 days under a light microscope and photographs were taken for documentation. The entire experiment was carried out twice.

3.5.6 Transfection of mammalian cells using Lipofectamin™

On the day before transfection of cells, these were plated in 1000µl of growth medium in 12-well format so that the cells would be 50–80% confluent at the time of transfection.

The next day complexes were prepared for each transfection sample as follows (according to supplier's manual, Invitrogen):

1. One µg of plasmid DNA was diluted in 200µl Opti-MEM® I Reduced Serum Medium and mixed thoroughly.

2. PLUS™ Reagent was mixed gently before use and added directly to the diluted DNA from step 1. The solution was gently mixed by inversion and incubated for 5 minutes at room temperature.

3. The Lipofectamine™ LTX solution was mixed by inversion and 2.5µl were added to the DNA solution. The DNA-lipid complex was incubated for 30 minutes at room temperature.

After incubation approximately 200µl of the complex was added drop-wise to the well containing the previously seeded cells. To dispense the complex evenly over the cells the plates were rocked gently back and forth.

The cells were incubated at 37°C in a CO_2 incubator for 18-48 hours prior to testing for transgene expression and the medium was exchanged after 12 hours post lipofection. As soon as the wells were around 90% confluent, cells were transferred to collagen-coated T25 cell culture flasks.

If necessary, it was possible to scale the lipofection mix down by using 24- or 48-well plates and amending the amounts of reagents and DNA used in the experiment.

3.5.7 Flow cytometry

Flow cytometry using fluorescently labelled antibodies offers the opportunity to characterise cell populations by specific markers. In this work only cell surface markers were analysed.

Cells were harvested, counted and $2x10^5$ to $1x10^6$ cells were re-suspended in 100µl PBS. Samples were treated with 5µl of fluorescently conjugated antibodies to markers of interest and incubated for 20 minutes in the dark. Afterwards the samples were washed twice with 1ml of PBS and centrifuged at 300g for 5 minutes. Following this, cells were re-suspended in 200µl PBS and were ready to be analysed on the FACS Canto or FACS Calibur (BD Bioscience). At least 100,000 events were acquired. An unstained sample was used as a negative control.

FITC-Mouse Anti-Human CD99 and APC-Mouse Anti-Human CD184 (also called CXCR4, clone 12G5) were both purchased from BD Bioscience.

3.5.8 Fluorescence activated cell sorting (FACS)

Where necessary, cells were prepared as described previously (3.5.7). Cells that harboured a plasmid containing an eGFP-gene were auto-fluorescing and thus did not have to be labelled.

Cells were harvested, counted and the solution was adjusted to a cell concentration of approximately $5x10^6$ cells per 100µl with the total volume of solution not exceeding 300µl in growth medium. The FCS contained within the medium was filtered using a 0.2µm Minisart syringe filter (Sartorius Stedim Biotech S.A., Aubagne Cedex, France) prior to being added to media. Prior to

cell sorting, the FACS Vantage SE cell sorter (BD Biosciences) was sterilised with 70% ethanol solution and washed with water and growth medium. Cells were acquired at a moderate event rate, typically 0.8-1.3x10^3 cells per second, and sorted fractions were collected in growth medium.

After sorting, at least 300-500 sorted cells were re-acquired to assess purity of the desired population.

Depending on the amount of sorted cells, these were taken back into culture in 96-well or 6-well plates or directly in T25-tissue culture flasks.

3.6 *In vivo* assays on mammalian cells

3.6.1 Keeping of animals

In vivo experiments performed at Newcastle University were done under Home Office license number PPL 60/3846 and ethical approval with the ERC Project ID 203. Experiments performed in Münster were approved by the district government licence number G54/2005. All care and experiments were carried out according to individual personal license and project license regulations. If necessary, advice or treatment was given from the on-site veterinary surgeon.

Animals selected for experiments in at the University Hospital in Münster were NOD/LtSz-*Prkdc*^{scid}/J mice (hereafter referred to as NOD/Scid, The Jackson Laboratory, Maine, USA) and at the Northern Institute for Cancer Research in Newcastle upon Tyne NOD.Cg-*Prkdc*^{scid} *Il2rg*^{tm1wjl}/SzJ mice (hereafter referred

to as NSG, The Jackson Laboratory, Maine, USA). The reasons for choosing these specific strains will be further discussed in chapter 3 and 5, respectively.

Due to the immunodeficiency of these mouse strains housing, handling and general care of these mice was carried out using aseptic techniques such as a laminar flow hood (Faster Ultrasafe Class II Microbiological safety cabinet, Wolf laboratories Ltd, Yorkshire, UK). It was not possible to image mice under sterile conditions but all possible safety precautions were taken such as wiping of surfaces with ethanol, wearing of gloves, disposable paper lab coats and face masks to avoid extensive exposure of mice to pathogens.

In Münster, as well as in Newcastle upon Tyne, mice were bred on site and maintained in single sex groups not exceeding five mice per cage. Bubble style isolators or individually ventilated cages were used for housing of mice, bedding and irradiated diet were exchanged once a week in a changing station. Water was provided in sterile disposable water packs or water bottles with autoclaved nozzles.

Handling was only performed when wearing disposable paper lab coats or clean surgical gowns and nitrile gloves. These were sprayed down with disinfectant between handling individual cages.

Once mice showed signs of tumour formation or generally appeared unwell (inactivity, breathing problems, hunched back, and untended fur), they were euthanized by high cervical dislocation.

3.6.2 Preparation of animals for surgical procedures

The induction of the anaesthesia of experimental animals was carried out in a small chamber connected to an Isofluorane vaporiser and oxygen supply (Mie Cavendish 500 anaesthetic machine, fitted with an Ohmeda Isotec 400 volatile anaesthetic vaporiser and Fluovac scavenge system, Key Health Solutions Ltd, Wiltshire, UK). Excess anaesthetic was scavenged for safety. Typically 4-5% Isofluorane (IsoFlo, Abbott Laboratories, Maidenhead, UK) was supplied in 1500cc/min oxygen. To determine suitable depth of anaesthesia the chamber was cautiously tilted to check if mice still had a righting reflex. Furthermore, the foot withdrawal in response to mild pain was used to determine suitable depth of anaesthesia.

Anaesthetised mice were afterwards transferred to a face mask supplying Isofluorane in oxygen and maintained at a suitable depth of anaesthesia. Usually, this required between 2.5-4% Isofluorane in oxygen dependent on the mice weight. To assure that mice would not suffer after the procedure, 10µl of Carprofen (Rimadyl, Pfizer, Kent, UK) per 10g body weight was injected subcutaneously (s. c.) into the skin over the back of the mouse.

All required anaesthetics and veterinary medicine were sourced through the responsible veterinarian of the Comparative Biology Centre, Newcastle University.

3.6.3 Intravenous transplantation

To obtain a systemic spread of disease and model late stages of ES/PNET with cells spreading and homing to different organs mice were transplanted intravenously (i. v.).

NOD/*Scid* mice were irradiated with 3.5Gy 24 hours in a ^{60}Co unit before planned transplantation of cells. The next day, mice were transferred into a laminar flow hood within their cage and an infrared heat-lamp was placed above the open cage for 5-10 minutes. This increased the circulation to the surface blood vessels (as the mouse regulates its body temperature) and led to expanding of the diameter of veins in the tail. Hereafter, mice were trapped in a restraining device, which was made of a 60ml syringe. The top which usually is attached to the needle was cut off and closed with a rubber plug that was slotted dent to allow the tail of the mouse to hang out of the device. The plunge was used to restrain the mouse in space.

Immediately, $5x10^6$ cells in 100-200µl growth medium were transplanted into the tail vein of these mice using a very small diameter needle with 27G. The mouse was marked and released back into the cage and observed for a while to ensure it recovered and calmed down after the procedure.

3.6.4 Intrafemoral transplantation

Orthotopic preclinical models are the gold standard for the characterisation of tumour cell interaction with the microenvironment. Therefore, an intrafemoral (i. f.) model for ES /PNET was developed within this thesis.

Male NSG mice where prepared for the procedure as described before and placed supine breathing further anaesthesia. Subsequently, the right knee of the mouse was shaved and disinfected.

The knee was flexed and grasped with the left hand to be able to puncture the femur with a 25G needle. The position of the drill needle was checked carefully to ensure, that the sample would be placed into the bone marrow cavity of the femur. Sample volumes of up to 30µl with $1x10^6$ cells were subsequently injected with a 30G insulin syringe through the previously drilled hole. Upon needle withdrawal the leg was straightened to close the femoral puncture site and minimise backflow of the cell suspension. Additionally, control transplantations with medium injected into the right femur were performed.

3.6.5 Positron emission tomography tracer preparation

^{18}F-2-Fluor-2-deoxy-D-glucose (FDG) for positron emission tomography (PET) experiments was purchased from Iba Molecular UK Ltd. (Sheffield, UK). Where possible, spare FDG originally delivered for patients was used. The tracer was diluted with sterile saline if required, to obtain a solution of which an appropriate amount could be used to inject 10MBq into mice.

The isotope ^{18}F emits positrons with a half-life of 109.8 minutes, which can be detected with a positron-emission tomography system. ^{18}F is not found naturally and has to be produced with the help of a cyclotron for example through positron bombardment of the oxygen-isotope ^{18}O.

3.6.6 Positron emission tomography

To be able to determine metastatic spread of ES/PNET and to characterise local tumours that arose after i. f. transplantation of cells, PET scans of previously injected mice were performed.

In Newcastle, all *in vivo* imaging experiments were performed in cooperation with the group "Drug Discovery and Imaging" (Northern Institute for Cancer Research, group leader Ross Maxwell).

PET scans were performed with the high-resolution Philips Mosaic HP (Philips Medical Systems, Eindhoven, The Netherlands) with a field of view (FOV) of 128 x 120mm. The first PET scan in each mouse was performed approximately two weeks after i. f. transplantation of tumour cells. Follow-up PET scans were performed in different intervals.

Before tracer injection, mice were anaesthetised by Isoflurane/oxygen inhalation for the entire experimental procedure or by an intraperitoneal (i. p.) injection of Ketamin/Medetomidine (75mg/kg and 1mg/kg, respectively). Rectal temperature was maintained at physiological values by use of a heating pad between the start of the anesthesia and the experimental procedures. Scans were performed 1 hour after i. v. injection of 10MBq FDG. Mice anaesthetised with Isoflurane/oxygen were kept under anesthesia during the experimental procedure using a Minerve Animal Anesthesia System (Equipement Vétérinaire Minerve, Esternay, France). Within the machine the body temperature was maintained by air flow through the animal bed. Once imaging had taken place, mice that had been anaesthetised with Ketamin/Medetomidine were recovered through i. p. injection of 0.5-1mg/kg Atipamezole. All mice were observed for 30 minutes after recovery from anaesthesia.

Reconstruction of PET images was performed using the 3D-RAMLA algorithm with no attenuation correction (Browne and de Pierro, 1996).

3.6.7 X-ray computed tomography

The technique of X-ray based computed tomography (CT) was used to visualise and characterise eventual changes to bones that could occur through the injection of tumour cells into the femur of mice. In this case NanoCT scans were carried out using the Bioscan NanoCT (Bioscan, Paris, France), which is able to produce data with resolution that is high enough to visualise the relatively fine bones of mice.

The FOV for the scans performed was 150 x 75mm. Parameters of whole-body images were: standard resolution, 180 projections, 55kVp, 1000ms exposure time and 10-12 minutes acquisition time, leading to a dose of ~150Sv. The parameters for scans of a higher resolution taken from just the lower limbs: ultra-fine resolution, 360 projections, 45kVp, 400ms exposure time, 2-3.5 minutes acquisition time, leading to a radiation dose of ~105Sv. The images were reconstructed using the Exact Cone Beam FBP (Filtered Back Projection) with the SheppLogan filter. The resulting voxel/pixel size is 0.10/0.096mm.

Mice were anaesthetised by Isoflurane/oxygen inhalation for the entire experimental procedure using a Minerve Animal Anesthesia System (Equipement Vétérinaire Minerve, Esternay, France) and a physiological body temperature was ensured by air flow through the animal bed.

If PET scans were performed the same day as CT scans these were performed before each PET scan using the same animal bed so that mice were kept in the same position and a fusion of PET and CT images was possible afterwards.

3.6.8 Magnetic resonance imaging

MRI was used to describe the soft tissue component of tumours.

One week after the last PET and CT scans transplanted mice underwent a final MRI scan. MRI scans were performed with a high-resolution 7T Varian MR system (Varian Inc., Palo Alto, USA) using a Coil-Rapid 72mm quadrature volume coil (RAPID Biomedical GmbH, Rimpar, Germany). Mice were anaesthetised for the entire experimental procedure by Isoflurane/oxygen inhalation and physiological temperatures were assured by the use of a rectal thermometer and a heating pad on which mice were placed through the whole procedure.

Parameters for the lung scans were: fast spin echo sequence with respiratory gating, repetition time (T_R) 2439ms, effective echo time (T_E) 39ms, FOV 30 x 35mm, in plane resolution 0.13mm and slice thickness 2mm.

Parameters for the leg scans were: spin echo sequence, T_R 500, T_E 17, FOV 30 x 35mm, in plane resolution 0.13mm and slice thickness 2mm.

For analysis of tumour volumes the software Vnmr J (Varian) Version 2.3 Rev. A was used.

3.6.9 Dissection of mice

In order to provide terminal analysis of tumour and metastasis development and to recover organs for pathology mice were dissected subsequent to euthanasia. Protocol limits were either a high tumour burden or a generally poor condition of a mouse. Mice used as controls were euthanized once all experimental mice had culled.

Intravenously injected mice were dissected and lungs, liver, kidneys and spleen were taken for pathology. At this stage of the experimental work (Münster) it was not possible to recover bone tissue for pathology. Thus, bone tissue was only taken from mice when there was a clear sign of tumour development.

Additionally, the bone marrow of both femurae was recovered. Therefore, a small section from each end of both femurs was clipped and bone marrow was extracted by flushing the lumen with transplant media repeatedly using an insulin syringe. Metastases from organs that were visible by eye and bone marrow flushes were taken into culture in RPMI growth medium containing Penicillin/Streptomycin. Using a sterile blade, tissues were disintegrated into fine pieces and incubated for 1 hour in trypsin/EDTA to ensure that tissue would break up. Following the enzymatic digest the tissue was pipetted up and down to apply shearing force to further separate the cells. To obtain a single cell solution for cultivation cells were forced through a fine mesh using a FACS tube with a Cell Strainer Cap (BD Biosciences).

Lungs, liver, kidneys and spleen were collected from all i. f. transplanted mice. Instead of collecting bone marrow from the hind limbs these were stripped of skin and separated from the rest of the body by transection of the spin just above the pelvis and the tail. Organs and hind limbs were fixed in formalin and

preserved in 70% ethanol. The hind limbs were decalcified to make them suitable for pathological sectioning (see chapter 3.7.1).

3.7 Pathology

3.7.1 Immunohistochemistry

Samples of organs and metastases were fixed in 10% neutral buffered formalin (4% formaldehyde in phosphate buffered saline), embedded in paraffin, and cut into 4–5 μm thick sections. These were stained with hematoxylin and eosin or used for immunohistochemistry to detect expression of huCD99 (commonly used as an ES/PNET marker). Typically, lung, liver, kidneys and spleen were screened for tumour cells also if no sign of metastases could be seen during dissection.

Staining for antigens was carried out as follows: slides were de-paraffinised, re-hydrated and neutralised in hydrogen peroxide solution. Antigen retrieval was performed by heating the slides twice for 5 minutes in 0.01M citrate buffer (pH 6.0) using a microwave. The slides were cooled down in the buffer and then rinsed under tap water. Slides were then washed twice for 5 minutes in 50mM Tris-buffered saline with a pH 7.6. A couple of drops Tween-20 were added to break the surface tension.

Immunohistochemical staining was carried out manually using the Menapath Kit (Menarini Diagnostics, Florence, Italy). Primary antibodies included monoclonal rat anti-human anti-CD99 (Dako, Carpinteria, CA, USA) diluted 1:50 and monoclonal rat anti-human anti-CD45 (Dako, Carpinteria, CA, USA) diluted

1:50. Diluted antibodies were dropped on the slides and incubated for 30-60 minutes. Slides were incubated for 10-20 minutes with the universal probe (Manapath Kit) then incubated for 20-30 minutes with HPR polymer, 30 minutes with VectaStain ABC reagent (Vector Laboratories, Peterborough, UK) and washed under tap water for 5 minutes. Slides were 10 seconds counter-stained with Harris's hematoxylin (BDH, VWR International, Lutterworth, UK), rinsed for 5 minutes under tap water, dehydrated, and cover-slipped. If not indicated differently, rinses were performed using Tris-buffered saline wash buffer.

3.7.2 Haematoxylin and Eosin staining

This method gives consistent results and is very simple to perform.

Hematoxylin is used because it produces a stained section with clearly defined nuclei in blue while the background stays completely colourless. The cytoplasm stains in various shades of pink which helps to identify different tissues.

Sections were prepared as described before (see section 3.7.1). Subsequent, the sections were stained for 15 minutes in hematoxylin solution and then wash in running tap water for 20 minutes. Sections were counterstain with eosin (Leica, Peterborough, UK) from 15 seconds up to 2 minutes depending on the age of the eosin, and the desired depth of counterstain.

Finally, for dehydration sections were transferred to 95% and absolute alcohol twice for 2 minutes each or until excess eosin was removed. Sections were cleared in xylene twice for 2 minutes each and mounted.

4. Chapter – Metastasis model for Ewing's sarcoma in Non-obese diabetic/Severe combined immunodeficient mice (NOD/Scid)

4.1 Introduction

In the first half of the 19th century clinicians realised that there were common features in the histology of ES/PNET and other sarcomas such as PNET, and Askin tumour of the thoracic wall (see Chapter 1). The development of new diagnostic techniques such as PCR has made it possible for these tumours to be grouped as one entity due to the characterisation of the first chromosomal translocation in this disease subtype. Thus, the Ewing's family of tumours serve as a model for understanding the biology of human sarcomas (Delattre et al., 1992, 1994).

Despite this similarity the group of sarcomas is heterogeneous in clinical and histochemical features and the exact cell or tissue of origin still remains unknown (see chapter 1). ES of the bone alone shows differences in course of disease and this heterogeneity reflects in treatment difficulties still present.

4.1.1 Metastasis in Ewing's sarcoma and patient outcomes

It has been known for many years that ES/PNET is radiosensitive (Ewing, 1939). Thus, for a long time radiotherapy combined with surgery was the gold standard for treatment of this sarcoma. Nevertheless, more than 90% of patients receiving immediate local radiotherapy died of systemic metastasis within two years of

diagnosis. This demonstrates that micrometastases establish early on in the course of this disease. Over the last 30 years, treatment protocols have combined radiotherapy, chemotherapy and surgery leading to an improved prognosis for ES/PNET patients and cure is achievable (see chapter 1).

Today, using modern multimodality therapy, one of the most important prognostic factors is the occurrence of primary metastasis (see Figure 4.1). The majority of tumours are primarily located in bony sites and while two thirds of ES/PNET patients with localized disease can be cured, the 5-year event free survival in patients presenting with osseous metastases or bone marrow infiltration is less than one fifth (accounting for approximately 10% of patients), while only 30% of patients with lung metastases survive (Paulussen et al., 1998a, 1998b, 2001).

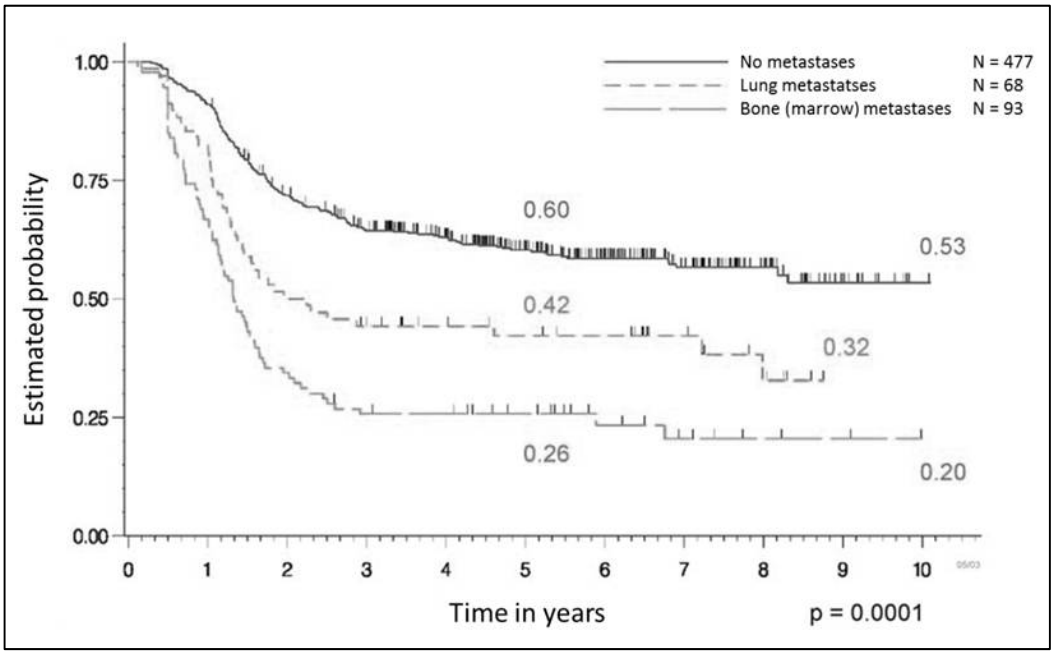

Figure 4.1: Event free survival of ES/PNET patients in correlation with existence and localisation of metastases. Localised disease (blue line), lung metastases (red line), bone (marrow) metastases (green line). (EI)CESS 81-92 study (modified from (Jürgens et al., 2006).

Metastatic disease is one of the most important factors influencing prognosis, and thus the intensity of treatment. The mechanisms of metastasis in ES/PNET remain unclear; therefore it is crucial to investigate the development of metastasis in order to improve treatment strategies and patient outcome.

4.1.2 Mouse model systems in cancer research

For more than 50 years it has been possible to use *in vivo* models to investigate complex correlations of cancerous diseases (Gellhorn and Hirschberg, 1955; Oettel and Wilhelm, 1955). The first studies were mainly performed by the National Cancer Institute (Bethesda, USA) with the three murine cell lines sarcoma 180, L1210 leukemia, and carcinoma 755. However, concerns arose due to the fact that the majority of studies were initially based on the murine L1210 leukemia model. Although relevant for some leukaemias, this model could have potentially selected for anti-cancer drugs only effective against rapidly growing tumours (Venditti et al., 1984).

During subsequent years, treatment of human leukaemia and lymphoma improved as a result of preclinical work on combinations of different chemotherapeutics in murine models of these malignancies (Zubrod, 1965; Frei et al., 1965; DeVita and Schein, 1973). In contrast, no significant improvements for human solid tumours were achieved (Suggitt and Bibby, 2005).

In 1966 a revolutionary publication describing a nude athymic (nu/nu) mouse strain (Flanagan, 1966) enabled the establishment of different human solid tumour xenografts, including breast, colon and lung tumours (Rygaard and Povlsen, 1969; Geran et al., 1972).

Many more mouse strains have since been developed and preclinical models have played a crucial role in medical research. They did not only help to improve the understanding of diseases but led to the development and improvement of therapy strategies and new drugs. Traditionally, these studies still are often carried out as s. c. experiments, which offer an easy approach and lead to tumours that are easily visible and palpable. Despite these advantages s. c. experimental protocols can be criticised as they simplify tumour formation due to the vigorous supply of blood from the skin. This leads to a quick vascularisation of the implant and subsequently to faster growth of the tumour. Furthermore it is usually only cell lines that engraft which may be due to the unnatural microenvironment they have to grow in.

In order to investigate metastasis intravenous models are also often used, which better reflect the late steps of metastasis that occur via dissemination in the blood stream, including organ-specific homing, extravasation, trans-endothelial migration, invasion into tissue, clonal expansion of tumour cells and tumour angiogenesis (Vormoor et al., 2001). Equally important to the choice of the method of transplantation is the selection of the most appropriate mouse strain. Mice have to be immunodeficient in order to allow human tumour cells to engraft in host tissues and to prevent the rejection of the xenograft by the host's immune system.

4.1.2.1 Nude Mice

The first immunodeficient mouse strain used in preclinical investigations was the Nude (nu/nu) strain discovered by Flanagan in the 1960s. Investigations showed

that the spontaneous mutation leading to nude mice is caused by a genetic change in the gene forkhead box N1 (Foxn1) on chromosome 11. Amongst others, one result of this pleiotropic mutation is the abnormal development of the thymic epithelium. These athymic mice lack functional T lymphocytes, which normally develop in the thymus from progenitors derived from haematopoietic stem cells of the bone marrow. Under normal circumstances haematopoietic progenitors are able to populate the thymus and expand by cell division to generate a large population of immature thymocytes subsequently resulting the generation of mature T cells (Pantelouris, 1968; Schwarz and Bhandoola, 2006). This lack of functional T cells in Nude mice results in an absent T cell-mediated immune response. As a direct result, Nude mice also carry a T cell-dependent defect in B cell maturation, function and immune response (Kaushik et al., 1995).

For a long time researchers used xenograft models of human solid tumours including ES/PNET characterised by s. c. transplantation into the flanks of Nude mice (Scotlandi et al., 1998). However, this model does not mirror the typical clinical occurrence and growth pattern. Additionally, it is not possible to grow all cell lines or even primary material in Nude mice as they have a residual immune function that prevents engraftment, tumour development and metastasis.

This fact and the observation that under suitable conditions even aging Nude mice can develop mature T cells deriving from haematopoietic progenitors (leakiness) made it necessary to develop mouse strains with less residual immune function. Nevertheless, although such profoundly immunodeficient strains were developed and used, Nude mice are still important in the preclinical evaluation of potential therapeutics in s. c. tumour models.

4.1.2.2 Scid Mice

In the early 1980s the discovery and promotion of another spontaneous mutation led to the development of a mouse strain termed "severe combined immunodeficient" (Scid), which was of great use in the studies of xenograft implantation (Bosma et al., 1983). In comparison to Nude mice, these have a more severe immunodeficiency and are thus less likely to reject implanted xenografts. This immune defect occurs as a result of a homozygous recessive mutation in the gene protein-kinase, DNA activated, catalytic polypeptide (Prkdc) on chromosome 16. This gene encodes for the DNA-dependent protein kinase catalytic subunit, which is a subunit of the DNA-dependent protein kinase (DNA-PK). The mutation in Prkdc hinders the interaction between the DNA-dependent protein kinase catalytic subunit and its ligands leading to a defect both in immunoglobulin and T cell receptor rearrangements. This results in the humoral and cellular immune systems failing to mature and Scid mice, therefore, present with impaired ability to produce mature T and B lymphocytes. This renders the mice ineffective at fighting infections, and unable to raise an adaptive immune response against any foreign antigen, including implanted tumour cells (Custer et al., 1985; Bosma et al., 1988b; Lieber et al., 1988).

The inability of the mutated Prkdc to bind the other components of the DNA-PK-complex additionally leads to a defect in DNA repair function of the complex. Thus, Scid mice are hypersensitive to ionising radiation (Fulop and Phillips, 1990). This effect is often used to further enhance the immune defect in Scid mice as ionising radiation removes all cells of the bone marrow.

One major disadvantage of the Scid mouse strain is the possibility that few Scid lymphocytes can have productive rearrangements at the appropriate Ig

(immunoglobulin) or T cell receptor loci and thus survive and express an antigen receptor despite the defect. When these "leaking" lymphocytes expand, mice are not sufficiently immunocompromised anymore. This effect may occur due to immune stimulus caused by housing animals in an environment that is not pathogen-free (Bosma et al., 1983, 1988a; Nonoyama et al., 1993).

However, Scid mice remain an important milestone in the research of xenograft models for human solid tumours (Phillips et al., 1989) but knowledge could be further advanced by the use of different strains of mice combining the Scid background.

4.1.2.3 NOD/Scid Mice

An important step in the development of immunodeficient mouse strains was the creation of the NOD/Scid mouse strain. By backcrossing the previously described spontaneously occurred Scid mutation (Prkdc mutation) onto the NOD/Lt strain background, a mouse strain with defective lymphoid function accompanied by reduced non adaptive immunologic function was created (Shultz et al., 1995). NOD/Lt mice harbour less functional NK cells (natural killer cells) (Kataoka et al., 1983; Serreze and Leiter, 1988), lack the complement system (Baxter and Cooke, 1993), and have defects in differentiation and function of antigen-presenting cells (Serreze et al., 1993). NOD/Lt mice show a high incidence of Type I insulin-dependent diabetes mellitus (IDDM), which is mediated by T cells. Backcrossing the Scid mutation onto this background, however, results in NOD/LtSz-*Prkdc*^{scid}/J (NOD/Scid mice, Jackson Laboratory) that do not develop IDDM (Christianson et al., 1993) but carry a complex

immunodeficiency which is characterised through the absence of T and B lymphocytes, macrophages, and the complement system as well as less efficient NK cells. This results in an almost complete inability to reject human xenotransplants, as the strain provides a more permissive environment for human cells than traditional Nude or Scid mice. However, remaining NK cell activity should be erased through immune depletion (e.g. ionising radiation) to minimise the remaining chances of rejection of transplants (Vormoor et al., 2001).

4.1.2.3 The established intravenous NOD/Scid mouse model

In the early 2000s, Vormoor et al. published a novel preclinical model for ES/PNET in immunocompromised mice (Vormoor et al., 2001) shortly after first models for other types of solid tumours in NOD/Scid mice had been introduced (Bogenmann, 1996; Klein et al., 1997). The aim of this study was to engraft ES/PNET cell lines and primary material *in vivo* via i. v. transplantation of single cell suspensions into NOD/Scid mice.

The motivation for the development of this model was the need to investigate the clonogenic frequency of ES/PNET cell lines and the proliferative ability of primary material *in vivo* as opposed to its often impaired growth *in vitro*. The NOD/Scid mice showed a pattern of disease spread similar to that found in patients with metastases in lung, kidney, ovary, bone, and s. c. tumours as well as involvement of bone marrow. Additionally, the time of tumour development of 1-6 months for cell lines and 4-9 month for primary material in mice was comparable to the occurrence of relapse in patients.

It can be assumed that the result of this study was a potential model for investigations not only for the clonogenic frequency of ES/PNET but also for its hematogenic spread. The fact that pattern of and time to metastasise were very similar to the clinical situation showed that the late and very complex stages of metastasis of ES/PNET seem to be reproducible in this mouse model. These include spread via the blood stream, organ-specific homing, adhesion to the endothelial wall, transendothelial migration and tissue invasion through chemotaxis as well as proliferation and the potential of self-renewal, and induction of angiogenesis. This proves as well that the interaction between human tumour cells and the specific microenvironment of the different organs of the mouse is sufficiently conserved.

Until now this model has been used successfully for different investigations on treatment opportunities and biological mechanisms of metastasis (Hotfilder et al., 2002; Staege et al., 2004; Hu-Lieskovan et al., 2005a).

Taking the advantages of this model into account, NOD/scid mice were chosen for studies of the metastasis of ES/PNET and to obtain different organ-specific tumours for further investigations. Since the development of this model the even more immunodeficient mouse strains NSG has been developed which were not available at the time (Shultz et al., 2005). NSG mice were used for the development of an orthotopic model for bone malignancies and are described in chapter 5.

4.1.3 The principles of expression profiling

Sequencing of the human genome has been a major breakthrough for biomedical research (McPherson et al., 2001; International Human Genome Sequencing Consortium, 2004). Together with new techniques of functional genomics it is now possible to perform global analyses of the expression of thousands of genes (Eisen and Brown, 1999) and to understand complex molecular processes involved in the development and progression of diseases such as cancer. During the years that expression profiling was available and got more and more important, microarray analysis has become the preferably used technique as it is a straightforward approach which does not require the sequencing of DNA. An alternative which offers the advantage of faster results is RNA-Seq (RNA sequencing). However, this method is a lot more expensive than microarrays at a comparable resolution of accuracy.

Thus, research could be performed to investigate gene profiles that correlate with a metastatic phenotype of tumour cells (Hynes, 2003). These profiles did not only discover genes responsible for the general ability of metastasis in specific tumours (van 't Veer et al., 2002), but furthermore identified clones within tumours and tumour cell lines that prefer specific organs as a site of metastasis (Kang et al., 2003). It may well be that solid tumours are maintained from rare cells within the tumour that have tumour initialising abilities. This is also the case in hematologic malignancies and may be accountable for metastasis of other malagnancies as well (Tu et al., 2002).

The analysis of different tumour systems, such as non-small cell lung cancer (Diederichs et al., 2004), breast cancer (Kang et al., 2003) and melanoma (Clark et al., 2000) has proven that there are organ-specific features driving metastasis

and this may give hints on the cellular mechanisms of organ-specific metastasis in general.

Gene microarrays represent a high throughput technology, which allows for the identification and quantification of thousands of genes from multiple samples in parallel that have pre-defined characteristics such as treatment versus no treatment (Mocellin and Rossi, 2007). The important advantages of this technique are

- the possibility to discover new genes and further investigate their functions.
- the opportunity to clarify gene regulation and regulatory networks.
- the chance to facilitate and improve diagnosis and prognosis by identification of disease- and stage-specific gene expression profiles.

Southern blotting is the technique, which led to the development of microarrays. This method requires the attachment of fragmented sample-DNA to a substrate. The DNA of the known gene of interest is then given onto the prepared substrate. This tests, whether the gene of interest is contained within the sample.

The underlying concept of microarray technique using GeneChips® is straightforward (see Figure 4.2). Briefly, RNA is isolated from cells or tissue, cDNA is synthesised, and biotin-labelled cRNA is generated in an IVT (*in vitro* transcription) reaction to obtain the target. This is fragmented and hybridised to the probes attached to the solid matrix of the microarray. The microarray with the hybridised sample is stained with PE-conjugated (phycoerythrin) streptavidin and scanned by the laser scanner of the system unit used. GeneChips® contain

several different 25-mer oligonucleotides matching one gene. Additionally, every oligonucleotide comes with a negative control containing a mismatch. From these match- and mismatch-oligonucleotide sets expression of the gene of interest can be derived and expression values of the different samples can subsequently be compared and analysed to obtain biological information (Staal et al., 2003).

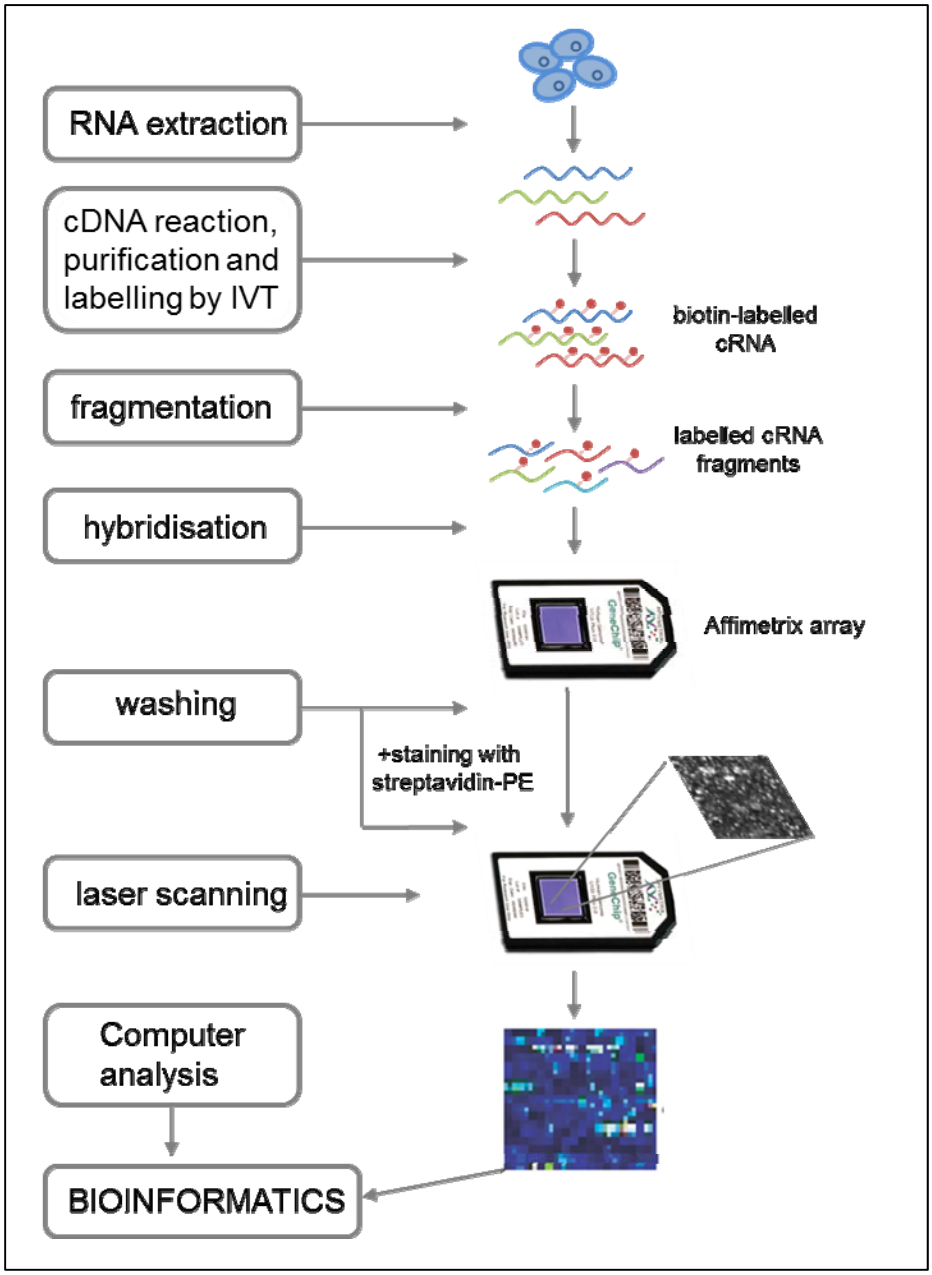

Figure 4.2: Scheme for the workflow of expression analysis using an Affymetrix GeneChip®. RNA is extracted from cells or tissue, cDNA is produced and in an IVT reaction cRNA is created and biotinylated (target). After fragmentation the template is hybridised to the probes on the GeneChip®, the chip is stained and finally scanned using a laser scanner.

Although, the human genome has been sequenced it still remains un-interpreted to a great extent and even the exact number of genes encoded is still unknown. Thus, analysis of expression profiling can only be an approximation and there

will always be unknown transcripts appearing in expression profiles that cannot yet give any biological information without further investigations on the function of that very gene.

4.1.3.1 Variations of gene expression data

Affymetrix oligonucleotide arrays have several advantages. The most important one is that several probes are used for one transcript. This leads to more reliable data with less variation. However, one of the major problems examining global gene expression is the reliability of resulting data at the lower end of the confidence scale. This is the case when the signal for a probe is extremely weak, or to the other extreme very saturated. It also has to be taken into account that fold changes in expression of transcribed genes compared between different samples (in this case parental cell line and mouse-derived organ-specific subclones) might not reflect the importance and emphasis of a down-stream occurring effect in biological pathways. For example, small changes on transcript level can be amplified through intracellular signalling pathways but may not be detected by the analysis of the expression arrays due to the set threshold of fold change (in this study 2-fold). However, it is likely that high fold changes detected in gene expression experiments have an impact in the cell and thus are important for the undertaken investigations.

Another drawback is that the sensitivity of oligonucleotide arrays has been found to differ between single arrays and the different platforms. This might be responsible for the mismatch between collected gene expression data from various studies handicapping meta-analysis of in theory comparable data.

4.1.3.2 Statistical and biological significance

Two types of replicates for gene expression microarray experiments ensure that collected data is statistically and biologically significant; these are technical and biological replicates. On the one hand, technical replicates are applied to determine variation of preparation of RNA samples, handling and its hybridisation onto the microarray GeneChip. On the other hand, biological replicates are achieved through testing of different samples derived from repeated experiments.

The Affymetrix platform is very well standardised leading to the biological variation outweighing any technically caused variation. Thus, only biological replicates had to be used in this set of experiments

4.2 Aims

The principle aim of this component of the project was to investigate cellular mechanisms of organ-specific metastasis in ES/PNET.

The working hypothesis was that patients with pulmonary metastases and patients with osseous metastases have different prognosis because the cells initiating the metastases have a different biological properties. The heterogeneity of ES/PNET cell lines and the resulting subclones with organ-specific metastasis could correlate with differences in expression of genes leading to organ-specific expression patterns. The identification and characterisation of these genes could potentially give insight about mechanisms pertaining to organ-specific metastasis and thus facilitate a better understanding of clinical differences between pulmonary and osseous metastasis. Furthermore, new targets for molecular

therapy strategies could be identified to improve diagnosis, treatment and prognosis of ES/PNET.

Concluding, the specific aims were:

- to isolate ES/PNET subclones with preferential tendency to metastasise to specific organs.
- to identify organ-specific gene expression signatures (lung versus bone versus bone marrow).

4.3 Materials and Methods

Most work for this part of the thesis in hand was performed at the Westfälische Wilhelms-University and University Hospital Münster, Germany.

4.3.1 Tracer preparation and positron emission tomography (Münster)

Tracer preparation [18F]fluoride was performed using an RDS 111e cyclotron (CTI, Knoxville, USA) according to Wieland et al. (Wieland et al., 1989). Subsequently, FDG was synthesised as previously described (Hamacher et al., 1986).

PET scans were performed as previously described (Franzius et al., 2006). The scanning was performed by a service unit of the research department of the University Hospital Münster which uses the high-resolution multi-wire chamber animal PET camera quadHIDAC (Oxford Positron Systems Ltd, Oxford, UK).

Mice were starved overnight, anaesthetised and handled as described before (3.6.1 and 3.6.3). One hour after i. v. injection of approximately 10MBq ^{18}F-FDG mice were scanned for 15 minutes. The FOV was 28cm axially and 17cm in diameter. The volumetric spatial resolution was 1.09mm^3 (using filtered back projection reconstruction) and constant over the whole FOV. The absolute sensitivity in the centre of the FOV was 18 cps/kBq. Whole-body emission images were reconstructed by the iterative OPL-EM algorithm, which offers an even higher spatial resolution of 0.7 mm full-width at half-maximum (FWHM).

4.3.2 Isolation of organ-specific subclones from metastases

Metastases were either localised by PET scanning or during dissection of mice. To achieve isolation of organ-specific metastases, mice were euthanized, dissected and metastases of the lung and bones as well as bone marrow flushes were collected in pre-warmed medium within a 50ml reaction tube and further treated as described before (see section 3.6.9).

Subsequently, subclones were cultivated along with the routine cell culture. Remaining mouse cells in the cultures died very rapidly so that subclone-cells could be frozen down as soon as the small culture flask was confluent. Therefore, cell pellets of 5x10^6 cells were aliquoted in 1.5ml reaction tubes and frozen in liquid nitrogen. Cells were stored at -80°C until RNA was isolated for microarray analysis (see chapter 3.3.4). For the validation of the quality of RNA see chapter 4.3.3.

4.3.3 Expression arrays

Microarrays were performed by the IZKF (Interdisziplinäres Zentrum für Klinische Forschung, Münster, an institutional research facility of the Medical Faculty of the Westfälische Wilhelms-University, Münster).

The IZKF is an Affymetrix Core Laboratory using the Agilent Bioanalyzer 2100 to control the quality of the sample RNA. The unit separates the sample using capillary electrophoresis. The Agilent Software offers an electropherogram (fluorescence against time), a "gel-like image" and is able to automatically judge about the quality. Therefore a database for RNA-analysis is used that offers 3000 electropherograms that were judged "by hand".

The Affymetrix GeneChip System® 3000 is used for the entire workflow of expression analysis.

4.3.3.1 Affymetrix U133 plus 2.0 array

For the analysis of gene expression the Affymetrix GeneChip® Human Genome U133 Plus 2.0 Array from Affymetrix (Affymetrix Inc., Santa Clara, USA) was used. This GeneChip® covers 1,300,000 unique oligonucleotide features which account for over 47,000 transcripts and variants representing approximately 39,000 of the best characterized human genes.

Transcripts were derived and selected from GenBank®, dbEST, and RefSeq and sequence clusters were created from the UniGene database (Build 133, April 20, 2001). The selection was then refined by analysis and comparison with a number of other publicly available databases. Further information is available on the Affymetrix Inc. homepage, www.affymetrix.com.

4.3.3.2 Probe sets on the GeneChip

In situ synthesised probes on the GeneChip are 25 nucleotides long. This ensures the specificity. For each transcript a probe set is created. This set consist of 11-16 probe pairs to allow multiple and independent measurements. A probe pair is made up of a perfect match and a mismatch, which contains a single mismatched base. The mismatch probe functions as an internal control to quantify levels of non-specific hybridisations of perfect match. The intensity of hybridised mismatch is subtracted from the intensity of the hybridised perfect match probe to be able to control and correct for the noise in the array results.

4.3.3.3 Planning the experiment and replicates

To be able to analyse the expression of ES/PNET derived from different organs, mice were transplanted with cells of different ES/PNET cell lines as mentioned before (see Figure 4.3 and chapter 3.6.3). Mice developed different tumours, which were isolated during dissection. Due to the isolation of tumours from the comparable organ in multiple mice it was possible to perform the experiment with biological replicates. Technical replicates (determining the variation in handling and hybridisation onto the GeneChip) were not necessary as the microarray platform used is very well standardised and validated. This means that the biological variation of samples outweighs the technical variations.

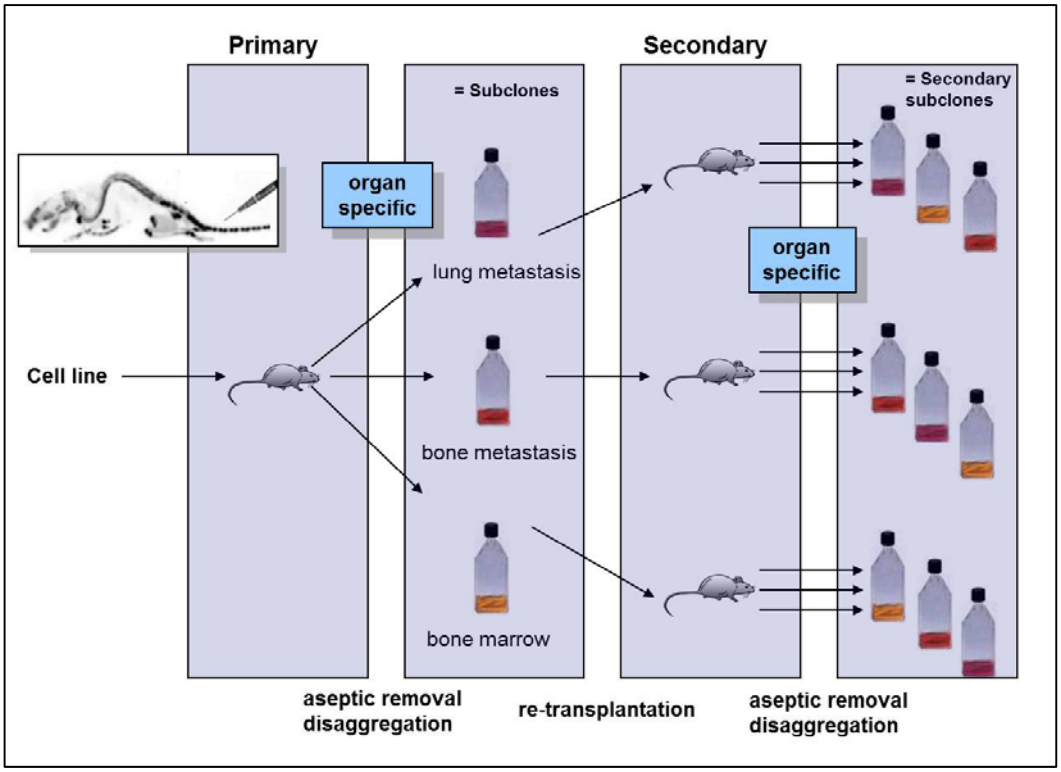

Figure 4.3: Scheme of transplantations and acquired metastases from primary and secondary mice.

Figure 4.3 shows the experimental plan with transplantation of cells, aseptic removal and isolation of metastases, re-cultivation of cells and secondary transplantation into further experimental animals with subsequent removal of metastases from secondary mice.

4.3.3.4 Sample preparation

RNA was isolated using the Qiagen kit as described before (3.3.4 and 3.3.5). Ideally, the amount of 5-15µg RNA of the different samples was sent in. The RNA had to be resuspended in ddH_2O and delivered to the IZKF at 4°C. Further steps were carried out by this institution as described in 4.3.3.

In total, 19 microarrays were performed with each two replicates of the parental cell lines VH-64 and TC-71 from which the subclones were derived.

4.3.4 Analysis of expression arrays

Raw data acquired directly from the microarray-chips was analysed using GeneSpring GX 11 (Agilent Technologies Inc., Santa Clara, USA) and BioConductor (Gentleman et al., 2004). Analysis was completed in cooperation with the bioinformatics department of Newcastle University.

Data was imported from the CEL files (raw data from chip scanning) and normalised with RMA (Robust Multi-array Average). Therefore, raw intensity values were background corrected, log2-transformed and then quantile normalized (Wu and Irizarry, 2005).

Data were filtered using MAS5 P/M/A calls (Microarray suite 5). Probe sets were discarded if they did not have present or marginal calls in all samples in any given experimental condition.

Finally, gene lists were filtered due to fold change. Transcripts whose abundance were significantly altered ($p<0.05$) after 100 permutation tests on the class labels and an absolute fold change greater than 2-fold were defined as differentially expressed and were therefore further analysed.

Where applicable, differences between experimental groups were determined using Rank Products (Breitling et al., 2004) and further analysed in GeneSpring.

Rank Products analysis provides a straightforward and statistically stringent way to determine the significance level for each transcript. It allows for a flexible control of the false-detection rate and family-wise error rate in the multiple

testing situation of a microarray experiment. This technique has been shown to reliably identify differentially expressed transcripts that do not originate from a sophisticated statistical model but rather from an analysis of biological reasoning.

4.3.5 Further biological analysis

For further, biological analysis of the normalised and processed data these were exported into EXEL (Microsoft Corp., Redmond, USA). Resulting gene list were then analysed through the use of Ingenuity Pathway Analysis 8.0 (IPA; Ingenuity Systems Inc., Redwood City, USA; www.ingenuity.com). IPA is a web-based software application, which allows the analysis and understanding of expression data in a biological context. It is backed by the Ingenuity Knowledge Base of highly structured, detail-rich biological and chemical findings. It is the largest knowledge base of its kind, with millions of findings generated from the full text literature and is updated on a weekly basis.

In more detail, IPA Core Analyses were performed on the comparison lists generated in GeneSpring containing the differentially regulated transcripts. This delivers a rapid assessment of the signalling and metabolic pathways, molecular networks, and biological processes that are most significantly perturbed in a dataset of interest.

IPA Core Analysis standard settings were used, including direct and indirect relationships with a maximum of 35 molecules per network and 25 networks per analysis.

IPA uses computational algorithms to identify local networks that are particularly enriched for the input genes, which are called focus genes by the IPA software. Furthermore, IPA uses a Fisher's exact test to determine which pathways (canonical pathways, toxicity pathways and biological functions) are significantly linked to the input gene set compared with the whole Ingenuity Knowledge Base.

4.3.6 Microarray validation experiment using qRT-PCR

Genes selected for validation of the microarray experiments via qRT-PCR are listed in Table 4.1.

Table 4.1: Details of qRT-PCR primers from Sigma.

Gene	Forward primer (5' – 3')	Reverse Primer(5' – 3')
ALDH1A1	AGCTCTGCCAGGTAGAAGAAGGA	ATCCAATCTGAAAAGCCTGTCTTG
APOC1	GGACAAGGCTCGGGAACTC	TGAAAACCACTCCCGCATCT
CXCR4	CTGAGAAGCATGACGGACAA	TGGAGTGTGACAGCTTGGAG
MEG3	ATCCCGGACCCAAGTCTTCT	CACGTAGGCATCCAGGTGATG
NRG1	GTCCACTGCGCCATCCTT (exon 1)	TTGTCCCAGTGGTGGATGTAGA
	CCCCGATTGAAAGAGATGAAAA (exons 2/3)	
VCAN	CCGGTGCTTAGGAAATGGAA	TTCATAGAATAAGTCCTTTGGTATGCA

The exact method for designing of qRT-PCR primers and the qRT-PCR itself are described in chapter 3.3.13.

4.4 Results

4.4.1 Intravenous transplantations and re-transplantation of subclones

To be able to isolate organ-specific metastases from immunocompromised mice, the mouse model previously established by Vormoor and co-workers was employed (Vormoor et al., 2001). Mice were scanned on a regular basis using the PET-technique. To get a full and reliable picture of metastasis and to isolate occurring metastases, mice were dissected and screened macroscopically. For this project, FDG-PET did not prove to be the technique of choice as a lot of metastases were not detected in sequential PET imaging but were discovered when mice were finally euthanized and dissected due to their poor general condition. In some cases, metastases were visible when the sections of the PET scan were not summed up but rather examinated individually (see Figure 4.4). Accumulation of FDG in the heart muscle continued to prevent the appearance of lung metastases on PET images.

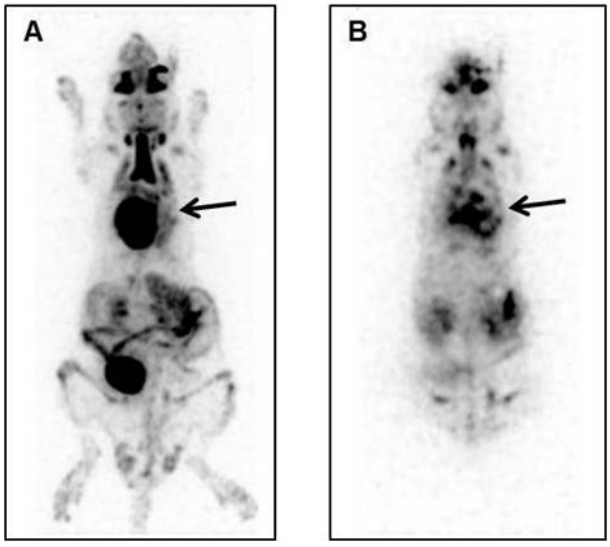

Figure 4.4: Representative PET images of a mouse transplanted intravenously with the cell line VH-64. A, image of all sections overlaid, accumulation of FDG in the heart (black arrow) prevents the appearance of lung metastases; **B,** one section alone allows visibility of lung metastases.

Mice that died due to transplantation-related toxicity within 3 weeks of transplantation (n=3) or due to unexpected circumstances, for example during PET scanning (n=13), were excluded from the analysis. The high number of unexpected deaths of experimental animals seems to result from disadvantageous housing conditions due to building activity on site. This might as well have accounted for decreased breeding success and resulting small transplantation numbers.

The remaining mice are listed in Table 4.2. Due to resulting small numbers there was insufficient statistical power to analyse tumour formation.

After i. v. transplantation of VH-64 and TC-71 into NOD/Scid mice metastases from lung, bone and bone marrow could be removed. From these metastases subclones were isolated and cultivated and subsequently re-transplanted into NOD/Scid mice.

Table 4.2: Ewing tumour formation in intravenously transplanted NOD/Scid mice. VH-64, TC-71 are ES/PNET cell lines; KM006, bone marrow derived subclone from mouse 006; K006, bone derived subclone from mouse 006; L006, lung derived subclone from mouse 006; BD-99, patient derived cell line. Mouse numbers in brackets had to be excluded from the study.

Cell lines	Mouse numbers	Number of transpl. cells	Tumour formation
VH-64	(001), (002), 003, 004, (005), 006	5×10^6	2/3
TC-71	(107), (108), 109, (128), (129), 130, 131, 132, (133)	2×10^6	3/4
KM006	r034, (r035), (r036)	5×10^6	1/1
K006	(r040), (r041), (r042), r052, (r053), r054	5×10^6	2/2
L006	r043, (r044), r045, (r049), r050, r051	$4.5\text{-}5 \times 10^6$	2/4
BD-99	455, 456	7×10^5	0/2

Re-transplanted organ-specific subclones developed in different organs (see Table 4.3). Although only relatively small numbers of transplantations were analysed it was obvious that the pattern of metastasis correlated very well with results reported previously (Vormoor et al., 2001). Specifically, all mice showed metastasis to the lung. Involvement of the bone only occurred after transplantation of VH-64 and re-transplantation of the bone-derived subclone K006. In total, nine out of ten mice developed bone marrow metastases. Cells of the re-transplanted lung metastases L006 were further able to establish a subcutaneous and an intraperitoneal metastasis.

Table 4.3: Pattern of metatstasis in tumour baring NOD/Scid mice. SC, subcutaneous tumour; IP, intraperitoneal tumour.

Cell lines	Mice with tumours	Lung	Bone	Bone marrow	Kidney	SC	IP
VH-64	004, 006	2/2	2/2	2/2	0/2	0/2	0/2
TC-71	130, 131, 132	3/3	0/3	2/3	0/3	0/3	0/3
KM006	r034	1/1	0/1	1/1	0/1	0/1	0/1
K006	r052, r054	2/2	1/2	2/2	1/2	0/2	0/2
L006	r043, r051	2/2	0/2	2/2	0/2	1/2	1/2

Analysis of the pattern of metastasis as well as the time to occurrence of clinical symptoms suggested that re-transplanted subclones derived from the lung or the bone marrow led to tumours in a shorter period of time. The difference in growth comparing lung-derived subclone to the parental cell line was statistically significant. In contrast, bone-derived subclones led to metastases in a comparable time to cell lines (see Figure 4.5). Analysis of the pattern of metastases for subclones shows additionally to the classically occurring lung, bone and bone marrow metastases subcutaneous and intraperitoneal as well as kidney involvement (see Table 4.3).

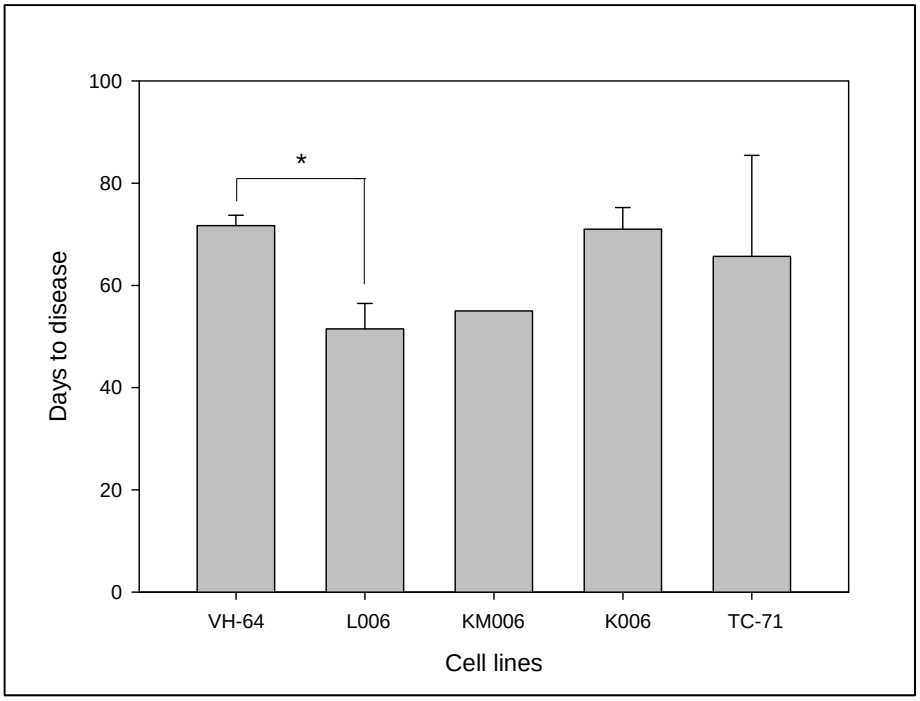

Figure 4.5: Mean time in days from transplantation to reaching of limits of the protocol. Asterisk marks P <0.050 in the comparison of cell line VH-64 to the deriving subclones (one way ANOVA, Bonferroni); L006, lung metastasis derived from mouse 006; KM006, bone marrow metastasis derived from mouse 006; K006, bone metastasis derived from mouse 006.

Therefore, these data suggest that the growth pattern as well as the shortened time to metastasis marks a more aggressive growth of subclones. However, taking the small transplantation numbers into account (due to breading problems on site and thus very low numbers of animals for the experiment) these data are not statistically robust and can only suggest a trend (see Table 4.3 and Figure 4.5).

4.4.2 *In vitro* characterisation of tissue specific subclones

The isolated subclones were validated as arising from the transplanted cell lines as well as further examined *in vitro* to characterise them and compare them to the parental cell lines.

4.4.2.1 Validation of clones – flow cytometry and PCR of fusion transcripts

All isolated secondary and tertiary subclones could be validated as human ES/PNET cells and therefore derived from the initially transplanted human cell line.

Therefore, the well-established ES/PNET marker CD99 was used in flow cytometry. All isolated metastases were positive for the surface-marker (see Figures 4.6 and 4.7).

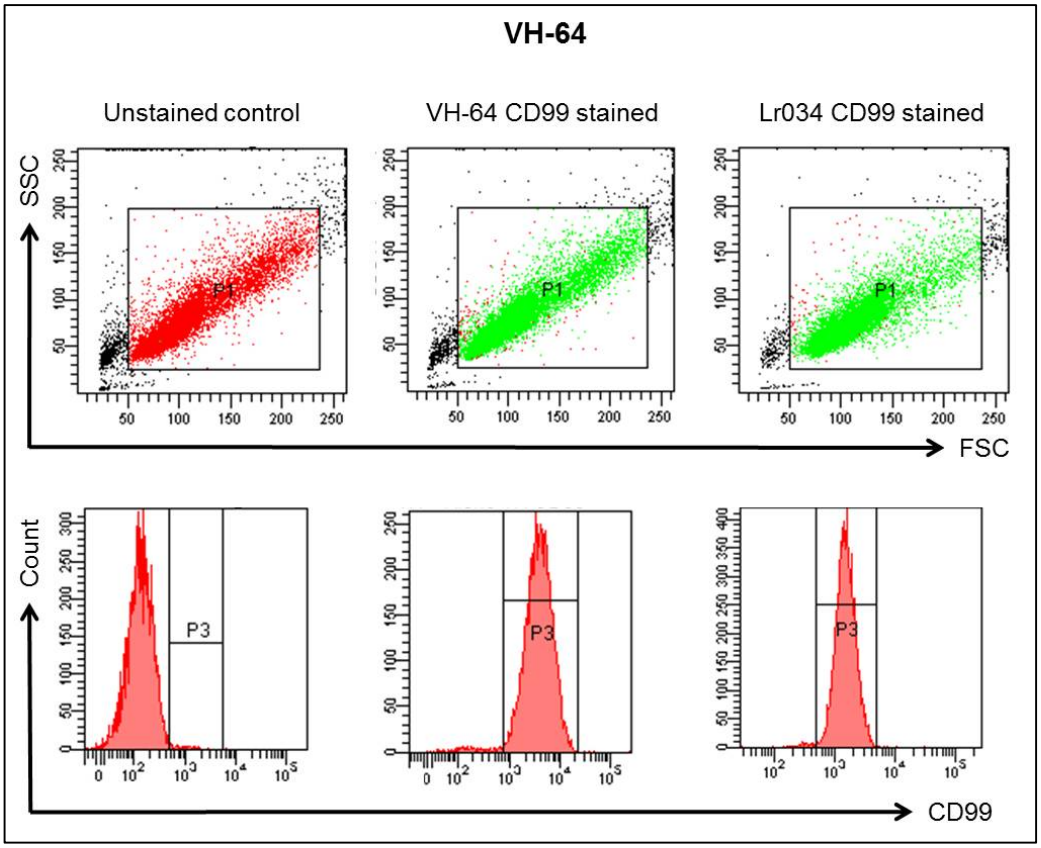

Figure 4.6: CD99 staining and flow-cytometric control of subclones derived from VH-64 transplanted mice. Additionally to the unstained and CD99-stained cells of the cell line VH-64 analysis of one representative subclone (Lr034) is shown. The first row shows forward and side scatter dot plots. Cells in P1 were analysed for their CD99-positivity which is shown in histograms in the second row. All subclones were positively tested for CD99 with more than 90% of cells being positive (above 10^3).

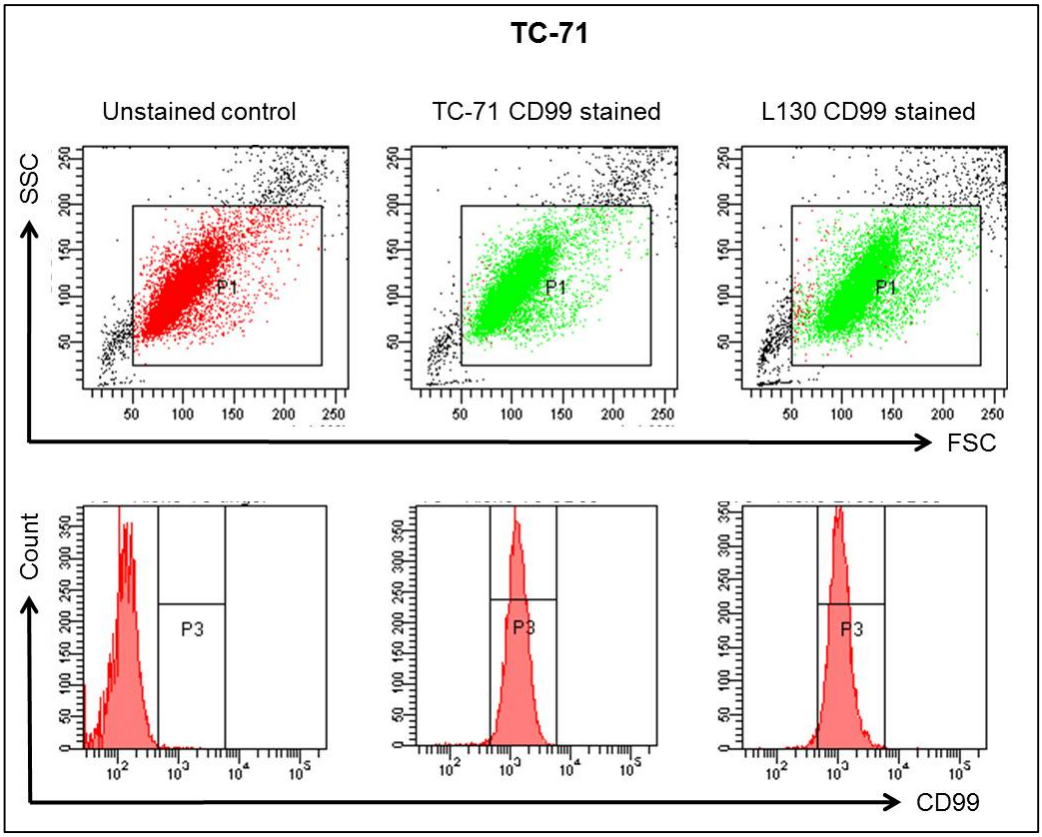

Figure 4.7: CD99 staining and flow-cytometric control of subclones derived from TC-71 transplanted mice. Additionally to the unstained and CD99-stained cells of the cell line TC-71 analysis of one representative subclone (L130) is shown. The first row shows forward and side scatter dot plots. Cells in P1 were analysed for their CD99-positivity which is shown in histograms in the second row. All subclones were positively tested for CD99 with more than 90% of cells being positive (above 10^3).

Additionally, all subclones were positively tested for the corresponding fusion transcripts by RT-PCR. Cells of the parental cell line TC-71 and subclones derived from this cell line harboured the EWS-FLI1 type 1 transcript, which results from the fusion of *EWS* exon 7 in frame with *FLI1* exon 6. VH-64 cells and deriving subclones harboured the EWS-FLI1 type 2 transcript occurring through fusion of *EWS* exon 7 in frame with *FLI1* exon 5. The resulting size

difference of the PCR products was distinguishable after agarose gel electrophoresis.

4.4.2.2 Colony assay

Colonies of the two cell lines VH-64 and TC-71 showed a slight difference in size. VH-64 colonies were smaller, which might be due to their smaller cell size (Figure 4.8; see also chapter 4.4.2.3). There was no difference visible between the parental cell lines and their derived subclones.

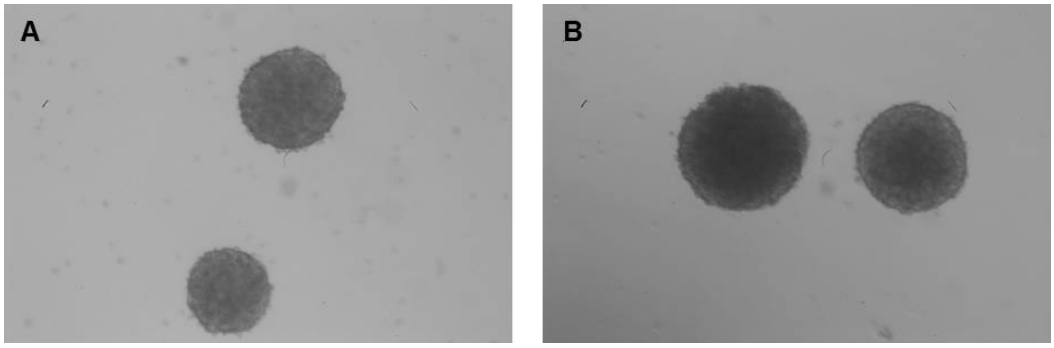

Figure 4.8: Appearance of colonies. A cell line VH-64, **B** cell line TC-71. Micrographs show the appearance of colonies in methylcellulose gels at x20 magnification.

No difference in clonogenicity of the parental cell lines VH-64 and TC-71 could be observed (data not shown).

4.4.2.3 Cytospins

Representative subclones were brought onto glass slides using the technique of cytospins to be able to analyse cells microscopically (Figure 4.9). Comparing cells of the cell lines VH-64 and TC-71 against each other, it is obvious that TC-71 cells and cells derived from this cell line are slightly bigger than VH-64 cells and its subclones.

However, all cells showed a relative high number and percentage of vacuoles also indicating a high metabolic activity and rate of replication.

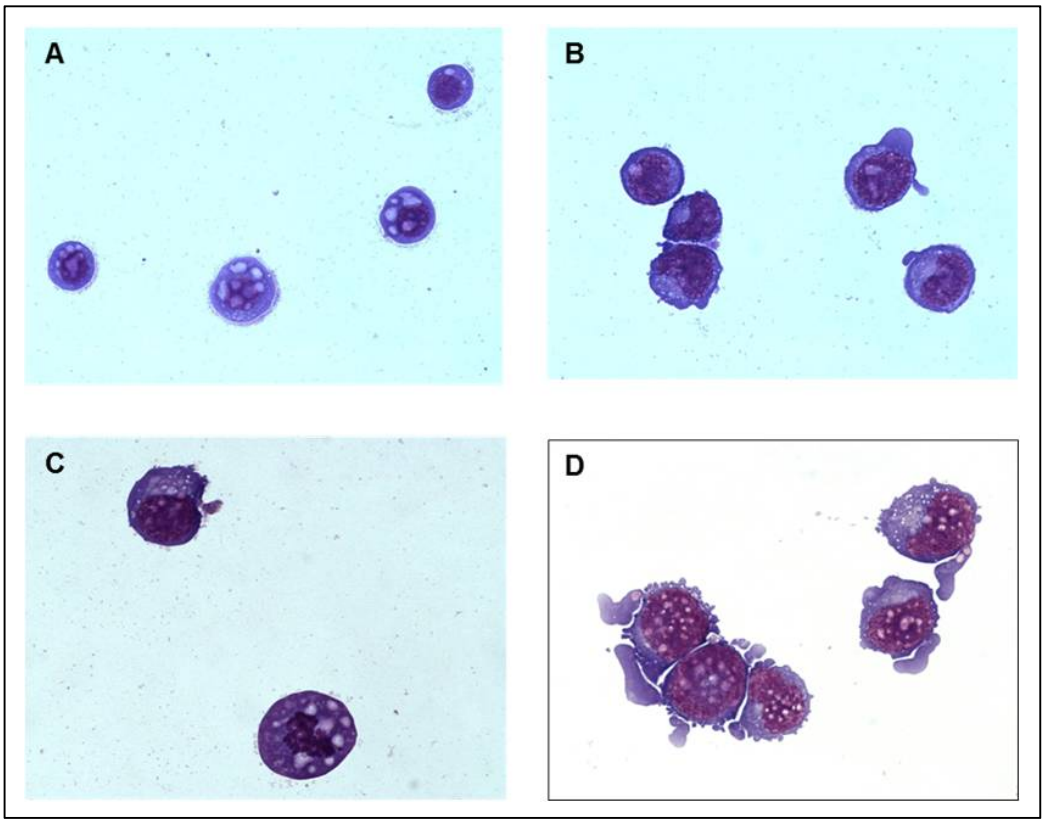

Figure 4.9: Microscopic examination of cytospins. A cell line VH-64, **B** cells of bone-derived subclone K006 after VH-64 transplantation, **C** cell line TC-71, **D** lung-derived subclone L131 after TC-71 transplantation. Magnification x64.

4.4.2.4 Further in vitro investigations

No differences in the proliferation of cell lines and their subclones could be observed *in vitro* in a MTT viability assay (data not shown).

Cell cycle analysis also did not reveal any changes comparing the organ-specific subclones against the parental cell lines (data not shown).

4.4.3 Expression profiling

Expression profiling was performed on selected subclones in comparison to the parental cell line. Microarrays were performed on cell lines VH-64 and TC-71 and 17 derived subclones. The project focussed on VH-64 and derived subclones and these could be analysed with statistical significance (see Tables 4.4 and 4.8). Due to small numbers of experimental mice and thus resulting small numbers of subclones it was not possible to include the second cell line TC-71 and derived subclones into the analysis.

4.4.3.1 Analysis of comparisons between organ-subclones directly

The analysis of microarrays of the different organ-specific subclones against each other was performed using the RankProd approach and subsequently GeneSpring and IPA (see also chapter 4.3.4) to be able to identify gene profiles that result from a more biological reasonable background. The performed comparisons are listed in Table 4.4.

Table 4.4: Comparisons of gene expression between the different VH-64-derived organ-specific subclones.

Name of comparison	1. group	2. group
Lung vs. bone	K004, K006, Kr054	L004, L006, L062, Lr034, Lr043, Lr051, Lr052, Lr054
Bone marrow vs. bone	K004, K006, Kr054	KM006, KM062, KMr043, KMr052, Kr054
Lung vs. bone marrow	KM006, KM062, KMr043, KMr052, Kr054	L004, L006, L062, Lr034, Lr043, Lr051, Lr052, Lr054

A comparison of "Lung vs. bone" metastases revealed that 314 genes were significantly higher expressed in lung than in bone while only three genes were significantly higher expressed in bone. "Bone marrow vs. bone" analysis of expression showed that 38 genes were significantly higher and five genes were less expressed in bone marrow compared to bone subclones. Comparing "Lung vs. bone marrow" metastases, 23 genes were recognised to be higher expressed in lung.

Possible organ-specific patterns for the different metastases could be filtered out of the three comparisons. This was achieved by looking at the differentially expressed gene profiles in more detail and comparing them against each other (see Table 4.5).

Table 4.5: Genes differentially expressed in more than one comparison. Values are fold-change values. Bm, bone marrow. Genes in bold were especially notable.

Gene	Description	Lung vs. bone	Lung vs. bm	Bm vs. bone	Specific for
AK1	adenylate kinase 1	-2.029		-2.923	bone
C9ORF16	chr 9 open reading frame 16	-2.486		-3.318	bone
CAMK2N1	calcium/calmodulin-dependent protein kinase II inhibitor 1	-2.377		-2.990	bone
CLPTM1	cleft lip and palate associated transmembrane protein 1	-2.026		-3.450	bone
CXCL10	chemokine (C-X-C motif) ligand 10	-5.101		-4.558	bone
FBXW2	F-box and WD repeat domain containing 2	-2.727		-3.302	bone
FCF1	FCF1 small subunit (SSU) processome component homolog	-2.323		-3.791	bone
GAMT	guanidinoacetate N-methyltransferase	-2.268		-2.337	bone
GAS1	growth arrest-specific 1	-2.690		-3.143	bone
GDF10	growth differentiation factor 10	-3.028		-3.929	bone
HERC6	hect domain and RLD 6	-2.638	-2.050		lung
IFI44	interferon-induced protein 44	-4.726		-2.855	bone
IFI44L	interferon-induced protein 44-like	-7.259		-4.433	bone
IFI6	interferon, alpha-inducible protein 6	-3.175		-3.726	bone
KRT8	keratin 8	-2.113		-2.979	bone
MDFI	MyoD family inhibitor	-2.176		-2.846	bone
MMP1	Matrix metallopeptidase 1	5.321	-2.999	15.955	
MRPL2	mitochondrial ribosomal protein L2	-2.271		-3.014	bone
OASL	2'-5'-oligoadenylate synthetase-like	-2.801	-2.138		lung
PDGFC	platelet derived growth factor C	-3.283		-3.508	bone
PRCC	papillary renal cell carcinoma	-2.630		-2.986	bone
PTP4A1	protein tyrosine phosphatase type IVA, member 1	-2.946		-3.137	bone
RAB4A	member RAS oncogene family	5.103		4.933	bone
RAD23B	RAD23 homolog B	-2.817		-3.752	bone

Table 4.6 continued.

Gene	Description	Lung vs. bone	Lung vs. bm	Bm vs. bone	Specific for
RPL23	ribosomal protein L23	-2.975		-3.459	bone
RPS11	ribosomal protein S11	4.987		7.652	bone
RSAD2	radical S-adenosyl methionine domain containing 2	-2.177	-2.554		lung
SLC16A3	solute carrier family 16, member 3	-2.338		-3.424	bone
SPAG16	sperm associated antigen 16	-3.335		-3.455	bone
UBE2M	ubiquitin-conjugating enzyme E2M	-2.452		-3.142	bone
ZYX	Zyxin	-2.888		-3.138	bone

The list shows 27 genes that might be specific for bone. Of these, 25 are less expressed in bone than in lung and bone marrow while two are higher expressed in bone than in the other metastases. Three genes were significantly up-regulated in lung metastases compared to bone and bone marrow metastases.

Several genes were especially noticeable due to their fold changes in the different comparisons of gene expressions. The genes CXCL10 (chemokine (C-X-C motif) ligand 10), GDF10 (growth differentiation factor 10), IFI44 (interferon-induced protein 44) and IFI44L (interferon-induced protein 44-like) were down-regulated in metastases isolated from the bone while the genes RAB4A (member RAS oncogene family) and PRS11 (ribosomal protein S11) were exclusively up-regulated in metastases taken from the bone.

The genes HERC6 (hect domain and RLD 6) and RSAD2 (radical S-adenosyl methionine domain containing 2) were up-regulated in lung metastases in comparison to bone and bone marrow metastases.

MMP1 (matrix metallopeptidase 1) showed very high expression values in especially bone-derived subclones and also lung metastases in comparison to bone marrow metastases.

4.4.3.2 Analysis of comparisons between VH-64 and the derived subclones

As described before, GeneSpring-derived comparative gene expression lists were analysed using IPA. A core analysis with default settings was performed for each comparison (for subclones included into the different comparisons see Table 4.6). The aim of these comparisons was to identify a sub-set of genes, which may be responsible for imprinting through the *in vivo* microenvironment.

Table 4.7: Comparisons of gene expression between the parental cell line VH-64 and deriving subclones. Microarrays from VH-64 were performed in biological replicates.

Name of created comparison	Parental line	Subclones
VH-64 vs. lung metastases	VH-64 (2x)	L004, L006, L062, Lr034, Lr043, Lr051, Lr052, Lr054
VH-64 vs. bone metastases	VH-64 (2x)	K004, K006, Kr054
VH-64 vs. bone marrow metastases	VH-64 (2x)	KM006, KM062, KMr043, KMr052, Kr054

In more detail, the numbers of up- and down-regulated genes listed for these comparisons varied. In the comparison of "VH-64 vs. lung metastases" the

expression of 523 genes was significantly up-regulated (> 2-fold) in lung metastases and for three genes was down-regulated. The comparison of "VH-64 vs. bone metastases" revealed up-regulation of the expression of 40 genes and down-regulation for six genes. Comparing "VH-64 vs. bone marrow metastases" 87 genes were discovered to be up-regulated, while three genes were down regulated.

The three comparisons showed 15 genes in common that were up-regulated and two genes that were down-regulated (see Table 4.7). When comparing the fold change of expression most genes showed values in the same range. Four genes have to be mentioned because their values were noticeable. CTCFL (CCCTC-binding factor (zinc finger protein)-like) showed an 6.9-fold up-regulation in bone marrow metastases, while it's up-regulation in metastases taken from the bone was nearly three times higher with a change of 18.7-fold and higher for lung metastases with a change of 10.3-fold.

A very high difference in fold changes for the different organ-specific subclones was also observable for RSAD2 (radical S-adenosyl methionine domain containing 2). While the fold change of bone and bone marrow metastases compared to the parental cell line was 6.0 and 5.1, respectively, it was 13.0 when comparing lung metastases against VH-64.

Furthermore, the genes RNF128 (ring finger protein 128) and TEX19 (testis expressed 19) were striking with extreme fold-changes in down-regulation compared to the parental cell line.

Table 4.8: Fold changes of genes differentially expressed in the organ-specific subclones in comparison to the parental cell line VH-64. Positive values indicate up-regulation, negative values indicate down-regulation in the subclones. Bm, bone marrow. Genes marked with 'D' were represented in duplicate. Genes in bold were especially noticeable.

Gene	Description	Mean fold change		
		VH-64 vs. lung metastases	**VH-64 vs. bone metastases**	**VH-64 vs. bm metastases**
AHNAK	AHNAK nucleoprotein	2.843	2.716	2.384
CTCFL	CCCTC-binding factor (zinc finger protein)-like	10.296	18.692	6.938
CTSK	cathepsin K	3.060	2.791	3.657
DLX1	distal-less homeobox 1	3.744	5.284	3.939
DLX2	distal-less homeobox 2	5.139	6.099	4.498
FAM26F	family with sequence similarity 26, member F	7.425	7.779	6.126
KCTD12	potassium channel tetramerisation domain containing 12	4.593	5.027	3.649
PPP1R9A	protein phosphatase 1, regulatory (inhibitor) subunit 9A	5.635	5.262	5.214
RNF128	ring finger protein 128	-10.207	-11.701	-14.697
RSAD2	radical S-adenosyl methionine domain containing 2	13.027	5.985	5.100
SOX11	SRY (sex determining region Y)-box 11	3.970	4.589	3.543
SPHK1	sphingosine kinase 1	3.216	2.269	3.226
TANC2	tetratricopeptide repeat, ankyrin repeat and coiled-coil containing 2	4.846	3.460	4.040
TBXA2R	thromboxane A2 receptor	3.331	4.393	2.760
TEX19	testis expressed 19	-17.495	-18.247	-17.159
TP53I3	tumor protein p53 inducible protein 3	3.375	3.240	3.492
ZNF618	zinc finger protein 618	4.734	2.969	4.531

Furthermore, some genes were regarded as interesting due to their functions and due in some cases to very high fold-changes in expression. In detail, these were ALDH1A1 (Aldehyde dehydrogenase 1 family, member A1) with a fold-change of -7.1 and IL-8 (Interleukin-8) with a fold-change -15.2 in the comparison of "VH-64 vs. bone metastases". Furthermore, in the comparisons of cell line against bone and lung NRG1 (Neuregulin 1) was differentially expressed with fold-change values of –8.6 and -7.5, respectively. VCAN (Versican) was up-regulated in lung and bone marrow metastases with fold changes of 6.5 and 5.8, respectively.

For the comparison of "VH-64 vs. lung metastases" the IPA core analysis revealed 143 canonical pathways that were most relevant based on the listed genes. For "VH-64 vs. bone metastases" IPA discovered 56 relevant canonical pathways and for the comparison of "VH-64 vs. bone marrow metastases" 161 canonical pathways were displayed as relevant.

The top canonical pathways for the comparisons of the parental cell line to the organ-specific metastases are listed in Table 4.9.

Table 4.9: Top Canonical pathways associated with the comparisons between VH-64 and the different organ-specific subclones.

Canonical Pathways	p-value	Ratio
VH-64 vs. lung metastases		
Hypoxia Signalling in the Cardiovascular System	0.0002	11.8%
Role of Pattern Recognition Receptors in Recognition of Bacteria and Viruses	0.0077	8.1%
Granzyme A Signalling	0.0079	17.6%
Cardiomyocyte Differentiation via BMP Receptors	0.0093	15.8%
Activation of IRF by Cytosolic Pattern Recognition Receptors	0.0163	7.8%
VH-64 vs. bone metastases		
Neuregulin Signalling	0.0123	2.1%
Glycerolipid Metabolism	0.0140	2.1%
Airway Pathology in Chronic Obstructive Pulmonary Disease	0.0157	12.5%
Hepatic Cholestasis	0.0253	1.5%
Aryl Hydrocarbon Receptor Signalling	0.0261	1.4%
VH-64 vs. bone marrow metastases		
p53 Signalling	0.0087	3.3%
T Cell Receptor Signalling	0.0095	3.0%
Sphingosin-1-phosphate Signalling	0.0119	2,7%
Glioma Invasiveness Signalling	0.0266	3.6%
Estrogen-Dependent Breast Cancer Signalling	0.0313	3.1%

Table 4.10 lists the biological and disease processes, which IPA discovered as most relevant to the gene lists of the comparisons.

The most relevant molecular and cellular process listed for all three comparisons is "Cellular Development". For the comparisons of lung and bone marrow metastases to the parental cell line the processes of "Cellular Growth and Proliferation" as well as "Cellular Movement" play a dominate role.

"Cancer" as a disease process is listed with very low p-values for all three organ-specific comparisons.

Table 4.10: Top biological functions of genes listed in the comparisons between VH-64 and the different organ-specific subclones.

Biological and disease processes	# molecules	p-value
VH-64 vs. lung metastases		
Diseases and Disorders		
Developmental Disorder	25	0.0000-0.0490
Cancer	104	0.0007-0.0490
Reproductive System Disease	17	0.0022-0.0248
Infectious Disease	9	0.0025-0.0025
Respiratory Disease	9	0.0025-0.0025
Molecular and Cellular Functions		
Cellular Development	65	0.0000-0.0497
Cellular Growth and Proliferation	74	0.0000-0.0490
Cellular Movement	42	0.0000-0.0490
Cell Morphology	25	0.0003-0.0490
Cellular Assembly and Organisation	25	0.0003-0.0490
VH-64 vs. bone metastases		
Diseases and Disorders		
Cancer	5	0.0013-0.0098
Neurological Disease	4	0.0015-0.0292
Dermatological Diseases and Conditions	2	0.0020-0.0121
Developmental Disorder	1	0.0020-0.0020
Genetic Disorders	5	0.0020-0.0425
Molecular and Cellular Functions		
Cellular Development	9	0.0001-0.0482
Cell Cycle	3	0.0001-0.0463
Cell Morphology	5	0.0001-0.0482
Cellular Movement	6	0.0002-0.0482
Cellular Assembly and Organisation	4	0.0002-0.0311
VH-64 vs. bone marrow metastases		
Diseases and Disorders		
Cancer	23	0.0047-0.0415
Connective Tissue Disorders	1	0.0047-0.0047
Developmental Disorder	4	0.0047-0.0233
Genetic Disorders	10	0.0047-0.0415
Hematological Diseases	4	0.0047-0.0130
Molecular and Cellular Functions		
Cellular Development	12	0.0006-0.0450
Cellular Growth and Proliferation	5	0.0016-0.0233
Cellular Movement	8	0.0026-0.0415
Amino Acid Metabolism	1	0.0047-0.0047
Cell-To-Cell-Signalling and Interaction	5	0.0047-0.0187

4.4.3.3 Validation of microarray results with qRT-PCR

Selected genes were used to validate the microarray results. ALDH1A1 as well as MEG3 showed differential expression when bone-derived subclones were compared with the parental cell line VH-64. Microarray results suggested up-regulation of ALDH1A1 and down-regulation of MEG3. NRG1 was chosen due to a suggested down-regulation in bone- and lung-derived subclones. Due to microarray results APOC1 was down-regulated in bone marrow metastases. All genes were selected because a literature research revealed research results for their function in proliferation, growth and other supportive functions and appearance in other types of cancer. Results of the performed qRT-PCRs are displayed in Figure 4.10.

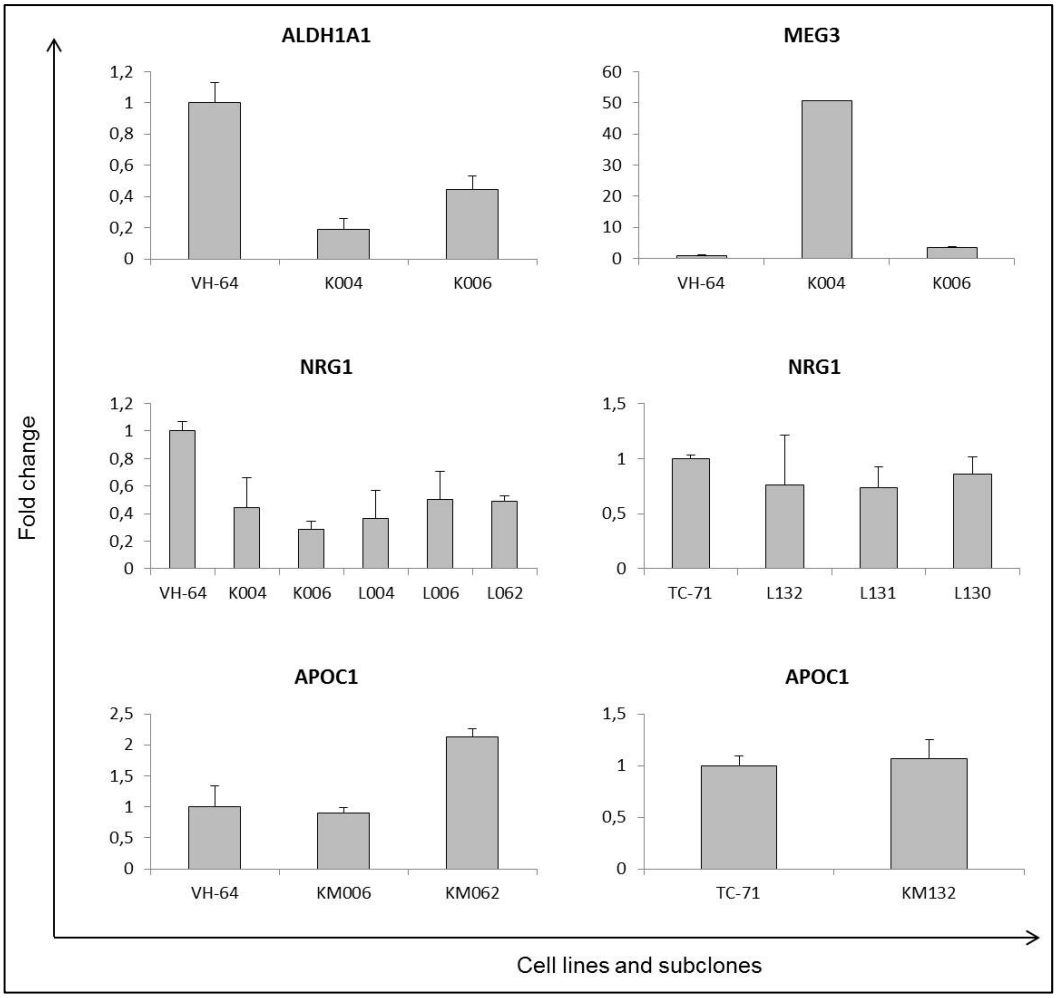

Figure 4.10: qRT-PCRs performed for the validation of the microarray experiment. Cell lines VH-64 and TC-71 as well as primary organ-specific subclones were tested for the expression of ALDH1A1, MEG3, NRG1 and APOC1. Values are displayed as fold changes relative to the according parental cell line. K004, K006 are bone-derived subclones; L004, L006, L062, L132, L131, L130 are lung-derived subclones; KM006, KM062, KM132 are bone marrow-derived subclones.

Although the same RNA samples were used for both experiments, fold-change values from qRT-PCR and microarrays cannot be directly compared as the methods are quite different and samples were handled in a different way.

For NRG1 and APOC1 TC-71 and -derived subclones from lung respectively bone marrow were tested additionally to VH-64 and derived subclones and showed the same trend as VH-64-derived subclones.

All verified genes showed the same trend previously suggested by microarray results. For ALDH1A1 fold-changes derived from the qRT-PCR data suggest a knock-down in subclones compared to the parental cell line (K004, 0.19; K006, 0.44). The qRT-PCR derived fold-changes for NRG1 in the VH-64-derived subclones varried with little variation from 0.28-fold to 0.5-fold (K004, 0.44; K006, 0.28; L004, 0.36; L006, 0.5; L062, 0.49). Down-regulation in the TC-71-derived subclones is less obvious with values of 0.73-fold to 0.86-fold (L132, 0.76; L131, 0.73; L130, 0.86).

For MEG3 the two tested bone-derived subclones showed up-regulation (K004, 50.6; K006, 3.63) compared to VH-64 but the values showed high variability. For APOC1 a suggested up-regulation in bone marrow could not be entirely verified as one of the VH-64-derived subclones showed a slight down-regulation in comparison to the parental cell line (KM006, 0.90; KM062, 2.13). For the only TC-71-derived bone marrow subclones the values was 1.06-fold.

However, due to the preliminary character of the data derived from qRT-PCR, it is not possible to make a reliable statement about significance and variability of values. The qRT-PCR experiments would have to be repeated with more subclones derived from the different tissues investigated (lung, bone and bone marrow).

4.5 Discussion

Using a previously established mouse model of ES/PNET metastasis it was possible to isolate organ-specific metastases (Vormoor et al., 2001). The initial hypothesis that subclones would develop a preferential tendency to metastasise to specific organs was not proven. It can only be assumed that after re-transplantation of subclones cells derived from lung metastases were able to establish in lung and bone marrow as the re-transplanted bone marrow-derived subclone was as well. However, it was not possible to analyse these results statistically due to small experimental numbers (see Table 4.3).

Analysis of the time to metastasis after re-transplantation of the lung-derived subclone showed that these cells were able to establish metastases in a significantly shorter period of time compared to the parental cell line and the bone-derived subclone. There was no difference between the cell lines VH-64 and TC-71. These data suggest that subclones were selected *in vivo* for their aggressiveness and proliferation rates. However, *in vitro* analysis of subclones showed that there was no difference in growth behaviour, cell cycle or clonogenicity. Morphologically subclones of VH-64 and TC-71 appeared to contain slightly more vacuoles and therefore might have a slightly higher metabolic rate compared to the parental cell lines which might indicate a higher activity (see Figure 4.8).

Expression profiling of cell lines and organ-specific subclones revealed a subset differentially expressed in all subclones compared to the parental cell line VH-64. This subset might be composed of genes that play a general role in metastasis of ES/PNET and that advance aggressiveness and proliferation of

cells. However, it remains possible that this subset might be influenced by the fact that metastases were taken back into culture after isolation from the mouse. Interesting candidate genes will have to be further analysed to clarify their role in metastasis of ES/PNET. Amongst these genes might be the two genes CTCFL and RSAD2 which were extremely up-regulated in all subclones compared to the cell line. Furthermore, RNF128 and TEX19 were down-regulated to a great extend in comparison with the cell line VH-64.

CTCFL, also known as BORIS, is an 11-zinc-finger factor involved in gene regulation. It utilizes different zinc fingers to bind varying DNA target sites thus activating transcription and is also able to influence histone methylation. CTCFL also positively influences hTERT (human telomerase reverse transcriptase) transcription, conferring cells with the ability to divide indefinitely (Nguyen et al., 2008; Renaud et al., 2010).

RSAD2 is best known for its vital role in the anti-viral response after infection with different types of viruses (Jiang et al., 2008), where it inhibits steps in viral proteins and/or RNA biosynthesis (Jiang et al., 2010).

RNF128, also known as GRAIL, is an E3 ubiquitin ligase associated with T cell tolerance. Until now not much is known about RNF128 in other contexts, however, GRAIL-deficient naive T cells, after activation, exhibited increased proliferation and cytokine expression (Nurieva et al., 2010). Thus, down-regulation of RNF128 in ES/PNET cells might influence proliferation positively.

The function and role of TEX19 remains to be fully elucidated. It is mainly expressed in adult testis and in undifferentiated embryonic stem cells (Kuntz et al., 2008).

The analysis of gene expression of organ-specific subclones directly against each other revealed subsets of genes that might harbour candidate genes that mirror the specific influence of the microenvironment in the organs from which the metastases were isolated. For bone down-regulation of CXCL10, GDF10, IFI44 and IFI44L as well as up-regulation of RAB4A and RPS11 seemed to be specific.

CXCL10 is secreted by several cell types in response to IFN-γ and binds to CXCR3. Expression of this chemokine leads to pleiotropic effects. These include stimulation of monocytes, migration of natural killer and T cells, as well as modulation of adhesion molecule expression. However, overexpression of CXCL10 is unfavourable for the survival and proliferation of cancer cells (Nagpal et al., 2006). Down-regulation of CXCL10 by bone-derived subclones might indicate that cells are trying to prevent a host immune response. This has been shown to play a role in tumour progression of ES/PNET (Zhang et al., 2003; Berghuis et al., 2011).

GDF10 is also known as BMP3B (bone morphogenetic protein 3B). BMPs are multifunctional cytokines involved in skeletal development and bone formation. In the exquisite interplay of BMPs, GDF10 is an antagonist of BMP2, which is usually expressed by osteoblasts and potently induces osteoblast differentiation in a variety of cell types (Marie et al., 2002). Thus it might be reasoned that down-regulation of GDF10 leads to increased osteoblast formation.

The function of IFI44 is not entirely understood. However, there is indication, that overexpression of IFI44 cDNA impairs proliferation *in vitro* through IFN-alpha activation, even in cells that are not responsive to IFN-alpha. A model was proposed suggesting that IFI44 binds intracellular GTP, thus abolishing

extracellular signal-regulated kinase (ERK) signalling and resulting in cell cycle arrest (Hallen et al., 2007).

Relatively little is known about RAB4A. It is, however, known that it plays a role in receptor recycling. Some receptors such as PDGF (platelet derived growth factor)-beta receptor recycle back to the membranes through vesicular transport dependent on the small GTPase Rab4a (Hellberg et al., 2009). Thus, up-regulation of RAB4A might be supportive for cell proliferation and migration through recycling of PDGF-beta receptor back to the cell surface.

RPS11 encodes a ribosomal protein that is a component of the 40S subunit of the ribosome. Up-regulation of RPS11 might indicate an increased protein synthesis and thus higher metabolic activity of the bone-derived subclones.

Furthermore, HERC6 and RSAD2 might be specific markers for lung metastases as they were significantly up-regulated in lung subclones compared to the parental cell line.

Comparing the three subclone-types it was also obvious that MMP1 is up-regulated especially in bone but also in lung metastases while it is not expressed to a greater extend in bone marrow metastases. MMP1 encodes for a secreted enzyme which breaks down the interstitial collagens, types I, II, and III. This is why it would have been expected to be up-regulated in metastases from the bone especially to support growth within the bone microenvironment, which contains collagen I to a great extent.

Interesting genes and their functions are finally summed up again in Table 4.10.

Table 4.11: Notable genes flagging up in the different comparisons and their most striking functions known so far.

Gene	Regulation	Functions and processes
VH-64 vs. Metastases		
CTCFL	↑ in metastases	DNA-binding, promoter binding, transcription activator activity
RSAD2	↑ in metastases	Relatively unknown, catalytic activity
RNF128	↓ in metastases	Ligase activity, ubiquination of transmembrane proteins
TEX19	↓ in metastases	unknown
Metastases amongst each other		
CXCL10	↓ in bone metastases	Chemokine-activity, receptor-binding, cell-cell-signalling
GDF10	↓ in bone metastases	Cytokine activity, growth factor activity
IFI44	↓ in bone metastases	Relatively unknown, response to virus
IFL44L	↓ in bone metastases	Relatively unknown, immune response
RAB4A	↑ in bone metastases	ATP-, GTP- and GDP-binding, signal mediation
RPS11	↑ in bone metastases	Gene expression, translation
HERC6	↑ in lung metastases	Ligase activity, protein-modification
RSAD2	↑ in lung metastases	See above
MMP1	↑ in bone and lung metastases	metalloendopeptidase activity, collagen catabolic process

A further point one has to bear in mind is that there is a clonal variation influencing the comparisons and the resulting gene lists. As each metastasis derives from one cell/clone the grouping of the organ-specific metastases has to be seen critical.

4.6 Conclusions

The described experiment indicates that there is no preference of cells derived from organ-specific metastases to re-metastasis to their organ of origin. This is why subsequent experiments will have to focus on specific genes, which were identified in the mentioned comparisons. Gain-of-function or loss-of–function experiments with certain genes of interest might clarify whether there is a mechanism regulating the organ-specific metastasis in ES/PNET and whether the specified genes have a potential to serve as markers or even therapeutic targets. However, to be able to give a final answer to the hypothesis this experiment will have to be repeated with primary material for transplantations. It is very likely that the fact of pre-selection for high proliferation rates and aggressiveness of cells in cell culture and the fact that cell lines lack a certain variety of cells influence this experimental setting negatively.

Furthermore, it can be concluded that the identified genes in the comparison of the parental cell line against the organ-specific metastases stand for an increased aggressiveness and proliferation potential. However, further experiments will have to follow as functions and role of most of the interesting genes is still not entirely clear. These experiments could involve knockdown experiments and subsequent *in vivo* examination as well as *in vitro* experiments on functions.

5. Chapter – The role of CXCL12 in metastasis of Ewing's sarcoma

5.1 Introduction

CXCR4 is overexpressed in a variety of different cancer types and cancer cell lines. The role of the CXCL12/CXCR4-axis in breast cancer, prostate cancer and melanoma has been well established (see chapter 1.3.2) and its potential role in ES/PNET is discussed in chapter 1.3.3.

RNA interference (RNAi) was used to knockdown CXCR4 in ES/PNET cell lines to be able to investigate features of the role of this cytokine/receptor-couple.

5.1.2 RNA interference

In 2006, Craig Mello and Andrew Fire were honoured with the Nobel Prize in Physiology or Medicine for their work on RNAi (Zamore, 2006). They and their co-workers were the first to demonstrate that double-stranded RNA (dsRNA) triggers gene-silencing in *Caenorhabditis elegans* (Fire et al., 1998). Shortly after the discovery, it became clear that mammalian cells operate with the same RNAi mechanism and that this could potentially be used for therapeutic approaches (Elbashir et al., 2001).

Subsequently, this landmark discovery developed into a technique that is now widely used to target genes directly by silencing through RNAi, enabling researchers to investigate the role of genes in a very elegant and isogenic way.

5.1.2.1 Gene expression control in eukaryotic cells

There are many mechanisms controlling the expression of genes. Pre-transcriptional control is achieved through epigenetic modifications of the DNA. Post-transcriptionally RNAi offers a natural possibility of gene expression control. This mechanism is believed to regulate vertebral differentiation and development. Due to the complexity of the RNAi processes and further features of gene expression control, the topic will not be described in all details (see review Carthew and Sontheimer, 2009).

After its discovery and alongside its investigation, the mechanism of RNAi has been used to develop techniques which are able to specifically knockdown and investigate genes of interest (see Figure 5.1).

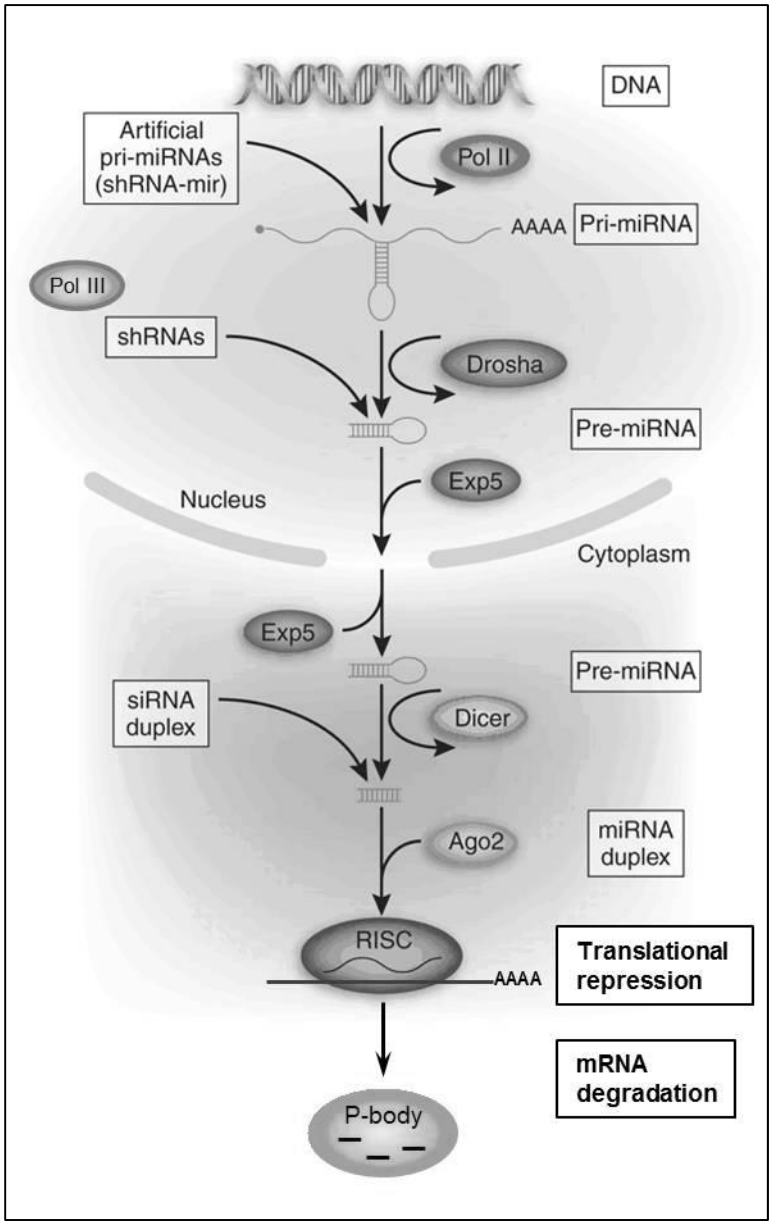

Figure 5.1: The RNAi pathway in vertebrate cells. The left side of the picture presents possibilities of interference into the natural process of RNAi by introducing siRNAs (small interfering), shRNAs (small hairpin RNAs) transcribed by RNA Pol III or artificial pri-miRNAs (primary micro RNA) into the cells. Not all factors involved in the process are shown. Ago2, Argonaute-2; Dicer, Helicase; Drosha, RNAse III; Exp5, Exportin-5; Pol II and Pol III, polymerases II and III; RISC, RNA-induced silencing complex (Cullen, 2005).

The natural process of RNAi in vertebrates is driven by endogenously encoded micro RNAs (miRNAs). These are single-stranded and composed of

~22 nucleotides (nt) which match part of the sequence of a specific mRNA. In the human organism the number is currently estimated to up to 1000 miRNAs which control the expression and activity of approximately 30% of the human genes (Kurreck, 2009). This gives RNAi an impact that is as important as the impact of transcription factors in gene regulation.

Polymerase II transcribes a ~85nt long primary miRNA (pri-miRNA). The miRNA is part of a hairpin loop as secondary structure. Subsequent to transcription, the pri-miRNA is processed by the RNAse III Drosha into a pre-miRNA by cleaving the hairpin ~22nt away from the loop structure leaving a characteristic 2nt 3'-overhang (Lee et al., 2002, 2003). Transported to the cytoplasm by Exportin-5, the pre-miRNA is bound by the helicase Dicer. It recognises the characteristic overhang and cleaves ~22nt away from the end so that the loop is removed and a second 2nt 3'-overhang is produced (Bernstein et al., 2001; Elbashir et al., 2001; Zhang et al., 2004).

The resulting duplex is bound by one of the four members of the Argonaute subfamily of proteins (Ago proteins) and becomes part of the forming RISC (RNA-induced silencing complex). This programming of RISC allows the specific down-regulation of homologous mRNA (Cullen, 2004).

Two steps are necessary to complete RISC assembly: loading and unwinding of the miRNA. Similar aspects apply to small interfering RNA (siRNA) duplexes that can be introduced artificially. It is not yet completely known how RISC is loaded in mammals. However, there seem to be two possible pathways – a Dicer-dependent one and a Dicer-independent one.

Once the duplex is loaded onto the RISC, one of the two strands has to be discarded in order to make a single strand able to bind to homologous mRNA.

The determination of the strand to be cleaved is not random but follows thermodynamic rules: The thermodynamic stability of the bases 1-4 at each end is determining and the strand with a less stable 5'-end serves as the guide strand and remains bound to RISC (Khvorova et al., 2003; Schwarz et al., 2003).

All four Ago proteins can repress translation of gene transcripts, but only one of them, AGO2, has a cleavage (slicer) activity (Liu et al., 2004). This leads to the passenger strand of the siRNA duplex being degraded as well as the bound mRNA that is supposed to be destroyed. As target cleavage requires extensive base pairing; only high complementary siRNA duplexes are processed by AGO2. Most endogenous duplexes, however, harbour some mismatches.

The Slicer-independent version of the unwinding process of small RNA duplexes is still not understood entirely. Recent findings suggest, that mismatches in specific regions of the small RNA duplexes guide the process of slicer-independent unwinding (Kawamata et al., 2009; Yoda et al., 2010). There is strong evidence for the assembly of many different factors involved in the decay of RNA, such as decapping proteins, nucleases and others in a complex called p-body (Franks and Lykke-Andersen, 2008). Further investigations, however, are required to fully understand this mechanism.

Both, slicer-dependent and –independent processes lead to elimination of passenger strand debris or the whole passenger strand from the RISC. Debris and whole strands are immediately degraded by nucleases so that the process is essentially irreversible (Kawamata and Tomari, 2010).

Furthermore, the Ago proteins can also be loaded with single-stranded siRNA via a so called "bypass loading". This fact can be used to specifically knockdown genes with exogenous siRNAs that are transferred into cells (Kurreck, 2009).

5.1.2.2 Using shRNA for silencing of genes

SiRNAs form a class of double-stranded RNAs which play a decisive role in biology. Amongst others, the most notable role is the involvement of siRNA in RNAi, where it interferes with the transcrips of specific genes and thus their expression.

Quickly, siRNA had been proven to offer a possibility of gene silencing *in vitro* and *in vivo* (de Fougerolles et al., 2007) although there are certain disadvantages of naked as well as of lipid-complexed siRNA. One of these is the delivered siRNA has a short half-life. The intracellular expression of siRNA for a sustained silencing of genes was achieved through especially constructed DNA vectors which were transferred into cells. In general, the so called short hairpin RNA (shRNA) is expressed through polymerase III (Pol III) promoters and the RNAi machinery can be employed for the purpose of post-translational gene control (Brummelkamp et al., 2002; Paddison et al., 2002).

The usage of viral approaches for transfection of plasmid-encoded shRNA leads to a stable expression of shRNA and subsequently knockdown of targeted mRNA following integration of the viral vector into the host genome. However, there are also certain disadvantages to viral systems such as antiviral responses being triggered through the presence of viral dsRNA resulting in expression of factors that lead to an inhibition of the complete translation and subsequently may lead to apoptosis of cells (Williams, 1997). Furthermore, the use of viral vectors that cause insertion of DNA might result in destruction or alteration of genes or their expression.

5.1.3 The vector pEPI-1 and the promoter H1

In this project, a shRNA approach was used to attempt knockdown of CXCR4 in ES/PNET cell lines using the vector pEPI-1 (see chapter 4.1.4) and the pol III promoter H1.

The pEPI-1 vector is a non-viral and episomal vector that does not integrate into the host's genome. Therefore, it is less likely to interfere with any existing genetic functions and furthermore does not rely on any position-depending expression and thus has predictable characteristics.

The central element of this vector is the scaffold/matrix attachment element (S/MAR) derived from the 5'-region of the human gene interferon β which allows the attachment of certain chromatin domains to the protein skeleton of the nucleus which makes vectors using this element very likely to be stabely expressed and to be passed on during division of cells (Bode et al., 1992). However, S/MARs have further advantages such as promotion of transcription and replication of the vector using the cells machinery as well as protection of the alien genetic material.

Furthermore, pEPI-1 harbours a Kanamycin/Neomycin-resistance gene allowing for selection of positive clones during the cloning process as well as for the resulting cell line.

This vector is stable within cells for several hundred generations without any necessity of selective pressure (Piechaczek et al., 1999).

The described vector was used as a basis construct. It was necessary to insert a pol III promoter for the expression of shRNA. In this case, the H1-RNA gene promoter was chosen as pol III promoter because it creates a small RNA transcript lacking a polyadenosine tail. Furthermore, it has a precise start of

transcription and a termination signal involving five thymidine bases in a row (T5). The most significant advantage is the fact that the transcribed shRNA is cleaved after the second uridine (U) of the termination site. This produces a transcript with ends resembling the ones of synthetic siRNAs as it also contains two 3' overhanging T or U nucleotides (Baer et al., 1990; Brummelkamp et al., 2002).

5.2 Aims

CXCR4 plays a role in different cancer types such as breast cancer and prostate carcinoma, and there is evidence that the CXCR4/CXCL12-axis might play a role in the metastasis of ES/PNET, including consistent high expression in nearly all ES/PNET cell lines and many primary tumours. Nevertheless, there is still a need for a direct proof of this assumption. Given this, a knockdown system for CXCR4 would allow researchers to investigate the importance and role of CXCR4 in ES/PNET and the consequences of a CXCR4-knockdown in ES/PNET cell lines.

The specific aims of this chapter were as follows:

- to create a knockdown vector against the cytokine receptor CXCR4
- to investigate functionality and influence of the knockdown vector

5.3 Methods and Materials

5.3.1 Cloning strategy for the knockdown construct

The extra-chromosomal vector pEPI-EGFP (Figure 5.2) is a derivate of pEPI-1 containing an additional sequence for the eGFP gene and was kindly provided by Prof. Dr. Lipps (University Witten-Herdecke, Witten, Germany). The aim of the cloning strategy was to insert a pol III promoter as well as a sequence coding for a shRNA directed against CXCR4 into pEPI-EGFP to create a knockdown plasmid.

The pSUPER (Oligoengine, Seattle, USA; Figure 4.2) vector system was used to create a cassette containing the H1-RNA pol III promoter and a custom DNA sequence encoding for a shRNA against CXCR4.

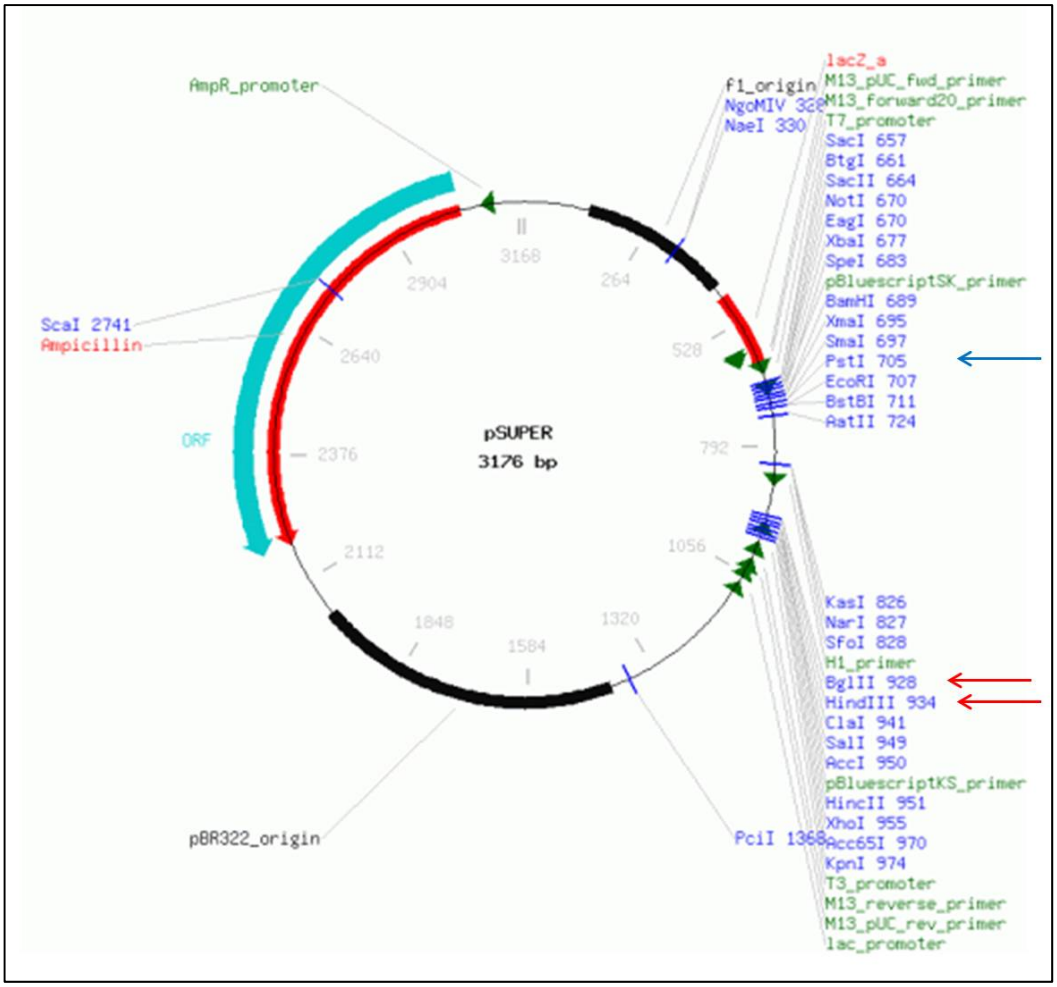

Figure 5.2: Map of the pSUPER vector. Important sites are H1 pol III promoter: 708-934; pUC origin: 1373-2040; PstI: 705; BglII: 928; HindIII: 934; KpnI 974. Restriction sites used for insertion of oligonucleotide for shRNA marked with red arrow, restriction sites used for excision of cassette containing H1 pol III promoter and oligonucleotide marked with blue arrow.

A pair of custom oligonucleotides was purchased (Purimex, Grebenstein, Germany) that contained amongst other features unique sequences in sense and antisense orientations (capital letters) derived from the mRNA transcript of CXCR4, separated by a spacer (Wang et al., 2005). The antisense strand of the resulting shRNA duplex hybridises to the target region of the CXCR4-mRNA (yellow).

```
5′  gatccccCACCCTGTTTCCGTGAAGAAttcaagagaTTCTTCACGGAAACAGGGtttt
3′      gggGTGGGACAAAGGCACTTCTTaagttctctAAGAAGTGCCTTTGTCCCaaaa

tctaga aag      3′
agatct ttcagct  5′
```

The 5'-end of the forward oligonucleotide formed an altered BglII restriction site (in red, alteration in blue), that is able to bind to a BglII overhang in the restricted vector but can afterwards not be used as a BglII restriction site again and a SalI restriction site (in green). Furthermore, an XbaI restriction site (in purple) was inserted after the T5 sequence.

The whole cassette containing the H1 pol III promoter, the sequence coding for the shRNA directed against CXCR4 and the additional XbaI restriction site was restricted using this XbaI restriction site and the PstI restriction site up-stream of the H1 pol III promoter. To avoid methylation of especially the XbaI restriction site a dam$^-$ *E. coli* strand was used (see chapter 2.1.1) which is impaired in its ability to methylate DNA.

Both restriction sites, XbaI and PstI are located within the MCS (multiple cloning site) of pEPI (see Figure 4.3) so that the cassette could be ligated into pEPI. Hereafter, the resulting vector is called pEPI-EGFP-shCXCR4.

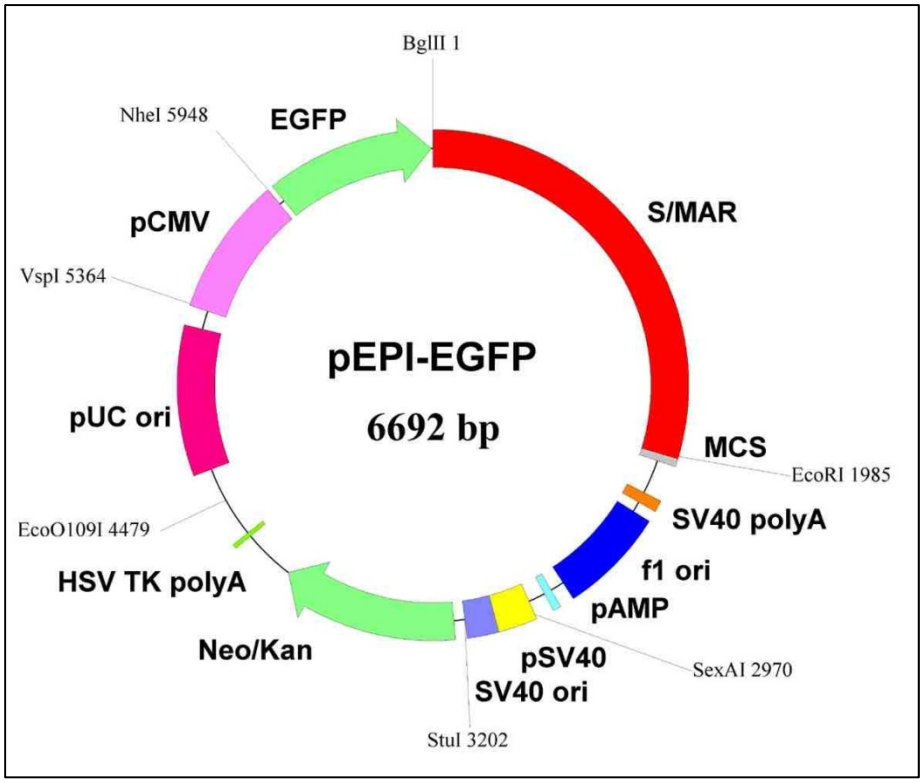

Figure 5.3: Map of the pEPI-EGFP vector. Important sites are S/MAR: 1-1983; Neomycin/Kanamycin resistance: 3251-4046; PstI: 1994; KpnI: 2006; XbaI: 2028. Restriction sites are located within the MCS (provided by Prof. Dr. Lipps).

All restrictions were verified by PCR, all ligations were tested with test restrictions and finally plasmids were sequenced (primers see chapter 3.3.15).

As a control construct the cassette containing H1 pol III promoter and a sequence coding for a shRNA directed against the fusion transcript MLL-AF4 was cloned into pEPI-EGFP which should not affect ES/PNET cells because this fusion does not occur in ES/PNET. The pSUPER containing the custom DNA construct coding for the shRNA was kindly provided by Dr. Frida Ponthan. The cassette was linearised using the restriction enzymes PstI upstream of the H1 promoter and KpnI downstream of the custom DNA sequence. KpnI is also contained in the MCS of pEPI-EGFP so that the cassette could be ligated into the

appropriately digested vector and be subsequently used as a control. Following, the resulting vector is called pEPI-EGFP-shMA6-Mut1.

5.3.2 Fluorescence activated cell sorting

TC-71 and VH-64 cell lines were transfected using Lipofectamin™ according to chapter 3.5.6. Cells were cultured until approximately 5×10^6 cells could be harvested from a T25 culture flask (90% confluence).

The protocol from chapter 3.5.8 was used to sort cells. When enough cells could be collected, 300-500 sorted cells were re-acquired to assess purity of the desired population.

5.3.3. G418 selection of clones

Enriched clones derived from fluorescence activated cell sorting were further treated with G418 (aminoglycoside antibiotic similar in structure to gentamicin B1; GIBCO). This blocks the polypeptide synthesis by inhibiting the elongation step in both prokaryotic and eukaryotic cells. Resistance to this antibiotic is delivered by the Neo/Kan gene from Tn5, which codes for an aminoglycoside 3'-phosphotransferase and is contained in the sequence of pEPI-EGFP.

Transfected and then FACS-sorted cultures were treated with different end concentrations of G418 ranging from 100 to 500µg/ml. The determined concentrations for selection of the different pEPI-EGFP clones were 200µg/ml

for transfected VH-64 cells and 300µg/ml for transfected TC-71 cells. Treatment was administered for a minimum of 14 days.

5.4 Results

5.4.1 Examination of stability of pEPI-EGFP in Ewing's sarcoma cell lines

To investigate the possibility of transfection and the stability of pEPI-EGFP in ES/PNET cell lines, TC-71 and VH-64 were transfected with the plasmid using Lipofectamin™. Subsequently, cells were tested for the production of eGFP using a flow-cytometer. Furthermore, the transfected cells were sequentially sorted using FACS and the cell lines resulting from the different and sequential sorts were examined for their fluorescence over a longer period of time. Data are shown for TC-71 and pEPI-EGFP-transfected TC-71 (Figure 5.4).

Transfection resulted in very low numbers of cells being positive for the plasmid and thus fluorescent. With sequential sorting using FACS fluorescence-positive cells could be enriched. Therefore, transfected cells were sorted, the selected cells were cultivated until enough cells for a second sort could be harvested. The resulting three different cultures were followed up with flow cytometry demonstrating that the cells of the second sort were still positive two month post-transfection (Figure 5.4B).

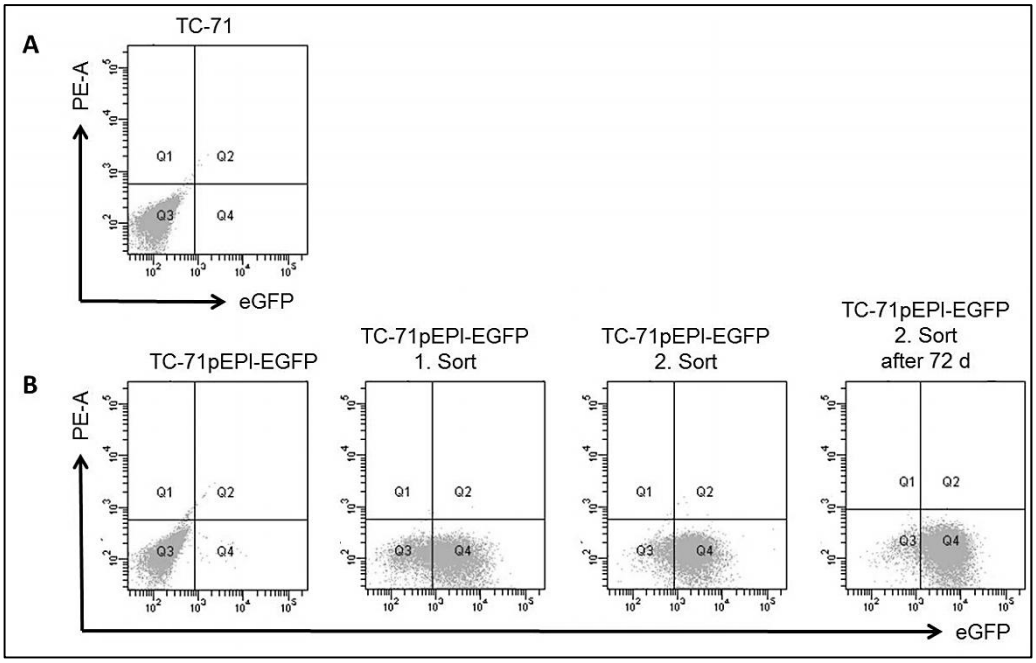

Figure 5.4: Flow-cytometric verification of e-GFP positivity of pEPI-EGFP-transfected TC-71 cells. A, negative control TC-71; **B**, pEPI-EGFP-transfected TC-71 cells, first sort, second sort and second sort after 72 days (cells in Q4 were judged as eGFP-positive in FITC-A channel).

The percentages of positive cells resulting from the flow-cytometric tests of TC-71, TC-71 pEPI-EGFP, TC-71pEPI-EGFP 1.sort and TC-71pEPI-EGFP 2.sort are visualised in Figure 5.5. All cultures were tested over time with the first sort performed between day 0 and day 24 and the second sort performed out of the cultured cells of the first sort between day 24 and day 35. At all times the very low positivity of the unsorted TC-71pEPI-EGFP culture remained visible. However, the variability of eGFP-positivity on days 24, 35, 72 and 93 can be assumed as a variation of handling and individual measurement. Follow-up measurements of eGFP-positivity on days 115 and 128 showed lower persentages. With a positivity of over 60% after 128 days the second sort of TC-71pEPI-EGFP suggests the applicability of pEPI-EGFP as a stably transfectable plasmid for knockdown experiments.

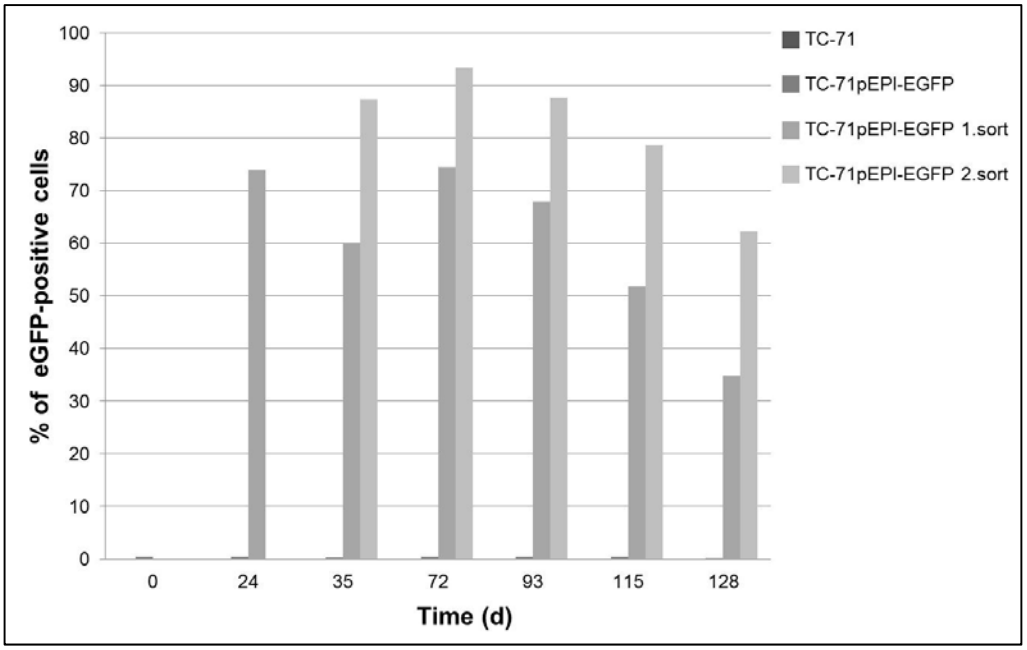

Figure 5.5: Examination of stability of pEPI-EGFP expression in TC-71 over time. Graph shows percentage of eGFP-positive and thus pEPI-EGFP positive cells from flow-cytometric analysis of the different sorts over the period of 128 days.

Taking all results into account it can be assumed that it is possible to transfect ES/PNET cell lines with the plasmid pEPI-EGFP, that the plasmid is expressed in the cells and stable over a long period of time. This suggests that it could allow for a stable knockdown of CXCR4 using a designed knockdown plasmid based on pEPI-EGFP without any long-term selection pressure on the positive cells. Thus, knockdown cells could be used for *in vivo* experiments without any additional treatment of mice necessary. This is why in this project pEPI-EGFP was used for further cloning of a knockdown plasmid against CXCR4 (strategy see chapter 5.3.1).

5.4.2 Verification of CXCR4-positivity of Ewing's sarcoma cell lines

Preliminary experiments on CXCR4 expression in ES cell lines were performed in Münster to be able to phrase a hypothesis for a knockdown project on CXCR4. To verify these results, preparing flow cytometry experiments were performed to investigate the expression of CXCR4 in ES cell lines. These showed that cell line VH-64 is positive for CXCR4, while cell line TC-71 showed a weaker positivity.

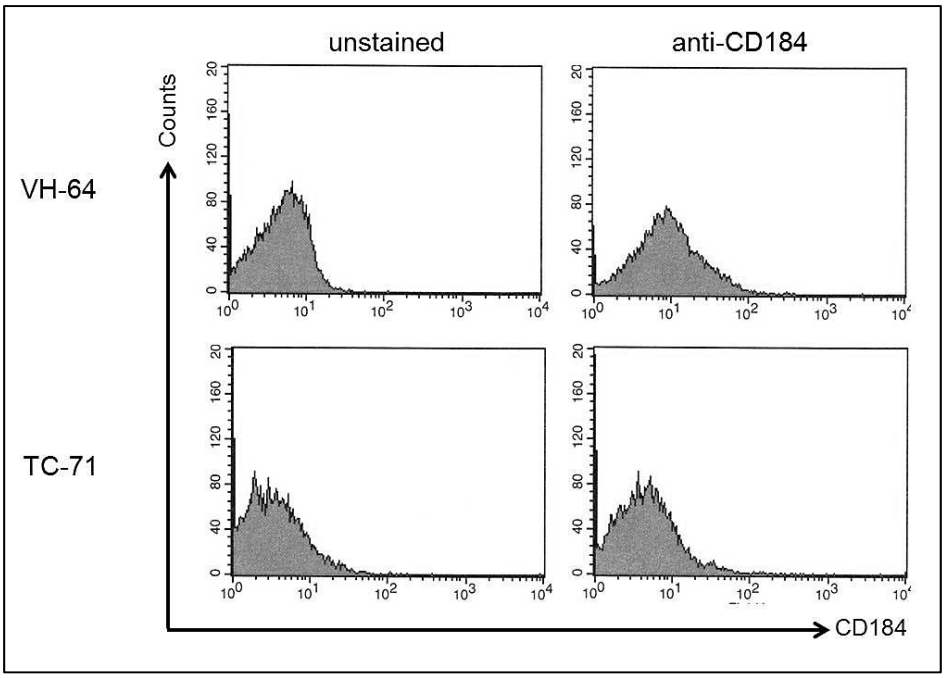

Figure 5.6: Examination of CXCR4 (CD184)-positivity of the ES cell lines VH-64 and TC-71. Cells were CD184 stained and flow-cytometrically examined with unstained cells as a control.

Flow-cytrometic examination of the CXCR4-positivity of the cell lines VH-64 and TC-71 showed, that expression and the resulting presentation of CXCR4 on

the cell surface of VH-64 cells was slightly higher than in TC-71 cells (see Figure 5.6).

Both cell lines were chosen for the following knockdown experiments using constructed vectors containing a DNA-sequence, which is able to form a shRNA for CXCR4-knockdown. This decision was made due to the fact that the majority of experiments in the differents project parts were performed on those two cell lines.

5.4.3 Verification of knockdown plasmid-positive Ewing's sarcoma cell lines

Before transfection of cells plasmids were sequenced using the service of Eurofins MWG Operon (compare chapter 3.2.15) to verify that pol III H1 promoter and the DNA-sequences coding for the shRNAs coding for mRNAs of CXCR4 (shCXCR4) and the fusion MLL-AF4 (shMA6-Mut1) were cloned into pEPI-EGFP resulting in the knockdown plasmid pEPI-EGFP-shCXCR4 and negative control plasmid pEPI-EGFP-shMA6-Mut1.

After transfection of ES/PNET cell lines TC-71 and VH-64 a first verification of plasmid uptake and eGFP production was performed. Therefore, pictures were taken of the resulting transfected cell lines using a fluorescence microscope (Figure 5.7).

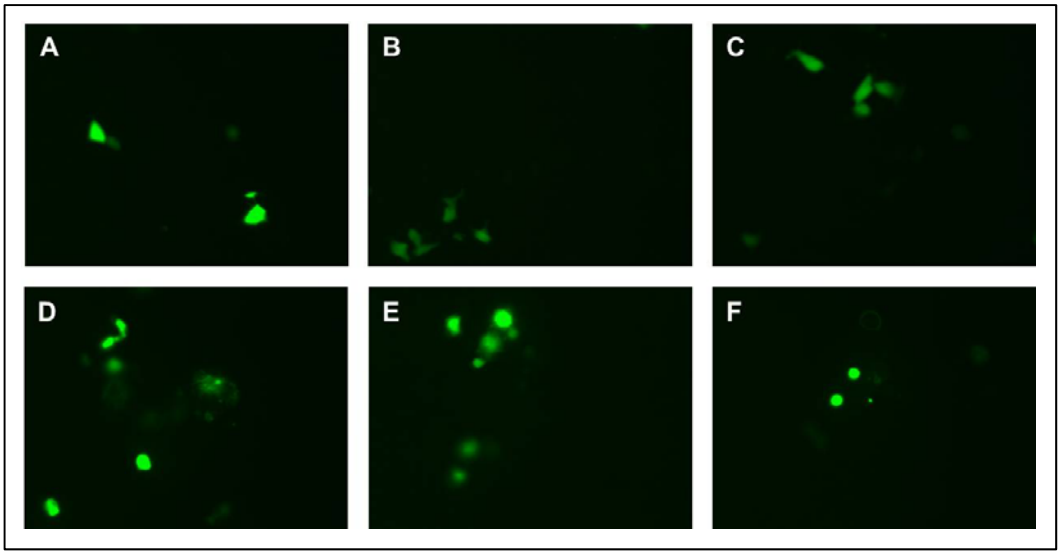

Figure 5.7: First examination of transfected cells using a fluorescence microscope. All transfected cells showed fluorescence. **A**, TC-71pEPI-EGFP; **B**, TC-71pEPI-EGFP-shCXCR4; **C**, TC-71pEPI-EGFP-shMA6-Mut1; **D**, VH-64pEPI-EGFP; **E**, VH-64pEPI-EGFP-shCXCR4; **F**, VH-64pEPI-EGFP -shMA6-Mut1.

All produced cell lines showed plasmid-uptake resulting in eGFP expression and thus green fluorescence of cells that could be visualised in the fluorescence microscope. This led to the assumption that cells could be analysed flow-cytometrically for plasmid expression as well as be sorted using FACS.

5.4.4 Selection of plasmid-positive cells

Subsequent to the first verification, transfected cells were sorted for eGFP-positivity using FACS and subsequently, enriched cell lines were further selected using G418.

As previously shown for the preliminary experiment in which cells were transfected with pEPI-EGFP, it was possible to serially FACS-sort for the positivity of the knockdown plasmid and the control plasmid as well.

5.5 Discussion

The plasmid pEPI-EGFP proved to offer a good opportunity for stable transfection of ES/PNET cell lines as transfected cells showed expression of eGFP encoded by the plasmid over a long period of time. After more than four months both transfected cell lines were still positive for the expression of eGFP through pEPI-EGFP.

Following these results, a knockdown-plasmid containing DNA coding for a shRNA against CXCR4 was constructed. Therefore, a cassette containing the promoter H1 and the DNA encoding the shRNA was cloned into pEPI-EGFP. All constructed plasmids were verified through sequencing.

First and very preliminary qRT-PCR experiments after transfection and selection of cells from the two cell lines TC-71 and VH-64 were performed. A slight knockdown of CXCR4 could be seen in TC-71pEPI-EGFP-hCXCR4. No knockdown, however, was detected in VH-64pEPI-EGFP-shRNA (data not shown due to missing repetitions and thus questionable significance). Due to restriction of time no further experiments were performed and it was not possible to fully examine the effect of CXCR4 knockdown on the cell phenotype. In the future, verification of expression knockdown using qRT-PCR will have to be performed. Furthermore, it will be necessary to perform functional experiments after knockdown has been confirmed in the transfected cell lines. As previous

work in CaP and breast cancer research has investigated the involvement of CXCR4 in the metastasis of cells of these types of cancer it would be of interest to investigate whether the knockdown of CXCR4 in ES/PNET cell lines influences migration, adhesion and proliferation of cells. Subsequently, it would be interesting to investigate the effect of a CXCR4-knockdown in the previously established preclinical i. v. model which reflects the metastasis of ES/PNET as seen in patients. Especially metastasis via the blood stream to bones in certain types of cancer positive for CXCR4 has been shown to take place in a CXCL12-dependent way (compare chapter 1.3.2).

There is evidence suggesting a role of the CXCL12/CXCR4 axis in ES/PNET as well. High expression of CXCR4 was discovered to be correlated with a metastatic behaviour and worse survival rates in ES/PNET patients. Moreover, knockdown experiments targeting the fusion transcript EWS/FLI1 discovered that CXCR4 expression seems to be up-regulated directly or indirectly through this aberrant transcription factor. This supports a role of CXCR4 in the biology of ES/PNET cells.

Subsequent to research performed in ES/PNET cell lines it should also be considered to investigate the role of CXCR4 on primary material if possible. As CXCR4 is currently considered to be a stem cell like marker, cultivation of cell lines for a long time might have selected cells for their *in vitro* growth and as a result of this might have left cells altered in their expression of several surface markers. Furthermore, it might be interesting to consider a closer look especially on the group of patients showing metastatic disease as the relation of metastatic behaviour of ES/PNET to the expression of CXCR4 has been suggested previously.

5.6 Conclusion

To date, there is still a need for a direct proof of the responsibility and role of the CXCL12/CXCR4-axis in the metastasis of ES/PNET. But taking the expression levels of CXCR4 in nearly all ES/PNET cell lines and many primary tumours as well as the role of this axis in other cancers into account there is strong indication for an involvement of CXCR4 in the metastasis or even the organ-specific metastasis of ES/PNET.

First results indicated that the constructed knockdown plasmid could be of value as a system to stably repress expression of CXCR4. This is why further investigations on the knockdown capacity of the constructed plasmid should be carried out to be able to subsequently investigate on the effect of CXCR4 knockdown.

6. Chapter – Development, establishment and validation of preclinical orthotopic mouse models for bone malignancies

6.1 Introduction

Many varying models for investigations of the different aspects of ES/PNET have been developed and used in studies (for a short overview see 6.1.2.2). However, only orthotopic models can reflect and discover the interactions of tumour cells in their "natural" microenvironment. Thus, i. f. transplantation into the bone marrow cavity of immunodeficient mice might offer a more relevant preclinical model for OS, ES/PNET and cancers that are known to metatstasise to the bone marrow.

6.1.1 Further malignancies of the bone

The continuity of bone tissue relies on the balance between osteoblasts and osteoclasts forming and resorbing new bone tissue, respectively. The presence of cancer cells in this tissue and their interaction with the normal cells disturbs this fragile equilibrium and can lead to aberrant new bone formation or destruction. Although typically both processes may be observed in bone cancers such as ES/PNET or OS, one is usually more prominent in each particular case (Coleman, 2001). Factors released from the bone through bone remodelling are believed to stimulate tumour growth and tumour cells are in turn able to produce factors that stimulate osteoclast differentiation and activity. This results in the establishment of a host-tumour relationship, often believed to be a "vicious

cycle" due to its progressively destructive nature (Chirgwin and Guise, 2000). The mechanisms of stimulation of osteogenesis through tumour cells associated with osteoblastic lesions are still not well understood (Goltzman et al., 2000).

In childhood and adolescents, OS is the most frequent primary malignancy of the bones and can originate in any bone, but is most commonly detected in the metaphyses of long bones. Most common sites are the proximal humerus, the distal femur or the proximal tibia with approximately 50% of cases occurring around the knee area (Dahlin and Coventry, 1967; Weinfeld and Dudley, 1962; Estrada-Aguilar et al., 1992). It develops mainly before the age of 30 years (Pringle, 1999) with a metastatic spread mainly to the lungs, as seen in 20% of presenting patients, which correlates with poor prognosis (Link et al., 1991; Saeter et al., 1997). Based on the radiologic appearance bone lesions caused by OS are characterized either as osteolytic, osteoblastic, or as mixed lesions (Mundy, 2002). However, osteolysis is a common feature associated with OS, as even predominantly osteoblastic lesions show osteolysis and this is mainly caused by activation of osteoclasts and their bone-resorbing activity (Goltzman, 2001).

Furthermore, bone tissue is one of the most common sites for a metastatic course of disease in many cancers including prostate carcinoma (CaP), breast and lung cancer (see also chapter 1). This destruction of bone causes severe symptoms in both bone sarcoma patients as well as cancer patients with metastatic disease of the bone.

As a prominent example for a cancer type metastasising to the bone, more than two thirds of advanced CaP cases develop bone metastases, with the axial skeleton being most frequently affected (Reid and Hamdy, 2007). Furthermore,

metastasis to weight-bearing bones can lead to pathological fractures and is indicative of a worse prognosis (Oefelein et al., 2002).

To be able to grow both, cells of primary tumours as well as cells of metastatic lesions need to interact with the matrix of the bone microenvironment so that the restricting nature of the mineralized bone tissue can be overcome. This is promoted by the mixed osteoblastic and osteolytic nature of bone tumours and secondary lesions (Roodman, 2004). While the basic mechanisms of metastasis of CaP to the metastatic niches have been explored (Lokeshwar et al., 1993; Birchmeier and Behrens, 1994; Nagle et al., 1994), details of the mechanisms still remain unknown. Furthermore, the process of bone remodelling in primary bone tumours is still unclear and requires further investigation.

This lack of understanding of the biology of the underlying mechanisms of bone remodelling has so far prevented the development of effective treatments for osseous disease. The validation of a clinically relevant preclinical model should provide a tool for both studying the mechanisms involved in disease progression, and to examine novel treatments targeting the interaction of tumour cells with the bone microenvironment.

6.1.2 Preclinical models for bone malignancies

Currently, many preclinical models of bone cancer still use s. c. xenografts, which clearly do not mirror well the site of disease in patients. If the effectiveness of a drug has been proven *in vitro*, it's tolerance *in vivo* can easily be tested in a simple mouse system. However, the more interesting and important question is, whether the distribution of the drug and it's interaction with the

designated target is given and comparable to the situation in patients. One of the experimental ways to address this problem is to employ an orthotopic model for the research of new drugs and their effectiveness (Bibby, 2004).

6.1.2.1 Preclinical models of primary bone malignancies

A lot of preclinical models were developed using s. c. or i. v. techniques for transplantation of xenografts. These techniques have their very own application areas.

Subcutaneously transplanted ES/PNET cell lines (such as TC-71 and VH-64 in own experiments) will form a solid tumour without difficulty so that this technique is the most common one for investigations on different aspects of tumour development and also used for pharmaceutical studies. There are, for example, several research projects employing s. c. models to test the efficiency of drugs against ES/PNET cells *in vivo* (Jia et al., 2006; Dalal and Burchill, 2009).

Injected into the flanks of athymic nude mice, development of tumours can be supervised by eye and tumour volumes can easily be assessed with a calliper. The measured length and width of the tumours are used to calculate the volume applying specific formulas (Scotlandi et al., 2002; Sancéau et al., 2002). This technique is applied vastly for the analysis of pharmacological aspects as it is a simple readout-system. However, no interaction of tumour cells with the suitable microenvironment of organs is given and thus tumours do not reflect the situation in patients very well.

As already mentioned before, i. v. transplantation of xenograft cells offers the possibility to analyse the haematogenous metastatic behaviour of ES/PNET and allows the interaction of these cells with the local microenvironment of tissues and organs (see chapter 3.1.2.3). Transplantation of ES/PNET cells into NOD/*Scid* mice leads to a pattern of metastasis similar to that seen clinically, providing research with a suitable and reliable system for studying metastasis of this disease. However, only relatively small numbers of the experimental mice in these studies developed assessable bone metastases (Scotlandi et al., 2000; Vormoor et al., 2001). This is why, it requires more effort to localise bone metastases within this i. v. model and ideally involves the possibility to use non-invasive imaging equipment.

OS can be induced in experimental animals through radiation. These tumours, however, usually grow at a very low rate and are no xenographs and thus not of human origin. This can hold problems for research (Witzel et al., 1992; Tinkey et al., 1998). The development of xenograft models has been challenging, because not all OS cell lines were able to manifest disease *in vivo* in immunocompromised mice. However, several s. c and i. v. models using the cell lines U2OS and SaOS-2 and derivates of those could be established (Zhou et al., 1996; Jia et al., 1999; Manara et al., 2000).

6.1.2.2 Orthotopic preclinical models for primary bone malignancies

On-going from these established types of preclinical models it was necessary to be able to model the primary tumour in its "natural" environment and tissue of origin. Placing the transplant in the normal physiological location, such models

would be more likely to mirror the human disease state. Therefore, more refined techniques were developed referred to as orthotopic models.

In small experimental animals such as mice, ideal locations for orthotopic transplantations would be the long bones of the leg: tibiae and femurs. An orthotopic approach is usually technically more difficult than i. v. transplantation, as animals have to be anaesthetised rather than simply restrained for the procedure. However, demonstrably better results in these models justify the additional effort and stress for the animals.

One of the methods uses transplantation of the xenograft directly into the tibia of the mice. Zhou et al. established an orthotopic bone tumour model by transplanting ES/PNET cells into the tibia of athymic nude mice. In this study transplanted mice where treated with zoledronic acid or paclitaxel to investigate the effect of these drugs on the developing tumours (Zhou et al., 2005). This i. t. model was also employed for the analysis of the effects after knockdown of VEGF (vascular endothelial growth factor) through siRNA (Guan et al., 2005).

There are more i. t. models for ES/PNET suggesting minimal-invasive transplantation of tumour cells into the tibia of mice being a good opportunity to investigate tumour-microenvironment interaction (Odri et al., 2010).

However, i. t. transplantation occasionally can imply an operation of the mouse tibia due to difficulties of achieving injection through a punctual percutaneous intraosseous intervention. This means a rather stressful procedure for the experimental animals as well as a risk of infection.

This is why we suggest the method of i. f. injection for induction of orthotopic tumours. As the state of research suggests a MSC to most likely be the cell of

origin for ES/PNET (see chapter 1.1.7), placement of tumour cells within the bone marrow cavity would be appropriate.

The method of i. f. transplantation provides a technically feasible and reproducible system for cancer types associated with the bone or bone marrow (Mazurier et al., 2003) and gives rise to tumours that are detectable by *in vivo* imaging or with a certain size by palpation of the animals. One of the advantages of an i. f. model is the relative good accessibility of the distal end of the femur which has a larger diameter than the tibia. Therefore, this preclinical model suggests being a good alternative orthotopic transplantation technique to the technique of i. t. transplantation.

Recently, several orthotopic models for OS mainly using i. t. transplantation have been established (Cao et al., 2005; Dass et al., 2005; Yuan et al., 2007). However, as it still remains problematic to establish tumour formation in mice after orthotopic transplantation some of these models employ genetically modified cell lines. Therefore, they cannot be a true representation of the human condition which has to be taken into account when using an orthotopic model.

6.1.2.3 Preclinical models for CaP metastases of the bone

In this project CaP was used as an exemplary type of cancer metastasising to the bone. The metastasis of CaP to the bone has been studied extensively. Metastatic behaviour of cell lines could be achieved through intracardiac as well as i. v. transplantation and bone metastases could be observed (Glinskii et al., 2005; Schneider et al., 2005). To be able to induce bone metastases directly, i. t.

injections were performed resulting in tumours located within the bone (Corey et al., 2002).

6.1.2.4 Development of the intrafemoral transplantation method

Orthotopic intraosseous transplantation could also be achieved through the development of an i. f. model. Originally, this model was developed for the transplantation of haematopoietic stem cells directly into the bone marrow cavity (Mazurier et al., 2003).

Mazurier et al. showed that a class of cells with repopulating capability usually found in the $CD34^{+}CD38^{low}CD36^{-}$ compartment of human bone marrow was detectable when human xenografts were injected directly into the murine femur. As the majority of normal and malignant haematopoietic cells are located within the bone marrow the process of homing through the circulatory system after i. v. injection could be avoided through employment of the direct transplantation of cells into the bone marrow cavity. This is especially important for cells which lack the ability to migrate as they will not survive and establish in the bone marrow. Thus, false negative results would be created. Indeed, previous research suggested that the lack of this ability to migrate and home to the bone marrow might be the cause for reported low seeding efficiency of no more than 10% of human repopulating cells in mice (van Hennik et al., 1999).

This indicates that orthotopic injection of human xenografts is able to better reflect the patient's primary tumour as opposed to tumours derived through other injection methods. The cell of origin for ES/PNET is still unknown but might most possibly be a primitive pluripotential cell that exists in the bone marrow

(Lin et al., 2011). This is why an orthotopic technique of transplantation is thought to be suitable for transplantation of human ES/PNET cells directly into their physiological appropriate microenvironment.

6.1.2.5 NSG mice

As described previously (chapter 3), immunocompromised mouse strains became more and more important for preclinical studies. One of the more recently developed mouse strains, offering an even higher grade of immunodeficiency than NOD/Scid mice is the mouse strain NOD.Cg-*Prkdc*^{scid} *Il2rg*^{tm1wjl}/SzJ (NSG, The Jackson Laboratory) developed by Shultz et al. (Shultz et al., 2005). The motivation for the development of this mouse strain resulted from the observation that NOD/Scid and other mouse strains with NOD background were less able to reject implanted xenografts when the NK cell activity was further depleted, e.g. through ionising radiation or anti-CD122 treatment (Hudson et al., 1998; Shultz et al., 2003). However, irradiation of mice bares the disadvantage that a strict and meticulous animal support is required and that significant mortality rates can be observed (Hayakawa et al., 2009).

To obtain a mouse strain with a complete lack of NK cell activity, NOD-*scid* females were crossed with B6.129S4-*IL2Rγ*$^{tm1Wjl/J}$ males (*IL2Rγ* mutation is X-chromosome-linked). The resulting (NOD x B6) F1 +/*scid IL2Rγ*^{null} hemizygous male offspring was backcrossed with NOD/Scid females for two generations. Subsequently, females homozygous for *scid* and heterozygous for the disrupted *IL2Rγ* gene were identified and the *IL2Rγ*^{null} allele was backcrossed for 8 generations onto the NOD-*scid* background. Resulting

NOD.Cg-*Prkdc*^{scid} *IL2Rγ*$^{Tm1Wjl/Sz}$ (hereafter named NOD-*scid IL2Rγ*$^{+/null}$) females were crossed with NOD-*scid IL2Rγ*^{null}/*Y* males. The NOD-*scid IL2Rγ*^{null} female and NOD-*scid IL2Rγ*^{null}/Y male offspring was identified and intercrossed to obtain the desired new mouse strain NOD.Cg-*Prkdc*^{scid} *Il2rg*^{tm1Wjl}/SzJ (Shultz et al., 2005). These mice have a high level of immunodeficiency as they lack mature T and B cells, functional NK cells and are depleted in cytokine signalling. Additionally, the latter leads to these mice lacking the predisposition to thymic lymphoma which is prevalent in the parental NOD/Scid strain. To avoid confusion with other strains that have a NOD/*scid* background, The Jackson Laboratories decided to give the strain the now common abbreviation of NSG (NOD *scid* gamma).

Recently, several publications described that this mouse strain allows better engraftment of human haematopoietic stem cells and cancer stem cells with almost no rejection of xenotransplants due to the almost total absence of a functional immune system. This makes this mouse strain a preferred tool for research using preclinical models of diseases in this field (Agliano et al., 2008; Goldstein et al., 2010). Based on these reports, the decision was made to use NSG mice for the development of a novel preclinical and orthotopic model for bone malignancies. Classically, NOD/Scid mice had been used for an i. v. model of ES/PNET. These mice had to be irradiated before transplantation to deplete the residual NK cell activity eventually causing rejection of xenografts. However, irradiation led to a high burden of stress for experimental mice and treatment-related deaths. Thus, the decision was made for NSG mice.

6.1.3 Imaging techniques

A major difficulty in using orthotopic models of any cancer preclinically has until now been the measurement of disease burden in a non-accessible site.

X-ray imaging was without a doubt a revolutionary innovation for medicine and improved diagnosis to a great extent. However, more distinct and elegant methods for imaging have been developed that allow to image and investigate more features of the body and its diseases.

The current way of diagnosing ES/PNET is to scan the patient by X-ray in two planes and take a biopsy of the possible tumour mass. MRI is used to examine the patient's stage of disease (Bernstein et al., 2006; Schmidt et al., 2007). Ideally, all bones making up involved joints are imaged to be able to identify possible skip lesions. CT is performed to be able to diagnose possible lung metastases. PET is usually not used as a primary imaging modality for ES/PNET and OS but may play a role in assessing treatment response. The variety of these methods can nowadays also be applied for small animals using NanoCT- (in the following referred to as CT), PET- or high-resolution MRI-machines.

The use of these newer *in vivo* imaging techniques offers the opportunity to detect and monitor development and progression of the disease in clinically relevant sites in transplanted mice and with the development of small animal imaging technologies it is possible to develop and monitor orthotopic models of disease investigating new drugs and cutting down animal numbers.

This chapter will not explain the techniques in detail but comment on advantages and disadvantages of the different imaging opportunities (for details refer to chapters 3.6.6, 3.6.7, and 3.6.8).

6.1.3.1 Computed tomography

CT uses the technique of X-ray imaging. While X-ray images show one defined plane and direction, a series of thousands of two-dimensional X-ray images taken from changing perspectives can be calculated into a three-dimensional image. Therefore, the exact absorption of radiation at a given location is recorded and the obtained data can be reconstructed by a computer.

On the one hand, a disadvantage of the CT is the high dose of radiation patients are exposed to. One abdominal CT is equivalent in radiation dose to 500 chest X-rays (Rajarubendra and Lawrentschuk, 2010). This is why the diagnostic benefit of a CT always has to be compared against the radiation exposure of the patient.

On the other hand, the technique of CT images is able to show bony metastases in detail. Bone structure, osteolytic as well as osteoblastic lesions, soft tissue involvement and bone marrow metastases can be judged at early stages. Thus, sensitivity of CT was reported to range from 71 to 100% (Gainford et al., 2005).

CT offers a good opportunity for preclinical research as images can be acquired relatively fast and, therefore, many animals can be scanned in a row with short anaesthesia times. Furthermore, newer small animal CT scanners offer high resolution images that allow judging on processes taking place in the skeleton of small experimental animals such as mice.

6.1.3.2 Positron emission tomography

FDG-PET imaging uses the fact that most malignant tumour cells exhibit increased glucolysis (Smith, 1998). Most commonly, FDG is used as it behaves

as a glucose analogue being accumulated by metabolically active cells. Thus, it is able to provide qualitative and quantitative metabolic information leading to an evaluation of a lesion.

The whole body can be scanned so that this technique also detects disease and metastases in regions not routinely included in other imaging studies (Rajarubendra and Lawrentschuk, 2010). Sensitivity of PET to detect metastases has been estimated to 62 to 100% (Gainford et al., 2005).

To follow the progress of metastasis of ES/PNET non-invasively in the living animal, high-resolution PET seems to constitute a useful tool and has been used in several studies (Franzius et al., 2006).

6.1.3.3 Magnetic resonance imaging

One of the biggest advances of MRI is the fact that no ionizing radiation has to be used to produce images. In the presence of a magnetic field the magnetic moments of some of the protons of H_2O change and align with the direction of the field. Applied radiofrequency radiation is used to produce an electromagnetic field which flips the spin of the aligned protons in the body. When the field is turned off, the protons decay to the original spin-down state. The difference in energy between the two states is released as a photon, which produces the electromagnetic signal that the scanner detects and which is used to calculate cross-sectional images of the body in any chosen plane (Rajarubendra and Lawrentschuk, 2010).

Differences in intensity between the scanned tissues e.g. between tumour tissue and bone or bone marrow make a detection and dimensioning of metastases

possible. Furthermore, MRI is the only imaging modality that directly visualises bone marrow and thus lesions can be found before destruction of the bone cortex and before any osteoblastic or osteolytic changes occur (Vanel et al., 1998). However, a disadvantage is the inability of MRI to depict destruction of the bone structure as cortical bone does not give any signal. This is why, the current use of imaging for diagnosis and staging of bone malignancies can only be a combination of the three imaging techniques and CT and PET are often used in combination as PET/CT with the images taken being overlaid.

6.2 Aims

The interaction between cells from certain types of cancer and the local microenvironment of the bone remain undefined. There is a vast field of preclinical research employing s. c. or i. v. models, but less work on orthotopic models of bone cancer. As such, the aims of this chapter were as follows:

- to develop an orthotopic *in vivo* model for malignant bone disease (primary and metastatic) for preclinical drug testing.
- to develop a model for studying the interaction between tumour cells and bone (remodelling of the tumour microenvironment).
- to investigate the opportunities for small animal *in vivo* bio-imaging to monitor local disease progression.

6.3 Results

6.3.1 Preliminary experiments

Preliminary experiments were performed to investigate whether the development and establishment of an orthotopic model for primary bone sarcomas was achievable through i. f. transplantation. Therefore, first i. f. transplantations in small numbers were performed to investigate whether chosen cell lines TC-71 and VH-64 (ES/PNET), SaOS-2 (OS) and PC3M (CaP) were able to form tumours in the desired orthotopic site. Furthermore, this preliminary experiment was used to establish the imaging techniques and histology. These data are included in the study and are presented together with the following results.
Additionally, mice that did not receive any treatment were used as controls in the preliminary experiments (see Figure 6.1).

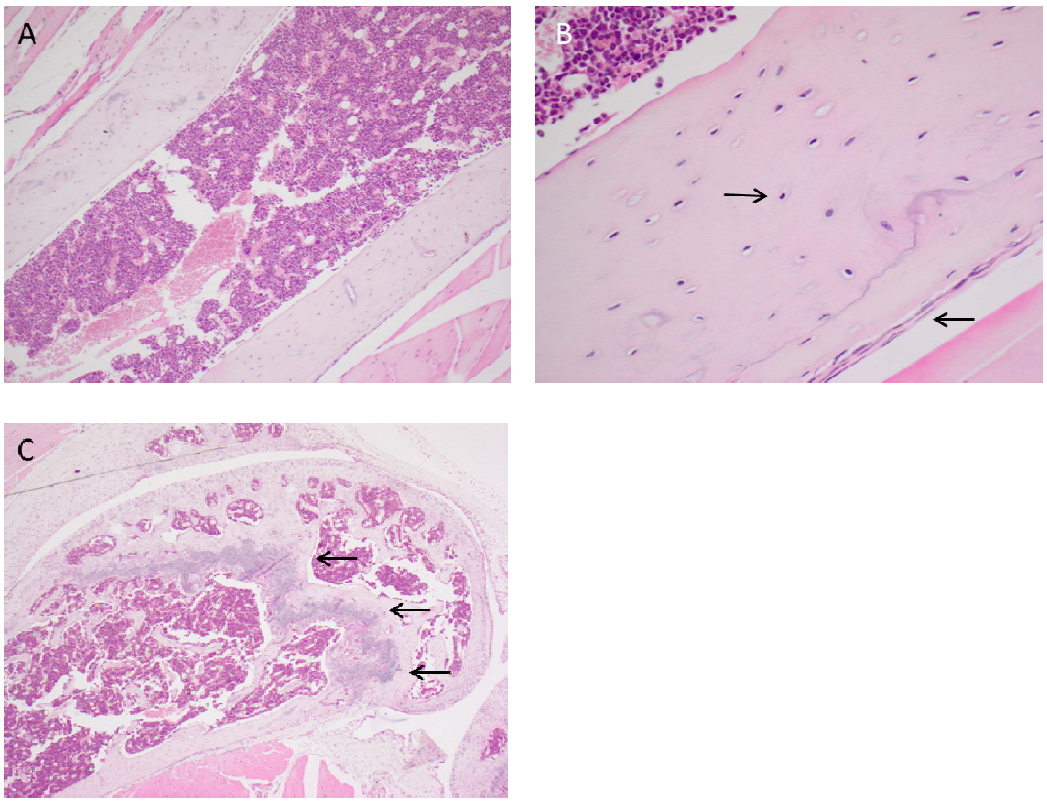

Figure 6.1: Normal structure of a murine femur. A, Femur shaft with bone marrow cavity in the centre (H&E staining, original magnification x10); **B,** detailed image of the cortex of a femur with osteocytes within the bone tissue and periosteum lining the cortex at the outer border (H&E staining, original magnification x40); **C,** distal end of the femur with growth plate and trabecular bone structures (H&E staining, original magnification x4).

Images taken of histological H&E-stained sections showed intact bone marrow (Figure 6.1 A), osteocytes within the cortical bone (Figure 6.1 B) and trabecular bone as well as the growth plate within the distal end of the murine femur (Figure 6.1C).

CT and PET images of transplanted mice were acquired as full-body images and generally were overlaid in the first set of experiments (as described in 3.6.6 and 3.6.7, see Figure 6.2 to 6.4).

Generally, eyes, heart, intestines and in some animals the brain showed FDG accumulation. Furthermore, the bladder and in some cases the kidneys as well

showed FDG signal due to the FDG excretion. Muscles showed background signal to a small extend in some cases.

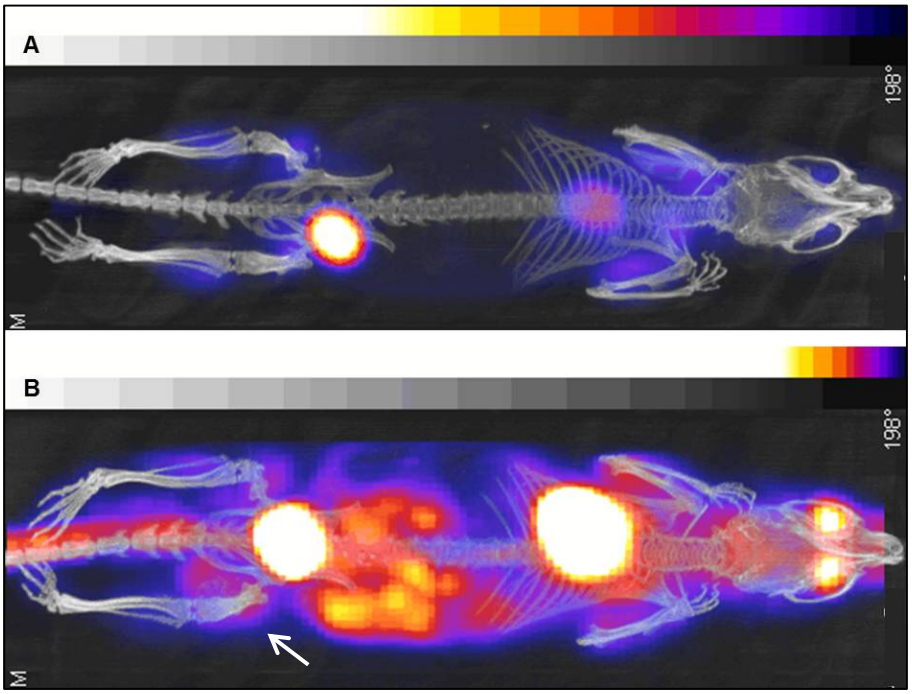

Figure 6.2: PET/CT image of a VH-64 i. f. transplanted mouse. A, Image taken after 21 days; **B,** Image taken after 42 days with the tumour marked with a white arrow (Maximum Intensity Projection (MIP) CT image overlaid with FDG-PET image, dorsal view).

The PET/CT image taken of the ES/PNET cell line VH-64 i. f. transplanted mouse did not show a tumour in the region of the right femur 21 days after transplantation. After 42 days the PET/CT image showed formation of a tumour surrounding the right femur. However, the contrast of the PET had to be very high to make the tumour visible. This led to a lot of background and a very bright heart signal making it impossible to judge whether there was pathologic involvement of the lung (Figure 6.2).

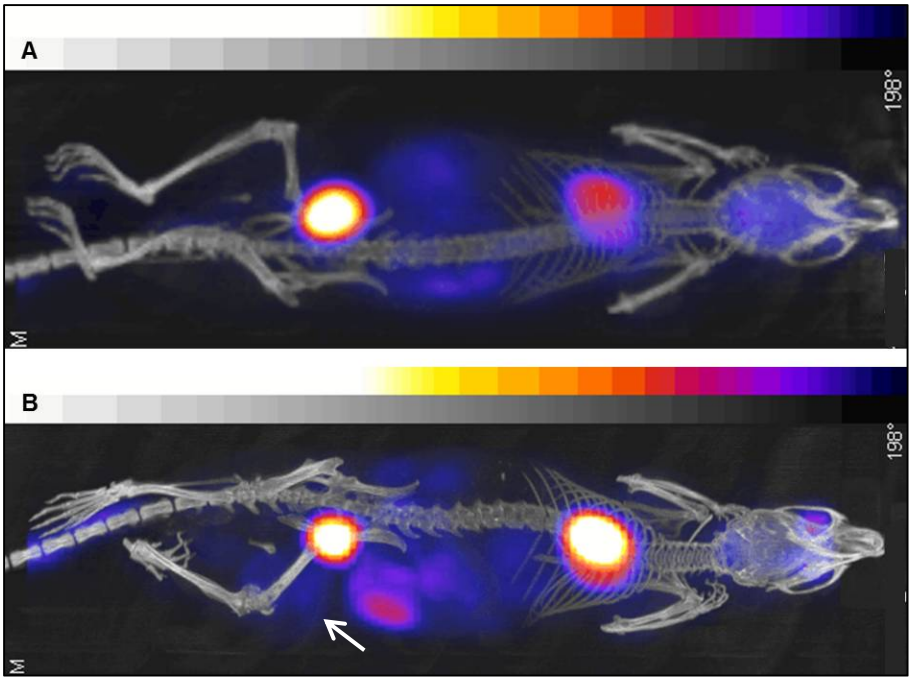

Figure 6.3: PET/CT image of a TC-71 i. f. transplanted mouse. A, Image taken after 22 days; **B,** Image taken after 42 days with the tumour marked with a white arrow (MIP-CT image overlaid with FDG-PET image, dorsal view).

The same accounts for the PET/CT image taken of the ES/PNET cell line TC-71 i. f. transplanted mouse. No tumour formation was visible in the region of the right femur 22 days after transplantation. Forty-two days after transplantation the PET/CT image showed a tumour surrounding the right femur. In this picture the contrast is not as high as in the image taken of the VH-64 transplanted mouse but there is still a lot of background and a very bright heart signal (Figure 6.3).

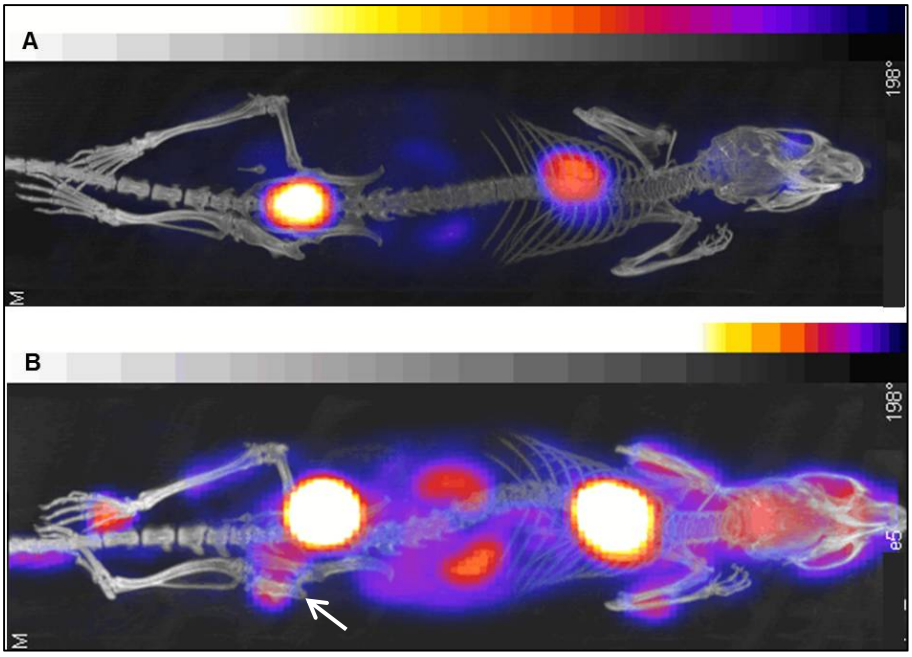

Figure 6.4: PET/CT image of a PC3M i.f. transplanted mouse. A, Image taken after 21 days; **B,** Image taken after 48 days with the tumour marked with a white arrow (MIP-CT image overlaid with FDG-PET image, dorsal view).

The PET/CT image taken of the CaP cell line PC3M i. f. transplanted mouse did not show tumour formation 21 days after transplantation. After 48 days the PET/CT image showed tumour formation around the right femur. Again, the contrast of the PET had to be very high to make the tumour visible. In this case the kidneys gave a bright signal, which might be due to the excretion of the FDG (Figure 6.4).

6.3.2 Reduction of background signal in positron emission tomography

To be able to image potential metastasis to the lung the bright heart signal had to be reduced. This is why, VH-64 and TC-71 cells were transplanted s. c to produce tumours that were easy to locate and monitor.

Three mice each were anaesthetised with the inhalable anaesthetic Isoflorane and with the injectable combination of Ketamine/Medetomidine (as described in 3.6.2). Thirty-three days after transplantation of VH-64 a palpable tumour had formed on the right flank of all six experimental animals. S. c. TC-71 tumours grew faster so that 5 out of 6 mice had to be culled before the planned FDG-PET procedure. However, one remaining mouse with an s. c. TC-71 tumour was imaged under Ketamine/Medetomidine anaesthesia and the tumour was visible comparable to the VH-64 tumour shown in Figure 6.5.

As expected and seen before, the mice anaesthetised with Isoflorane showed a bright signal of the heart muscle. In contrast to this, mice injected with Ketamine/Medetomidine showed no signal of the heart muscle (see Figure 6.5). This is why it can be assumed that possible lung metastases could be identified easier when mice are anaesthetised with this injectable anaesthesia.

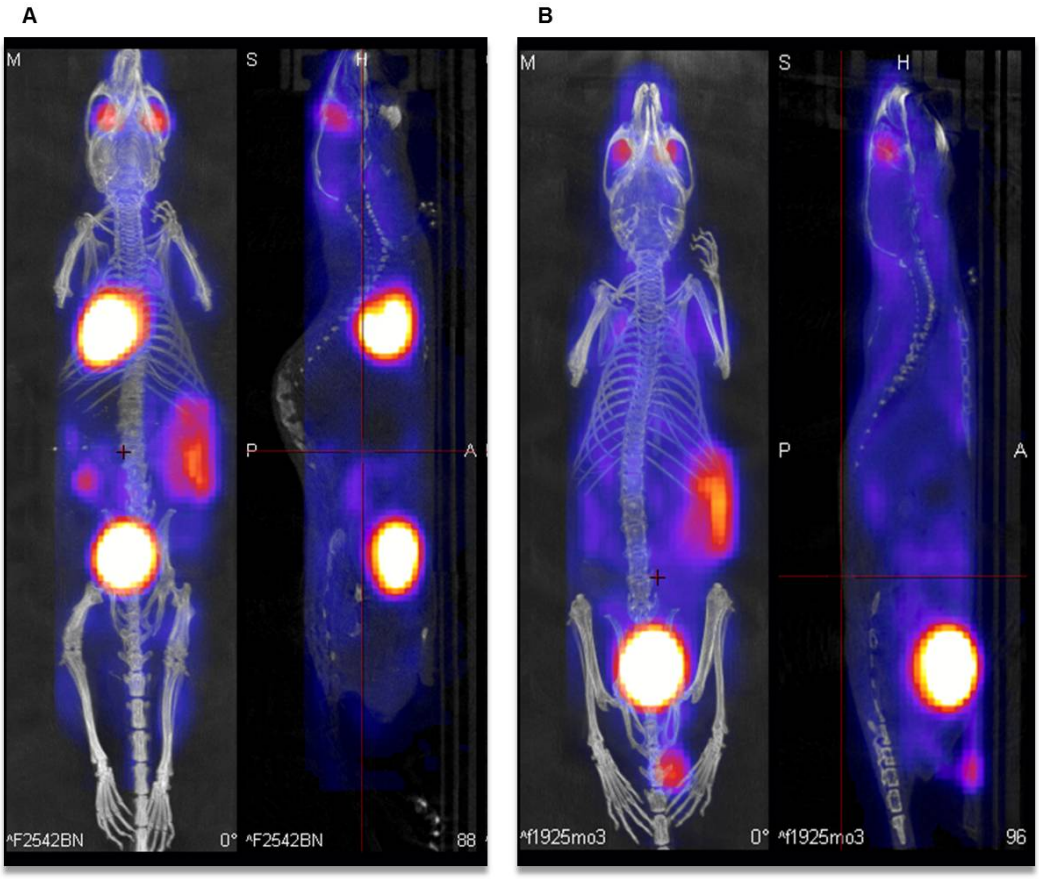

Figure 6.5: PET/CT images comparing inhalable and injectable anaesthesia. A, Exemplary mouse with s. c. VH-64 tumour anaesthetised with inhalable Isolflurane, picture showing accumulation of FDG within the tumour but as well in the heart and bladder; **B**, Exemplary mouse with s. c. VH-64 tumour anaesthetised with injectable Ketamin/Medetomidine. (each right picture, MIP-CT; each left picture, section through the sagittal plane in the heart region).

However, due to a high noise to signal ratio of the PET images in the preliminary experiment this technique was not used in the further development of the orthotopic model for bone malignancies.

6.3.3 Development of an orthotopic model for bone malignancies

Previous work has used i. v. transplantation to investigate the metastasis of ES/PNET cell lines *in vivo* or i.t transplantations to achieve tumours in the bone. To be able to study the direct interaction of different malignant cell types with bone we developed a preclinical orthotopic model by injecting cells of different tumour types directly into the femur of young NSG mice (see Table 6.1), a method that is easily to perform even on young and not full-grown mice.

Table 6.1: Experimental mice for the development of an orthotopic model for bone malignancies. VH-64 and TC-71, ES/PNET cell lines; SaOS-2, OS cell line; PC3M, CaP cell line; Medium, mice were injected with medium alone.

Transplant	Identification of mice	Age at transplantation (weeks, median, range)	Time to reach protocol limits (d, median, range)	Tumour formation
VH-64	F1921LN, F1921BN, F4901RN, F4901BN, F4901NN, F4968LN, F4968N	12 (11-12)	38 (29-42)	100% (7/7)
TC-71	F1920RN, F4968BN, F4968NN, F4965LN, F4965RN, F4965BN	12 (11-12)	31 (15-42)	83.3% (5/6)
SaOS-2	F4967LN, F4967RN, F4905LN, F5187LN, F5187RN	12 (10-12)	70 (70-83)	100% (5/5)
PC3M	F1927RN, F1927NN, F4902LN, F4902RN, F4902BN, F4902NN, F4901LN	12 (12-13)	29 (29-31)	100% (7/7)
Medium	F4965NN, F4970LN, F4970RN, F4970BN, F4970NN	11 (11-12)	na	0% (0/5)

Mice were transplanted with a median age of 11 to 12 weeks. Transplanted ES/PNET cell lines VH-64 and TC-71 developed tumours leading to euthanasia

after 38 and 31 days, respectively. PC3M-transplanted mice had to be euthanized after 29 days and SaOS-2-transplanted mice lived at mean 70 days. Except one TC-71 transplanted mouse all experimental animals developed tumours at the site of injection.

6.3.3.1 Induction of pathological new bone formation

CT images of the femurs injected with ES/PNET and OS cell lines showed remodelling of the murine bone with induction of pathological new bone formation. In all cases, the ES/PNET cell line VH-64 led to formation of calcified structures, which were clearly visible in CT. In most cases these new formations were manifested as sunray spicules, directly coming of the murine femur (see Figure 6.6 A).

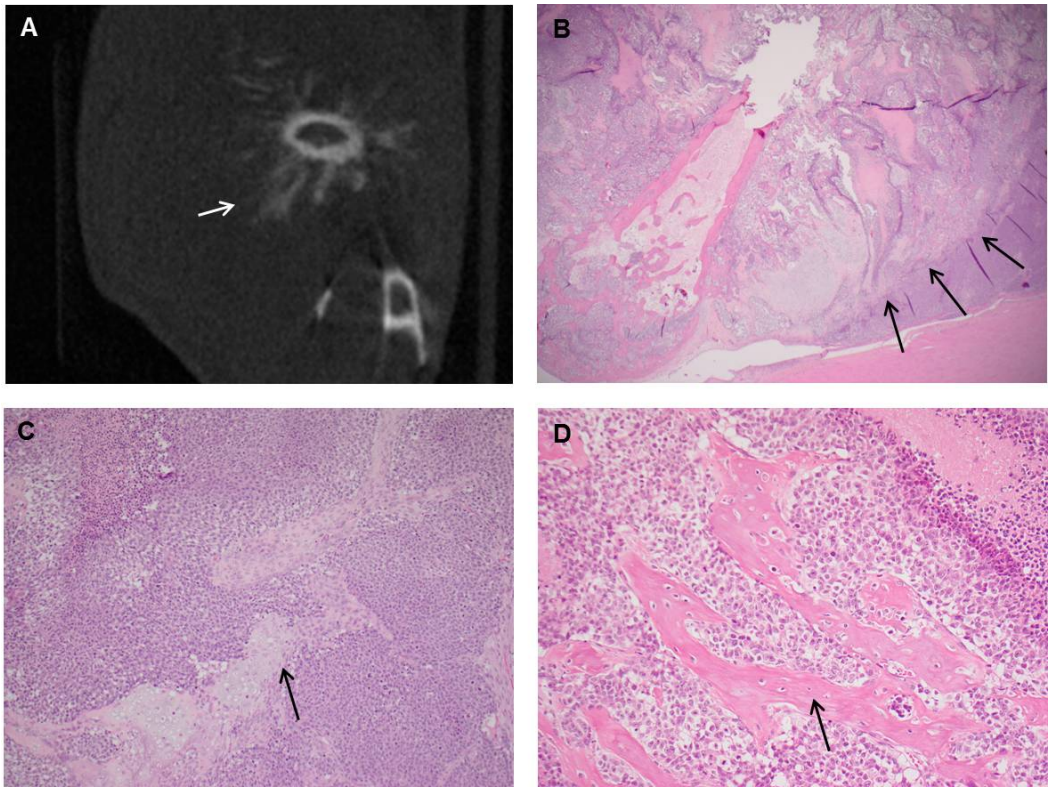

Figure 6.6: Induction of new bone formation after VH-64 transplantation. A, Exemplary CT image 42 days after transplantation (cross section of a femur, white arrow indicates sunray spicules); **B,** Large periosteal reaction induced by the tumour and reactive bone (H&E staining, original magnification 2x, arrows indicate the periosteum); **C,** Formation of cartilage in fibrous bands (H&E staining, original magnification 10x); **D,** Spicules of new bone formation most probably coming off the murine femur (H&E staining, original magnification 40x).

H&E stained histological sections of femurs injected with the ES/PNET cell line VH-64 confirmed findings of the CT scans. Structures identified as sunray spicules of immature bone arose directly from the murine femurs (Figure 6.6 A, B, D) and led to progressively destroyed cortical bone. Furthermore, tumours invaded the surrounding soft tissues. However, different from findings in patients transplanted ES/PNET cells in this model seemed to induce formation of cartilage as well.

The ES/PNET cell line TC-71 showed a mixed pattern with CT pictures giving evidence of both bone resorption as well as very weak induction of bone growth (see Figure 6.7).

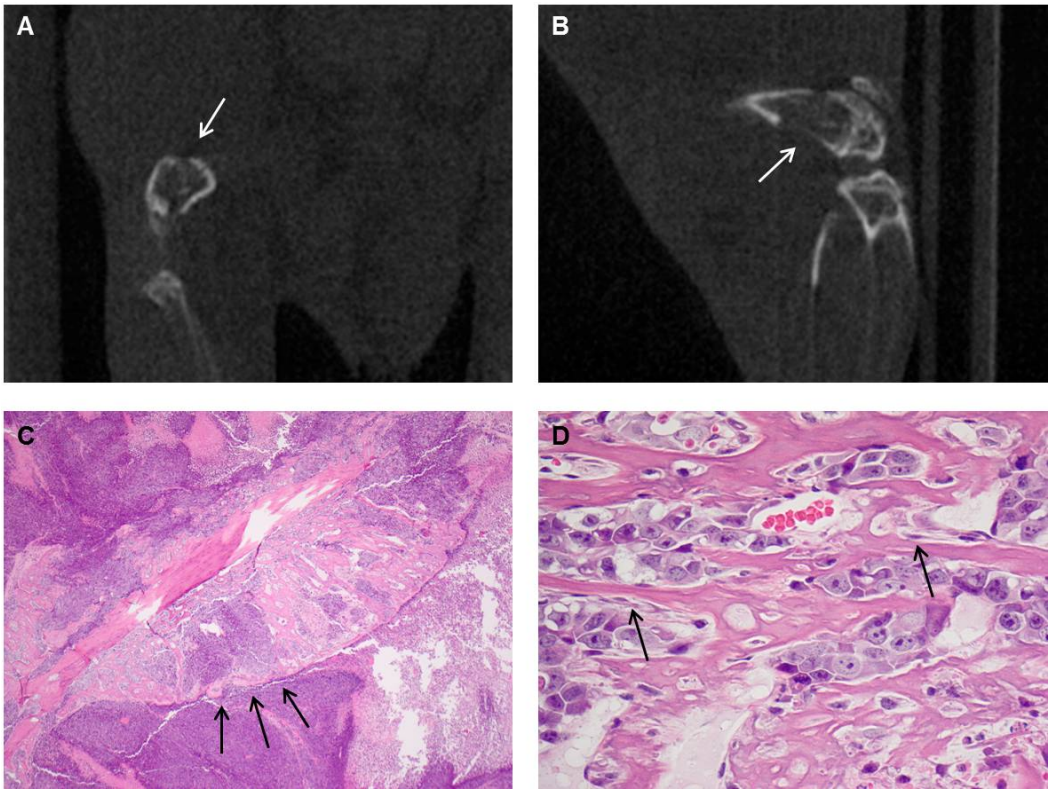

Figure 6.7: Lysis of bone and induction of new bone formation after TC-71 transplantation. **A,** Exemplary CT image 15 days after transplantation (cross section of a femur, white arrow indicates lysis of bone); **B,** Exemplary CT image 15 days after transplantation (longitudinal section of a femur, white arrow indicates lysis of bone); **C,** Large periosteal reaction induced by the tumour and reactive bone (H&E staining, original magnification 4x, arrows indicate the location of the periosteum); **D,** Spicules of immature bone formation most probably coming off the murine femur (H&E staining, original magnification 60x, arrows indicate flattened cells on the bone surface).

Therein some areas of bone was resorbed and the cortical bone destroyed to a great extent as seen in histology, whilst in others new and immature bone

formation was induced with the periosteum lifted of the cortical bone like in VH-64 transplanted mice (see Figure 6.7).

The fact that newly induced bone was not explicitly visible in CT suggests the immaturity and thus poor calcification of bone. However, flattened cells were visible on the surface of the reactive bone, which most probably are osteoclasts induced through the presence of tumour cells (see Figure 6.7 D).

Murine femurs injected with the OS cell line SaOS-2 showed induction of new bone formation in CT. In some cases lifting of the periosteum could be observed in histological slides that resulted in formation of sub-periosteal new bone that seemed to come of the murine cortical bone as it was the case in ES/PNET transplanted mice (see Figure 6.8). However, the induction of reactive bone was to a lesser extent than reactive bone formation as induced by VH-64 cells.

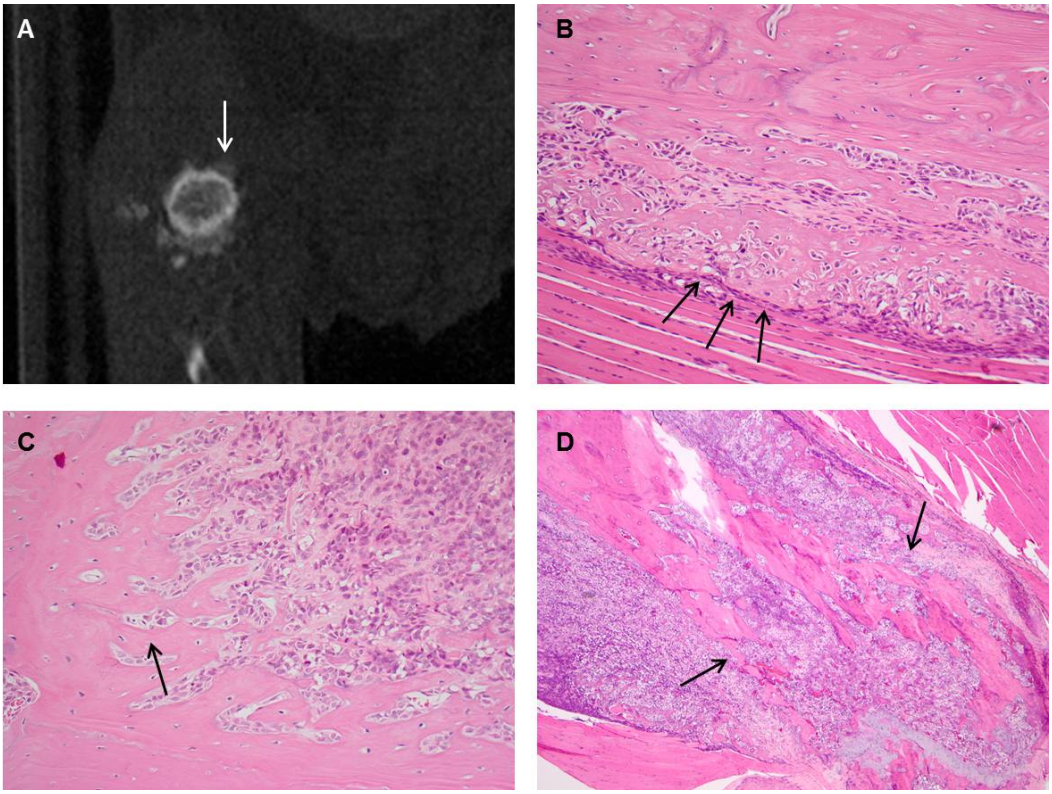

Figure 6.8: Lysis of bone and induction of new bone formation after SaOS-2 transplantation. A, Exemplary CT image 77 days after transplantation (cross section of a femur, white arrow indicates lysis of bone); **B,** Large periosteal reaction induced by the tumour and reactive bone (H&E staining, original magnification 20x, arrows indicate the location of the periosteum); **C,** Massive induction of reactive bone coming of the murine cortical bone of the femur (H&E staining, original magnification 20x, arrow indicates reactive bone); **D,** Destruction of the cortical bone by tumour cells growing through the existing bone (H&E staining, original magnification 4x).

6.3.3.2 Malignant new bone formation

In addition to the induction of reactive bone, CT scans of femurs transplanted with the OS cell line SaOS-2 showed formation of calcified structures within the tumour mass itself. The destructive and permissive growth of the cells (see Figure 6.9) had led to big tumour masses outside the femoral shaft as well and the calcified structures within this tumour mass were not directly linked to the

cortical bone of the murine femurs but appeared to be arising from the tumour cells themselves.

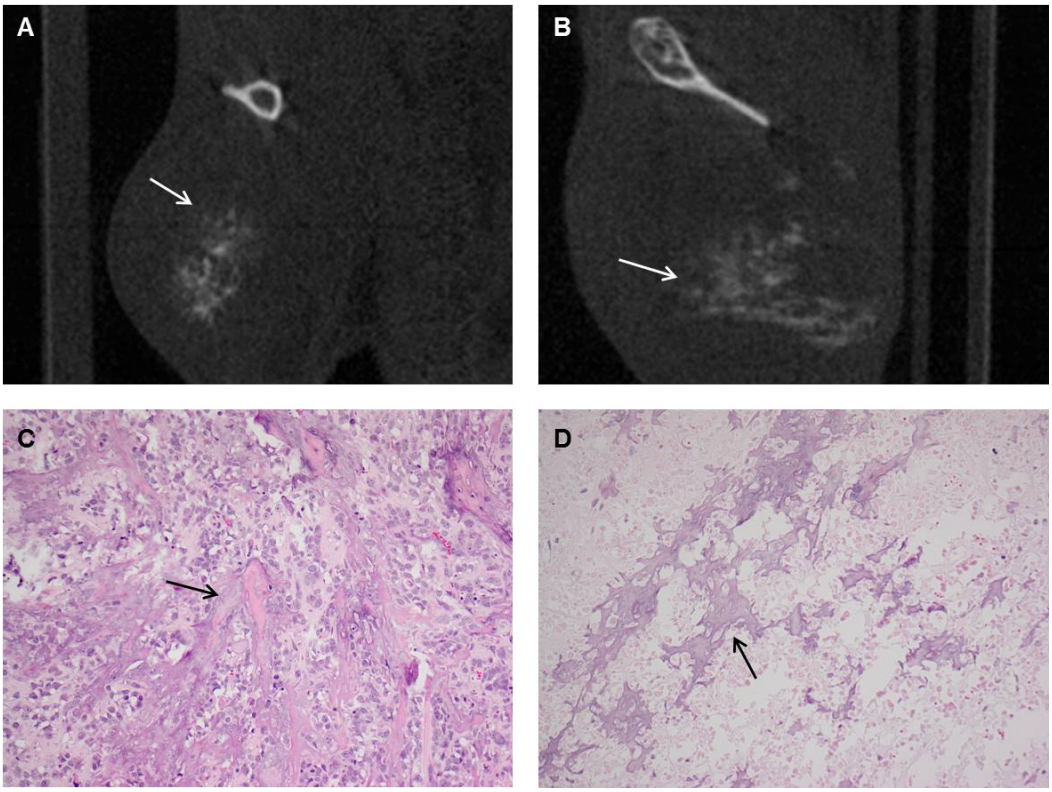

Figure 6.9: Malignant bone formation within the tumour mass after SaOS-2 transplantation. A, Exemplary CT image 77 days after transplantation (cross section of a femur, white arrow indicates malignant bone formation); **B,** Exemplary CT image 15 days after transplantation (longitudinal section of a femur, white arrow indicates malignant bone formation); **C,** Immature malignant bone within tumour mass (H&E staining, original magnification 20x); **D**, Malignant bone within necrotic part of the tumour mass (H&E staining, original magnification 20x).

These findings could be verified histologically. The malignant bone formed within the tumour mass was unstructured and less organised than the normal murine bone. Furthermore, the malignant bone seemed to arise from fibrous

structures within the tumour mass. In necrotic parts of the tumour malignant bone remained as pointy sclerotic structures.

6.3.3.3 Induction of osteolytic lesions

As a comparison to the primary bone tumour cell lines the CaP cell line PC3M was used to create a model for CaP in bone as its most common site of metastasis. On CT images injected femurs showed mainly heavy signs of resorption of bone leading to pathological fractures of the femur in two out of seven injected mice (see Figure 6.10).

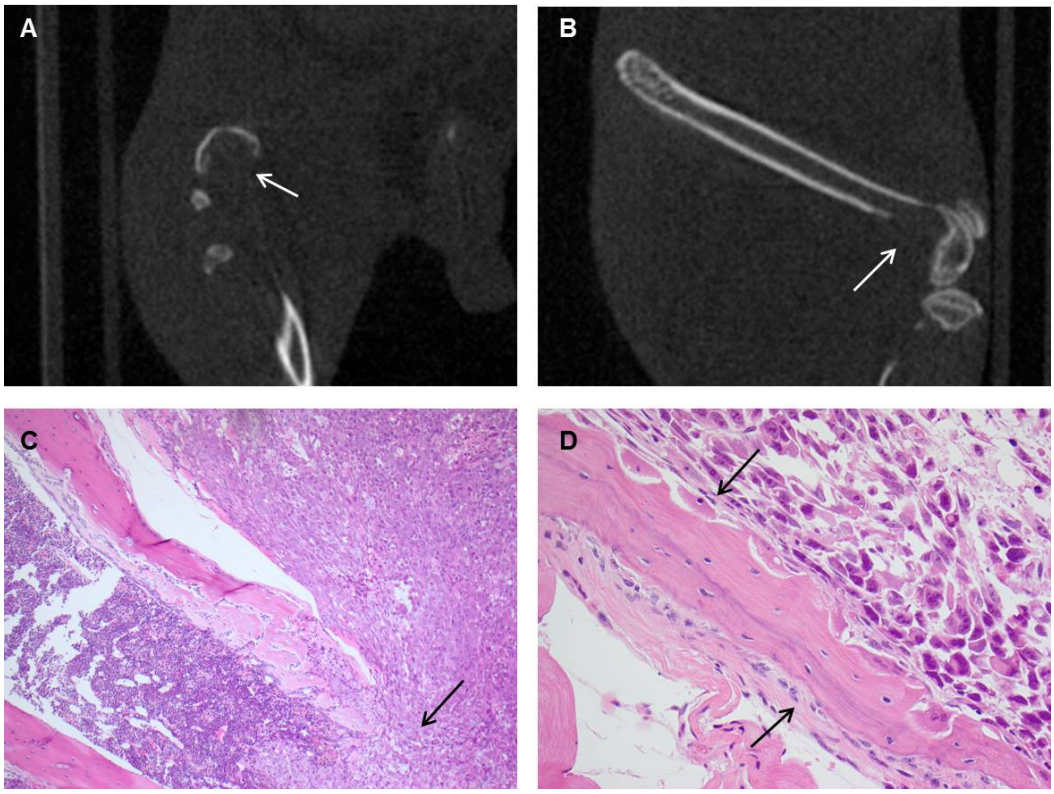

Figure 6.10: Osteolytic lesion caused by injection of PC3M. A, Exemplary CT image 29 days after transplantation (cross section of a femur, white arrow indicates lysis of the femur); **B,** Exemplary CT image 29 days after transplantation (longitudinal section of a femur, white arrow indicates lysis of the femur); **C**, Tumour mass destroying and dislocating femoral bone (H&E staining, original magnification 10x, black arrow indicating gap in the cortex); **D**, lysis of the bone with resorption pits of osteoclasts (upper black arrow) and osteoblastic reaction (lower black arrow, H&E staining, original magnification 40x).

In histological H&E stained slides PC3M injected femurs showed a vigorous resorption of bone material. The resorptive pits formed by active osteoclasts could be visualised in histological sections. The outer shape of the femurs did not appear as smooth as in controls but showed multiple sites of bone resorption (see Figures 6.10 C and D). Furthermore, on the opposite site of the cortical bone, osteoblastic formation of bone appeared as a compensational reaction. However, this bone appeared less organised and mature.

6.3.3.4 Documentation of soft tissue involvement using MRI

Where possible, tumour mass was documented by MR imaging immediately before dissection. In all cases MRI was a useful technique to visualise and investigate the tumour mass growing at the site of previous injection. It was possible to calculate volumes of tumours by selecting the region of interest (ROI) in sections that showed tumour mass (see Figure 6.11). In all investigated cases (VH-64, PC3M and SaOS-2 transplanted mice) it was possible to measure the ROI with results showing that the tumour volume had a nearly Gaussian distribution.

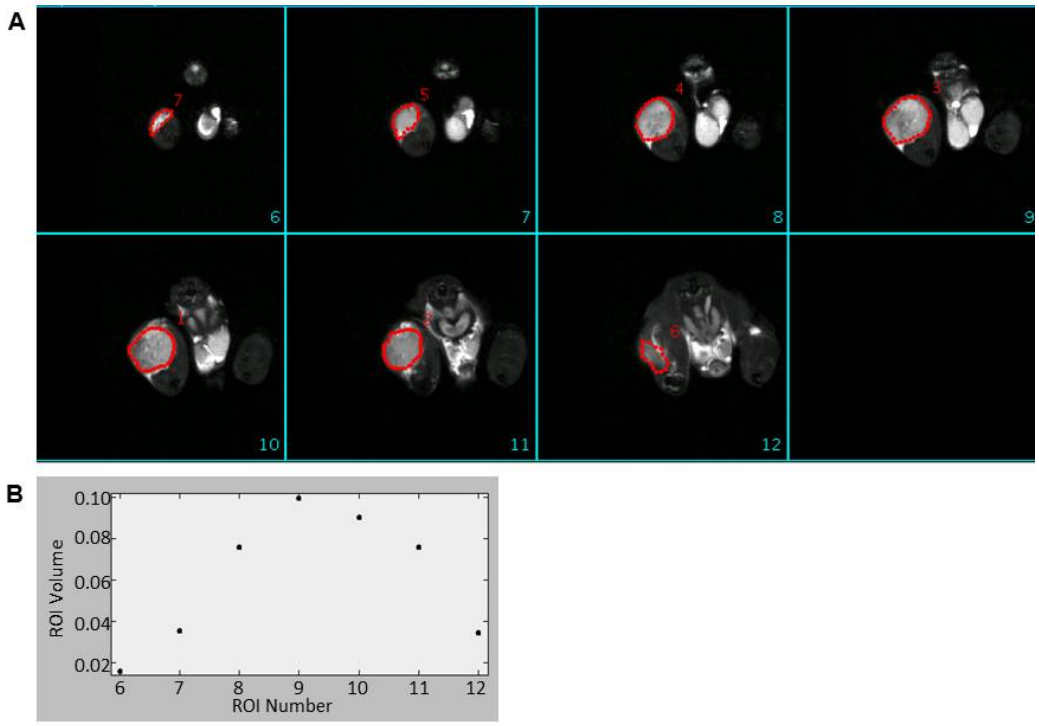

Figure 6.11: MR imaging of VH-64 Ewing sarcoma of the injected femur showing a larger extra-osseous tumour component. A, The region of interest (red circle) was measured in slices that showed tumour and from these the volume of the tumour was calculated. Thickness of slices was 2 mm; **B**, graphical distribution of region of interest volume showing a Gaussian distribution.

MRI was also able to pick up metastases that were located in the liver of TC-71 and PC3M transplanted mice. Due to the small size of mice and the high frequency of their respiration resulting images were of poor quality with the given equipment. Thus, it was not possible to make reliable judgment about metastases in the lungs in the given circumstances. Furthermore, due to respiration abdominal metastases were also hard to judge. No metastases could be documented for i. f. transplanted VH-64 and SaOS-2 in MRI.

Organs of representative mice of the experiment were analysed immunohistochemically. TC-71 and PC3M i. f. transplanted mice showed liver metastases and furthermore in a mouse transplanted with PC3M numerous very small lung metastases could be observed in immunohistology. Therefore, tissue slices were stained with huCD99 (staining process involved universal probe from Menapath Kit, HPR polymer, and VectaStain ABC as well as counterstaining with Harris' hematoxylin; see 3.7.1) and examined microscopically. Cells of metastases with human origin stained positively and thus could be distinguished form the murine organ-tissue (Figure 6.12).

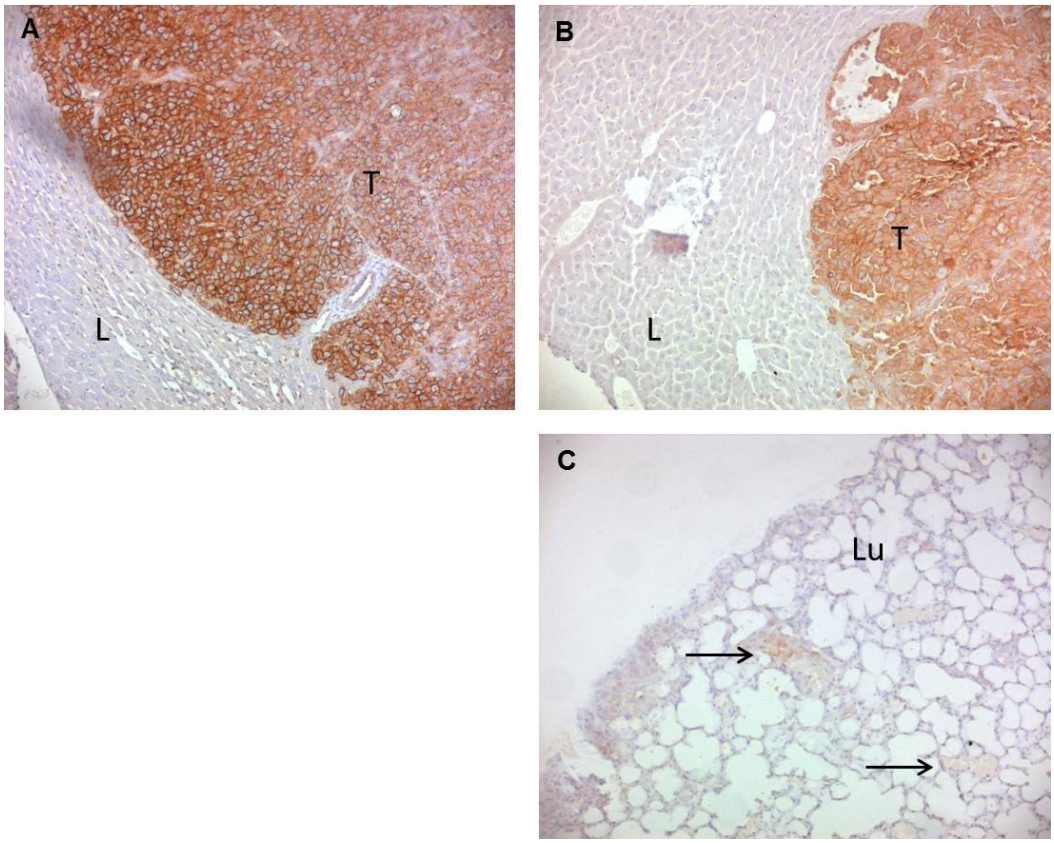

Figure 6.12: Metastases identified in histology. A, Liver metastasis after i. f. transplantation of ES cell line TC-71; **B**, Liver metastasis after i. f. transplantation of CaP cell line PC3M; **C**, Small lung metastases after i. f. transplantation of CaP cell line PC3M (T, tumour; L, liver tissue; Lu, lung tissue; all sections stained with huCD99).

Occasionally, it was possible to image metastases by MRI. However, due to the distance between housing of the animals and the MRI facility it was not possible to image all mice as these mice had to be euthanized as soon as they showed signs of disease. Figure 6.13 displays an exemplary image of a metastasis occurring in the liver of a PC3M-transplanted mouse.

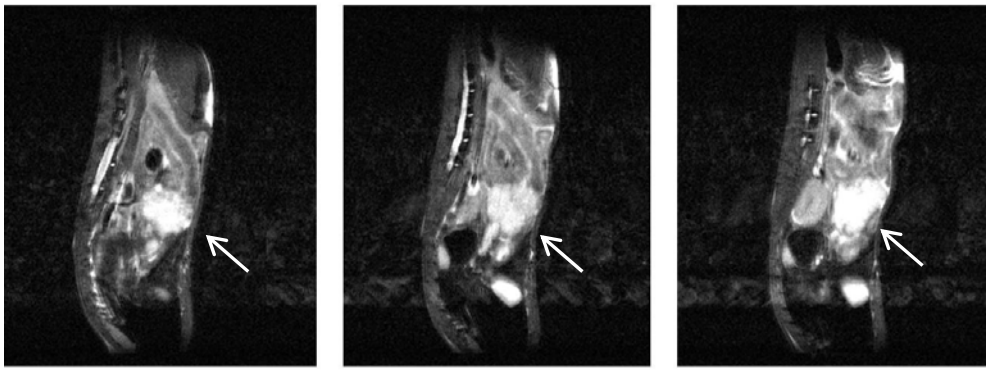

Figure 6.13: Series of three MRI images of the abdomen of a PC3M-transplanted mouse. The white arrows indicates the tumour mass within the abdomen.

6.4 Discussion

The described findings show that all human cell lines tested were able to interact with the murine bone microenvironment and to induce development of tumours. While the ES cell lines induced reactive bone growth, the OS cell line was additionally able to form malignant bone within the tumour mass itself. These findings correlate to a great extent with the clinical situation of ES/PNET and OS patients.

The CaP cell line PC3M formed tumours inducing lysis of the murine bone and in two cases even caused pathological fractures. This correlates with the clinical findings. However, most commonly osteoblastic lesions are observed in CaP patients with metastatic disease. Nevertheless, pathological fractures are frequently seen in CaP patients with osseous lesions as well (compare introduction chapter 6). Until today, there are only very few preclinical models that are able to mirror the osteoblastic features of bone metastases caused by

CaP. In the majority of models in which CaP cells are transplanted directly into the bone osteolysis is observed.

Mice transplanted with the ES/PNET cell lines VH-64 and TC-71 had to be euthanized 38 and 31 days after transplantation, respectively. Mice transplanted with the prostate cancer cell line PC3M reached protocol limits after 29 days. However, the development of tumour sizes leading to euthanasia after SAOS-2 transplantation took 70 days which is significantly longer than development of all other investigated tumour cell lines.

For a long time there has been the need for the development of orthotopic models for bone malignancies. Currently, there are several orthotopic models available; however, one of the advantages of an i. f. model is the relative accessibility of the femur by simply bending the knee and accessing it through the distal end. Compared to other systems such as transplantation of tumour cells into the ribs, i. f. injection is a minimally invasive and a non-traumatic procedure, which provides us with a reliable preclinical orthotopic model for bone malignancies. In comparison to i. t. transplantation, transplantation into the bigger femur during i. f. transplantation offers an easier approach. As the state of research suggests a MSC to most likely be the cell of origin for ES/PNET (see chapter 1.1.7), it can be assumed that the placement of tumour cells within the bone marrow cavity would be appropriate and leave the ES/PNET cells in the orthotopic environment.

New imaging techniques such as CT, PET and MRI can be of great help in following the progression of disease in a preclinical model. Furthermore, numbers of experimental animals can be cut down dramatically. In more detail, CT proved to be a reliable tool for the investigation of bone reactions to

transplanted cells while MRI was able to describe the soft tissue component of the developed tumours. FDG-PET was not the technique of choice for this project as the background signal was quite high so that the primary tumour was difficult to define on the images. Furthermore, there was a high signal of the heart muscle due to the routinely used Isoflorane. An experiment with s. c. tumours induced through ES/PNET cell transplantation showed that by using the injectable anaesthetics with Ketamine/Medetomidin avoids the strong background signal from the heart. Therefore, this type of anaesthesia might be the better choice for future PET studies. However, Ketamine/Medetomidin is not as well-tolerated as inhalable anaesthesia with Isoflorane is (personal experience).

PET was used in i. v. experiments performed before although it was here shown not to be the technique of choice. This is due to the fact that the i. v. experiments were performed in Münster, where PET was the only modern imaging technology available at that time point. Even with input from clinically very experienced radiologists metastases on PET images could only be detected when analysing individual planes rather than looking at summation images. For the experiments of the i. f. model, which was developed and investigated in Newcastle, different PET equipment was used and thus results of PET imaging performed here demonstrated that FDG-PET is not a very sensitive technique to study local progression and systemic dissemination of ES/PNET in preclinical models.

As by now, however, there are a lot of different radiolabelled compounds used as tracers for tumour cells, which allow to study basically any biochemical process of cellular function *in vivo* (Chatziioannou, 2002; Lewis et al., 2002). Thus,

employing this orthotopic model of bone malignancies it will be possible to investigate, if these components are more suitable for imaging of ES/PNET *in vivo*. Succesfully tested tracers can than be employed in clinics and patients will ultimately be able to benefit from this.

There are more *in vivo* imaging opportunities such as fluorescence and bioluminescence imaging that can be used to visualise labelled cells in preclinical models. Bioluminescence can visualise cells that are for example transfected with plasmids encoding for appropriate genes such as luciferase. This leads to light emission without the need of excitation when luciferin is injected. This fact and the longer wavelength of the produced signal lead to better images than images produced using cells labelled with eGFP. Currently, our group is in the progress of developing preclinical models using bioluminescence to track human tumour cells *in vivo* in the mice. This will provide further experimental opportunities for this orthotopic model in the future.

6.5 Conclusions

The orthotopic model for bone malignancies offers a reliable and highly reproducible tool for research on primary malignancies of the bone such as ES/PNET and OS and other cancers that induce bone metastases. Further to the development using different cell lines it will be necessary and interesting to investigate the behaviour of primary material in this preclinical model.

The described i. f. model is established within the Northern Institute for Cancer Research and will be used in further and on-going studies on pharmaceuticals for therapy of ES/PNET. Furthermore, it offers a great opportunity for studying the

interaction between tumour cells and their microenvironment in the bone and thus for dissecting the biology of ES/PNET, OS as well of bone metastases caused by other types of cancers. It will also give the possibility to further investigate the effects of CXCR4-knockdown on ES/PNET cell lines as well as the involvement of different genes and their products that were found to be differentially expressed in different organ-specific metastases.

7. Chapter – General Discussion and Conclusions

The aim of this thesis has been to investigate different aspects of the mechanisms of organ-specific metastasis in ES/PNET and whether it would be possible to identify an organ-specific pattern of gene expression that would correlate with organ-specific metastasis. Furthermore, a knockdown system was designed to investigate the role of CXCR4 as a possible driver for metastasis in ES/PNET.
Finally, to be able to focus on the interaction of ES/PNET cells with their orthotopic environment in the bm/bone, an i. f. mouse model was developed using *in vivo* imaging.

7.1 General Discussion

Although in the past decades great progress has been made in our understanding and the treatment of ES/PNET the knowledge of the basic mechanisms underlying metastasis and tumour progression is still limited. Furthermore, although treatment has changed immensely with the introduction of chemotherapy and patients have better outcomes than ever, differences between patients with localised and metastatic disease are still enormous. Patients with metastases to the bones still have a particularly poor and unsatisfying outcome.
A first step to understanding the differences between patients with metastasis to different organs has been undertaken. It was possible to identify differentially expressed genes when comparing metastases from different organs in a preclinical model of ES/PNET metastasis.

The initial hypothesis of the presence of subclones within tumour cell lines with the ability of inducing organ-selective metastases could not be verified. After re-transplantation tumour cells recovered from lungs or bone/bone marrow were able to metastasise to other organs as well. However, (although no statistical analysis could be performed due to the small number of experimental mice) it appeared that re-transplanted clones derived from lungs of primary mice were able to form metastases in secondary mice after a shorter period of time.

Furthermore, the results suggest that transplantation selected for an aggressive type of cells as these were able to establish in different organs again after re-transplantation. The function of some of the genes that could be identified in all comparisons of gene expression lists of the parental cell line versus the different metastases fit this hypothesis and may be responsible for the more aggressive growth and increased proliferation *in vivo*. Future research will need to identify the key drivers of this aggressive phenotype, particularly as the functions of many of the genes on the list are unknown.

Genes that were noticeable in comparisons of microarrays of clones derived from different organs directly against each other might mirror the influence of the specific microenvironments on the cells that settled in these.

A further fact that has to be taken into account in this experiment is clonal variation as every metastasis originates from one single cell that homed, settled and subsequently developed a metastasis. This might also have influenced the set of genes that is regarded as specific for the organ-specific metastases grouped together and, therefore, the analysis needs to be extended to a higher number of clones.

Most importantly, cell lines may not reflect tumour cell heterogeneity in primary material. These cells have undergone selection in cell culture over a long period of time and are expected to be less microenvironment-dependent as compared with primary tumour cells. Thus, it would be of interest to underline and strengthen these results with transplantation of primary material.

Attempts have been made to analyse specific gene patterns that would allow to predict the course of disease and outcomes (prognostic biomarkers). Ohali et al. suggest a gene pattern that might be able to give a classification of patients into high- and low-risk subgroups and they have the identified overexpressed genes from tumours with a poor prognosis that might be targets for the new cancer therapies (Ohali et al., 2004).

Further work tried to describe molecular signatures that distinguish localised and metastatic disease (Schaefer et al., 2008) or to identify marker genes which reflect tumour resistance to chemotherapy using material from primary tumours and metastases (Scotlandi et al., 2009).

However, to date there is a lack of research on the molecular programme that drives the metastatic phenotype in ES/PNET and results in the different outcome in patients with localised and metastatic disease.

Any hypotheses derived from the described xenograft mouse model will need to be validated in primary patients. It would be especially interesting to analyse the differences in gene expression in cells of different metastases from patients directly. However, it is ethically difficult to obtain not only material from primary tumours but also material from metastases as most patients are children or adolescents and biopsing metastases would be purely for scientific reasons and of no benefit for the patient. Material from metastases might be available after

treatment, if metastases have to be removed. However, cells of this material have undergone at least chemotherapy and thus will have altered characteristics and biology. This is why, it will remain a challenge to investigate why outcomes for patients with pulmonary and bone metastases remains so poor.

As mentioned before, some cancer types such as breast and prostate cancer as well as melanoma metastasise in a CXCL12/CXCR4-dependant manner. This involves metastasis via the blood stream and subsequent homing to CXCL12 rich tissues such as bone.

In previous research high expression of CXCR4 was correlated with a metastatic behaviour and worse prognosis for ES/PNET patients, which might indicate a role of the CXCL12/CXCR4 axis in the biology of ES/PNET cells. Due to this evidence, investigations involving knockdown of this cytokine-receptor was undertaken.

For the construction of a knockdown plasmid pEPI-EGFP was selected and proved to be stable in ES/PNET cell lines without the need of a constant selection pressure. It was possible to construct a knockdown plasmid against CXCR4. But due to lack of time, it was not possible to investigate the consequences of CXCR4 knockdown in this thesis.

If knockdown of CXCR4 in ES/PNET cell lines leads to a phenotype it would be essential to validate these findings on primary material. Most ES/PNET cell lines only show a weak expression of CXCR4 while it has been shown that primary material expresses CXCR4. This lack of CXCR4 expression in cell lines might result from the fact that cultivation of these for a long time might have left cells altered in their expression of several surface markers and ES/PNET cell lines

have become less dependent on signals from their normal microenvironment (here CXCL12). The role of CXCR4 expression as a prognostic biomarker that predicts a metastatic phenotype would then need to be explored and confirmed in a prospective clinical study.

Concluding, it could be demonstrated that the constructed vector pEPI-EGFP with the pol III promoter H1 can be used in ES/PNET cells as a tool for knockdown of different target genes as well. The pEPI-EGFP vector with the pol II promoter H1 will be a useful tool to analyse candidate genes for ES/PNET metastasis.

To be able to perform research focused on the interaction of ES/PNET cells in the "natural" microenvironment an orthotopic model was developed by injecting tumour cells directly into the easily assessable femur of mice. The significance and great importance of orthotopic transplantation becomes obvious through the proof that the whole process of metastasis is more efficient, closely mimics human metastasis and metastases manifest in clinically relevant sites (Bibby, 2004).

The primary tumours developed in this orthotopic i. f. model for ES/PNET and OS mirror to a great extent the clinical situation of primary bone tumours and their interaction with the bone tissue in patients. CT images showed the influence transplanted cells had on remodelling murine femur. In ES/PNET transplanted mice bones reacted with formation of new bone material that appeared in form of sunray spicules and lifting of the periosteum. In OS transplanted mice the formation of reactive bone was visible as well. In addition to this malignant bone formation within the tumour mass was visible. Further studies with improved

imaging techniques that visualise metastatic disease reliably will have to be carried out to be able to also focus on metastatic progression in the experimental mice.

The proposed model of i. f. transplantation in combination with NanoCT imaging, MRI and histology promises to be a valuable and reliable tool for future experiments on the interaction between tumour cells and the bone microenvironment. It will be possible to directly investigate the influence of tumour cells on the different cell types within this microenvironment. As the cell of origin for ES/PNET is most probably a mesenchymal stem cell, a model employing transplantation into the bone marrow cavity can be postulated to be very likely orthotopic. However, this remains speculative as long as the cell of orgin is open to debate. As ES/PNET metastasis is considered to be via haematogenic spread and ES/PNET cells can be found in the bone marrow, this model is likely to represent a model reflecting bone marrow and bone metastasis.

However, it has to be kept in mind that the "resolution" is very different with $5x10^6$ cells being transplanted where usually one cell turns malignant. And thus interaction between injected tumour cells and the microenvironment has to be understood as different in comparison to the interaction between a single malignant cell of origin and its "natural" microenvironment (always bearing in mind that there is also the difference between human and murine cells in the microenvironment of the bone marrow). Further experiments should thus also be carried out with down-scalled numbers of human ES/PNET cells transplanted onto experimental mice.

Furthermore, studies on novel treatments will benefit from this model as it is highly reproducible and easy to handle and could thus be used in addition to s. c.

models that are routinely used in drug development. Results of studies will have high significance against the background of the employment of an orthotopic model, particularly when using primary tumour cells that will be more micronenvironment-dependent as compared with cell lines.

In conclusion, this model will provide an excellent tool for functional studies of the metastatic phenotype using an RNAi approach; in particular to dissect the role of CXCR4 and other candiate genes identified here through gene expression studies.

7.2 Future Directions

Metastatic disease is the clinically most important adverse risk factor and associated with a dismal outcome. Therefore, there is a great need of understanding the biology of metastasis in ES/PNET. A mechanistic understanding will be fundamental for the identification of new targets against which drugs could be developed that are specifically active in metastatic disease.

One candidate mechanism that was studied in the thesis was CXCR4. CXCR4 is expressed in a variety of cancer types and has been shown to play a role in metastasis of these cancers. As CXCR4 is up-regulated by the EWS/FLI1 fusion gene the key molecular event in ES/PNET and as CXCR4 is expressed on the cell surface it is likely to play a role in migration and homing of ES/PNET cells. A vector-based knockdown-system has been developed to study the role of CXCR4 *in vitro* and *in vivo*. With this tool it will be possible to further investigate the role of CXCR4 in migration, adhesion and invasion of ES/PNET cells *in vitro* and on the metastatic phenotype in preclinical *in vivo* models. CXCR4 might constitute a potential target for treatment and CXCR4 antagonists that can disrupt CXCR4-mediated tumour cell adhesion to stromal cells and sensitise cancer cells to chemotherapy are already in clinical development.

One key focus of this thesis has been a detailed investigation of the interactions between human ES/PNET, OS and CaP cells and the murine bone and bone marrow microenvironment in an orthotopic xenograft model. The human cancer cells induce re-modelling of the murine bone in a fashion similar to that seen in patients, including induction of reactive bone growth (spiculae fomation) and osteolysis; and also formation of malignant bone within OS. Thus, this model provides a good basis for future research in this field and will be a reliable tool

for investigations on the biology of these cancers as well as an addition to s. c. models applied in investigations on new pharmaceuticals.

Beyond this, identification of the cell of origin still remains a goal that has to be achieved. This is of specific interest as the knowledge about the cell of origin or cells of origin for different types of ES/PNET will greatly influence our understanding of the biology and thus the clinical behaviour of ES/PNET.

8. Chapter – Bibliography

Aggarwal, R., Ghobrial, I. M., and Roodman, G. D. (2006). Chemokines in multiple myeloma. Exp. Hematol *34*, 1289-1295.

Agliano, A., Martin-Padura, I., Mancuso, P., Marighetti, P., Rabascio, C., Pruneri, G., Shultz, L. D., and Bertolini, F. (2008). Human acute leukemia cells injected in NOD/LtSz-scid/IL-2Rgamma null mice generate a faster and more efficient disease compared to other NOD/scid-related strains. Int. J. Cancer *123*, 2222-2227.

Aiuti, A., Tavian, M., Cipponi, A., Ficara, F., Zappone, E., Hoxie, J., Peault, B., and Bordignon, C. (1999). Expression of CXCR4, the receptor for stromal cell-derived factor-1 on fetal and adult human lympho-hematopoietic progenitors. Eur. J. Immunol *29*, 1823-1831.

Allinen, M., Beroukhim, R., Cai, L., Brennan, C., Lahti-Domenici, J., Huang, H., Porter, D., Hu, M., Chin, L., Richardson, A., et al. (2004). Molecular characterization of the tumor microenvironment in breast cancer. Cancer Cell *6*, 17-32.

Armengol, G., Tarkkanen, M., Virolainen, M., Forus, A., Valle, J., Böhling, T., Asko-Seljavaara, S., Blomqvist, C., Elomaa, I., Karaharju, E., et al. (1997). Recurrent gains of 1q, 8 and 12 in the Ewing family of tumours by comparative genomic hybridization. Br. J. Cancer *75*, 1403-1409.

Aryee, D. N. T., Niedan, S., Kauer, M., Schwentner, R., Bennani-Baiti, I. M., Ban, J., Muehlbacher, K., Kreppel, M., Walker, R. L., Meltzer, P., et al. (2010). Hypoxia modulates EWS-FLI1 transcriptional signature and

enhances the malignant properties of Ewing's sarcoma cells in vitro. Cancer Res *70*, 4015-4023.

Baer, M., Nilsen, T. W., Costigan, C., and Altman, S. (1990). Structure and transcription of a human gene for H1 RNA, the RNA component of human RNase P. Nucleic Acids Res *18*, 97-103.

Bailly, R. A., Bosselut, R., Zucman, J., Cormier, F., Delattre, O., Roussel, M., Thomas, G., and Ghysdael, J. (1994). DNA-binding and transcriptional activation properties of the EWS-FLI-1 fusion protein resulting from the t(11;22) translocation in Ewing sarcoma. Mol. Cell. Biol *14*, 3230-3241.

Batson, O. V. (1940). THE FUNCTION OF THE VERTEBRAL VEINS AND THEIR ROLE IN THE SPREAD OF METASTASES. Ann. Surg *112*, 138-149.

Baxter, A. G., and Cooke, A. (1993). Complement lytic activity has no role in the pathogenesis of autoimmune diabetes in NOD mice. Diabetes *42*, 1574-1578.

Bendre, M. S., Margulies, A. G., Walser, B., Akel, N. S., Bhattacharrya, S., Skinner, R. A., Swain, F., Ramani, V., Mohammad, K. S., Wessner, L. L., et al. (2005). Tumor-derived interleukin-8 stimulates osteolysis independent of the receptor activator of nuclear factor-kappaB ligand pathway. Cancer Res *65*, 11001-11009.

Bennani-Baiti, I. M., Cooper, A., Lawlor, E. R., Kauer, M., Ban, J., Aryee, D. N. T., and Kovar, H. (2010). Intercohort gene expression co-analysis reveals chemokine receptors as prognostic indicators in Ewing's sarcoma. Clin. Cancer Res *16*, 3769-3778.

Berghuis, D., Santos, S. J., Baelde, H. J., Taminiau, A. H., Maarten Egeler, R., Schilham, M. W., Hogendoorn, P. C., and Lankester, A. C. (2011). Pro-inflammatory chemokine-chemokine receptor interactions within the Ewing sarcoma microenvironment determine CD8(+) T-lymphocyte infiltration and affect tumour progression. J. Pathol *223*, 347-357.

Bernstein, E., Caudy, A. A., Hammond, S. M., and Hannon, G. J. (2001). Role for a bidentate ribonuclease in the initiation step of RNA interference. Nature *409*, 363-366.

Bernstein, M., Kovar, H., Paulussen, M., Randall, R. L., Schuck, A., Teot, L. A., and Juergens, H. (2006). Ewing's sarcoma family of tumors: current management. Oncologist *11*, 503-519.

Berrettoni, B. A., and Carter, J. R. (1986). Mechanisms of cancer metastasis to bone. J Bone Joint Surg Am *68*, 308-312.

Beyer Nardi, N., and da Silva Meirelles, L. (2008). Mesenchymal Stem Cells: Isolation, In Vitro Expansion and Characterisation. In Stem Cells (Springer).

Bianco, P., Robey, P. G., and Simmons, P. J. (2008). Mesenchymal stem cells: revisiting history, concepts, and assays. Cell Stem Cell *2*, 313-319.

Bibby, M. C. (2004). Orthotopic models of cancer for preclinical drug evaluation: advantages and disadvantages. Eur. J. Cancer *40*, 852-857.

Birchmeier, W., and Behrens, J. (1994). Cadherin expression in carcinomas: role in the formation of cell junctions and the prevention of invasiveness. Biochim. Biophys. Acta *1198*, 11-26.

Bode, J., Kohwi, Y., Dickinson, L., Joh, T., Klehr, D., Mielke, C., and Kohwi-Shigematsu, T. (1992). Biological significance of unwinding capability of nuclear matrix-associating DNAs. Science *255*, 195-197.

Bogenmann, E. (1996). A metastatic neuroblastoma model in SCID mice. Int. J. Cancer *67*, 379-385.

Bosma, G. C., Custer, R. P., and Bosma, M. J. (1983). A severe combined immunodeficiency mutation in the mouse. Nature *301*, 527-530.

Bosma, G. C., Fried, M., Custer, R. P., Carroll, A., Gibson, D. M., and Bosma, M. J. (1988a). Evidence of functional lymphocytes in some (leaky) scid mice. J. Exp. Med *167*, 1016-1033.

Bosma, M., Schuler, W., and Bosma, G. (1988b). The scid mouse mutant. Curr. Top. Microbiol. Immunol *137*, 197-202.

Boyle, W. J., Simonet, W. S., and Lacey, D. L. (2003). Osteoclast differentiation and activation. Nature *423*, 337-342.

Breitling, R., Armengaud, P., Amtmann, A., and Herzyk, P. (2004). Rank products: a simple, yet powerful, new method to detect differentially regulated genes in replicated microarray experiments. FEBS Lett *573*, 83-92.

Browne, J., and de Pierro, A. B. (1996). A row-action alternative to the EM algorithm for maximizing likelihood in emission tomography. IEEE Trans Med Imaging *15*, 687-699.

Brummelkamp, T. R., Bernards, R., and Agami, R. (2002). A system for stable expression of short interfering RNAs in mammalian cells. Science *296*, 550-553.

Burdach, S., Plehm, S., Unland, R., Dirksen, U., Borkhardt, A., Staege, M. S., Müller-Tidow, C., and Richter, G. H. S. (2009). Epigenetic maintenance of stemness and malignancy in peripheral neuroectodermal tumors by EZH2. Cell Cycle *8*, 1991-1996.

Burgert, E. O., Nesbit, M. E., Garnsey, L. A., Gehan, E. A., Herrmann, J., Vietti, T. J., Cangir, A., Tefft, M., Evans, R., and Thomas, P. (1990). Multimodal therapy for the management of nonpelvic, localized Ewing's sarcoma of bone: intergroup study IESS-II. J. Clin. Oncol *8*, 1514-1524.

Burns, J. M., Summers, B. C., Wang, Y., Melikian, A., Berahovich, R., Miao, Z., Penfold, M. E. T., Sunshine, M. J., Littman, D. R., Kuo, C. J., et al. (2006). A novel chemokine receptor for SDF-1 and I-TAC involved in cell survival, cell adhesion, and tumor development. J. Exp. Med *203*, 2201-2213.

Burr, D. B. (2002). Targeted and nontargeted remodeling. Bone *30*, 2-4.

Bussard, K. M., Gay, C. V., and Mastro, A. M. (2008). The bone microenvironment in metastasis; what is special about bone? Cancer Metastasis Rev *27*, 41-55.

Cao, Y., Zhou, Z., de Crombrugghe, B., Nakashima, K., Guan, H., Duan, X., Jia, S.-F., and Kleinerman, E. S. (2005). Osterix, a transcription factor for osteoblast differentiation, mediates antitumor activity in murine osteosarcoma. Cancer Res *65*, 1124-1128.

Carthew, R. W., and Sontheimer, E. J. (2009). Origins and Mechanisms of miRNAs and siRNAs. Cell *136*, 642-655.

Castillero-Trejo, Y., Eliazer, S., Xiang, L., Richardson, J. A., and Ilaria, R. L. (2005). Expression of the EWS/FLI-1 oncogene in murine primary bone-

derived cells Results in EWS/FLI-1-dependent, ewing sarcoma-like tumors. Cancer Res *65*, 8698-8705.

Cavazzana, A. O., Miser, J. S., Jefferson, J., and Triche, T. J. (1987). Experimental evidence for a neural origin of Ewing's sarcoma of bone. Am. J. Pathol *127*, 507-518.

Chaffer, C. L., and Weinberg, R. A. (2011). A perspective on cancer cell metastasis. Science *331*, 1559-1564.

Chambers, T. J., and Fuller, K. (1985). Bone cells predispose bone surfaces to resorption by exposure of mineral to osteoclastic contact. J. Cell. Sci *76*, 155-165.

Chansky, H. A., Barahmand-Pour, F., Mei, Q., Kahn-Farooqi, W., Zielinska-Kwiatkowska, A., Blackburn, M., Chansky, K., Conrad, E. U., Bruckner, J. D., Greenlee, T. K., et al. (2004). Targeting of EWS/FLI-1 by RNA interference attenuates the tumor phenotype of Ewing's sarcoma cells in vitro. J. Orthop. Res *22*, 910-917.

Chiao, J. W., Moonga, B. S., Yang, Y. M., Kancherla, R., Mittelman, A., Wu-Wong, J. R., and Ahmed, T. (2000). Endothelin-1 from prostate cancer cells is enhanced by bone contact which blocks osteoclastic bone resorption. Br. J. Cancer *83*, 360-365.

Chinni, S. R., Sivalogan, S., Dong, Z., Filho, J. C. T., Deng, X., Bonfil, R. D., and Cher, M. L. (2006). CXCL12/CXCR4 signaling activates Akt-1 and MMP-9 expression in prostate cancer cells: the role of bone microenvironment-associated CXCL12. Prostate *66*, 32-48.

Chinni, S. R., Yamamoto, H., Dong, Z., Sabbota, A., Bonfil, R. D., and Cher, M. L. (2008). CXCL12/CXCR4 transactivates HER2 in lipid rafts of prostate

cancer cells and promotes growth of metastatic deposits in bone. Mol. Cancer Res *6*, 446-457.

Chirgwin, J. M., and Guise, T. A. (2000). Molecular mechanisms of tumor-bone interactions in osteolytic metastases. Crit. Rev. Eukaryot. Gene Expr *10*, 159-178.

Christianson, S. W., Shultz, L. D., and Leiter, E. H. (1993). Adoptive transfer of diabetes into immunodeficient NOD-scid/scid mice. Relative contributions of CD4+ and CD8+ T-cells from diabetic versus prediabetic NOD.NON-Thy-1a donors. Diabetes *42*, 44-55.

Cironi, L., Riggi, N., Provero, P., Wolf, N., Suvà, M.-L., Suvà, D., Kindler, V., and Stamenkovic, I. (2008). IGF1 is a common target gene of Ewing's sarcoma fusion proteins in mesenchymal progenitor cells. PLoS ONE *3*, e2634.

Clark, E. A., Golub, T. R., Lander, E. S., and Hynes, R. O. (2000). Genomic analysis of metastasis reveals an essential role for RhoC. Nature *406*, 532-535.

Clarke, B. (2008). Normal bone anatomy and physiology. Clin J Am Soc Nephrol *3 Suppl 3*, S131-139.

Clines, G. A., Mohammad, K. S., Bao, Y., Stephens, O. W., Suva, L. J., Shaughnessy, J. D., Fox, J. W., Chirgwin, J. M., and Guise, T. A. (2007). Dickkopf homolog 1 mediates endothelin-1-stimulated new bone formation. Mol. Endocrinol *21*, 486-498.

Coleman, R. E. (2001). Metastatic bone disease: clinical features, pathophysiology and treatment strategies. Cancer Treat. Rev *27*, 165-176.

Coleman, R. E. (2006). Clinical features of metastatic bone disease and risk of skeletal morbidity. Clin. Cancer Res *12*, 6243s-6249s.

Collins, A. T., and Maitland, N. J. (2006). Prostate cancer stem cells. Eur. J. Cancer *42*, 1213-1218.

Colter, D. C., Sekiya, I., and Prockop, D. J. (2001). Identification of a subpopulation of rapidly self-renewing and multipotential adult stem cells in colonies of human marrow stromal cells. Proc. Natl. Acad. Sci. U.S.A *98*, 7841-7845.

Corey, E., Quinn, J. E., Bladou, F., Brown, L. G., Roudier, M. P., Brown, J. M., Buhler, K. R., and Vessella, R. L. (2002). Establishment and characterization of osseous prostate cancer models: intra-tibial injection of human prostate cancer cells. Prostate *52*, 20-33.

Corral, D. A., Amling, M., Priemel, M., Loyer, E., Fuchs, S., Ducy, P., Baron, R., and Karsenty, G. (1998). Dissociation between bone resorption and bone formation in osteopenic transgenic mice. Proc. Natl. Acad. Sci. U.S.A *95*, 13835-13840.

Cotterill, S. J., Ahrens, S., Paulussen, M., Jürgens, H. F., Voûte, P. A., Gadner, H., and Craft, A. W. (2000a). Prognostic factors in Ewing's tumor of bone: analysis of 975 patients from the European Intergroup Cooperative Ewing's Sarcoma Study Group. J. Clin. Oncol *18*, 3108-3114.

Cotterill, S. J., Ahrens, S., Paulussen, M., Jürgens, H. F., Voûte, P. A., Gadner, H., and Craft, A. W. (2000b). Prognostic factors in Ewing's tumor of bone: analysis of 975 patients from the European Intergroup Cooperative Ewing's Sarcoma Study Group. J. Clin. Oncol *18*, 3108-3114.

Craft, A., Cotterill, S., Malcolm, A., Spooner, D., Grimer, R., Souhami, R., Imeson, J., and Lewis, I. (1998). Ifosfamide-containing chemotherapy in Ewing's sarcoma: The Second United Kingdom Children's Cancer Study Group and the Medical Research Council Ewing's Tumor Study. J. Clin. Oncol *16*, 3628-3633.

Cullen, B. R. (2005). RNAi the natural way. Nat. Genet *37*, 1163-1165.

Cullen, B. R. (2004). Transcription and processing of human microRNA precursors. Mol. Cell *16*, 861-865.

Custer, R. P., Bosma, G. C., and Bosma, M. J. (1985). Severe combined immunodeficiency (SCID) in the mouse. Pathology, reconstitution, neoplasms. Am. J. Pathol *120*, 464-477.

Dahlin, D. C., and Coventry, M. B. (1967). Osteogenic sarcoma. A study of six hundred cases. J Bone Joint Surg Am *49*, 101-110.

Dalal, S., and Burchill, S. A. (2009). Preclinical evaluation of vascular-disrupting agents in Ewing's sarcoma family of tumours. Eur. J. Cancer *45*, 713-722.

Dass, C. R., Nadesapillai, A. P. W., Robin, D., Howard, M. L., Fisher, J. L., Zhou, H., and Choong, P. F. M. (2005). Downregulation of uPAR confirms link in growth and metastasis of osteosarcoma. Clin. Exp. Metastasis *22*, 643-652.

Delattre, O., Zucman, J., Melot, T., Garau, X. S., Zucker, J. M., Lenoir, G. M., Ambros, P. F., Sheer, D., Turc-Carel, C., and Triche, T. J. (1994). The Ewing family of tumors--a subgroup of small-round-cell tumors defined by specific chimeric transcripts. N. Engl. J. Med *331*, 294-299.

Delattre, O., Zucman, J., Plougastel, B., Desmaze, C., Melot, T., Peter, M., Kovar, H., Joubert, I., de Jong, P., and Rouleau, G. (1992). Gene fusion with an ETS DNA-binding domain caused by chromosome translocation in human tumours. Nature *359*, 162-165.

Le Deley, M.-C., Delattre, O., Schaefer, K.-L., Burchill, S. A., Koehler, G., Hogendoorn, P. C. W., Lion, T., Poremba, C., Marandet, J., Ballet, S., et al. (2010). Impact of EWS-ETS fusion type on disease progression in Ewing's sarcoma/peripheral primitive neuroectodermal tumor: prospective results from the cooperative Euro-E.W.I.N.G. 99 trial. J. Clin. Oncol *28*, 1982-1988.

DeVita, V. T., and Schein, P. S. (1973). The use of drugs in combination for the treatment of cancer: rationale and results. N. Engl. J. Med *288*, 998-1006.

Diederichs, S., Bulk, E., Steffen, B., Ji, P., Tickenbrock, L., Lang, K., Zänker, K. S., Metzger, R., Schneider, P. M., Gerke, V., et al. (2004). S100 family members and trypsinogens are predictors of distant metastasis and survival in early-stage non-small cell lung cancer. Cancer Res *64*, 5564-5569.

Dirksen, U., and Jürgens, H. (2010). Approaching Ewing sarcoma. Future Oncol *6*, 1155-1162.

Dong, Z., Bonfil, R. D., Chinni, S., Deng, X., Trindade Filho, J. C., Bernardo, M., Vaishampayan, U., Che, M., Sloane, B. F., Sheng, S., et al. (2005). Matrix metalloproteinase activity and osteoclasts in experimental prostate cancer bone metastasis tissue. Am. J. Pathol *166*, 1173-1186.

Dontu, G., Al-Hajj, M., Abdallah, W. M., Clarke, M. F., and Wicha, M. S. (2003). Stem cells in normal breast development and breast cancer. Cell Prolif *36 Suppl 1*, 59-72.

van Doorninck, J. A., Ji, L., Schaub, B., Shimada, H., Wing, M. R., Krailo, M. D., Lessnick, S. L., Marina, N., Triche, T. J., Sposto, R., et al. (2010). Current treatment protocols have eliminated the prognostic advantage of type 1 fusions in Ewing sarcoma: a report from the Children's Oncology Group. J. Clin. Oncol *28*, 1989-1994.

Du, Y.-F., Shi, Y., Xing, Y.-F., Xing, Y.-fei, Zeng, F.-Q., and Zeng, F.-qing (2008). Establishment of CXCR4-small interfering RNA retrovirus vector driven by human prostate-specific antigen promoter and its biological effects on prostate cancer in vitro and in vivo. J. Cancer Res. Clin. Oncol *134*, 1255-1264.

Eisen, M. B., and Brown, P. O. (1999). DNA arrays for analysis of gene expression. Meth. Enzymol *303*, 179-205.

Elbashir, S. M., Lendeckel, W., and Tuschl, T. (2001). RNA interference is mediated by 21- and 22-nucleotide RNAs. Genes Dev *15*, 188-200.

Endo, Y., Beauchamp, E., Woods, D., Taylor, W. G., Toretsky, J. A., Uren, A., and Rubin, J. S. (2008). Wnt-3a and Dickkopf-1 stimulate neurite outgrowth in Ewing tumor cells via a Frizzled3- and c-Jun N-terminal kinase-dependent mechanism. Mol. Cell. Biol *28*, 2368-2379.

Estrada-Aguilar, J., Greenberg, H., Walling, A., Schroer, K., Black, T., Morse, S., and Hvizdala, E. (1992). Primary treatment of pelvic osteosarcoma. Report of five cases. Cancer *69*, 1137-1145.

Everts, V., Delaissé, J. M., Korper, W., Jansen, D. C., Tigchelaar-Gutter, W., Saftig, P., and Beertsen, W. (2002). The bone lining cell: its role in cleaning Howship's lacunae and initiating bone formation. J. Bone Miner. Res *17*, 77-90.

Ewing, J. (1939). A review of the classification of bone tumors. Surg Gynecol Obstet *68*, 971–976.

Ewing, J. (1921). Diffuse endothelioma of bone. Proc NY Pathol Soc *21*, 17-24.

Ewing, J. (1924). Further report of endothelial myeloma of bone. Proc NY Patho l Soc *24*, 93–100.

Fidler, I. J., and Kripke, M. L. (1977). Metastasis results from preexisting variant cells within a malignant tumor. Science *197*, 893-895.

Fire, A., Xu, S., Montgomery, M. K., Kostas, S. A., Driver, S. E., and Mello, C. C. (1998). Potent and specific genetic interference by double-stranded RNA in Caenorhabditis elegans. Nature *391*, 806-811.

Flanagan, S. P. (1966). "Nude", a new hairless gene with pleiotropic effects in the mouse. Genet. Res *8*, 295-309.

de Fougerolles, A., Vornlocher, H.-P., Maraganore, J., and Lieberman, J. (2007). Interfering with disease: a progress report on siRNA-based therapeutics. Nat Rev Drug Discov *6*, 443-453.

Franks, T. M., and Lykke-Andersen, J. (2008). The control of mRNA decapping and P-body formation. Mol. Cell *32*, 605-615.

Franzius, C., Hotfilder, M., Poremba, C., Hermann, S., Schäfers, K., Gabbert, H. E., Jürgens, H., Schober, O., Schäfers, M., and Vormoor, J. (2006). Successful high-resolution animal positron emission tomography of

human Ewing tumours and their metastases in a murine xenograft model. Eur. J. Nucl. Med. Mol. Imaging *33*, 1432-1441.

Fraumeni, J. F., and Glass, A. G. (1970). Rarity of Ewing's sarcoma among U.S. Negro children. Lancet *1*, 366-367.

Frei, E., Karon, M., Levin, R. H., Freireich, E. J., Taylor, R. J., Hananian, J., Selawry, O., Holland, J. F., Hoogstraten, B., Wolman, I. J., et al. (1965). The effectiveness of combinations of antileukemic agents in inducing and maintaining remission in children with acute leukemia. Blood *26*, 642-656.

Fulop, G. M., and Phillips, R. A. (1990). The scid mutation in mice causes a general defect in DNA repair. Nature *347*, 479-482.

Furusato, B., Mohamed, A., Uhlén, M., and Rhim, J. S. (2010). CXCR4 and cancer. Pathol. Int *60*, 497-505.

Gainford, M. C., Dranitsaris, G., and Clemons, M. (2005). Systemic treatment of bone metastases from breast cancer: is it all that it's cracked up to be? J. Clin. Oncol *23*, 4802-4803.

Gellhorn, A., and Hirschberg, E. (1955). Investigation of diverse systems for cancer chemotherapy screening. Cancer Res *15*, 1-125.

Geminder, H., Sagi-Assif, O., Goldberg, L., Meshel, T., Rechavi, G., Witz, I. P., and Ben-Baruch, A. (2001). A possible role for CXCR4 and its ligand, the CXC chemokine stromal cell-derived factor-1, in the development of bone marrow metastases in neuroblastoma. J. Immunol *167*, 4747-4757.

Gentleman, R. C., Carey, V. J., Bates, D. M., Bolstad, B., Dettling, M., Dudoit, S., Ellis, B., Gautier, L., Ge, Y., Gentry, J., et al. (2004). Bioconductor:

open software development for computational biology and bioinformatics. Genome Biol *5*, R80.

Geran, R. I., Greenberg, N. H., Macdonald, M. M., Schumacher, A. M., and Abbott, B. J. (1972). Protocols for screening chemical agents and natural productsagainst animal tumours and other biological systems. Cancer Chemother Rep Part 3 *3*.

Gladson, C. L., and Welch, D. R. (2008). New insights into the role of CXCR4 in prostate cancer metastasis. Cancer Biol. Ther *7*, 1849-1851.

Glinskii, O. V., Huxley, V. H., Glinsky, G. V., Pienta, K. J., Raz, A., and Glinsky, V. V. (2005). Mechanical entrapment is insufficient and intercellular adhesion is essential for metastatic cell arrest in distant organs. Neoplasia *7*, 522-527.

Goldstein, A. S., Huang, J., Guo, C., Garraway, I. P., and Witte, O. N. (2010). Identification of a cell of origin for human prostate cancer. Science *329*, 568-571.

Goltzman, D. (2001). Osteolysis and cancer. J. Clin. Invest *107*, 1219-1220.

Goltzman, D., Karaplis, A. C., Kremer, R., and Rabbani, S. A. (2000). Molecular basis of the spectrum of skeletal complications of neoplasia. Cancer *88*, 2903-2908.

Grier, H. E., Krailo, M. D., Tarbell, N. J., Link, M. P., Fryer, C. J. H., Pritchard, D. J., Gebhardt, M. C., Dickman, P. S., Perlman, E. J., Meyers, P. A., et al. (2003). Addition of ifosfamide and etoposide to standard chemotherapy for Ewing's sarcoma and primitive neuroectodermal tumor of bone. N. Engl. J. Med *348*, 694-701.

Guan, H., Zhou, Z., Wang, H., Jia, S.-F., Liu, W., and Kleinerman, E. S. (2005). A small interfering RNA targeting vascular endothelial growth factor inhibits Ewing's sarcoma growth in a xenograft mouse model. Clin. Cancer Res *11*, 2662-2669.

Guise, T. A., and Chirgwin, J. M. (2003). Transforming growth factor-beta in osteolytic breast cancer bone metastases. Clin. Orthop. Relat. Res, S32-38.

Guise, T. A., Mohammad, K. S., Clines, G., Stebbins, E. G., Wong, D. H., Higgins, L. S., Vessella, R., Corey, E., Padalecki, S., Suva, L., et al. (2006). Basic mechanisms responsible for osteolytic and osteoblastic bone metastases. Clin. Cancer Res *12*, 6213s-6216s.

Hahm (1999). Repression of the gene encoding the TGF-beta type II receptor is a major target of the EWS-FLI1 oncoprotein. Nat. Genet *23*, 481.

Hallen, L. C., Burki, Y., Ebeling, M., Broger, C., Siegrist, F., Oroszlan-Szovik, K., Bohrmann, B., Certa, U., and Foser, S. (2007). Antiproliferative activity of the human IFN-alpha-inducible protein IFI44. J. Interferon Cytokine Res *27*, 675-680.

Hamacher, K., Coenen, H. H., and Stöcklin, G. (1986). Efficient stereospecific synthesis of no-carrier-added 2-[18F]-fluoro-2-deoxy-D-glucose using aminopolyether supported nucleophilic substitution. J. Nucl. Med *27*, 235-238.

Hancock, J. D., and Lessnick, S. L. (2008). A transcriptional profiling meta-analysis reveals a core EWS-FLI gene expression signature. Cell Cycle *7*, 250-256.

Harada, S.-ichi, and Rodan, G. A. (2003). Control of osteoblast function and regulation of bone mass. Nature *423*, 349-355.

Harris, S. E., Harris, M. A., Mahy, P., Wozney, J., Feng, J. Q., and Mundy, G. R. (1994). Expression of bone morphogenetic protein messenger RNAs by normal rat and human prostate and prostate cancer cells. Prostate *24*, 204-211.

Hart, I. R., and Fidler, I. J. (1980). Role of organ selectivity in the determination of metastatic patterns of B16 melanoma. Cancer Res *40*, 2281-2287.

Hattinger, C. M., Pötschger, U., Tarkkanen, M., Squire, J., Zielenska, M., Kiuru-Kuhlefelt, S., Kager, L., Thorner, P., Knuutila, S., Niggli, F. K., et al. (2002). Prognostic impact of chromosomal aberrations in Ewing tumours. Br. J. Cancer *86*, 1763-1769.

Hauben, E. I., and Hogendoorn, P. C. W. (2010). Epidemiology of Primary Bone Tumors and Economical Aspects of Bone Metastases. In Bone Cancer: Progression and Therapeutic Approaches (London, UK: Academic Press), pp. 3-8.

Hayakawa, J., Hsieh, M. M., Uchida, N., Phang, O., and Tisdale, J. F. (2009). Busulfan produces efficient human cell engraftment in NOD/LtSz-Scid IL2Rgamma(null) mice. Stem Cells *27*, 175-182.

Hellberg, C., Schmees, C., Karlsson, S., Ahgren, A., and Heldin, C.-H. (2009). Activation of protein kinase C alpha is necessary for sorting the PDGF beta-receptor to Rab4a-dependent recycling. Mol. Biol. Cell *20*, 2856-2863.

van Hennik, P. B., de Koning, A. E., and Ploemacher, R. E. (1999). Seeding efficiency of primitive human hematopoietic cells in nonobese

diabetic/severe combined immune deficiency mice: implications for stem cell frequency assessment. Blood *94*, 3055-3061.

Hense, H. W., Ahrens, S., Paulussen, M., Lehnert, M., and Jürgens, H. (1999). Deskriptive Epidemiologie der Ewing-Tumoren□: Analysen der deutschen Patienten von (EI)CESS 1980-1997. Klinische Pädiatrie *211*, 360-380.

Herrero-Martín, D., Osuna, D., Ordóñez, J. L., Sevillano, V., Martins, A. S., Mackintosh, C., Campos, M., Madoz-Gúrpide, J., Otero-Motta, A. P., Caballero, G., et al. (2009). Stable interference of EWS-FLI1 in an Ewing sarcoma cell line impairs IGF-1/IGF-1R signalling and reveals TOPK as a new target. Br. J. Cancer *101*, 80-90.

Hildebrand (1890). Über das tubuläre Angiosarkom oder Endotheliom des Knochens. Dtsch Z Chir. *31*, 261-281.

Horwood, N. J., Elliott, J., Martin, T. J., and Gillespie, M. T. (1998). Osteotropic agents regulate the expression of osteoclast differentiation factor and osteoprotegerin in osteoblastic stromal cells. Endocrinology *139*, 4743-4746.

Hotfilder, M., Lanvers, C., Jürgens, H., Boos, J., and Vormoor, J. (2002). c-KIT-expressing Ewing tumour cells are insensitive to imatinib mesylate (STI571). Cancer Chemother. Pharmacol *50*, 167-169.

Hudson, W. A., Li, Q., Le, C., and Kersey, J. H. (1998). Xenotransplantation of human lymphoid malignancies is optimized in mice with multiple immunologic defects. Leukemia *12*, 2029-2033.

Hu-Lieskovan, S., Heidel, J. D., Bartlett, D. W., Davis, M. E., and Triche, T. J. (2005a). Sequence-specific knockdown of EWS-FLI1 by targeted,

nonviral delivery of small interfering RNA inhibits tumor growth in a murine model of metastatic Ewing's sarcoma. Cancer Res *65*, 8984-8992.

Hu-Lieskovan, S., Zhang, J., Wu, L., Shimada, H., Schofield, D. E., and Triche, T. J. (2005b). EWS-FLI1 fusion protein up-regulates critical genes in neural crest development and is responsible for the observed phenotype of Ewing's family of tumors. Cancer Res *65*, 4633-4644.

Hynes, R. O. (2003). Metastatic potential: generic predisposition of the primary tumor or rare, metastatic variants-or both? Cell *113*, 821-823.

International Human Genome Sequencing Consortium (2004). Finishing the euchromatic sequence of the human genome. Nature *431*, 931-945.

Ishikawa, T., Kamiyama, M., Tani-Ishii, N., Suzuki, H., Ichikawa, Y., Hamaguchi, Y., Momiyama, N., and Shimada, H. (2001). Inhibition of osteoclast differentiation and bone resorption by cathepsin K antisense oligonucleotides. Mol. Carcinog *32*, 84-91.

Janknecht, R. (2005). EWS-ETS oncoproteins: the linchpins of Ewing tumors. Gene *363*, 1-14.

Janowski, M. (2009). Functional diversity of SDF-1 splicing variants. Cell Adh Migr *3*, 243-249.

Jeon, I. S., Davis, J. N., Braun, B. S., Sublett, J. E., Roussel, M. F., Denny, C. T., and Shapiro, D. N. (1995). A variant Ewing's sarcoma translocation (7;22) fuses the EWS gene to the ETS gene ETV1. Oncogene *10*, 1229-1234.

Jia, S. F., Worth, L. L., and Kleinerman, E. S. (1999). A nude mouse model of human osteosarcoma lung metastases for evaluating new therapeutic strategies. Clin. Exp. Metastasis *17*, 501-506.

Jia, S.-F., Duan, X., Worth, L. L., Guan, H., and Kleinerman, E. S. (2006). Intratumor murine interleukin-12 gene therapy suppressed the growth of local and distant Ewing's sarcoma. Cancer Gene Ther *13*, 948-957.

Jiang, D., Guo, H., Xu, C., Chang, J., Gu, B., Wang, L., Block, T. M., and Guo, J.-T. (2008). Identification of three interferon-inducible cellular enzymes that inhibit the replication of hepatitis C virus. J. Virol *82*, 1665-1678.

Jiang, D., Weidner, J. M., Qing, M., Pan, X.-B., Guo, H., Xu, C., Zhang, X., Birk, A., Chang, J., Shi, P.-Y., et al. (2010). Identification of five interferon-induced cellular proteins that inhibit west nile virus and dengue virus infections. J. Virol *84*, 8332-8341.

Jiang, Y., Jahagirdar, B. N., Reinhardt, R. L., Schwartz, R. E., Keene, C. D., Ortiz-Gonzalez, X. R., Reyes, M., Lenvik, T., Lund, T., Blackstad, M., et al. (2002). Pluripotency of mesenchymal stem cells derived from adult marrow. Nature *418*, 41-49.

Jürgens, H., Paulussen, M., and Zoubek, A. (2006). Ewing-Tumoren. In Pädiatrische Hämatologie und Onkologie (Berlin, Germany: Springer), pp. 894-910.

Jung, Y., Wang, J., Schneider, A., Sun, Y.-X., Koh-Paige, A. J., Osman, N. I., McCauley, L. K., and Taichman, R. S. (2006). Regulation of SDF-1 (CXCL12) production by osteoblasts; a possible mechanism for stem cell homing. Bone *38*, 497-508.

Kaneko, Y., Yoshida, K., Handa, M., Toyoda, Y., Nishihira, H., Tanaka, Y., Sasaki, Y., Ishida, S., Higashino, F., and Fujinaga, K. (1996). Fusion of an ETS-family gene, EIAF, to EWS by t(17;22)(q12;q12) chromosome

translocation in an undifferentiated sarcoma of infancy. Genes Chromosomes Cancer *15*, 115-121.

Kang, Y., Siegel, P. M., Shu, W., Drobnjak, M., Kakonen, S. M., Cordón-Cardo, C., Guise, T. A., and Massagué, J. (2003). A multigenic program mediating breast cancer metastasis to bone. Cancer Cell *3*, 537-549.

Katagiri, T., Yamaguchi, A., Komaki, M., Abe, E., Takahashi, N., Ikeda, T., Rosen, V., Wozney, J. M., Fujisawa-Sehara, A., and Suda, T. (1994). Bone morphogenetic protein-2 converts the differentiation pathway of C2C12 myoblasts into the osteoblast lineage. J. Cell Biol *127*, 1755-1766.

Kataoka, S., Satoh, J., Fujiya, H., Toyota, T., Suzuki, R., Itoh, K., and Kumagai, K. (1983). Immunologic aspects of the nonobese diabetic (NOD) mouse. Abnormalities of cellular immunity. Diabetes *32*, 247-253.

Kauer, M., Ban, J., Kofler, R., Walker, B., Davis, S., Meltzer, P., and Kovar, H. (2009). A molecular function map of Ewing's sarcoma. PLoS ONE *4*, e5415.

Kaushik, A., Kelsoe, G., and Jaton, J. C. (1995). The nude mutation results in impaired primary antibody repertoire. Eur. J. Immunol *25*, 631-634.

Kawamata, T., and Tomari, Y. (2010). Making RISC. Trends Biochem. Sci *35*, 368-376.

Kawamata, T., Seitz, H., and Tomari, Y. (2009). Structural determinants of miRNAs for RISC loading and slicer-independent unwinding. Nat. Struct. Mol. Biol *16*, 953-960.

Khurana, J. S., and Safadi, P. J. (2009). Bone Structure, Development and Bone Biology. In Essentials in Bone and Soft-Tissue Pathology (New York: Springer), pp. 1-16.

Khvorova, A., Reynolds, A., and Jayasena, S. D. (2003). Functional siRNAs and miRNAs exhibit strand bias. Cell *115*, 209-216.

Klein, K. A., Reiter, R. E., Redula, J., Moradi, H., Zhu, X. L., Brothman, A. R., Lamb, D. J., Marcelli, M., Belldegrun, A., Witte, O. N., et al. (1997). Progression of metastatic human prostate cancer to androgen independence in immunodeficient SCID mice. Nat. Med *3*, 402-408.

Kong, Y. Y., Feige, U., Sarosi, I., Bolon, B., Tafuri, A., Morony, S., Capparelli, C., Li, J., Elliott, R., McCabe, S., et al. (1999). Activated T cells regulate bone loss and joint destruction in adjuvant arthritis through osteoprotegerin ligand. Nature *402*, 304-309.

Kotz, R., Dominkus, M., Zettl, T., Ritschl, P., Windhager, R., Gadner, H., Zielinski, C., and Salzer-Kuntschik, M. (2002). Advances in bone tumour treatment in 30 years with respect to survival and limb salvage. A single institution experience. Int Orthop *26*, 197-202.

Krishnan, V., Bryant, H. U., and Macdougald, O. A. (2006). Regulation of bone mass by Wnt signaling. J. Clin. Invest *116*, 1202-1209.

Kucia, M., Reca, R., Miekus, K., Wanzeck, J., Wojakowski, W., Janowska-Wieczorek, A., Ratajczak, J., and Ratajczak, M. Z. (2005). Trafficking of normal stem cells and metastasis of cancer stem cells involve similar mechanisms: pivotal role of the SDF-1-CXCR4 axis. Stem Cells *23*, 879-894.

Kuntz, S., Kieffer, E., Bianchetti, L., Lamoureux, N., Fuhrmann, G., and Viville, S. (2008). Tex19, a mammalian-specific protein with a restricted expression in pluripotent stem cells and germ line. Stem Cells *26*, 734-744.

Kurreck, J. (2009). RNA interference: from basic research to therapeutic applications. Angew. Chem. Int. Ed. Engl *48*, 1378-1398.

Ladenstein, R., Pötschger, U., Le Deley, M. C., Whelan, J., Paulussen, M., Oberlin, O., van den Berg, H., Dirksen, U., Hjorth, L., Michon, J., et al. (2010). Primary disseminated multifocal Ewing sarcoma: results of the Euro-EWING 99 trial. J. Clin. Oncol *28*, 3284-3291.

Lambert, G., Bertrand, J. R., Fattal, E., Subra, F., Pinto-Alphandary, H., Malvy, C., Auclair, C., and Couvreur, P. (2000). EWS fli-1 antisense nanocapsules inhibits ewing sarcoma-related tumor in mice. Biochem. Biophys. Res. Commun *279*, 401-406.

Lapidot, T., Sirard, C., Vormoor, J., Murdoch, B., Hoang, T., Caceres-Cortes, J., Minden, M., Paterson, B., Caligiuri, M. A., and Dick, J. E. (1994). A cell initiating human acute myeloid leukaemia after transplantation into SCID mice. Nature *367*, 645-648.

Leavey, P. J., Mascarenhas, L., Marina, N., Chen, Z., Krailo, M., Miser, J., Brown, K., Tarbell, N., Bernstein, M. L., Granowetter, L., et al. (2008). Prognostic factors for patients with Ewing sarcoma (EWS) at first recurrence following multi-modality therapy: A report from the Children's Oncology Group. Pediatr Blood Cancer *51*, 334-338.

Lee, R. L., Westendorf, J., and Gold, M. R. (2007). Differential role of reactive oxygen species in the activation of mitogen-activated protein kinases and

Akt by key receptors on B-lymphocytes: CD40, the B cell antigen receptor, and CXCR4. J Cell Commun Signal *1*, 33-43.

Lee, Y., Ahn, C., Han, J., Choi, H., Kim, J., Yim, J., Lee, J., Provost, P., Rådmark, O., Kim, S., et al. (2003). The nuclear RNase III Drosha initiates microRNA processing. Nature *425*, 415-419.

Lee, Y., Jeon, K., Lee, J.-T., Kim, S., and Kim, V. N. (2002). MicroRNA maturation: stepwise processing and subcellular localization. EMBO J *21*, 4663-4670.

Leppä, S., Saarto, T., Vehmanen, L., Blomqvist, C., and Elomaa, I. (2004). A high serum matrix metalloproteinase-2 level is associated with an adverse prognosis in node-positive breast carcinoma. Clin. Cancer Res *10*, 1057-1063.

Lessnick, S. L., Braun, B. S., Denny, C. T., and May, W. A. (1995). Multiple domains mediate transformation by the Ewing's sarcoma EWS/FLI-1 fusion gene. Oncogene *10*, 423-431.

Lessnick, S. L., Dacwag, C. S., and Golub, T. R. (2002). The Ewing's sarcoma oncoprotein EWS/FLI induces a p53-dependent growth arrest in primary human fibroblasts. Cancer Cell *1*, 393-401.

Li, F. P., Tu, J. T., Liu, F. S., and Shiang, E. L. (1980). Rarity of Ewing's sarcoma in China. Lancet *1*, 1255.

Lieber, M. R., Hesse, J. E., Lewis, S., Bosma, G. C., Rosenberg, N., Mizuuchi, K., Bosma, M. J., and Gellert, M. (1988). The defect in murine severe combined immune deficiency: joining of signal sequences but not coding segments in V(D)J recombination. Cell *55*, 7-16.

Lin, P. P., Wang, Y., and Lozano, G. (2011). Mesenchymal Stem Cells and the Origin of Ewing's Sarcoma. Sarcoma *2011*.

Link, M. P., Goorin, A. M., Horowitz, M., Meyer, W. H., Belasco, J., Baker, A., Ayala, A., and Shuster, J. (1991). Adjuvant chemotherapy of high-grade osteosarcoma of the extremity. Updated results of the Multi-Institutional Osteosarcoma Study. Clin. Orthop. Relat. Res, 8-14.

Liu, B. Y., Guo, J., Lanske, B., Divieti, P., Kronenberg, H. M., and Bringhurst, F. R. (1998). Conditionally immortalized murine bone marrow stromal cells mediate parathyroid hormone-dependent osteoclastogenesis in vitro. Endocrinology *139*, 1952-1964.

Liu, J., Carmell, M. A., Rivas, F. V., Marsden, C. G., Thomson, J. M., Song, J.-J., Hammond, S. M., Joshua-Tor, L., and Hannon, G. J. (2004). Argonaute2 is the catalytic engine of mammalian RNAi. Science *305*, 1437-1441.

Lokeshwar, B. L., Selzer, M. G., Block, N. L., and Gunja-Smith, Z. (1993). Secretion of matrix metalloproteinases and their inhibitors (tissue inhibitor of metalloproteinases) by human prostate in explant cultures: reduced tissue inhibitor of metalloproteinase secretion by malignant tissues. Cancer Res *53*, 4493-4498.

Lu, D.-Y., Tang, C.-H., Yeh, W.-L., Wong, K.-L., Lin, C.-P., Chen, Y.-H., Lai, C.-H., Chen, Y.-F., Leung, Y.-M., and Fu, W.-M. (2009). SDF-1alpha up-regulates interleukin-6 through CXCR4, PI3K/Akt, ERK, and NF-kappaB-dependent pathway in microglia. Eur. J. Pharmacol *613*, 146-154.

Lücke, A. (1866). Beiträge zur Geschwulstlehre: III. Lympho-sarcom der Achseldrüse: embolische Geschwülste der Lungen; allgemeine Leukämie. Tod. Virchows Arch *35*, 524-539.

Lynch, C. C., Hikosaka, A., Acuff, H. B., Martin, M. D., Kawai, N., Singh, R. K., Vargo-Gogola, T. C., Begtrup, J. L., Peterson, T. E., Fingleton, B., et al. (2005). MMP-7 promotes prostate cancer-induced osteolysis via the solubilization of RANKL. Cancer Cell *7*, 485-496.

Manara, M. C., Baldini, N., Serra, M., Lollini, P. L., De Giovanni, C., Vaccari, M., Argnani, A., Benini, S., Maurici, D., Picci, P., et al. (2000). Reversal of malignant phenotype in human osteosarcoma cells transduced with the alkaline phosphatase gene. Bone *26*, 215-220.

Mani, S. A., Guo, W., Liao, M.-J., Eaton, E. N., Ayyanan, A., Zhou, A. Y., Brooks, M., Reinhard, F., Zhang, C. C., Shipitsin, M., et al. (2008). The epithelial-mesenchymal transition generates cells with properties of stem cells. Cell *133*, 704-715.

Mao, X., Miesfeldt, S., Yang, H., Leiden, J. M., and Thompson, C. B. (1994). The FLI-1 and chimeric EWS-FLI-1 oncoproteins display similar DNA binding specificities. J. Biol. Chem *269*, 18216-18222.

Marie, P. J., Debiais, F., and Haÿ, E. (2002). Regulation of human cranial osteoblast phenotype by FGF-2, FGFR-2 and BMP-2 signaling. Histol. Histopathol *17*, 877-885.

Matsuo, K., and Irie, N. (2008). Osteoclast-osteoblast communication. Arch. Biochem. Biophys *473*, 201-209.

May, W. A., Gishizky, M. L., Lessnick, S. L., Lunsford, L. B., Lewis, B. C., Delattre, O., Zucman, J., Thomas, G., and Denny, C. T. (1993a). Ewing

sarcoma 11;22 translocation produces a chimeric transcription factor that requires the DNA-binding domain encoded by FLI1 for transformation. Proc. Natl. Acad. Sci. U.S.A *90*, 5752-5756.

May, W. A., Lessnick, S. L., Braun, B. S., Klemsz, M., Lewis, B. C., Lunsford, L. B., Hromas, R., and Denny, C. T. (1993b). The Ewing's sarcoma EWS/FLI-1 fusion gene encodes a more potent transcriptional activator and is a more powerful transforming gene than FLI-1. Mol. Cell. Biol *13*, 7393-7398.

Mazurier, F., Doedens, M., Gan, O. I., and Dick, J. E. (2003). Rapid myeloerythroid repopulation after intrafemoral transplantation of NOD-SCID mice reveals a new class of human stem cells. Nat. Med *9*, 959-963.

McGrath, K. E., Koniski, A. D., Maltby, K. M., McGann, J. K., and Palis, J. (1999). Embryonic expression and function of the chemokine SDF-1 and its receptor, CXCR4. Dev. Biol *213*, 442-456.

McPherson, J. D., Marra, M., Hillier, L., Waterston, R. H., Chinwalla, A., Wallis, J., Sekhon, M., Wylie, K., Mardis, E. R., Wilson, R. K., et al. (2001). A physical map of the human genome. Nature *409*, 934-941.

Miyagawa, Y., Okita, H., Nakaijima, H., Horiuchi, Y., Sato, B., Taguchi, T., Toyoda, M., Katagiri, Y. U., Fujimoto, J., Hata, J.-I., et al. (2008). Inducible expression of chimeric EWS/ETS proteins confers Ewing's family tumor-like phenotypes to human mesenchymal progenitor cells. Mol. Cell. Biol *28*, 2125-2137.

Mocellin, S., and Rossi, C. R. (2007). The principles of gene microarray data analysis. In Microarray Technology and Cancer Gene Profiling.

Advances in Experimental Medicine and Biology. (Austin, USA: Landes Bioscience), pp. 19-30.

Möhle, R., Moore, M. A., Nachman, R. L., and Rafii, S. (1997). Transendothelial migration of CD34+ and mature hematopoietic cells: an in vitro study using a human bone marrow endothelial cell line. Blood *89*, 72-80.

Morel, A.-P., Lièvre, M., Thomas, C., Hinkal, G., Ansieau, S., and Puisieux, A. (2008). Generation of breast cancer stem cells through epithelial-mesenchymal transition. PLoS ONE *3*, e2888.

Müller, A., Homey, B., Soto, H., Ge, N., Catron, D., Buchanan, M. E., McClanahan, T., Murphy, E., Yuan, W., Wagner, S. N., et al. (2001). Involvement of chemokine receptors in breast cancer metastasis. Nature *410*, 50-56.

Mundy, G. R. (2002). Metastasis to bone: causes, consequences and therapeutic opportunities. Nat. Rev. Cancer *2*, 584-593.

Nagasawa, T., Hirota, S., Tachibana, K., Takakura, N., Nishikawa, S., Kitamura, Y., Yoshida, N., Kikutani, H., and Kishimoto, T. (1996). Defects of B-cell lymphopoiesis and bone-marrow myelopoiesis in mice lacking the CXC chemokine PBSF/SDF-1. Nature *382*, 635-638.

Nagle, R. B., Knox, J. D., Wolf, C., Bowden, G. T., and Cress, A. E. (1994). Adhesion molecules, extracellular matrix, and proteases in prostate carcinoma. J. Cell. Biochem. Suppl *19*, 232-237.

Nagpal, M. L., Davis, J., and Lin, T. (2006). Overexpression of CXCL10 in human prostate LNCaP cells activates its receptor (CXCR3) expression and inhibits cell proliferation. Biochim. Biophys. Acta *1762*, 811-818.

Nakamura, E. S., Koizumi, K., Kobayashi, M., Saitoh, Y., Arita, Y., Nakayama, T., Sakurai, H., Yoshie, O., and Saiki, I. (2006). RANKL-induced CCL22/macrophage-derived chemokine produced from osteoclasts potentially promotes the bone metastasis of lung cancer expressing its receptor CCR4. Clin. Exp. Metastasis *23*, 9-18.

Nannuru, K. C., and Singh, R. K. (2010). Tumor-stromal interactions in bone metastasis. Curr Osteoporos Rep *8*, 105-113.

Navarro, D., Agra, N., Pestaña, A., Alonso, J., and González-Sancho, J. M. (2010). The EWS/FLI1 oncogenic protein inhibits expression of the Wnt inhibitor DICKKOPF-1 gene and antagonizes beta-catenin/TCF-mediated transcription. Carcinogenesis *31*, 394-401.

Nesbit, M. E., Gehan, E. A., Burgert, E. O., Vietti, T. J., Cangir, A., Tefft, M., Evans, R., Thomas, P., Askin, F. B., and Kissane, J. M. (1990). Multimodal therapy for the management of primary, nonmetastatic Ewing's sarcoma of bone: a long-term follow-up of the First Intergroup study. J. Clin. Oncol *8*, 1664-1674.

Nguyen, P., Bar-Sela, G., Sun, L., Bisht, K. S., Cui, H., Kohn, E., Feinberg, A. P., and Gius, D. (2008). BAT3 and SET1A form a complex with CTCFL/BORIS to modulate H3K4 histone dimethylation and gene expression. Mol. Cell. Biol *28*, 6720-6729.

Nonoyama, S., Smith, F. O., Bernstein, I. D., and Ochs, H. D. (1993). Strain-dependent leakiness of mice with severe combined immune deficiency. J. Immunol *150*, 3817-3824.

Nurieva, R. I., Zheng, S., Jin, W., Chung, Y., Zhang, Y., Martinez, G. J., Reynolds, J. M., Wang, S.-L., Lin, X., Sun, S.-C., et al. (2010). The E3

ubiquitin ligase GRAIL regulates T cell tolerance and regulatory T cell function by mediating T cell receptor-CD3 degradation. Immunity *32*, 670-680.

Odri, G. A., Dumoucel, S., Picarda, G., Battaglia, S., Lamoureux, F., Corradini, N., Rousseau, J., Tirode, F., Laud, K., Delattre, O., et al. (2010). Zoledronic acid as a new adjuvant therapeutic strategy for Ewing's sarcoma patients. Cancer Res *70*, 7610-7619.

Oefelein, M. G., Ricchiuti, V., Conrad, W., and Resnick, M. I. (2002). Skeletal fractures negatively correlate with overall survival in men with prostate cancer. J. Urol *168*, 1005-1007.

Oettel, H., and Wilhelm, G. (1955). Tests of compounds against Ehrlich ascites tumor, sarcoma 180 and Walker carcino-sarcoma 256. Cancer Res *Suppl. 2*, 129-144.

Ohali, A., Avigad, S., Zaizov, R., Ophir, R., Horn-Saban, S., Cohen, I. J., Meller, I., Kollender, Y., Issakov, J., and Yaniv, I. (2004). Prediction of high risk Ewing's sarcoma by gene expression profiling. Oncogene *23*, 8997-9006.

Olsen, B. R., Reginato, A. M., and Wang, W. (2000). Bone development. Annu. Rev. Cell Dev. Biol *16*, 191-220.

Paddison, P. J., Caudy, A. A., Bernstein, E., Hannon, G. J., and Conklin, D. S. (2002). Short hairpin RNAs (shRNAs) induce sequence-specific silencing in mammalian cells. Genes Dev *16*, 948-958.

Paget, S. (1889). The distribution of secondary growths in cancer of the breast. Lancet *133*, 571-573.

Palmqvist, P., Persson, E., Conaway, H. H., and Lerner, U. H. (2002). IL-6, leukemia inhibitory factor, and oncostatin M stimulate bone resorption

and regulate the expression of receptor activator of NF-kappa B ligand, osteoprotegerin, and receptor activator of NF-kappa B in mouse calvariae. J. Immunol *169*, 3353-3362.

Pantelouris, E. M. (1968). Absence of thymus in a mouse mutant. Nature *217*, 370-371.

Parfitt, A. M. (2001). The bone remodeling compartment: a circulatory function for bone lining cells. J. Bone Miner. Res *16*, 1583-1585.

Paulussen, M., Ahrens, S., Burdach, S., Craft, A., Dockhorn-Dworniczak, B., Dunst, J., Fröhlich, B., Winkelmann, W., Zoubek, A., and Jürgens, H. (1998a). Primary metastatic (stage IV) Ewing tumor: survival analysis of 171 patients from the EICESS studies. European Intergroup Cooperative Ewing Sarcoma Studies. Ann. Oncol *9*, 275-281.

Paulussen, M., Ahrens, S., Craft, A. W., Dunst, J., Fröhlich, B., Jabar, S., Rübe, C., Winkelmann, W., Wissing, S., Zoubek, A., et al. (1998b). Ewing's tumors with primary lung metastases: survival analysis of 114 (European Intergroup) Cooperative Ewing's Sarcoma Studies patients. J. Clin. Oncol *16*, 3044-3052.

Paulussen, M., Ahrens, S., Dunst, J., Winkelmann, W., Exner, G. U., Kotz, R., Amann, G., Dockhorn-Dworniczak, B., Harms, D., Müller-Weihrich, S., et al. (2001). Localized Ewing tumor of bone: final results of the cooperative Ewing's Sarcoma Study CESS 86. J. Clin. Oncol *19*, 1818-1829.

Paulussen, M., Craft, A. W., Lewis, I., Hackshaw, A., Douglas, C., Dunst, J., Schuck, A., Winkelmann, W., Köhler, G., Poremba, C., et al. (2008). Results of the EICESS-92 Study: two randomized trials of Ewing's

sarcoma treatment--cyclophosphamide compared with ifosfamide in standard-risk patients and assessment of benefit of etoposide added to standard treatment in high-risk patients. J. Clin. Oncol *26*, 4385-4393.

Paulussen, M., Ranft, A., Dirksen, U., and Jürgens, H. (2007). Ewing tumours: Outcome in children, adolescents and adult patients. European Journal of Cancer Supplements *5*, 209-215.

Peter, M., Couturier, J., Pacquement, H., Michon, J., Thomas, G., Magdelenat, H., and Delattre, O. (1997). A new member of the ETS family fused to EWS in Ewing tumors. Oncogene *14*, 1159-1164.

Phillips, R. A., Jewett, M. A., and Gallie, B. L. (1989). Growth of human tumors in immune-deficient scid mice and nude mice. Curr. Top. Microbiol. Immunol *152*, 259-263.

Piechaczek, C., Fetzer, C., Baiker, A., Bode, J., and Lipps, H. J. (1999). A vector based on the SV40 origin of replication and chromosomal S/MARs replicates episomally in CHO cells. Nucleic Acids Res *27*, 426-428.

Pieper, S., Ranft, A., Braun-Munzinger, G., Jurgens, H., Paulussen, M., and Dirksen, U. (2008). Ewing's tumors over the age of 40: a retrospective analysis of 47 patients treated according to the International Clinical Trials EICESS 92 and EURO-E.W.I.N.G. 99. Onkologie *31*, 657-663.

Pittenger, M. F., Mackay, A. M., Beck, S. C., Jaiswal, R. K., Douglas, R., Mosca, J. D., Moorman, M. A., Simonetti, D. W., Craig, S., and Marshak, D. R. (1999). Multilineage potential of adult human mesenchymal stem cells. Science *284*, 143-147.

Plougastel, B., Zucman, J., Peter, M., Thomas, G., and Delattre, O. (1993). Genomic structure of the EWS gene and its relationship to EWSR1, a site of tumor-associated chromosome translocation. Genomics *18*, 609-615.

Ponomaryov, T., Peled, A., Petit, I., Taichman, R. S., Habler, L., Sandbank, J., Arenzana-Seisdedos, F., Magerus, A., Caruz, A., Fujii, N., et al. (2000). Induction of the chemokine stromal-derived factor-1 following DNA damage improves human stem cell function. J. Clin. Invest *106*, 1331-1339.

Price, J. S., Oyajobi, B. O., and Russell, R. G. (1994). The cell biology of bone growth. Eur J Clin Nutr *48 Suppl 1*, S131-149.

Prieur, A., Tirode, F., Cohen, P., and Delattre, O. (2004). EWS/FLI-1 silencing and gene profiling of Ewing cells reveal downstream oncogenic pathways and a crucial role for repression of insulin-like growth factor binding protein 3. Mol. Cell. Biol *24*, 7275-7283.

Pringle, J. A. S. (1999). Bone-forming neoplasms arisingwithin bone. In Pathology of bone and joint neoplasms. (Philadelphia: Saunders).

Rajarubendra, N., and Lawrentschuk, N. (2010). Imaging of Bone Cancer. In Bone Cancer: Progression and Therapeutic Approaches (London, UK: Academic Press), pp. 269-282.

Reid, S. H., and Hamdy, F. C. (2007). Epidemiology, Pathology, and Pathogenesis. In Urological Oncology (New York: Springer), pp. 451-469.

Renaud, S., Loukinov, D., Alberti, L., Vostrov, A., Kwon, Y.-W., Bosman, F. T., Lobanenkov, V., and Benhattar, J. (2010). BORIS/CTCFL-mediated

transcriptional regulation of the hTERT telomerase gene in testicular and ovarian tumor cells. Nucleic Acids Res.

Riggi, N., Cironi, L., Provero, P., Suvà, M.-L., Kaloulis, K., Garcia-Echeverria, C., Hoffmann, F., Trumpp, A., and Stamenkovic, I. (2005). Development of Ewing's sarcoma from primary bone marrow-derived mesenchymal progenitor cells. Cancer Res *65*, 11459-11468.

Riggi, N., Suvà, M.-L., Suvà, D., Cironi, L., Provero, P., Tercier, S., Joseph, J.-M., Stehle, J.-C., Baumer, K., Kindler, V., et al. (2008). EWS-FLI-1 expression triggers a Ewing's sarcoma initiation program in primary human mesenchymal stem cells. Cancer Res *68*, 2176-2185.

Riggi, N., Suvà, M.-L., De Vito, C., Provero, P., Stehle, J.-C., Baumer, K., Cironi, L., Janiszewska, M., Petricevic, T., Suvà, D., et al. (2010). EWS-FLI-1 modulates miRNA145 and SOX2 expression to initiate mesenchymal stem cell reprogramming toward Ewing sarcoma cancer stem cells. Genes Dev *24*, 916-932.

Roberts, P., Burchill, S. A., Brownhill, S., Cullinane, C. J., Johnston, C., Griffiths, M. J., McMullan, D. J., Bown, N. P., Morris, S. P., and Lewis, I. J. (2008). Ploidy and karyotype complexity are powerful prognostic indicators in the Ewing's sarcoma family of tumors: a study by the United Kingdom Cancer Cytogenetics and the Children's Cancer and Leukaemia Group. Genes Chromosomes Cancer *47*, 207-220.

Rodriguez-Galindo, C., Spunt, S. L., and Pappo, A. S. (2003). Treatment of Ewing sarcoma family of tumors: current status and outlook for the future. Med. Pediatr. Oncol *40*, 276-287.

Roessner, A., and Jürgens, H. (1993). Round cell tumours of bone. Pathol. Res. Pract *189*, 111-136.

Roodman, G. D. (2004). Mechanisms of bone metastasis. N. Engl. J. Med *350*, 1655-1664.

Ross, F. P., and Teitelbaum, S. L. (2005). alphavbeta3 and macrophage colony-stimulating factor: partners in osteoclast biology. Immunol. Rev *208*, 88-105.

Rygaard, J., and Povlsen, C. O. (1969). Heterotransplantation of a human malignant tumour to "Nude" mice. Acta Pathol Microbiol Scand *77*, 758-760.

Saad, S., Bendall, L. J., James, A., Gottlieb, D. J., and Bradstock, K. F. (2000). Induction of matrix metalloproteinases MMP-1 and MMP-2 by co-culture of breast cancer cells and bone marrow fibroblasts. Breast Cancer Res. Treat *63*, 105-115.

Saeter, G., Alvegård, T. A., Elomaa, I., Wiebe, T., Björk, O., Strander, H., and Solheim, O. P. (1997). Chemotherapy for osteosarcoma and Ewing's sarcoma. Acta Orthop Scand Suppl *273*, 120-125.

Safadi, F. F., Barbe, M. F., Abdelmagid, S. M., Rico, M. C., Aswad, R. A., Litvin, J., and Popoff, S. N. (2009). Bone Structure, Development and Bone Biology. In Bone Pathology (New York: Springer), pp. 1-50.

Salcedo, R., Wasserman, K., Young, H. A., Grimm, M. C., Howard, O. M., Anver, M. R., Kleinman, H. K., Murphy, W. J., and Oppenheim, J. J. (1999). Vascular endothelial growth factor and basic fibroblast growth factor induce expression of CXCR4 on human endothelial cells: In vivo

neovascularization induced by stromal-derived factor-1alpha. Am. J. Pathol *154*, 1125-1135.

Sancéau, J., Poupon, M.-F., Delattre, O., Sastre-Garau, X., and Wietzerbin, J. (2002). Strong inhibition of Ewing tumor xenograft growth by combination of human interferon-alpha or interferon-beta with ifosfamide. Oncogene *21*, 7700-7709.

Schaefer, K.-L., Eisenacher, M., Braun, Y., Brachwitz, K., Wai, D. H., Dirksen, U., Lanvers-Kaminsky, C., Juergens, H., Herrero, D., Stegmaier, S., et al. (2008). Microarray analysis of Ewing's sarcoma family of tumours reveals characteristic gene expression signatures associated with metastasis and resistance to chemotherapy. Eur. J. Cancer *44*, 699-709.

Schleiermacher, G., Peter, M., Oberlin, O., Philip, T., Rubie, H., Mechinaud, F., Sommelet-Olive, D., Landman-Parker, J., Bours, D., Michon, J., et al. (2003). Increased risk of systemic relapses associated with bone marrow micrometastasis and circulating tumor cells in localized ewing tumor. J. Clin. Oncol *21*, 85-91.

Schmid, C., Schläpfer, I., Futo, E., Waldvogel, M., Schwander, J., Zapf, J., and Froesch, E. R. (1992). Triiodothyronine (T3) stimulates insulin-like growth factor (IGF)-1 and IGF binding protein (IGFBP)-2 production by rat osteoblasts in vitro. Acta Endocrinol *126*, 467-473.

Schmidt, D., Herrmann, C., Jürgens, H., and Harms, D. (1991). Malignant peripheral neuroectodermal tumor and its necessary distinction from Ewing's sarcoma. A report from the Kiel Pediatric Tumor Registry. Cancer *68*, 2251-2259.

Schneider, A., Kalikin, L. M., Mattos, A. C., Keller, E. T., Allen, M. J., Pienta, K. J., and McCauley, L. K. (2005). Bone turnover mediates preferential localization of prostate cancer in the skeleton. Endocrinology *146*, 1727-1736.

Schuck, A., Ahrens, S., Paulussen, M., Kuhlen, M., Könemann, S., Rübe, C., Winkelmann, W., Kotz, R., Dunst, J., Willich, N., et al. (2003). Local therapy in localized Ewing tumors: results of 1058 patients treated in the CESS 81, CESS 86, and EICESS 92 trials. Int. J. Radiat. Oncol. Biol. Phys *55*, 168-177.

Schwarz, B. A., and Bhandoola, A. (2006). Trafficking from the bone marrow to the thymus: a prerequisite for thymopoiesis. Immunol. Rev *209*, 47-57.

Schwarz, D. S., Hutvágner, G., Du, T., Xu, Z., Aronin, N., and Zamore, P. D. (2003). Asymmetry in the assembly of the RNAi enzyme complex. Cell *115*, 199-208.

Scotlandi, K., Benini, S., Manara, M. C., Serra, M., Nanni, P., Lollini, P. L., Nicoletti, G., Landuzzi, L., Chano, T., Picci, P., et al. (2000). Murine model for skeletal metastases of Ewing's sarcoma. J. Orthop. Res *18*, 959-966.

Scotlandi, K., Benini, S., Nanni, P., Lollini, P. L., Nicoletti, G., Landuzzi, L., Serra, M., Manara, M. C., Picci, P., and Baldini, N. (1998). Blockage of insulin-like growth factor-I receptor inhibits the growth of Ewing's sarcoma in athymic mice. Cancer Res *58*, 4127-4131.

Scotlandi, K., Avnet, S., Benini, S., Manara, M. C., Serra, M., Cerisano, V., Perdichizzi, S., Lollini, P.-L., De Giovanni, C., Landuzzi, L., et al. (2002). Expression of an IGF-I receptor dominant negative mutant

induces apoptosis, inhibits tumorigenesis and enhances chemosensitivity in Ewing's sarcoma cells. Int. J. Cancer *101*, 11-16.

Scotlandi, K., Remondini, D., Castellani, G., Manara, M. C., Nardi, F., Cantiani, L., Francesconi, M., Mercuri, M., Caccuri, A. M., Serra, M., et al. (2009). Overcoming resistance to conventional drugs in Ewing sarcoma and identification of molecular predictors of outcome. J. Clin. Oncol *27*, 2209-2216.

Scotton, C. J., Wilson, J. L., Milliken, D., Stamp, G., and Balkwill, F. R. (2001). Epithelial cancer cell migration: a role for chemokine receptors? Cancer Res *61*, 4961-4965.

Sela, J., Amir, D., Schwartz, Z., and Weinberg, H. (1987). Ultrastructural tissue morphometry of the distribution of extracellular matrix vesicles in remodeling rat tibial bone six days after injury. Acta Anat (Basel) *128*, 295-300.

Serreze, D. V., and Leiter, E. H. (1988). Defective activation of T suppressor cell function in nonobese diabetic mice. Potential relation to cytokine deficiencies. J. Immunol *140*, 3801-3807.

Serreze, D. V., Gaskins, H. R., and Leiter, E. H. (1993). Defects in the differentiation and function of antigen presenting cells in NOD/Lt mice. J. Immunol *150*, 2534-2543.

Shultz, L. D., Schweitzer, P. A., Christianson, S. W., Gott, B., Schweitzer, I. B., Tennent, B., McKenna, S., Mobraaten, L., Rajan, T. V., and Greiner, D. L. (1995). Multiple defects in innate and adaptive immunologic function in NOD/LtSz-scid mice. J. Immunol *154*, 180-191.

Shultz, L. D., Banuelos, S. J., Leif, J., Appel, M. C., Cunningham, M., Ballen, K., Burzenski, L., and Greiner, D. L. (2003). Regulation of human short-term repopulating cell (STRC) engraftment in NOD/SCID mice by host CD122+ cells. Exp. Hematol *31*, 551-558.

Shultz, L. D., Lyons, B. L., Burzenski, L. M., Gott, B., Chen, X., Chaleff, S., Kotb, M., Gillies, S. D., King, M., Mangada, J., et al. (2005). Human lymphoid and myeloid cell development in NOD/LtSz-scid IL2R gamma null mice engrafted with mobilized human hemopoietic stem cells. J. Immunol *174*, 6477-6489.

Siligan, C., Ban, J., Bachmaier, R., Spahn, L., Kreppel, M., Schaefer, K.-L., Poremba, C., Aryee, D. N. T., and Kovar, H. (2005). EWS-FLI1 target genes recovered from Ewing's sarcoma chromatin. Oncogene *24*, 2512-2524.

Sims, N. A., and Gooi, J. H. (2008). Bone remodeling: Multiple cellular interactions required for coupling of bone formation and resorption. Semin. Cell Dev. Biol *19*, 444-451.

Singh, S. K., Hawkins, C., Clarke, I. D., Squire, J. A., Bayani, J., Hide, T., Henkelman, R. M., Cusimano, M. D., and Dirks, P. B. (2004). Identification of human brain tumour initiating cells. Nature *432*, 396-401.

Smith, T. A. (1998). FDG uptake, tumour characteristics and response to therapy: a review. Nucl Med Commun *19*, 97-105.

Sollazzo, M. R., Benassi, M. S., Magagnoli, G., Gamberi, G., Molendini, L., Ragazzini, P., Merli, M., Ferrari, C., Balladelli, A., and Picci, P. (1999).

Increased c-myc oncogene expression in Ewing's sarcoma: correlation with Ki67 proliferation index. Tumori *85*, 167-173.

Sorensen, P. H., Lessnick, S. L., Lopez-Terrada, D., Liu, X. F., Triche, T. J., and Denny, C. T. (1994). A second Ewing's sarcoma translocation, t(21;22), fuses the EWS gene to another ETS-family transcription factor, ERG. Nat. Genet *6*, 146-151.

Staal, F. J. T., van der Burg, M., Wessels, L. F. A., Barendregt, B. H., Baert, M. R. M., van den Burg, C. M. M., van Huffel, C., Langerak, A. W., van der Velden, V. H. J., Reinders, M. J. T., et al. (2003). DNA microarrays for comparison of gene expression profiles between diagnosis and relapse in precursor-B acute lymphoblastic leukemia: choice of technique and purification influence the identification of potential diagnostic markers. Leukemia *17*, 1324-1332.

Staege, M. S., Hansen, G., Baersch, G., and Burdach, S. (2004). Functional and molecular characterization of interleukin-2 transgenic Ewing tumor cells for in vivo immunotherapy. Pediatr Blood Cancer *43*, 23-34.

Stiller, C. A., Craft, A. W., and Corazziari, I. (2001). Survival of children with bone sarcoma in Europe since 1978: results from the EUROCARE study. Eur. J. Cancer *37*, 760-766.

Strauss, S. J., Ng, T., Mendoza-Naranjo, A., Whelan, J., and Sorensen, P. H. B. (2010). Understanding micrometastatic disease and Anoikis resistance in ewing family of tumors and osteosarcoma. Oncologist *15*, 627-635.

Suda, T., Takahashi, N., Udagawa, N., Jimi, E., Gillespie, M. T., and Martin, T. J. (1999). Modulation of osteoclast differentiation and function by the

new members of the tumor necrosis factor receptor and ligand families. Endocr. Rev *20*, 345-357.

Suggitt, M., and Bibby, M. C. (2005). 50 Years of Preclinical Anticancer Drug Screening: Empirical to Target-Driven Approaches. Clinical Cancer Research *11*, 971 -981.

Sun, X., Cheng, G., Hao, M., Zheng, J., Zhou, X., Zhang, J., Taichman, R. S., Pienta, K. J., and Wang, J. (2010). CXCL12 / CXCR4 / CXCR7 chemokine axis and cancer progression. Cancer Metastasis Rev *29*, 709-722.

Sun, Y.-X., Wang, J., Shelburne, C. E., Lopatin, D. E., Chinnaiyan, A. M., Rubin, M. A., Pienta, K. J., and Taichman, R. S. (2003). Expression of CXCR4 and CXCL12 (SDF-1) in human prostate cancers (PCa) in vivo. J. Cell. Biochem *89*, 462-473.

Sutow, W. W., and Sullivan, M. P. (1962). Cyclophosphamide therapy in children with Ewing's sarcoma. Cancer Chemother Rep *23*, 55-60.

Suvà, M.-L., Riggi, N., Stehle, J.-C., Baumer, K., Tercier, S., Joseph, J.-M., Suvà, D., Clément, V., Provero, P., Cironi, L., et al. (2009). Identification of cancer stem cells in Ewing's sarcoma. Cancer Res *69*, 1776-1781.

Tachibana, K., Hirota, S., Iizasa, H., Yoshida, H., Kawabata, K., Kataoka, Y., Kitamura, Y., Matsushima, K., Yoshida, N., Nishikawa, S., et al. (1998). The chemokine receptor CXCR4 is essential for vascularization of the gastrointestinal tract. Nature *393*, 591-594.

Takahashi, M., Miyazaki, H., Furihata, M., Sakai, H., Konakahara, T., Watanabe, M., and Okada, T. (2009). Chemokine CCL2/MCP-1 negatively regulates

metastasis in a highly bone marrow-metastatic mouse breast cancer model. Clin. Exp. Metastasis *26*, 817-828.

Takashima, Y., Era, T., Nakao, K., Kondo, S., Kasuga, M., Smith, A. G., and Nishikawa, S.-I. (2007). Neuroepithelial cells supply an initial transient wave of MSC differentiation. Cell *129*, 1377-1388.

Takuwa, Y., Masaki, T., and Yamashita, K. (1990). The effects of the endothelin family peptides on cultured osteoblastic cells from rat calvariae. Biochem. Biophys. Res. Commun *170*, 998-1005.

Teitell, M. A., Thompson, A. D., Sorensen, P. H., Shimada, H., Triche, T. J., and Denny, C. T. (1999). EWS/ETS fusion genes induce epithelial and neuroectodermal differentiation in NIH 3T3 fibroblasts. Lab. Invest *79*, 1535-1543.

Thiery, J. P., Acloque, H., Huang, R. Y. J., and Nieto, M. A. (2009). Epithelial-mesenchymal transitions in development and disease. Cell *139*, 871-890.

Thiolloy, S., Halpern, J., Holt, G. E., Schwartz, H. S., Mundy, G. R., Matrisian, L. M., and Lynch, C. C. (2009). Osteoclast-derived matrix metalloproteinase-7, but not matrix metalloproteinase-9, contributes to tumor-induced osteolysis. Cancer Res *69*, 6747-6755.

Thomas, R. J., Guise, T. A., Yin, J. J., Elliott, J., Horwood, N. J., Martin, T. J., and Gillespie, M. T. (1999). Breast cancer cells interact with osteoblasts to support osteoclast formation. Endocrinology *140*, 4451-4458.

Thompson, A. D., Teitell, M. A., Arvand, A., and Denny, C. T. (1999). Divergent Ewing's sarcoma EWS/ETS fusions confer a common tumorigenic phenotype on NIH3T3 cells. Oncogene *18*, 5506-5513.

Tinkey, P. T., Lembo, T. M., Evans, G. R., Cundiff, J. H., Gray, K. N., and Price, R. E. (1998). Postirradiation sarcomas in Sprague-Dawley rats. Radiat. Res *149*, 401-404.

Tirode, F., Laud-Duval, K., Prieur, A., Delorme, B., Charbord, P., and Delattre, O. (2007). Mesenchymal stem cell features of Ewing tumors. Cancer Cell *11*, 421-429.

Toretsky, J. A., Erkizan, V., Levenson, A., Abaan, O. D., Parvin, J. D., Cripe, T. P., Rice, A. M., Lee, S. B., and Uren, A. (2006). Oncoprotein EWS-FLI1 activity is enhanced by RNA helicase A. Cancer Res *66*, 5574-5581.

Tran Van, P., Vignery, A., and Baron, R. (1982). An electron-microscopic study of the bone-remodeling sequence in the rat. Cell Tissue Res *225*, 283-292.

Tu, S.-M., Lin, S.-H., and Logothetis, C. J. (2002). Stem-cell origin of metastasis and heterogeneity in solid tumours. Lancet Oncol *3*, 508-513.

Urano, F., Umezawa, A., Hong, W., Kikuchi, H., and Hata, J. (1996). A novel chimera gene between EWS and E1A-F, encoding the adenovirus E1A enhancer-binding protein, in extraosseous Ewing's sarcoma. Biochem. Biophys. Res. Commun *219*, 608-612.

Uren, A., Tcherkasskaya, O., and Toretsky, J. A. (2004a). Recombinant EWS-FLI1 oncoprotein activates transcription. Biochemistry *43*, 13579-13589.

Uren, A., Wolf, V., Sun, Y.-F., Azari, A., Rubin, J. S., and Toretsky, J. A. (2004b). Wnt/Frizzled signaling in Ewing sarcoma. Pediatr Blood Cancer *43*, 243-249.

Väänänen, H. K., Zhao, H., Mulari, M., and Halleen, J. M. (2000). The cell biology of osteoclast function. J. Cell. Sci *113 (Pt 3)*, 377-381.

Vanel, D., Bittoun, J., and Tardivon, A. (1998). MRI of bone metastases. Eur Radiol *8*, 1345-1351.

van 't Veer, L. J., Dai, H., van de Vijver, M. J., He, Y. D., Hart, A. A. M., Mao, M., Peterse, H. L., van der Kooy, K., Marton, M. J., Witteveen, A. T., et al. (2002). Gene expression profiling predicts clinical outcome of breast cancer. Nature *415*, 530-536.

Venditti, J. M., Wesley, R. A., and Plowman, J. (1984). Current NCI preclinical antitumor screening in vivo: results of tumor panel screening, 1976-1982, and future directions. Adv Pharmacol Chemother *20*, 1-20.

Vormoor, J., Baersch, G., Decker, S., Hotfilder, M., Schäfer, K. L., Pelken, L., Rübe, C., Van Valen, F., Jürgens, H., and Dockhorn-Dworniczak, B. (2001). Establishment of an in vivo model for pediatric Ewing tumors by transplantation into NOD/scid mice. Pediatr. Res *49*, 332-341.

Wang, J., Wang, J., Sun, Y., Song, W., Nor, J. E., Wang, C. Y., and Taichman, R. S. (2005). Diverse signaling pathways through the SDF-1/CXCR4 chemokine axis in prostate cancer cell lines leads to altered patterns of cytokine secretion and angiogenesis. Cell. Signal *17*, 1578-1592.

Watson, D. K., Robinson, L., Hodge, D. R., Kola, I., Papas, T. S., and Seth, A. (1997). FLI1 and EWS-FLI1 function as ternary complex factors and ELK1 and SAP1a function as ternary and quaternary complex factors on the Egr1 promoter serum response elements. Oncogene *14*, 213-221.

Weinfeld, M. S., and Dudley, H. R. (1962). Osteogenic sarcoma. A follow-up study of the ninety-four cases observed at the Massachusetts General Hospital from 1920 to 1960. J Bone Joint Surg Am *44-A*, 269-276.

Wennberg, C., Hessle, L., Lundberg, P., Mauro, S., Narisawa, S., Lerner, U. H., and Millán, J. L. (2000). Functional characterization of osteoblasts and osteoclasts from alkaline phosphatase knockout mice. J. Bone Miner. Res *15*, 1879-1888.

Westendorf, J. J., Kahler, R. A., and Schroeder, T. M. (2004). Wnt signaling in osteoblasts and bone diseases. Gene *341*, 19-39.

Widhe, B., and Widhe, T. (2000). Initial symptoms and clinical features in osteosarcoma and Ewing sarcoma. J Bone Joint Surg Am *82*, 667-674.

Wieland, B. W., Bida, G. T., Padgett, H. C., and Go, H. (1989). Current status of CTI target systems for the production of PET radiochemicals. In Proceedings of the 3rd workshop of Targetry and Target Chemistry (Vancouver, British Columbia, Canada).

Williams, B. R. (1997). Role of the double-stranded RNA-activated protein kinase (PKR) in cell regulation. Biochem. Soc. Trans *25*, 509-513.

Wilson, T. J., Nannuru, K. C., and Singh, R. K. (2009). Cathepsin G-mediated activation of pro-matrix metalloproteinase 9 at the tumor-bone interface promotes transforming growth factor-beta signaling and bone destruction. Mol. Cancer Res *7*, 1224-1233.

Wilson, T. J., Nannuru, K. C., Futakuchi, M., and Singh, R. K. (2010). Cathepsin G-mediated enhanced TGF-beta signaling promotes angiogenesis via upregulation of VEGF and MCP-1. Cancer Lett *288*, 162-169.

Witzel, J. G., Prescher, A., and Weisser, H. (1992). Experimental animal model for the evaluation of chemotherapeutical effects on osteosarcoma. Chemotherapy *38*, 251-260.

Wu, Z., and Irizarry, R. A. (2005). Stochastic models inspired by hybridization theory for short oligonucleotide arrays. J. Comput. Biol *12*, 882-893.

Yang, J., and Weinberg, R. A. (2008). Epithelial-mesenchymal transition: at the crossroads of development and tumor metastasis. Dev. Cell *14*, 818-829.

Yang, L., Chansky, H. A., and Hickstein, D. D. (2000). EWS.Fli-1 fusion protein interacts with hyperphosphorylated RNA polymerase II and interferes with serine-arginine protein-mediated RNA splicing. J. Biol. Chem *275*, 37612-37618.

Yasuda, H., Shima, N., Nakagawa, N., Mochizuki, S. I., Yano, K., Fujise, N., Sato, Y., Goto, M., Yamaguchi, K., Kuriyama, M., et al. (1998). Identity of osteoclastogenesis inhibitory factor (OCIF) and osteoprotegerin (OPG): a mechanism by which OPG/OCIF inhibits osteoclastogenesis in vitro. Endocrinology *139*, 1329-1337.

Yoda, M., Kawamata, T., Paroo, Z., Ye, X., Iwasaki, S., Liu, Q., and Tomari, Y. (2010). ATP-dependent human RISC assembly pathways. Nat. Struct. Mol. Biol *17*, 17-23.

Yu, L., Cecil, J., Peng, S.-B., Schrementi, J., Kovacevic, S., Paul, D., Su, E. W., and Wang, J. (2006). Identification and expression of novel isoforms of human stromal cell-derived factor 1. Gene *374*, 174-179.

Yu, X., Huang, Y., Collin-Osdoby, P., and Osdoby, P. (2004). CCR1 chemokines promote the chemotactic recruitment, RANKL development, and motility of osteoclasts and are induced by inflammatory cytokines in osteoblasts. J. Bone Miner. Res *19*, 2065-2077.

Yu, X., Huang, Y., Collin-Osdoby, P., and Osdoby, P. (2003). Stromal cell-derived factor-1 (SDF-1) recruits osteoclast precursors by inducing

chemotaxis, matrix metalloproteinase-9 (MMP-9) activity, and collagen transmigration. J. Bone Miner. Res *18*, 1404-1418.

Yuan, K., Chung, L. W. K., Siegal, G. P., and Zayzafoon, M. (2007). alpha-CaMKII controls the growth of human osteosarcoma by regulating cell cycle progression. Lab. Invest *87*, 938-950.

Zagzag, D., Lukyanov, Y., Lan, L., Ali, M. A., Esencay, M., Mendez, O., Yee, H., Voura, E. B., and Newcomb, E. W. (2006). Hypoxia-inducible factor 1 and VEGF upregulate CXCR4 in glioblastoma: implications for angiogenesis and glioma cell invasion. Lab. Invest *86*, 1221-1232.

Zamore, P. D. (2006). RNA interference: big applause for silencing in Stockholm. Cell *127*, 1083-1086.

Zhang, H., Kolb, F. A., Jaskiewicz, L., Westhof, E., and Filipowicz, W. (2004). Single processing center models for human Dicer and bacterial RNase III. Cell *118*, 57-68.

Zhang, H., Merchant, M. S., Chua, K. S., Khanna, C., Helman, L. J., Telford, B., Ward, Y., Summers, J., Toretsky, J., Thomas, E. K., et al. (2003). Tumor expression of 4-1BB ligand sustains tumor lytic T cells. Cancer Biol. Ther *2*, 579-586.

Zhang, P. J., Barcos, M., Stewart, C. C., Block, A. W., Sait, S., and Brooks, J. J. (2000). Immunoreactivity of MIC2 (CD99) in acute myelogenous leukemia and related diseases. Mod. Pathol *13*, 452-458.

Zhao, C., Irie, N., Takada, Y., Shimoda, K., Miyamoto, T., Nishiwaki, T., Suda, T., and Matsuo, K. (2006). Bidirectional ephrinB2-EphB4 signaling controls bone homeostasis. Cell Metab *4*, 111-121.

Zhao, W., Byrne, M. H., Boyce, B. F., and Krane, S. M. (1999). Bone resorption induced by parathyroid hormone is strikingly diminished in collagenase-resistant mutant mice. J. Clin. Invest *103*, 517-524.

Zhou, Y., Mohan, S., Linkhart, T. A., Baylink, D. J., and Strong, D. D. (1996). Retinoic acid regulates insulin-like growth factor-binding protein expression in human osteoblast cells. Endocrinology *137*, 975-983.

Zhou, Z., Guan, H., Duan, X., and Kleinerman, E. S. (2005). Zoledronic acid inhibits primary bone tumor growth in Ewing sarcoma. Cancer *104*, 1713-1720.

Zou, Y. R., Kottmann, A. H., Kuroda, M., Taniuchi, I., and Littman, D. R. (1998). Function of the chemokine receptor CXCR4 in haematopoiesis and in cerebellar development. Nature *393*, 595-599.

Zubrod, C. G. (1965). Combinations of drugs in the treatment of acute leukemias. Proc. R. Soc. Med *58*, 988-990.

Zucman, J., Melot, T., Desmaze, C., Ghysdael, J., Plougastel, B., Peter, M., Zucker, J. M., Triche, T. J., Sheer, D., and Turc-Carel, C. (1993). Combinatorial generation of variable fusion proteins in the Ewing family of tumours. EMBO J *12*, 4481-4487.

9. Chapter – Appendix

9.1 Abstracts and posters for scientific meetings

Abstract for the XXth Annual Research Meeting of the Kind-Philipp Foundation for Leukemia Research, June 6th-9th, 2007 (Wilsede, Germany).

(Klin Padiatr. 2007 May-Jun;219(3):181-96):

Oral presentation

Identifying Cellular Mechanisms of Organ-Specific Metastasis of Ewing Tumours

H Knizia[1], M Hotfilder[1], J Vormoor[2]

Dep. of Paediatric Haematology/Oncology, U of Muenster[1], and NICR[2], Newcastle, UK

The most important factor in the prognosis of Ewing sarcomas is the presentation of primary metastasis. The 5-year-outcome of patients with lung metastases and with bone tumours or involvement of bone marrow it is 36% resp. only 20%. Patients with a localised tumour can be cured in 50% of the cases. The metastasis model for Ewing sarcoma in NOD/scid-mice shows a metastasis pattern equal to patients. So the conservation of interaction between human tumour cells and the microenvironment of the different mouse organs can be assumed. After intravenous application of Ewing tumour cells, tumour clones are isolated,

preferentially from lung, bone and bone marrow. These tumour clones are analysed in vitro, and re-transplanted into mice. Global gene expression analysis will identify genes, whose expression is correlated to organ specific metastasis. Functional analysis of these genes will be done with the NOD/scid-mouse model. (e.g. by siRNA technology). Intention of our work is the identification of genes, which are involved in organ-specific metastasis and may function as new targets for molecular therapies and diagnostic.

Abstract for XXIth Annual Research Meeting of the Kind-Philipp Foundation for Leukemia Research, June 11th-14th, 2008 (Wilsede, Germany):

Oral presentation

Identifying Cellular Mechanisms of Organ-Specific Metastasis of Ewing's Sarcoma

H Knizia[1], R Unland[1], M Hotfilder[1], E Korsching[2], U Dirksen[1], H Jürgens[1], J Vormoor[3]

Dep. of Paediatric Haematology/Oncology[1], Dep. of Pathology[2], University of Münster, and NICR[3], Newcastle, UK

Prognosis of Ewing sarcomas is mainly influenced by the occurrence of primary metastasis. While 2/3 of patients with localized disease can be cured, the 3-year ETS in patients with lung metastases only is ~50% and the prognosis of patients with bony metastases is <20%. The metastasis model for Ewing sarcoma in NOD/scid-mice shows a metastasis pattern equal to patients. So the conservation of interaction between human tumour cells and the microenvironment of the different mouse organs can be assumed.

Via transplantation of cell lines TC-71 and VH-64 onto NOD/scid-mice 14 subclones preferentially from lung, bone and bone marrow could be generated. The tumour clones where analysed in vitro and re-transplanted into mice. First global gene expression analysis identified 247 genes with different expression levels in bone metastases resp. lung metastases. These genes may be correlated to

organ specific metastasis. Functional analysis of these genes will be done with the NOD/scid-mouse model. (e.g. by shRNA technology).

Intention of our work is the identification of genes, which are involved in organ-specific metastasis and may function as new targets for molecular therapies and diagnostic.

Abstract for BACR/RSM Oncology Section/APS Joint Meeting: "Preclinical models, biomarkers and targeted therapy", November 27th, 2008 (London, UK):

Selected for poster presentation and oral presentation (poster talk)

Identifying Cellular Mechanisms of Organ-Specific Metastasis of Ewing's Sarcoma

Knizia[1,2] H, Batey[1] M, Unland[2] R, Korsching[3] E, Dirksen[2] U, Jürgens[2] H, Heidenreich[1] O, Hotfilder[2] M, Hempel[2] G, Vormoor[1] J

Northern Institute for Cancer Research[1], Newcastle University, UK and Dep. of Paediatric Haematology/Oncology[2], Dep. of Pathology[3], University of Münster, Germany

Ewing's sarcoma is the second most common bone tumour in children and adolescents. The prognosis of Ewing's sarcomas is mainly influenced by the occurrence of primary metastasis. While 2/3 of patients with localized disease can be cured, the 3-year event free survival in patients with lung metastases is only ~50% and <20% in patients with bony metastases. Metastatic models of Ewing's sarcoma in Rag2-/-□c-/-and Nod/Scid mice show a pattern of disease spread similar to that found in patients, providing us with a suitable system for studying this disease.

Transplantation of the TC-71 and VH-64 Ewing's sarcoma cell lines into NOD/scid-mice leads to the development of metastases in lung, bone and bone marrow. Following aseptic removal and disaggregation of tumour cells from

each of these sites, these cells were analysed in vitro and re-transplanted into mice. Global gene expression analysis of clones and subclones identified several genes with differential expression levels in bone metastases compared to lung metastases. Functional analysis of these genes will be carried out in our immunocompromised animal models.

Transplanted mice are imaged using PET and MRI to detect and monitor growing metastases from early stages of development. We are utilising bone density assessment software to interpret some of the MRI data. With this analysis the correlation between possible bone metastases and a loss of bone density will be determined.

Understanding the molecular mechanisms that underlie metastatic spread in Ewing's sarcoma, will allow us to develop more specific therapies for patients with advanced stage Ewing's sarcoma in the future.

Identifying Cellular Mechanisms of Organ-Specific Metastasis of Ewing's Sarcoma

Knizia H[1,2], Batey M[1], Unland R[2], Korsching E[3], Dirksen U[2], Jürgens H[2], Heidenreich O[1], Hotfilder M[2], Hempel G[4], Vormoor J[1]

Northern Institute for Cancer Research[1], Newcastle University, UK and Dep. of Paediatric Haematology/Oncology[2], Dep. of Pathology[3], Dep. of Pharmaceutical and Medical Chemistry[4], University of Münster, Germany

Henrike.Knizia@ncl.ac.uk

Introduction and aims

Ewing's sarcoma is the second most common bone tumour in children and adolescents. The most important factor in prognosis is the presentation of primary metastasis: While 2/3 of patients without metastases can be cured, the 5-year event free survival in patients with lung metastases is only ~50% and ~30% in patients with bony metastases (Fig. 1).

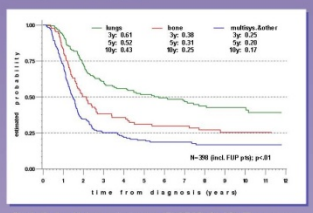

Fig 1: Kaplan-Meier survival curve (EI(CESS) 81-92). The outcome of patients is related to their metastatic pattern.

Using metastatic models of Ewing's sarcoma in *Rag2*$^{-/-}$*yc*$^{-/-}$ and NOD/*Scid* mice, a pattern of disease spread similar to that found in patients can be shown (Ref. 1). This system allows for the study of cellular mechanisms of organ-specific metastasis of this disease. Intravenous (i. v.) transplantation of patient derived TC-71 and VH-64 Ewing's sarcoma cell lines into immuno-compromised mice leads to the development of extensive tumour metastases. These clones are removed aseptically and disaggregated before *in vitro* analysis and re-transplantation into secondary mice to study the consistency of the metastatic pattern. We have recently introduced the orthotopic intrafemoral (i. f.) model of transplantation for our Ewing's sarcoma cell lines, where the cells are injected directly into the bone marrow of the mouse (Fig. 2).

Global gene expression analysis of cell lines, clones and subclones indicates differences in gene expression levels between bone and lung metastases. Further functional analysis of candidate genes will be carried out in our immunocompromised animal models.

Furthermore, we aim to utilise *in vivo* imaging to detect and monitor development of disease in transplanted mice. Previous work has used PET to examine metastatic tumour sites. Following the recent acquisition at Newcastle of a PET scanner, a small animal MRI machine, and a microCT, our intention is to compare and combine these imaging modalities to study mechanisms of tumour metastasis and progression in animals engrafted with Ewing's sarcoma as well as to compare our orthotopic (i. f.) and systemic (i. v.) models.

Methods

- Transplantation of *Rag2*$^{-/-}$*yc*$^{-/-}$ and NOD/*Scid* (NOD/LtSz-*Prkdc*^{scid}/J) mice i. v. and i. f. with resp. 5x10^5 or 1x10^5 cells of cell lines TC-71 and VH-64
- PET (Muenster): high-resolution multi-wire chamber animal PET camera quadHIDAC (Oxford Positron Systems Ltd, Oxford, UK); PET (Newcastle): Philips Mosaic HP (Philips Medical Sysems, Eindhoven, The Netherlands)
- MRI: high-resolution Varian DirectDrive MR system with 7 Tesla 210mm horizontal bore Magnex magnet (Varian Inc., Palo Alto, USA)
- CT: Bioscan NanoCT (Bioscan Inc.Washington, USA)
- Global gene expression analysis by Affymetrix chip HG U133 Plus 2.0

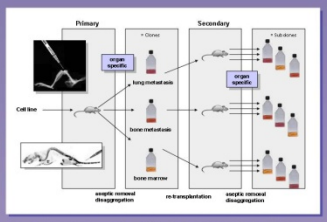

Fig 2: Scheme of the i. v. and i. f. model for Ewing's Sarcoma in NOD/*Scid* and *Rag2*$^{-/-}$*yc*$^{-/-}$. Primary: i. v. or i. f. transplantation of the cell lines, secondary: re-transplantation of the metastases derived clones.

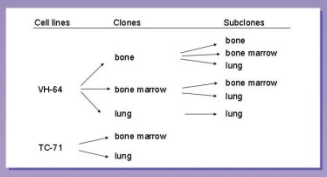

Fig 3: Pattern of metastasis in i. v. transplanted tumour-bearing NOD/*Scid* mice. Clones generated from primary mice, subclones generated from secondary mice transplanted with the same clone respectively from bone, bone marrow or lung.

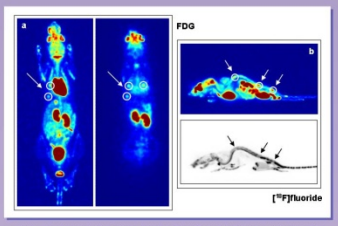

Fig 4: i. v. transplanted Ewing tumour cell line VH-64 in a NOD/*scid* mouse. Whole-body PET, **a** coronal slice (FDG) showing pulmonary metastases; **b** sagittal slice (FDG, [^{18}F]fluoride below) showing vertebral metastases (Ref. 2).

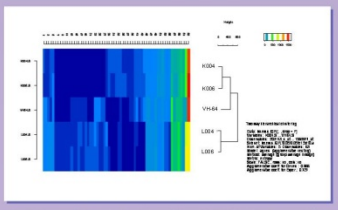

Fig 5: Two way hierarchical clustering of the cell line VH-64, two bone and two lung metastases, respectively: K004, K006 are bone metastases of mice 004 and 006; L004, L006 are lung metastases of mice 004 and 006. A set of 63 exemplary genes was used as a basis.

Results

After i. v. transplantation the pattern of metastasis in NOD/*Scid* mice was found to be comparable to that in patients (Ref. 1). Metastases from the lung, bone and bone marrow were removed aseptically and disaggregated (Fig. 2). Although further analysis of these results is required it would appear that re-transplantation of these generated subclones shows that bone metastases migrate more aggressively than subclones from other tissues of interest (Fig. 3). At the moment an i. f. model for the metastasis of Ewing's sarcoma cells is in development as well as the expansion of both of these models into the *Rag2*$^{-/-}$*yc*$^{-/-}$ strain.

The non invasive detection of metastases was carried out by high-resolution PET. Coronal slices of the FDG PET scan show small pulmonary metastases that were depicted with moderately increased FDG uptake (Fig. 4 a). A FDG PET scan and a [^{18}F]fluoride PET scan demonstrate small vertebral body metastases that show moderately increased FDG uptake and decreased [^{18}F]fluoride uptake (osteolysis) (Fig. 4 b). Images were analysed visually and semi-quantitatively by a region of interest (ROI)-based method in maximum intensity projections (MIP) using coronal and sagittal slices.

Early results from our MRI analysis of tumour bearing mice, show that metastases can easily be detected by MRI (Fig. 6). We are currently in the process of validating our MRI and microCT methodology for comparison to the PET image data.

Preliminary data regarding the gene expression analysis of the subclones derived from primary and secondary transplantations suggest a difference in expression. Bone and lung metastases cluster separately in a hierarchical analysis (Fig. 5).

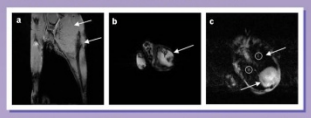

Fig 6: i. f. transplanted Ewing tumour cell line TC-71 in a *Rag2*$^{-/-}$*yc*$^{-/-}$ mouse, **a** coronal slice showing a bone metastasis located in the hip region and a transformation of the femur, **b** transverse slice of the femur region, **c** transverse slice of the thorax region of an i. v. injected *Rag2*$^{-/-}$*yc*$^{-/-}$ mouse showing lung metastases.

Conclusion

- i. v. transplantation of Ewing's sarcoma cell lines into NOD/*Scid* shows a similar metastatic spread of disease to that found in patients
- we are in the process of isolating subclones from secondary animals (implanted with cells taken from primary animals) with an organ-specific metastasis pattern
- we are in the process of investigating whether there are differences in gene expression between different metastatic sites (Affymetrix)
- Initial imaging studies show that metastases can be readily identified via PET or MRI

References

1. *Vormoor J* et al. Pediatr Res. 2001 Mar; 49 (3): 332-41.
2. *Franzius C* et al. Eur J Nucl Med Mol Imaging. 2006 Dec; 33 (12): 1432-41.

Acknowledgements

Thanks to Dr. Ross Maxwell and Ian Wilson for the MRI work.

Abstract for AACR 101st Annual Meeting 2010, April 17th-21st, 2010 (Washington D.C., USA): Selected for poster presentation

Development of an orthotopic model for human malignant bone diseases in immunocompromised NOD.Cg-*Prkdc*^{scid} *Il2rg*^{tm1wjl}/SzJ (NSG) mice

Knizia H, Batey MA, Almeida GS, Wilson I, Maxwell RJ, Dildey P, Hide IG, Bacon CM, Vormoor J

Northern Institute for Cancer Research, Newcastle University, UK

Bone is the third most common site for metastatic disease in cancer. The continuity of bone tissue relies on the delicate balance between osteoblasts and osteoclasts and the formation and resorbtion of new bone tissue. The presence of cancer cells disturbs this equilibrium and can lead to aberrant new bone formation or destruction. In Ewing's Sarcoma (ES) the 3-year event free survival in patients with osseous metastases or bone marrow infiltration is less than 20%, which accounts for 10% of patients. Clinically, the morphological changes to bone caused by ES differ from those of other cancer types such as prostate cancer (CaP).

To better address the interaction between ES and bone, we have developed a preclinical orthotopic bone model. Intrafemoral (i. f.) transplantation is a technically feasible and convenient method for the study of cancer types associated with bone or bone marrow. Cells are injected directly into the bone marrow cavity of the femur via the knee. ES cell lines TC-71 and VH-64 and the CaP cell line PC3M were injected into the right femur of NSG mice at varying

cell doses. The course of the disease was tracked using Computed Tomography (CT) and 2-[18F]fluoro-2-deoxy-D-glucose-Positron Emission Tomography (FDG-PET); a final MR documented the tumor before dissection. Areas of interest, identified by imaging, were taken for immunohistochemistry (IHC) and compared to patient images and IHC.

Seven weeks post injection, CT images of mice transplanted with the ES cell line VH-64 showed development of structures identified as sunray spicules. The ES cell line TC-71 did not initiate the development of such structures, but appeared mottled and thickened compared to the left femur in the same mouse matching the permeative growth of Ewing sarcoma in human patients. Conversely, 66% of PC3M transplanted mice developed a pathological fracture of the right femur. In addition to palpable tumors in the thigh, all experimental mice had developed metastases at distant sites including liver and lungs. IHC analysis of the right femurs confirmed the findings of CT, and both ES cell lines were shown to have induced new bone formation. A review of ES patient images and IHC shows that a considerable number of patients present with new bone formation demonstrating the good concordance and clinical relevance of our proposed model.

As 20% of ES arise in the diaphysis region of the femur and patients develop lung or bone metastases, this i. f. model better reflects the situation in patients than s. c. or i. v. models. All ES implanted animals developed bone tumors, suggesting that this model may be useful in preclinical studies. I. f. injection is a minimally invasive and non-traumatic procedure, which provides us with a preclinical orthotopic model for ES and a model of primary metastasis in CaP. In addition to examining the biology of bone malignancies to the model can be used

study new drugs disturbing the interaction between cancer cells and bone microenvironment.

Development of an orthotopic model for human malignant bone diseases in immunocompromised NOD.Cg-*Prkdc*^{scid} *Il2rg*^{tm1wjl}/SzJ (NSG) mice

Abstract # 478

Knizia H[1], Batey MA[1], Almeida GS[1], Wilson I[1], Maxwell RJ[1], Dildey P[2], Hide IG[2], Bacon C[1], Vormoor J[1,2]

[1]Northern Institute for Cancer Research, Newcastle University, Newcastle upon Tyne, NE2 4HH, Newcastle upon Tyne, UK and

[2]Newcastle upon Tyne Hospitals, NHS Foundation Trust, Newcastle upon Tyne, UK

Henrike.Knizia@ncl.ac.uk

Introduction

- Bone is the third most common site of metastasis for any type of cancer and, more importantly, bone metastasis is one of the most significant adverse prognostic factors both for primary bone tumors (such as Ewing sarcoma and osteosarcoma) and other types of cancer (e.g. prostate cancer).
- Understanding how tumor cells remodel the bone microenvironment may be crucial to develop novel therapies targeting malignant bone disease.
- However, there are no experimental *in vivo* models available that allow studying and imaging of the interaction between tumor cells and normal bone.
- Previously, it had been shown that in an intravenous model for Ewing sarcoma metastasis to the bones was achieved in only 23% of the transplanted mice (1, 2). However, in order to study new treatments as well as the underlying mechanisms of the interaction between tumor cells and bone, it was felt necessary to develop a new and improved orthotopic *in vivo* model.
- Intrafemoral (i.f.) injection of cells in immunocompromised mice provides a technically feasible, minimally invasive and non-traumatic reproducible system for many cancer types infiltrating the bone or bone marrow (3, Fig 1) and offers new small animal *in vivo* bioimaging opportunities (Figs 2, 3 and 4).

Aims

- To develop an orthotopic *in vivo* model for malignant bone disease (primary and metastatic) for pre-clinical drug testing.
- To develop a model for studying the interaction between tumor cells and bone (re-modeling of the tumor microenvironment).
- To investigate the opportunities for small animal *in vivo* bio-imaging to monitor local disease progression (imaging biomarkers).

Methods

- Intrafemoral transplantation of male NOD.Cg-Prkdc^{scid}Il2rg^{tm1wjl}/SzJ (NSG) and Rag2(-/-)gamma(c)(-/-) mice with 1x10^5 cells of the following cell lines:
  - Ewing sarcoma: TC-71 and VH-64
  - Osteosarcoma: SaOS-2
  - Prostate cancer: PC3M
- *In vivo* imaging performed with:
  - CT: Bioscan NanoCT (Bioscan , Paris, France)
  - PET: Philips Mosaic HP (Philips, Eindhoven, NL)
  - MR: Varian 7T magnetic resonance system (Varian, Palo Alto, CA, USA)
- ImageJ was used for analysis of the CT pictures.

Fig 1: Scheme of intrafemoral transplantation.

Results

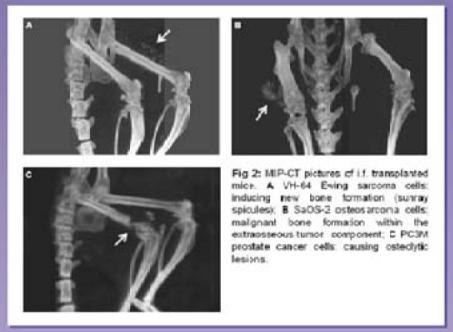

Fig 2: MIP-CT pictures of i.f. transplanted mice. **A** VH-64 Ewing sarcoma cells: inducing new bone formation (sunray spicules). **B** SaOS-2 osteosarcoma cells: malignant bone formation within the extraosseous tumor component; **C** PC3M prostate cancer cells: causing osteolytic lesions.

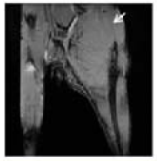

Fig 3: MR imaging of TC-71 Ewing sarcoma of the femur showing a larger extra-osseous tumor component (similar to patients).

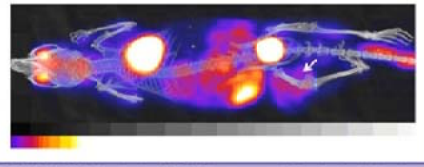

Fig 4: FDG-PET/CT fusion imaging of TC-71 Ewing sarcoma cells 7 weeks after injection (low tumor to background ratio).

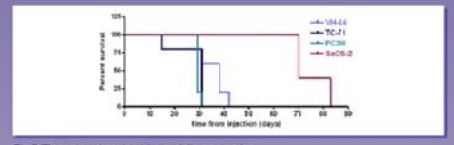

Fig 5: Time to reach protocol limits of disease burden.

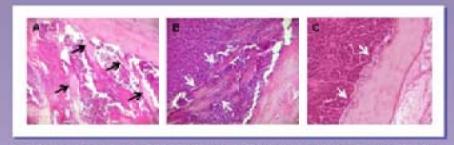

Fig 6: H&E stained histological slides of transplanted femurs (x20). **A** VH-64 induces new bone formation (histological correlate of the sunray spicules), **B** TC-71 shows similar induction of new immature bone, **C** PC3M showing lysis of the bone with activation of osteoclasts.

Conclusion

- Human Ewing sarcoma (VH-64, TC-71) cells induce formation of new and immature murine bone in an orthotopic xenograft model.
- Human osteosarcoma (SaOS-2) cells appear to be able to mature and form new malignant bone.
- Human prostate cancer (PC3M) cells cause osteolytic lesions of the murine femurs, sometimes causing pathological fractures.
- All cell lines are also able to metastasize to other organs (data not shown).
- CT offers excellent results for the visualization of tumor-associated bone alterations, while MRI imaging is superior for visualizing the extraosseous tumor component and tumor metastasis throughout the mice.
- In conclusion, we have been able to establish a new orthotopic model for malignant bone remodeling. As demonstrated here, human tumor cells are able to interact and activate both murine osteoblasts and osteoclasts similar to the situation in human patients.

References

1. Vormoor J et al. *Pediatr Res*. 2001 Mar; 49 (3): 332-41.
2. Franzius C et al. *Eur J Nucl Med Mol Imaging*. 2006 Dec; 33 (12): 1412-4.
3. Mazurier F et al. *Nature Medicine*. 2003 Jul; 9 (7): 959-963.

This work was supported by grants from the Bone Cancer Research Trust (BCRT), the North of England's Children's Cancer Research Fund (NECCR) and the Newcastle Healthcare Charity. There are no relevant conflicts of interest to disclose.

Abstract for the BACR 50th Anniversary Celebration meeting 'Hallmarks of Cancer: from Mechanisms to Therapies', June 13th-15th, 2010 (Edinburgh, UK):

Selected for poster presentation

Development of an orthotopic model for human malignant bone diseases in immunocompromised NOD.Cg-*Prkdc*^{scid} *Il2rg*^{tm1wjl}/SzJ (NSG) mice

Knizia H[1], Batey MA[1], Almeida GS[1], Wilson I[1], Maxwell RJ[1], Dildey P[2], Hide IG[2], Bacon C[1], Vormoor J[1,2]

[1]Northern Institute for Cancer Research, Newcastle University, Newcastle upon Tyne, NE2 4HH, Newcastle upon Tyne, UK and

[2]Newcastle upon Tyne Hospitals, NHS Foundation Trust, Newcastle upon Tyne, UK

The continuity of bone tissue relies on the delicate balance between osteoblasts and osteoclasts and the formation and resorption of new bone tissue. The presence of cancer cells disturbs this equilibrium. Ewing's sarcoma (ES) and osteosarcoma (OS) are the two most frequent primary osseous sarcomas in childhood and adolescence and primary osseous metastasis is the main adverse prognostic factor in patients. Clinically, the morphological changes to bone caused by ES differ from those of other cancer types metastasizing to the bone, such as prostate cancer (CaP).

We developed a preclinical orthotopic intrafemoral (i. f.) model addressing the interaction between tumour and bone directly. For this, ES cell lines TC-71 and VH-64, OS cell line SaOS-2 and CaP cell line PC3M were injected into the right femur of NSG mice via the knee. The course of the disease was tracked using Computed Tomography (CT) and 2-[18F]fluoro-2-deoxy-D-glucose-Positron Emission Tomography (FDG-PET); a final MR documented the tumour. Areas of interest, identified by imaging, were taken for histopathology.

Post injection CT images of femurs injected with the ES cell line VH-64 showed induction of sunray spicules, while femurs of TC-71 transplanted mice appeared mottled. CT images of SaOS-2 transplanted mice showed, that the tumour cells appear to be able to mature and form new malignant bone. Conversely, 66% of PC3M transplanted mice developed a pathological fracture of the injected femur. Histopathological analysis of the right femurs confirmed the findings of CT and a review of patient images and pathology shows that a considerable number of patients present with different forms of new bone formation. This demonstrates the good concordance and clinical relevance of the proposed model and as all implanted animals developed bone tumours, this model may be useful for examining the biology of bone malignancies and in preclinical studies.

Development of an orthotopic model for human malignant bone diseases in immunocompromised NOD.Cg-*Prkdc*^{scid} *Il2rg*^{tm1wjl}/SzJ (NSG) mice

Knizia H[1], Batey MA[1], Almeida GS[1], Wilson I[1], Maxwell RJ[1], Dildey P[2], Hide IG[2], Bacon C[1], Vormoor J[1,2]

[1]Northern Institute for Cancer Research, Newcastle University, Newcastle upon Tyne, NE2 4HH, Newcastle upon Tyne, UK and [2]Newcastle upon Tyne Hospitals, NHS Foundation Trust, Newcastle upon Tyne, UK

Henrike.Knizia@ncl.ac.uk

Newcastle University

Introduction

- Bone is the third most common site of metastasis for any type of cancer. Furthermore, bone metastasis is one of the most significant adverse prognostic factors both for primary bone tumours (such as Ewing sarcoma and osteosarcoma) and other types of cancer (e.g. prostate cancer).
- Understanding how tumour cells remodel the bone microenvironment may be crucial to develop novel therapies targeting malignant bone disease.
- However, there are no experimental *in vivo* models available that allow studying and imaging of the interaction between tumour cells and normal bone.
- Previously, it had been shown that in an intravenous model for Ewing sarcoma metastasis to the bones was achieved in only 23% of the transplanted mice (1, 2). In order to study new treatments as well as the underlying mechanisms of the interaction between tumour cells and bone, it was felt necessary to develop a new and improved orthotopic *in vivo* model.
- Intrafemoral (i.f.) injection of cells in immuno-compromised mice provides a technically feasible, minimally invasive and non-traumatic reproducible system for many cancer types infiltrating the bone or bone marrow (3, Fig 1) and offers new small animal *in vivo* bioimaging opportunities (Figs 2, 3 and 4).

Aims

- To develop an orthotopic *in vivo* model for malignant bone disease (primary and metastatic) for pre-clinical drug testing.
- To develop a model for studying the interaction between tumour cells and bone (re-modeling of the tumour microenvironment).
- To investigate the opportunities for small animal *in vivo* bio-imaging to monitor local disease progression (imaging biomarkers).

Methods

- Intrafemoral transplantation of male NOD.Cg-Prkdc^{scid}Il2rg$^{tm1wjl/szj}$ (NSG) and Rag2(-/-)gamma(c)(-/-) mice with 1x10^6 cells of the following cell lines:
  - Ewing sarcoma: TC-71 and VH-64
  - Osteosarcoma: SaOS-2
  - Prostate cancer: PC3M
- *In vivo* imaging performed with:
  - CT: Bioscan NanoCT (Bioscan, Paris, France)
  - PET: Philips Mosaic HP (Philips, Eindhoven, NL)
  - MR: Varian 7T magnetic resonance system (Varian, Palo Alto, CA, USA)
- ImageJ was used for analysis of the CT pictures

Fig 1: Scheme of intrafemoral transplantation.

Results

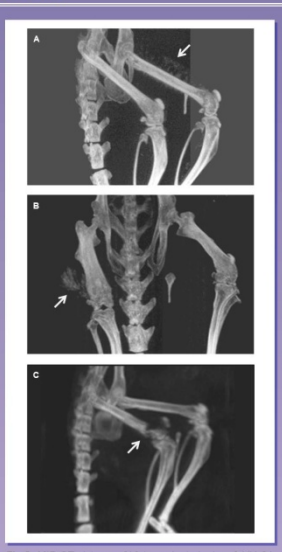

Fig 2: MIP-CT pictures of i.f. transplanted mice. **A** VH-64 Ewing sarcoma cells: inducing new bone formation (sunray spicules); **B** SaOS-2 osteosarcoma cells: malignant bone formation within the extraosseous tumour component; **C** PC3M prostate cancer cells: causing osteolytic lesions.

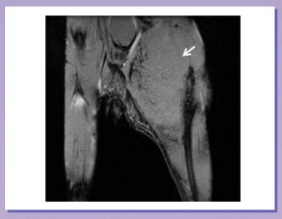

Fig 3: MR imaging of TC-71 Ewing sarcoma of the femur showing a larger extra-osseous tumour component (similar to patients).

Fig 4: FDG-PET/CT fusion imaging of TC-71 Ewing sarcoma cells 7 weeks after injection (low tumour to background ratio).

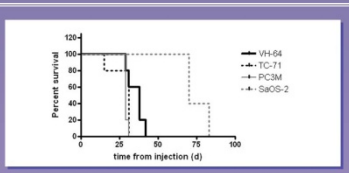

Fig 5: Time to reach protocol limits of disease burden.

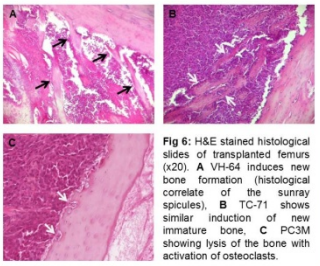

Fig 6: H&E stained histological slides of transplanted femurs (x20). **A** VH-64 induces new bone formation (histological correlate of the sunray spicules), **B** TC-71 shows similar induction of new immature bone, **C** PC3M showing lysis of the bone with activation of osteoclasts.

Conclusion

- Human Ewing sarcoma (VH-64, TC-71) cells induce formation of new and immature murine bone in an orthotopic xenograft model.
- Human osteosarcoma (SaOS-2) cells appear to be able to mature and form new malignant bone.
- Human prostate cancer (PC3M) cells cause osteolytic lesions of the murine femurs, sometimes causing pathological fractures.
- All cell lines are also able to metastasise to other organs (data not shown).
- CT offers excellent results for the visualization of tumour-associated bone alterations, while MRI imaging is superior for visualizing the extraosseous tumour component and tumour metastasis throughout the mice.
- In conclusion, we have been able to establish a new orthotopic model for malignant bone re-modeling. As demonstrated here, human tumour cells are able to interact and activate both murine osteoblasts and osteoclasts similar to the situation in human patients.

References

1. Vormoor J et al. *Pediatr Res.* 2001 Mar; 49 (3): 332-41.
2. Franzius C et al. *Eur J Nucl Med Mol Imaging.* 2006 Dec; 33 (12): 1432-41.
3. Mazurier F et al. *Nature Medicine.* 2003 Jul; 9 (7): 959-963

BONE CANCER RESEARCH TRUST

NECCR

Abstract for the NCRI Cancer Conference 2010, November 7th-10th 2010 (Liverpool, UK): Selected for poster presentation

Establishment of a preclinical orthotopic model for human malignant bone disease in immunocompromised NSG mice using small animal PET, CT and MRI imaging

Knizia H[1], Batey MA[1], Almeida GS[1], Wilson I[1], Maxwell RJ[1], Dildey P[2], Hide IG[2], Bacon CM[1], Vormoor HJ[1,2]

[1]Northern Institute for Cancer Research, Newcastle University, Newcastle upon Tyne, NE2 4HH, UK and

[2]Newcastle upon Tyne Hospitals NHS Foundation Trust, Newcastle upon Tyne, NE2 4HH, UK

Background: Ewing sarcoma (ES) and osteosarcoma (OS) are the two most frequent primary osseous sarcomas in childhood and adolescence. In both primary bone tumours and other cancers, bone metastases are the main adverse prognostic factor. Through complex interactions with cells such as osteoblasts and osteoclasts, cancer cells disturb the delicately balanced bone microenvironment causing different patterns of bone remodelling. Orthotopic models are needed both to study the biology of the interaction between tumour cells and bone and as preclinical models for drug development.

Methods: To develop a preclinical orthotopic intrafemoral model addressing interaction between tumour and bone, ES cell lines VH-64 and TC-71, OS cell line SaOS-2 and prostate cancer (CaP) cell line PC3M were injected into the right femurs of NSG mice. The disease was tracked using Computed

Tomography (CT) and 2-[18F]fluoro-2-deoxy-D-glucose-Positron Emission Tomography (FDG-PET); final Magnetic Resonance Imaging (MRI) documented tumours. Areas of interest identified by imaging were taken for histopathology.

Results: CT images of femurs injected with ES and OS cell lines showed remodelling of the murine bone with induction of pathological new bone formation. Additionally, OS transplanted mice showed formation of new malignant bone within the tumour mass itself. However, CaP cells caused osteolytic lesions and 28% of transplanted mice developed pathological fractures of the injected femur.

Histopathological analysis of the femurs confirmed the findings of CT imaging. Comparison of the model with images and pathology from patients with bone tumours showed a considerable similarity, demonstrating the clinical and biological relevance of the model. Finally, small animal MRI proved to be a good tool to quantify tumour volumes.

Conclusions: We have established a consistent orthotopic xenograft mouse model to study remodelling of the bone microenvironment by malignant cells. Moreover, this model can be used as a quantitative assay for preclinical drug testing.

Establishment of a preclinical orthotopic model for human malignant bone disease in immunocompromised NSG mice using small animal PET, CT and MRI imaging

Knizia H[1], Batey MA[1], Almeida GS[1], Wilson I[1], Maxwell RJ[1], Dildey P[2], Hide IG[2], Bacon CM[1], Vormoor J[1,2]

[1]Northern Institute for Cancer Research, Newcastle University, Newcastle upon Tyne, NE2 4HH, Newcastle upon Tyne, UK and [2]Newcastle upon Tyne Hospitals, NHS Foundation Trust, Newcastle upon Tyne, UK

Henrike.Knizia@ncl.ac.uk

Introduction

- Bone is the third most common site of metastasis for any type of cancer. Furthermore, bone metastasis is one of the most significant adverse prognostic factors both for primary bone tumours (such as Ewing sarcoma and osteosarcoma) and other types of cancer (e.g. prostate cancer).
- Understanding how tumour cells remodel the bone microenvironment may be crucial to develop novel therapies targeting malignant bone disease.
- However, there are no experimental *in vivo* models available that allow studying and imaging of the interaction between tumour cells and normal bone.
- Previously, it had been shown that in an intravenous model for Ewing sarcoma metastasis to the bones was achieved in only 23% of the transplanted mice (1, 2). In order to study new treatments as well as the underlying mechanisms of the interaction between tumour cells and bone, it was felt necessary to develop a new and improved orthotopic *in vivo* model.
- Intrafemoral (i.f.) injection of cells in immuno-compromised mice provides a technically feasible, minimally invasive and non-traumatic reproducible system for many cancer types infiltrating the bone or bone marrow (3, Fig 1) and offers new small animal *in vivo* bioimaging opportunities (Figs 2, 3 and 4).

Aims

- To develop an orthotopic *in vivo* model for malignant bone disease (primary and metastatic) for pre-clinical drug testing.
- To develop a model for studying the interaction between tumour cells and bone (re-modeling of the tumour microenvironment).
- To investigate the opportunities for small animal *in vivo* bio-imaging to monitor local disease progression (imaging biomarkers).

Methods

- Intrafemoral transplantation of male NOD.Cg-*Prkdc*^{scid} *Il2rg*^{tm1Wjl}/SzJ (NSG) and Rag2(-/-)gamma(c)(-/-) mice with 1x10^6 cells of the following cell lines:
  - Ewing sarcoma: TC-71 and VH-64
  - Osteosarcoma: SaOS-2
  - Prostate cancer: PC3M
- *In vivo* imaging performed with:
  - CT: Bioscan NanoCT (Bioscan, Paris, France)
  - PET: Philips Mosaic HP (Philips, Eindhoven, NL)
  - MR: Varian 7T magnetic resonance system (Varian, Palo Alto, CA, USA)
- Analysis: Imalytics (Philips), Amide (free software)

Fig 1: Scheme of intrafemoral transplantation.

Results

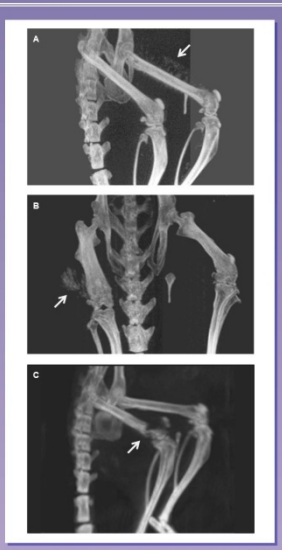

Fig 2: MIP-CT pictures of i.f. transplanted mice. **A** VH-64 Ewing sarcoma cells: inducing new bone formation (sunray spicules); **B** SaOS-2 osteosarcoma cells: malignant bone formation within the extraosseous tumour component; **C** PC3M prostate cancer cells: causing osteolytic lesions.

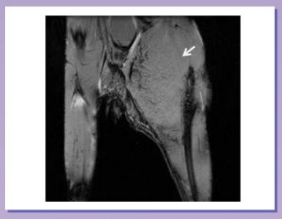

Fig 3: MR imaging of TC-71 Ewing sarcoma of the femur showing a larger extra-osseous tumour component (similar to patients).

Fig 4: FDG-PET/CT fusion imaging of TC-71 Ewing sarcoma cells 7 weeks after injection (low tumour to background ratio).

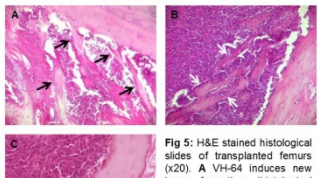

Fig 5: H&E stained histological slides of transplanted femurs (x20). **A** VH-64 induces new bone formation (histological correlate of the sunray spicules), **B** TC-71 shows similar induction of new immature bone, **C** PC3M showing lysis of the bone with activation of osteoclasts.

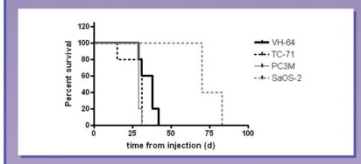

Fig 6: Time to reach protocol limits of disease burden.

Conclusion

- Human Ewing sarcoma (VH-64, TC-71) cells induce formation of new and immature murine bone in an orthotopic xenograft model.
- Human osteosarcoma (SaOS-2) cells appear to be able to mature and form new malignant bone.
- Human prostate cancer (PC3M) cells cause osteolytic lesions of the murine femurs, sometimes causing pathological fractures.
- CT offers excellent results for the visualization of tumour-associated bone alterations, while MRI imaging is superior for visualizing the extraosseous tumour component and tumour metastasis throughout the mice.
- In conclusion, we have been able to establish a new orthotopic model for malignant bone re-modeling. As demonstrated here, human tumour cells are able to interact and activate both murine osteoblasts and osteoclasts similar to the situation in human patients.

References

1. Vormoor J et al. *Pediatr Res.* 2001 Mar; 49 (3): 332-41.
2. Franzius C et al. *Eur J Nucl Med Mol Imaging.* 2006 Dec; 33 (12): 1432-41.
3. Mazurier F et al. *Nature Medicine.* 2003 Jul; 9 (7): 959-963

9.2 Internal Presentations

Research days of the Pediatric Oncology, University Hospital Münster, Mittelberg, Kleinwalsertal, Austria:

March 2007

February 2008

March 2009

Friday Research Forum, Northern Institute for Cancer Research, Newcastle upon Tyne, UK:

May 22nd 2009

March 12th 2010

Diverse Journal-Club presentations in the working groups in Münster and Newcastle upon Tyne.

9.3 External Presentations

Cellular Tumour Immune-Therapy Meeting, University Hospital Münster, Münster, Germany (invited):

September 2007

April 2008

Newcastle Cancer Centre Drug Discovery and Imaging Group Meeting, General Hospital, Newcastle upon Tyne, UK (invited):

September 29th 2009

9.4 Publications

Prepared manuscript which will be submitted to Neoplasia:

Knizia, H. K., Batey, M. A., Almeida, G. S., Wilson, I., O'Toole, K., Dildey, P., Hide, G. I., Maxwell, R. J., Bacon, C. M., Vormoor, H. J.

Development of an orthotopic model for human malignant bone diseases in immunocompromised NOD.Cg-*Prkdc*^{scid} *Il2rg*^{tm1wjl}/SzJ (NSG) mice using *in vivo* imaging techniques.

Manuscript in preparation:

Gene expression patterns in organ-specific metastases of Ewing's sarcoma in an *in vivo* model of NOD/Scid mice.